THÈSE

Pour obtenir le grade de

DOCTEUR DE L'UNIVERSITÉ GRENOBLE ALPES

et de l'UNIVERSITÉ FÉDÉRALE DE SÃO CARLOS

École doctorale : IMEP-2 – Ingénierie, Matériaux, Mécanique, Environnement, Énergétique, Procédés, Production

Spécialité : Matériaux, Mécanique, Génie Civil, Électrochimie et Science et Ingénierie des Matériaux

Unité de recherche : Laboratoire du Génie de Procédés Papetiers et Département d'Ingénierie des Matériaux

Optimisation des mousses de PLA produites par methode supercritique : Influence de la modification chimique et de l'incorporation de CNC sur les structures cellulaires resultantes

Optimization of PLA foams produced by supercritical method: Influence of chemical modification and incorporation of CNC on the resulting cellular structures

Présentée par :

Ana Beatriz VALIM SUQUISAQUI

Direction de thèse

Dr. Julien BRAS Professor at Université Grenoble Alpes	Directeur de thèse
Dr. Sílvia H. Prado BETTINI Professor at Universidade Federal de São Carlos	Directrice de thèse

Rapporteurs :

Dr. Tatiana BUDTOVA
Senior Scientis at Mines Paris
Dr. Antonio José Felix de CARVALHO
Professor at Universidade de São Paulo

Thèse soutenue publiquement le **30 Septembre 2024,** devant le jury composé de:

Dr. Julien BRAS Professor at Université Grenoble Alpes	Directeur de thèse
Dr. Sílvia H. Prado BETTINI Professor at Universidade Federal de São Carlos	Directrice de thèse
Dr. Tatiana BUDTOVA Senior Scientist at Mines Paris	Rapporteure
Dr. Antonio José Felix de CARVALHO Professor at Universidade de São Paulo	Président
Dr. Carlos Henrique SCURACCHIO Professor at Universidade Federal de São Carlos	Examinateur
Dr. Mohamed Naceur BELGACEM Professor at Université Grenoble Alpes	Examinateur

Titre : Optimisation des mousses de PLA produites par methode supercritique : Influence de la modification chimique et de l'incorporation de CNC sur les structures cellulaires resultantes

Mots clés : Acide poly(lactique); modification chimique; mécanochimie; nanocomposites ; nanocristaux de cellulose ; mousses polymères; cryogels de NFC.

Résumé : L'objectif principal de cette recherche était d'étudier l'influence de la modification chimique et de l'introduction de nanocristaux de cellulose (CNC) sur les propriétés du PLA, visant la production de mousses, utilisant du CO_2 supercritique comme agent moussant. Dans le même temps, dans le but de produire un matériau matriciel poreux en cellulose, un cryogel de nanofibres de cellulose (NFC) a été produit avec un caractère hydrophobe accru, sans nécessiter de traitements chimiques. Pour la modification chimique du PLA, le GMA a été utilisé comme agent modificateur, en présence de peroxyde comme initiateur. Concernant la stratégie d'incorporation des charges, le CNC a été modifié chimiquement par mécanochimie, à l'aide de n-isocyanate d'octadécyle, dans le but d'augmenter la compatibilité avec la matrice PLA. Les nanocomposites ont été produits dans différentes concentrations de CNC pure et modifiée. Des cryogels à base de cellulose ont été produits en lyophilisant une suspension de de NFC et de nanoparticules de PLA qui, après avoir été lyophilisées, ont été soumises à un traitement thermique. Les résultats ont montré que la modification chimique du PLA entraînait des changements significatifs dans les structures cellulaires des mousses. L'introduction de la CNC était plus significative pour la concentration la plus élevée étudiée (10 %), où la CNC pure à cette concentration entraînait la plus petite taille de cellule et le taux d'expansion le plus élevé. Quant au cryogel NFC, l'introduction de 10 % de nanoparticules de PLA suivie d'un traitement thermique s'est avérée efficace pour augmenter le caractère hydrophobe du matériau, sans subir d'impacts majeurs sur la structure interne des pores.

Title: Optimization of PLA foams produced by supercritical method: Influence of chemical modification and incorporation of CNC on the resulting cellular structures

Keywords: Poly(lactic acid) ; chemical modification; mechanochemistry; nanocomposites; cellulose nanocrystals; polymeric foams; CNF cryogels;

Abstract: The main objective of this research was to study the influence of chemical modification and the introduction of cellulose nanocrystals (CNC) on the properties of PLA, with a view to producing foams using supercritical CO_2 as a foaming agent. In parallel, in order to produce a cellulose-based porous material, an CNF cryogel was produced with an increased hydrophobic character, without the need for chemical treatments. For the chemical modification of PLA, GMA was used as a modifying agent, in the presence of peroxide as an initiator. For the strategy of incorporating fillers, the CNC was chemically modified by mechanochemistry using n-octadecyl isocyanate in order to increase compatibility with the PLA matrix. The nanocomposites were produced in different concentrations of neat and modified CNC. The cellulose-based cryogels were produced by freeze-drying a suspension of CNF with PLA nanoparticles which, after being freeze-dried, were subjected to thermal treatment. The results showed that the chemical modification of PLA resulted in significant changes in the cell structures of the foams. The introduction of CNC was more significant at the highest concentration studied (10 wt%), which neat CNC at this concentration resulted in the smallest cell size and highest expansion ratio. As for the CNF cryogel, the introduction of 10 wt% PLA nanoparticles followed by heat treatment proved to be efficient in increasing the material hydrophobic character, without impacting on the internal structure of the pores.

AKNOWLEDGEMENTS

Meus agradecimentos não podem começar sem agradecer minha família, acima de tudo. Aos meus pais, Sandra e Gilberto, que sempre admiraram e demonstraram respeito aos professores, pesquisadores e à ciência. Hoje eu sei que minha escolha para seguir na academia não foi aleatória: eu queria ser aquelas pessoas que sempre vi meus pais admirando! E durante esses meus 29 anos, eles não mediram esforços para me proporcionarem a melhor educação que eu poderia ter. Obrigada também à minha irmã, Giovana, que depois de passar uma vida inteira sendo minha cópia (rs) hoje é uma das minhas maiores inspirações. Ela não sabe, mas durante os momentos mais desafiadores e difíceis da escrita desta tese, uma frase dela, dita no auge de seus 16 anos, ecoou na minha mente "*Você tá com medo do que? De sentir dor? Vai doer e vai passar. E acabou.*". Obrigada Djodjo por ser destemida e me inspirar a ser também! Obrigada aos meus avós que me deram os meus bens mais preciosos que são meus pais, por terem proporcionado as melhores lembranças de infância que eu tenho, por terem nos amado e demonstrado isso dia após dia. À minha Bá, que teve a oportunidade de me vir crescer e me tornar doutora, que cuidou de mim e me ensinou tanto, obrigada por ser você. A vida não faria sentido sem vocês, minha família! Obrigada por serem meus! Eu amo vocês com todo meu coração!

Meu outro bem mais precioso dessa vida: meus amigos! Meus amigos me permitem ser quem eu sou, da forma mais pura. Obrigada por me acompanharem em todas as fases da minha vida e por construírem juntos comigo, uma vida de histórias. Vocês sabem quem são e sabem o quanto eu amo vocês. Obrigada pelo carinho durante esse período, pelas palavras de incentivo (ou bolinho de cenoura no meio da tarde) e por não me deixarem esquecer que eu sou doutora! Vocês fizeram a diferença nesse processo: Amilgas, Role suavão (que nunca é suave), Interajets, Somos 7, Neidocas e todos meus amigos que se tornaram minha família do coração, eu amo e sou apaixonada por vocês!!

Gostaria de agradecer também aos professores que fizeram parte da minha vida durante essa caminhada e me inspiraram e contribuíram para que eu fosse capaz de realizar esse doutorado.

Ao professor Paulo e aos funcionários e alunos que tive o prazer de conhecer no Instituto de Química da Unicamp, obrigada pela parceria na produção das minhas espuminhas e por todo suporte durante minhas estadias na universidade. Foi um prazer dividir meus dias com vocês!

To all my friends in France, merci for receiving me with open arms, for all the help and support. You were my home for one entire year and I am sure this experience would not be the same without you. Thanks to all the staff, engineers, technicians and students from LGP2 and Cermav, for everything. Thank you so much to my supervisor, Julien Bras, for giving me this opportunity and for support me (and

save me from the French bureaucracy) during this period. It was an honor and a pleasure to be supervised by this great professor! C'était pas trop mal!!

Special thanks to my close friends who made my lab life much more funny during this year: Rene, Laura, Thaís, Marina, Rafael, Emma, Jean Pierre, Randy and Stefania thank you so much for all the moments we shared. I hope to be with you asap!

Aos meus amigos brasileiros na França, vocês foram minha casa e minha família durante esse ano maluco! Eu não canso de dizer o quanto eu fui sortuda por ter vocês ao meu lado: João tupanjo, Kauã, Helga, Gabs, Thaís, Rafael, Marina, Tati, Igor, Berrrrrnarrrrrdo, Bruna, Letícia. Espero ter a oportunidade de viver muitas outras histórias com vocês! Obrigada por terem me aguentado em todas as minhas versões: a apocalíptica e a que sumia! Amo vocês!

No Brasil, gostaria de agradecer muito meu grupo de pesquisa, meus colegas de laboratório, técnicos, funcionários e professores do departamento que acompanharam e de alguma forma fizeram parte dos meus dias durante esses anos. Queria agradecer especialmente as pessoas que me ensinaram, ajudaram e me deram suporte para iniciar minha história na engenharia de materiais, no laboratório, durante as disciplinas e nessa reta final do doutorado: Talita, Lívia, Laís, Marcos (o nosso e o da Lidi rsrs), Iago, Franklin, Saccardo, Daniel.

Finalmente, minha eterna gratidão a pessoa que me deu a chance de realizar esse sonho: minha amiga e orientadora Sílvia Bettini! Obrigada Sil por ter me dado essa chance, sem me conhecer, sabendo que eu teria que aprender tudo do zero. Obrigada por tantos ensinamentos e por confiar em mim! Foi um prazer imenso ter sido formada por você. Espero que o futuro nos dê outras oportunidades para trabalharmos juntas!

This study was financed in part by the Coordenação de Aperfeiçoamento de Pessoal de Nível Superior - Brasil (CAPES) - Finance Code 001.

This study was financed by CAPES – grant: 88887.501080/2020-00.

This study was financed, in part, by the São Paulo Research Foundation (FAPESP), Brasil. Process Number 2020/07633-2.

This study was financed, in part, by CNPq – Conselho Nacional de Desenvolvimento Científico e Tecnológico – Brasil, grant: 200206/2022-2.

Suquisaqui, 2024

SCIENTIFIC CONTRIBUITIONS (2020-2024)

SUQUISAQUI, A.B.V.; BETTINI, S.H.P.; BRAS, J. Cellulose nanofibers (CNF) cryogels hydrophobicity enhancement by using poly(lactic acid) (PLA) nanoparticles physisorption and melting templating. Submitted to *ACS Applied Biomaterials.*

SUQUISAQUI, A.B.V; GONÇALVES, L.M.G.; POSSALI, L.T.; BRETAS, R.E.S.; ROSA, P.T.V; BRAS, J.; BETTINI, S.H.P. The role of chemical modification in producing PLA foams: balance between branches, macroradical recombination, and linear reaction. Submitted to *ACS Applied Polymer Materials.*

SUQUISAQUI, A.B.V.S.; BETTINI, S.H.P.; BRAS, J. CNC-based nanocomposites functionalized with long aliphatic chains by mechanochemistry: a green and solvent-free method. In preparation.

SUQUISAQUI, A.B.V.; BRAS, J.; BETTINI, S.H.P. PLA/CNC nanocomposites foams produced by supercritic method. In preparation.

SUQUISAQUI, A.B.V.; BRAS, J.; BETTINI, S.H.P. Rheological and crystallinity influence in cellular structures of modified PLA foam. In preparation.

Conference presentations:

SUQUISAQUI, A.B.V; BRAS, J.; BETTINI, S.H.P. Rheological Analysis of modified PLA by reactive process aiming at the production of foams. Oral presentation. 39th International Conference of Polymer Processing Society. Cartagena de Indias, Colômbia. May 2024.

SUQUISAQUI, A.B.V. GONÇALVES, L.M.G.; POSSALI, L.T.; SILVA, E. A.; LIMA NETO, B.S.; BRETAS, R.E.S.; ROSA, P.T.V.; BETTINI, S.H.P. Foaming of modified poly(lactic acid) obtained by reactive processing as a sustainable solution for single-use packaging. Poster presentation. 39th International Conference of Polymer Processing Society. Cartagena de Indias, Colômbia. May 2024.

BRAS J, PESCHEUX-SERGIENKO J, SUQUISAQUI A.BV., DOUARD L., BELGACEM N., Mechanochemistry as a solution to produce and functionalize various types of nanocellulose, TAPPI NANO, Atlanta, 10-13th of June 2024.

SUQUISAQUI, A.B.V.; SILLARD,C.; BETTINI, S.H.P. ; BRAS, J. Cellulose nanofibers (CNF) cryogel incorporated with poly(lactide acid) (PLA) nanoparticles. Poster presentation. EPNOE, Graz, Austria. September 2023.

SUQUISAQUI, A..B.V.; GONÇALVES, L.M.G.; BRETAS, R.E.S.; BETTINI, S.H.P. PLA chain extension by reactive processing aiming foaming. Oral presentation. Biopol, Alicante, Spain. November 2022.

TABLE OF CONTENT

Page

AKNOWLEDGEMENTS i

SCIENTIFIC CONTRIBUITIONS (2020-2024) iv

TABLE INDEX xii

FIGURES INDEX xiv

GENERAL INTRODUCTION 2

CHAPTER I - FUNDAMENTALS AND LITERATURE REVIEW 10

Introduction to Chapter I 10

1 Polymeric Foams: context, history and definitions 11

1.1 Polymer foaming 14

1.1.1 Blowing agents 14

1.1.2 Principle of foaming 17

1.1.3 Methods for foams production 19

1.2 Factors influencing the foaming process using supercritical CO_2 as a blowing agent 22

1.2.1 Rheological characteristics 23

1.2.2 Crystallinity 25

1.2.3 Blowing agents 26

1.2.4 Processing conditions 26

1.2.4.1 Influence of Pressure, Temperature, and Time on Gas Solubility During CO_2 Saturation 26

1.2.4.2 Effects of foaming temperature 27

1.2.4.3 Influence of the presence of fillers in the polymer matrix 29

1.3 Final considerations on polymeric foams 29

2 Biobased polymers contextualization 31

3 Poly(Lactic Acid) 34

3.1 Structure and production 36

3.1.1 Degradation and biodegradation 39

3.1.2 PLA properties 41
3.2 PLA reactive processing for production of foams 42
3.3 PLA nanocomposites for foams 45
4 Nanocellulose 49
4.1 From cellulose to nanocellulose 49
4.2 Nanocelluloses productions and application 52
4.2.1 Cellulose nanofibers (CNF) 52
4.2.1.1 CNF-based porous materials 55
4.2.2 Cellulose nanocrystals (CNC) 59
4.2.2.1 CNC-based nanocomposites 61
4.2.2.2 CNC funcionalization 62
4.2.2.3 Methods for CNC nanocomposites production 69
4.3 Market of nanocellulose 70

Conclusion Chapter I 71

CHAPTER II - PLA CHEMICAL MODIFICATION AND FOAMS 74
Introduction to Chapter II 74

II.1 The role of chemical modification in producing different PLA chain structures: balance between branches, macroradical recombination, and liner reaction. 75
1 Introduction 75
2 Materials and Methods 78
2.1 Materials 78
2.2 Chemical Modification of PLA 78
2.3 Characterization 79
2.3.1 Size Exclusion Chromatography (SEC) 79
2.3.2 Determination of acids groups 79
2.3.3 Rheological analysis 80
2.3.4 DSC 80
2.3.5 Crosslinking content 81

2.3.6 NMR analysis 81
2.3.7 Statistical analysis 82
3 Results 83
3.1 Torque results during chemical modification of PLA 83
3.2 Influence of chemical modification on final chemical structures 85
4 Conclusions 96

II.2 Rheological properties and crystallinity influence on modified PLA foams 97
1 Introduction 97
2 Materials and Methods 100
2.1 Materials 100
2.2 Methods 100
2.2.1 Chemical modification 100
2.2.2 Batch foaming 100
2.2.3 Rheological characterization 102
2.2.4 Differential scanning calorimetry (DSC) 102
2.2.5 Foam characterization 102
2.2.6 Statistical analysis 103
3 Results 104
3.1 Rheological properties 104
3.2 Foamability of modified PLA 109
3.3 Crystallinity influence on foams 113
4 Conclusion 117

Conclusion Chapter II 118

CHAPTER III - CNC FUNCTIONALIZATION AND NANOCOMPOSITES FOAMS 120
Introduction to Chapter III 120

III.1 CNC functionalized with long aliphatic chains by mechanochemistry: a green and solvent-free method 121

1 Introduction 121
2 Materials and Methods 123
2.1 Materials 123
2.2 CNC chemical modification 123
2.3 CNC characterization 124
2.3.1 Fourier-transform infrared (FTIR) spectroscopy 124
2.3.2 X-ray photoelectron spectroscopy (XPS) 124
2.3.3 Elemental Analysis 125
2.3.4 X-ray diffraction (XRD) 125
2.3.5 Transmission electron microscopy (TEM) 125
2.3.6 Dynamic light scattering (DLS) 126
2.3.7 Contact Angle 126
3 Results 127
3.1 CNC chemical modification 127
4 Conclusion 140

III.2 PLA/CNC nanocomposites foams produced by supercritical methode 141
1 Introduction 141
2 Material and Methods 144
2.1 Materials 144
2.2 Methods 144
2.2.1 CNC functionalization 144
2.2.2 Nanocomposite foams production 144
2.2.3 Fourier-transform infrared spectroscopy (FTIR) 146
2.2.4 Nanocomposites rheological analysis 146
2.2.5 Differential Scanning Calorimetry (DSC) 147
2.2.6 Transmission Electron Microscopy TEM 147
2.2.7 Foam characterization 148
2.2.8 Statistical analysis 149
3 Results 150
3.1 Properties of nanocomposites 150
3.2 Foams characterization 162

4 Conclusion 169

Conclusion Chapter III 170

CHAPTER IV - CELLULOSE NANOFIBERS (CNF) AS A MATRIX FOR POROUS MATERIALS 172

Introduction to Chapter IV 172

IV.1 Cellulose nanofibers (CNF) cryogels hydrophobicity enhancement by using poly(lactic acid) (PLA) nanoparticles physisorption and melting templating 173

1 Introduction 173

2 Materials and Methods 177

2.1 Materials 177

2.2 Methods 177

2.2.1 PLA nanoemulsion preparation 177

2.2.2 CNF/PLA cryogel preparation 178

2.2.3 Characterization 179

2.2.3.1 CNF Morphological analysis 179

2.2.3.2 Dynamic Light Scattering (DLS) 180

2.2.3.3 Multi-SPR (Multi-Parameter Surface Plasmon Resonance) 180

2.2.3.4 Cryogels characterization 182

2.2.3.5 Fourier-transform infrared spectroscopy (FTIR) 183

2.2.3.6 Specific surface area (SSA) 183

2.2.3.7 Contact angle 183

2.2.3.8 Dynamic mechanical analysis (DMA) 184

2.2.3.9 Cryogel morphological analysis 184

3 Results 185

3.1 CNF and PLA Nanoemulsion characterization 185

3.2 PLA Nanoemulsion interaction with CNF 188

3.3 Preparation of CNF/PLA nanoparticles Cryogel 190

3.4 Influence of PLA with or without thermal treatment in mechanical properties and water resistance of ensued cryogel 196
4 Conclusion 200

GENERAL CONCLUSION 202
PERSPECTIVES AND FUTURE WORKS 205
APPENDIX 207
EXTENDED PORTUGUESE ABASTRACT 221
REFERENCES 234

TABLE INDEX

Chapter I

Table I.1 - Main advantages and drawbacks of polymeric foams compared to solid materials. 12
Table I.2 - Key characteristics of foam production processes using supercritical fluids. 19
Table I.3 - List of the largest PLA producers 34
Table I.4 – Advantages and drawbacks of ball milling 68

Chapter II

Table II.1 – Nomenclature of samples with different DCP and GMA concentrations. 79
Table II.2 – Results of SEC and titration of acid groups. 86
Table II.3 – Crosslinking percentage of the samples. 89
Table II.4 – Thermal results from second heating curves by DSC analysis, from 0°C to 200°C, at 10°C/min. 92
Table II.5 - Experimental design. 100
Table II.6 – Terminal slope, cross-over, and $\eta 0*$ values obtained from the graphs presented. 105

Chapter III

Table III.1 – Experimental values of XPS and values of decomposition peaks of C1s curve. 130
Table III.2 – Elemental analysis results of experimental values and corrected values 131
Table III.3 - Length and diameter of neat CNC and neat CNC cryomilled for 15 minutes. 136
Table III.4 – Comparison between results found in the literature of CNC modification using n-OI. 139
Table III.5 – Nanocomposites formulations and nomenclature. 145
Table III.6 – Values of terminal slope (0.05-0.3 rad/s) and crossover for all samples. 156

Table III.7 – DSC results for all nanocomposites formulations. 158

Chapter IV

Table IV.1 – Identification of cryogel samples according to experimental design. 179
Table IV.2 – MorFi analysis of CNF samples. 186
Table IV.3 – Stress values (Pa) for 50% and 80% of strain for all cryogels.... 197

FIGURES INDEX

Chapter I

Figure I.1 – Main applications for polymeric foams. 12
Figure I.2- Classification of Polymeric Foams. 13
Figure I.3 - Most commonly used thermoplastic polymers to produce foams and their classifications 14
Figure I.4 – Typical decomposition process of ADC. 15
Figure I.5 – Decomposition of sodium bicarbonate when thermally exposed.. . 15
Figure I.6 - Typical phase diagram illustrating the possible physical states of substances under different temperatures and pressures. The critical point is reached at specific critical temperature and pressure values (Tc and Pc, respectively). 16
Figure I.7 – Main steps of foaming processing. 17
Figure I.8 - Two-stage, temperature-induced foaming process 21
Figure I.9 - One-step foaming process induced by a pressure decrease 22
Figure I.10 - Main factors influencing the foaming ability of polymers 23
Figure I.11 – Representation of strain-hardening curves for the same sample at different strain rates, where a>b>c are different strain rates. 24
Figure I.12 - Typical SEM images and schematic representation of open and closed cellular structures in foams 28
Figure I.13- Classifications of bioplastics 31
Figure I.14 - Nanoparticles commonly used to improve the properties of bioplastic nanocomposites 32
Figure I.15 - Global production capacity of bioplastics in 2023. 33
Figure I.16 - PLA applications in different areas. 35
Figure I.17 - Repeating unit of poly(lactic acid). 36
Figure I.18 – Lactic acid enantiomers. 37
Figure I.19 – Isomers of lactide. 38
Figure I.20 - Scheme of the three main PLA production routes. 38
Figure I.21 - General molecular structure of the multifunctional chain extender Joncryl®, where R1-R5 can be H, CH3, long alkyl chains, or combinations thereof; R6 represents an alkyl group, and x, y, z range from 1 to 20 units. 44

Figure I.22 – Typical behavior of melting polymers under rheological dynamic analysis 46
Figure I.23 – Proposed model for the dynamic rheological response of polymeric matrix filled with nanoclays, where $n_a<n_b<n_c<n_d$ are the number of particles per unit volume 47
Figure I.24 - Molecular structure of cellulose (where n represents the degree of polymerization) 50
Figure I.25 - Cellulose polymorphs and the main steps involved in their formation 50
Figure I.26 - Hierarchical organization of cellulose fiber 51
Figure I.27 – Different types of nanocelluloses..... 52
Figure I.28 - Mechanical processes for producing CNF.. 53
Figure I.29 - Representative scheme for obtaining CNFs from cellulose fibers.. 54
Figure I.30 – Different methods to produce porous materials..... 56
Figure I.31 – Formation of porous structures from ice crystals sublimation..... 57
Figure I.32 – Different ice crystals structures during freezing for cryogels production..... 58
Figure I.33 – Aerogel, cryogel and xerogel produced from microcrystalline cellulose 58
Figure I.34 – Steps for obtaining CNC from acid hydrolysis 59
Figure I.35 - Representative scheme for obtaining CNC from acid hydrolysis by sulfuric acid, resulting in sulfate half-ester surface groups 60
Figure I.36 – Representation of modification methods of CNC..... 62
Figure I.37 – Common chemical modifications of CNC, where PEG: poly(ethylene glycol); PEO: poly(ethylene oxide); PLA: poly(lactic acid); PAA: poly(acrylic acid); PNiPAAm: poly(N-isopropylacrylamide); and PDMAEMA: poly(N,N-dimethylaminoethyl methacrylate) 63
Figure I.38- Mono- and di-isocyanates, aliphatic and aromatics, most commonly used in nanocellulose functionalization. 64
Figure I.39 – Chemical reaction between n-OI and hydroxyl group from CNC. 65
Figure I.40 - Formation of the allophanate group when excess isocyanate is present in the reaction medium, reacting with the urethane group formed 65

Figure I.41 - By-products produced in the reaction between isocyanate and water 66
Figure I.42 – Methods studied for functionalizing CNC using n-OI 66
Figure I.43 – Different types of instruments used to the ball milling process: a) tumbler ball mill; b) vibratory mill; c) planetary ball mill..... 68

Chapter II

Figure II.1 – Chemical structure: (a) DCP; (b) GMA. 78
Figure II.2: Reactive processing of the formulations: (a) reference formulations (b) experimental design 2^2. Code: PLA_C_{DCP}_C_{GMA}..... 84
Figure II.3 - Possible reactions between the epoxy group present in PLA-g-GMA and the a) hydroxyl group at the end of the chain of another PLA molecule and b) carboxylic acid group at the end of the chain of another PLA molecule. 84
Figure II.4: Reaction mechanisms for PLA chemical modification, where: R1: Decomposition of DCP into two peroxyl radicals; R2- Formation of PLA radical in the presence of a peroxide; R3- Stabilization of PLA radical by chain scission; R4- Stabilization of PLA radical by recombination between different PLA radicals; R5' – Stabilization of PLA radical by insertion of GMA monomer; R5'' – Linear chain extension of GMA branched after reaction between epoxy group from GMA and carboxylic group from PLA. 87
Figure II.5 – Percentage of crosslinking structures obtained by Soxhlet extraction during 6 hours at two concentrations of peroxide (0.5 and 1phr)..... 88
Figure II.6 – Possible chain structures formed as a result of variation of DCP and GMA concentration during the reactive process, where: a) represents sample 0.5_1; b) sample 1.5_1 which presented crosslinked structure; c) sample 0.5_3 and; d) sample 1.5_3..... 91
Figure II.7: Steady-state shear at T=180°C: (a) Viscosity *versus* shear rate (b) First normal stress difference (N_1) *versus* shear rate. 93
Figure II.8 – a) Rheological analysis in the oscillatory state for modified and neat PLA samples of tan δ *versus* frequency; b) Cole-Cole graphics for neat PLA and modified PLA. T=180°C..... 94
Figure II.9 – Scheme of the in-house made foaming device. 101
Figure II.10 – Steps for the foaming process with sc-CO_2. 101

Figure II.11 – Complex viscosity obtained from 0.05 to 500 rad/s, at 180°C.. 104
Figure II.12 – Plots of log G’ and G’’ *versus* log angular frequency from 0.05 to 500 rad/s, at 180ºC..... 106
Figure II.13 – Log G’ *versus* log angular frequency performed at 180°C, from 0.05 to 500 rad/s. 107
Figure II.14 - van Gurp-Palmen (vGP) graph for the samples studied..... 108
Figure II.15 – SEM images of neat and modified PLA at a magnification of 250x. 110
Figure II.16 – Morphologies of cell structures obtained by SEM at 1200x magnification, with graphs of the respective cell size distributions. 111
Figure II.17 - Density, volume expansion ratio (VER), cell size and cell density values. Equal letters correspond to statistically similar samples. 112
Figure II.18 - Differences in the crystallinity percentages of the foamed and non-foamed samples (Following Equation II.4). 114
Figure II.19 - Relationship between crystallinity and complex viscosity for the production of foams with controlled and uniform sizes. 116

Chapter III

Figure III.1– Chemical structure of n-octadecyl Isocyanate. 123
Figure III.2 – Grinding jar made of zirconium dioxide filled with 50 zirconium dioxide balls..... 124
Figure III.3 – Chemical reaction between the OH group from CNC and isocyanate groups from n-OI. 127
Figure III.4 – FTIR curves of neat CNC and CNC modified with n-OI..... 128
Figure III.5 – XPS results a) peaks b) Deconvolution of carbon peaks for neat and modified CNC. 128
Figure III.6 – XRD curves for all neat CNC, neat CNC after milling and modified CNC. 132
Figure III.7 – DLS of neat CNC, milled CNC, and modified CNC. 133
Figure III.8 – TEM of a) neat CNC in water; b) neat milled CNC in water; c) modified CNC in ethanol. 134

Figure III.9 – Comparison between a) neat CNC and; b) neat cryomilled CNC, at the same magnification. Arrows show some agglomeration after cryomilling process. 135
Figure III.10 – Different aggregates obtained after CNC chemical modification with n-OI. 136
Figure III.11 – Contact angle for neat and modified CNC, for 30 seconds. 137
Figure III.12 – Scheme of the in-house made foaming device and the steps of the foaming process. 146
Figure III.13 – FTIR spectra for PLA and PLA/CNC nanocomposites: a) full spectra and; b) Zoom at region of 3000 cm^{-1} showing the presence of long aliphatic chains present in n-OI. 151
Figure III.14 – Apparent viscosity of PLA and PLA/CNC nanocomposites, at 180°C. 152
Figure III.15 – Log G' *versus* log angular frequency of nanocomposites performed at 180°C from a) 0.05 a 500 rad/s and; b) 0.05 a 0.3 rad/s. 154
Figure III.16 – Log G' and G'' *versus* log angular frequency of nanocomposites performed at 180°C from 0.05 to 500 rad/s. 155
Figure III.17 – DSC second heating curves for all studied nanocomposites formulations. 157
Figure III.18 –CNC and CNCm DSC curves, from 25°C to 200°C, at 10°C/min. 158
Figure III.19 – TEM images of nanocomposites at a magnification of 45000 x. 161
Figure III.20 - First heating curves in the DSC analysis of the foams produced. 163
Figure III.21 – Crystallinity percentage of the foams obtained in the first DSC heating, at 10°C/min, representing the percentage of crystallization during the foaming process. 164
Figure III.22 – SEM images in two different magnifications (400x and 800x) for all nanocomposites formulations and its size distribution. 165
Figure III.23 – Cell morphology characterization. Different letters are statistically different. 166

Chapter IV

Figure IV.1 – a) CNF at 3 wt% dry content; b) SEM image of CNF at magnification of 600x; c) TEM image of CNF; d) optical microscopy of CNF. 185
Figure IV.2 – Picture of PLA nanoemulsion 6 months after its preparation, at a concentration of 1.8 wt% and stored at room temperature, followed by characterization of PLA nanoparticles size and PDI before (emulsion) and after (nanoemulsion) ultrasonic treatment. 186
Figure IV.3 – SPR sensogram and a representation of what happens in each step of injection: 1) First layer with PEI as a substrate for CNF adsorption; 2) second layer with CNF; 3) third layer with PLA. 188
Figure IV.4 - Different structures formed in cryogels as a result of the a) presence of excess surfactant; b) absence of excess surfactant after several centrifuging cycles. 190
Figure IV.5 – Produced cryogels before and after thermal treatment: a) CNF; b) CNF/PLA10; c) CNF/PLA20; d) CNF_180; e) CNF/PLA10_180; f) CNF/PLA20_180. 191
Figure IV.6 – Comparison between FTIR curves of neat PLA, CNF cryogel, and CNF/PLA cryogel with 10 and 20 wt% of PLA. 192
Figure IV.7 – Cryogel characterization: a) shrinkage; b) Specific Surface Area (SSA). 193
Figure IV.8 – SEM images of cryogels samples in cross-section direction. 195
Figure IV.9 – Compressive resistance of cryogels samples in 50% HR, 23°C monitored room. 197
Figure IV.10 – Changes in contact angle and volume of water during 30 seconds and pictures of water droplets and their respective contact angle after 5 seconds. 198
Figure IV.11– Water resistance of cryogels after 24 hours. a) Cryogels without thermal treatment; b) cryogels thermal treated at 180°C. 199

ABBREVIATIONS

Chemicals and Materials

CNC	Cellulose Nanocrystals
CNF	Cellulose Nanofibers
DCP	Dicumyl peroxide
GMA	Glycidyl Methacrylate
PEI	Polyethyleneimine
PLA	Poly(lactic acid)
PLA-NE	Poly(lactic acid) nanoemulsion
THF	Tetrahydrofuran
AGU	Anhydroglucose unit

Methods

BET	Brunauer-Emmett-Teller
CI	Crystallinity Index
DLS	Dynamic light scattering
DSC	Differential scanning calorimetry
FTIR	Fourier transform infrared spectroscopy
G'	Storage modulus
G''	Loss modulus
LCB	Long chain branches
MP-SPR	Multi-Parameter Surface Plasmon Resonance
N_1	First normal stress difference
NMR	Nuclear Magnetic Resonance
n-OI	n-Octadecyl isocyanate
phr	Per hundred of resin
Sc-CO_2	Supercritical CO_2
SEC	Size Exclusion Chromatography
SEM	Scanning Electron Microscopy
SSA	Surface Specific Area
TEM	Transmission electron microscopy

VER	Volume expansion ratio
vGP	van Gurp-Palmen
XPS	X-ray photoelectron spectroscopy
XRD	X-ray diffraction
ω	Angular frequency
η^*	Complex viscosity
η_0	Apparent zero shear viscosity
η_e	Extensional viscosity

General Introduction

GENERAL INTRODUCTION

Polymeric materials have been an instrument of growth and development in society for over 70 years and have gained prominence for being light, cheap, durable, and suitable for both consumer and industrial purposes. Since the end of the 20th century, the low cost of this material has led to growth in its market, but it has also accelerated the culture of disposal and single use of these products [1].

Since then, the use of plastic products has grown every year. In 2019, the world produced around 460 million tons of plastics [2], two-thirds of which are destined for short life-cycle products, which quickly become waste. This has led to significant impacts on the environment, health and the economy [3].

Within the class of polymeric materials, foams have been used for years in various applications. However, these materials produced from fossil-based polymers present some post-consumer challenges, such as incorrect waste disposal and low recyclability rates [4].

In Brazil, for example, it has been identified that the factors that most hinder the recycling of expanded polystyrene (EPS) are logistical (distance between cooperatives and recycling centers) and economic [5].

In this way, difficulties in management can lead to the accumulation of this waste in the environment, which results in continuous degradation of the material due to external factors. This degradation generates small particles currently known as microplastics [6], which can be classified into [7]:

(i) nanoplastics: 1 to <1000 nm (to comply with existing definitions of nanomaterials, a subdivision into nanoplastics (1 to <100 nm) and submicroplastics (100 to <1000 nm) can be made);
(ii) microplastics: 1 to <1000 µm;
(iii) mesoplastics: 1 to <10 mm;
(iv) macroplastics: 1 cm or more.

For this reason, considering the depletion of non-renewable resources and the negative externalities associated with the post-consumption of petrochemical polymeric materials, especially those that present challenges in their management, the development and study of alternative materials becomes a promising opportunity. In this context, biobased and biodegradable/compostable polymers are materials produced from renewable resources that biodegrade in the environment or under composting conditions.

Poly(lactic acid) (PLA) is a polymer from a renewable source, biodegradable under composting conditions and biocompatible, produced on a large scale and in various grades. For this reason, PLA is an alternative for the production of polymeric foams. However, it has low resistance in the molten state, an essential requirement for the production of foams with controlled and homogeneous cell structures. Therefore, strategies such as chemical modification of the material or the introduction of nanoparticles can be adopted to increase the material's melt strength.

Among the various reinforcement options for producing nanocomposites, cellulose, considered to be the most abundant polymer on the planet, can currently be used in various ways due to its hierarchical organization. One of these well-established forms is cellulose nanocrystals (CNC), which can alter the rheological properties of the material. Therefore, studying the introduction of CNC into the PLA matrix becomes a potential strategy for understanding the final properties of the material and its respective cellular structures obtained by foaming the PLA/CNC nanocomposite.

Furthermore, since cellulose is the most abundant polymer on the planet, obtained from renewable sources, biodegradable and biocompatible, the production of materials in which cellulose is the main compound could also be an alternative to the problems above mentioned. However, cellulose cannot be melted, which prevents the production of foam using conventional method employed for polymeric foams in the molten state.

As an alternative, the freeze-drying method allows the production of a cellulose-based porous material, which is called cryogel. Cryogels produced from nanofibrillated cellulose have the disadvantage of having low resistance in the

presence of water, which leads to the possibility of further studies to remedy this challenge.

Therefore, two methods were used to explore the production of biobased foams: foaming using supercritical CO_2 and lyophilization.

For the supercritical CO_2 method, two strategies were used. The first was the adjustment of PLA properties through chemical modification by reactive processing, in which the aim was to verify if it would be possible to foam PLA just by modifying its chemical structure, without the addition of nucleating agents. The second strategy was to foam the PLA/CNC nanocomposite, intending to check whether the introduction of CNC, pure or modified, would result in smaller and more homogeneous cell structures. Finally, a cellulose matrix cryogel was produced using the freeze-drying method and incorporated with PLA nanoparticles in order to increase the hydrophobic character of the material.

Figure 1 shows a representative diagram of the strategies used to carry out the research.

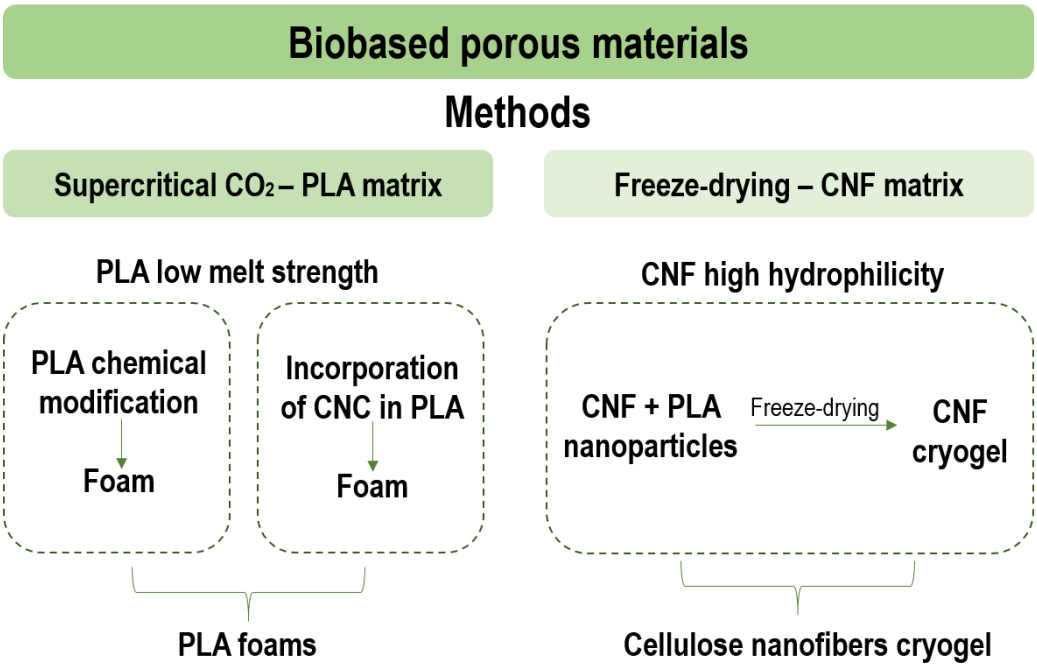

Figure 1 - Representation of the strategies used to produce PLA foams and CNF cryogels.

Therefore, the general objective of this doctoral thesis was to study the influence of chemical modification, by reactive processing, and the introduction of cellulose nanocrystals (CNC) on the properties of poly(lactic acid) (PLA) with a view to producing foams using supercritical CO_2 as a foaming agent. In parallel, the study also aimed to produce cellulose-based porous materials with an improved hydrophobic character, without the use of chemical modifications.

In this way, the thesis aimed to meet the following specific objectives:

- Evaluate the influence of different concentrations of reagents during the chemical modification of PLA on the chemical structures formed and the resulting properties;
- Chemically modify the cellulose nanocrystals to increase the surface hydrophobic character and improve their compatibility with the PLA matrix;
- Investigate the influence of properties obtained by PLA chemical modification and PLA/CNC nanocomposite on the final cellular structures of their foams;
- Propose a method for increasing the hydrophobic character of CNF cryogels without the need for chemical modifications.

In order to achieve the proposed objectives, the collaboration between Biodegradable Polymers Laboratory at UFSCar (Brazil) and the Laboratory of Pulp and Paper Science and Graphic Arts (France) was essential to achieve the results developed during 4 years of joint PhD. This thesis is organized into 4 chapters, based on scientific papers, as explained below.

Chapter I presents a fundamental background of the main topics covered in the thesis. This chapter will present the main mechanisms of how the foaming process of polymeric materials occurs and the different types of foaming agents that can be used, with special attention to the supercritical CO_2 foaming agent. In addition, the main properties required for the production of polymeric foams will be presented. This will be followed by a brief introduction involving the definitions and use of bioplastics, and a more detailed discussion of the main materials that will be investigated in this work: PLA, nanofibrillated cellulose and cellulose nanocrystals. In this discussion, the main processing challenges faced by these

materials will be presented: the low resistance of PLA in the molten state, the low compatibility of CNC with hydrophobic polymeric matrices and the low resistance to the water of CNF cryogels.

Chapter II will detail the chemical modification of PLA and its subsequent effects on the material's properties and the cellular structures of the resulting foams. A comprehensive description of the chemical modification procedure will be provided, including proposed reaction mechanisms for the various reagent concentrations used, as well as the characterization of these formulations. The rheological properties of the modified PLA will be analyzed to elucidate the chemical structures formed, which will have a direct impact on the foam morphology.

Chapter III explores the strategy of incorporating cellulose nanocrystals (CNCs) into the PLA matrix to tailor its properties for foam production. Part of the chapter will be dedicated to the mechanochemical process of modifying and characterizing the CNCs, comparing the modified and unmodified materials. Additionally, the chapter will cover the production and characterization of nanocomposites. Finally, the foams and their respective cell structures will be presented, with a focus on correlating these structures to the properties of the nanocomposites.

Finally, **Chapter IV** presents an alternative strategy for producing porous materials within a nanofibrillated cellulose (NFC) matrix. A significant challenge in creating cellulose-based materials is their inherent high hydrophilicity, typically addressed through chemical modifications or surface treatments. As a non-chemical alternative, this chapter outlines the production of a cryogel derived from CNF integrated with PLA nanoparticles and subjected to thermal treatment, aimed at enhancing the cryogel's hydrophobicity without the need for chemical modifications.

Therefore, the findings of this research are expected to enhance the understanding of the relationship between the properties of PLA and their foams, as well as to introduce new methods for optimizing the performance of CNF-based cryogels. These insights can serve as a foundation for the study and development of materials across various applications.

Figure 2 shows a summary of the organization of this thesis.

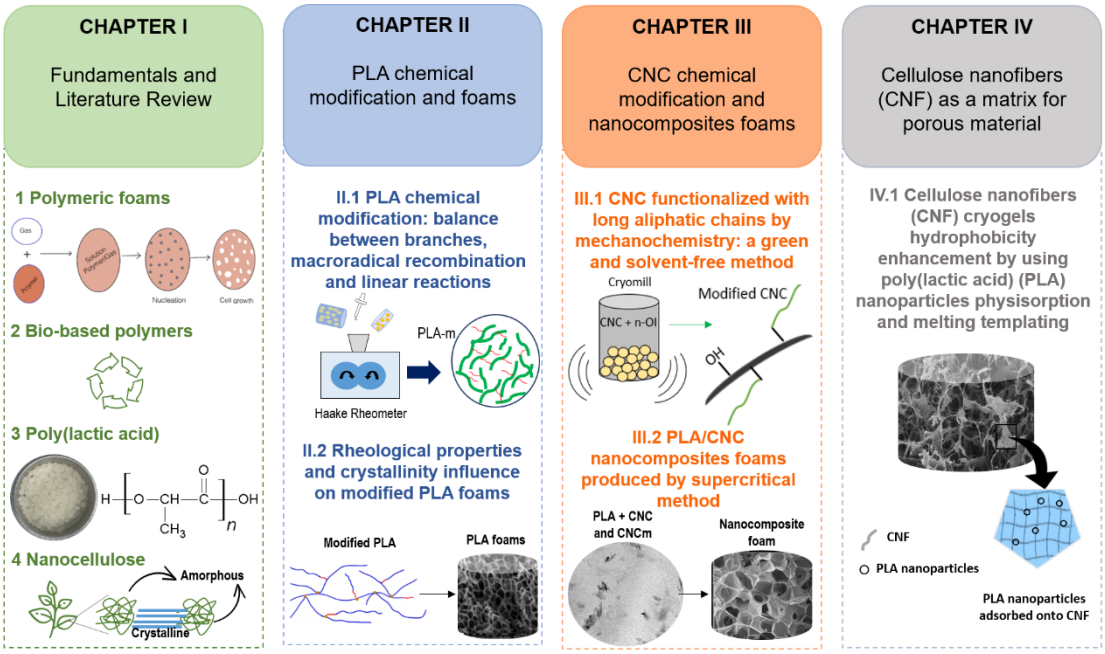

Figure 2 - Representation of the organization of the thesis into chapters and the respective subjects that will be covered.

Chapter I

Fundamentals and Literature Review

CHAPTER I - FUNDAMENTALS AND LITERATURE REVIEW

Introduction to Chapter I

Chapter I aims to provide a comprehensive background to the main topics covered in this doctoral thesis. The section entitled **"Polymeric Foams"** is intended to present definitions, mechanisms, process parameters, and desirable properties for producing polymeric foams, emphasizing PLA foams and PLA-based nanocomposites foams.

The **"Biobased Polymers Contextualization"** section will define and differentiate terms that are often used generically or incorrectly, as well as discuss the main applications and materials defined as bioplastics.

Considering that one of the focuses of this research is the study of biobased materials, the section **"Poly(lactic acid)"** will provide an overview of the world's most widely produced bioplastic. The molecular structure of PLA, synthesis routes and its main applications will be discussed. The fundamental properties of the material and its limitations will be analyzed, along with potential strategies for improving some of its characteristics. Given that one of the alternatives for adjusting PLA's properties involves the inclusion of cellulose nanoparticles, the fourth section will cover the theoretical background of this natural polymer.

Therefore, in **"Nanocellulose,"** the structure and main properties associated with this material will be explored, as well as its hierarchical organization, which makes it possible to obtain cellulose nanofibers and cellulose nanocrystals. The differences between these types of nanocellulose will be discussed, as well as their main applications, whether as reinforcing agents or as a matrix for producing porous materials.

1 Polymeric Foams: context, history and definitions

According to the International Union of Pure and Applied Chemistry (IUPAC) [8] foams are defined as "A dispersion in which a large proportion of gas by volume in the form of gas bubbles, is dispersed in a liquid, solid or gel. The diameter of the bubbles is usually larger than 1 μm, but the thickness of the lamellae between the bubbles is often in the usual colloidal size range".

Polymeric foams are formed when gas bubbles are embedded within a polymer matrix. As defined by ASTM D883-24 [9], the terms "cellular plastic," "expanded plastic," and "foamed plastic" are synonymous with "plastic foam," which, in this study, will be referred to as "polymeric foam." According to the standard's definition, polymeric foams are plastics containing intentionally introduced cells, which may be either interconnected or isolated.

The development of microcellular polymeric foams dates back to the 1930s, marked by the production of polystyrene (PS) foams with cell sizes exceeding 100 μm [10]. Subsequent research efforts concentrated on generating foams with progressively smaller cells, culminating in the development of the batch foaming process in 1980, which enabled the production of foams with cell sizes below 100 μm. Since then, the production of foams has been extensively leveraged to create materials with tailored properties for various applications, including packaging, automotive, and biomedical sectors, as illustrated by Figure I.1 [11–14].

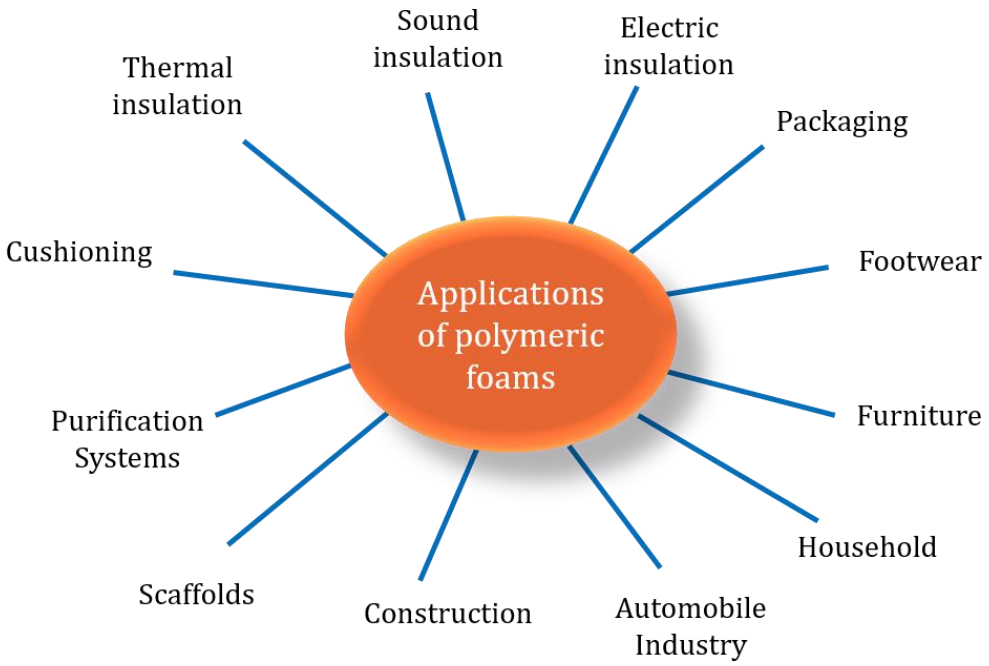

Figure I.1 – Main applications of polymeric foams.

Polymeric foams are of particular interest due to their low density, which results in reduced material usage, along with other significant properties as outlined in Table I.1:

Table I.1 - Main advantages and drawbacks of polymeric foams compared to solid materials [11,15,16].

Advantages	**Drawbacks**
Low cost (reduced amount of material)	Low adhesion to recycling
Low density	High flammability
High protective effect in packaging	Low fracture resistance for rigid foams (PU, PVC, among others)
High thermal insulation	
High sound insulation	
High specific strength	
Mechanical stability	

To gain a deeper understanding of these diverse applications, it is crucial to explore the various classifications of polymeric foams, which can be categorized by type, nature, density, and other pertinent characteristics. Figure I.2 summarizes the most common classifications of polymeric foams [10,15,17–20].

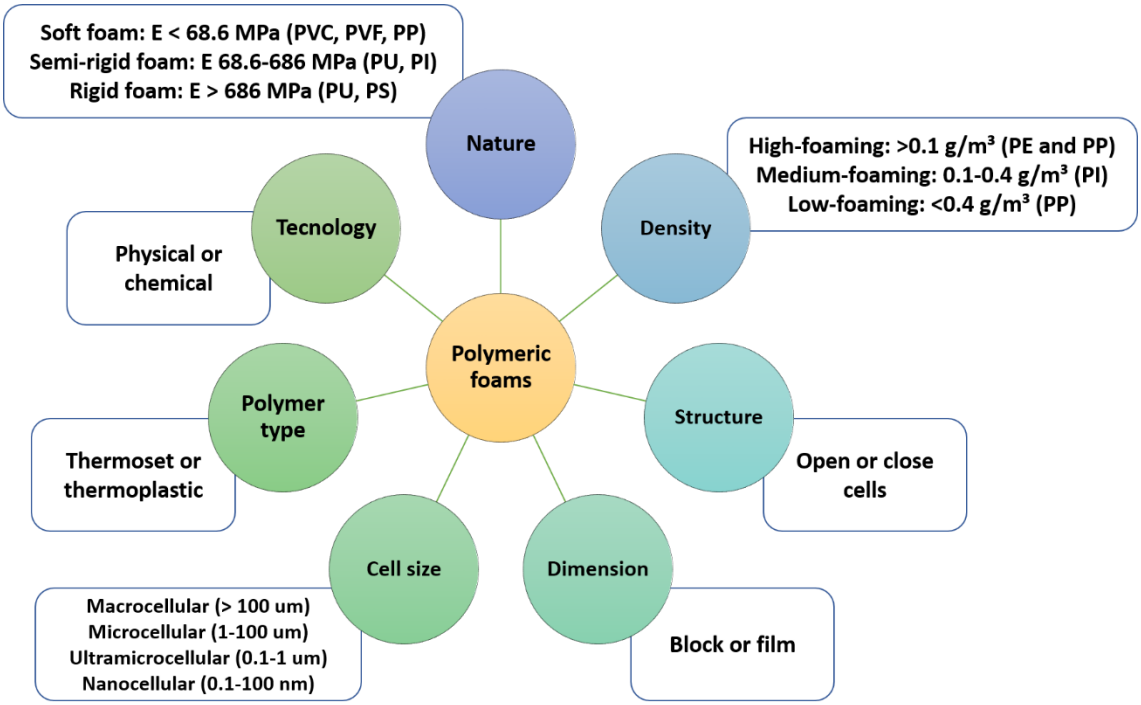

Figure I.2- Classification of Polymeric Foams.

Thermoplastic polymers, which are the focus of this study, can be used in foam production and are broadly categorized into two main groups: homopolymers and multiphase polymers. Each of these groups encompasses several subcategories, as depicted in Figure I.3.

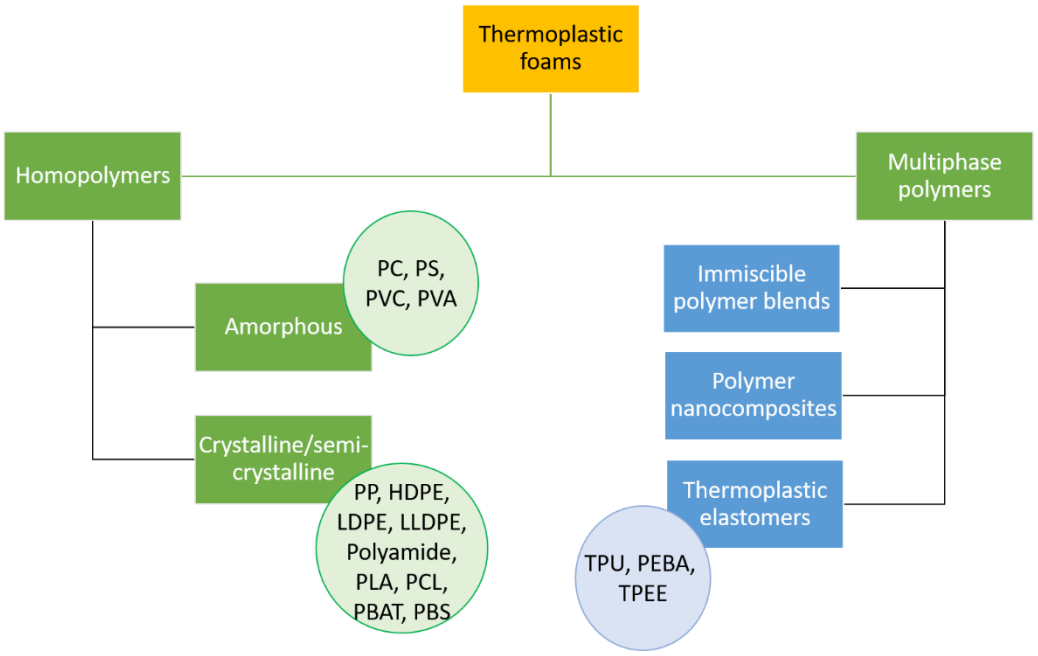

Figure I.3 - Most commonly used thermoplastic polymers to produce foams and their classifications [12].

1.1 Polymer foaming

1.1.1 Blowing agents

The polymer foaming process can be described in three primary stages: cell formation, growth, and stabilization. To achieve material expansion, the use of blowing agents is essential. These agents enable the formation of a cellular structure within the polymer matrix. Depending on the method of gas generation during the foaming process, these agents can be classified as either chemical or physical [15,18].

Chemical blowing agents are compounds that release gas under the processing conditions of polymer foams, either through thermal decomposition or chemical reactions. The decomposition of the original molecule of the blowing agent results in gases that facilitate the expansion of the material and may generate some residues that remain in the expanded polymer. These chemical agents can be categorized as exothermic or endothermic. Exothermic agents produce heat during decomposition, with azodicarbonamide (ADC) being the most commonly used exothermic chemical blowing agent [21]. The

decomposition of ADC generates a mixture of gases, including cyanic acid, ammonia, carbon monoxide, and nitrogen, as well as solid residues such as urazole and hydrazodicarbinamide [22], as shown in Figure I.4.

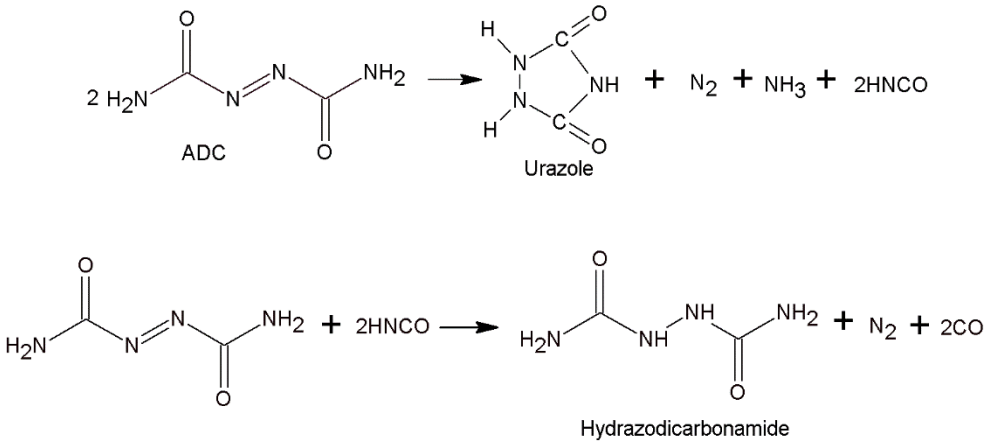

Figure I.4 – Typical decomposition process of ADC. Adapted from [22].

The endotherms, on the other hand, absorb heat during decomposition, with sodium bicarbonate being the most used [23]. Figure I.5 illustrates the decomposition reaction of sodium bicarbonate when exposed to heat.

$$2NaHCO_3 \longrightarrow Na_2CO_3 + H_2O + CO_2$$

Figure I.5 – Decomposition of sodium bicarbonate when thermally exposed. Adapted from [22].

Physical blowing agents provide the gas required to expand the polymer by altering its physical state, which may involve the volatilization of a liquid or the depressurization of a compressed gas incorporated into the polymer [18]. Common physical agents include nitrogen (N_2), carbon dioxide (CO_2), air, water, pentane, hexane, and dichloroethane, among others [15].

With growing environmental concerns, the use of physical blowing agents in the supercritical state is particularly attractive due to its clean technique. This

technique enables the production of microcellular foams with higher cell density, smaller cell sizes, and greater compressive strength than those produced using chemical agents [24].

Pure substances can undergo phase transitions between gas, liquid, and solid states, depending on the temperature and pressure applied. The liquid-gas interface ceases to exist at a specific pressure and temperature, marking the substance's supercritical point [11]. A substance is considered to be in a supercritical fluid state when the temperature and pressure exceed its critical values [25]. Under these conditions, the substance exhibits a hybrid gas-liquid behavior, characterized by diffusivity values similar to those of the gas phase and solvent properties as those in the liquid phase. Figure I.6 presents a general scheme of a phase diagram, highlighting the region where materials are in the supercritical state [11].

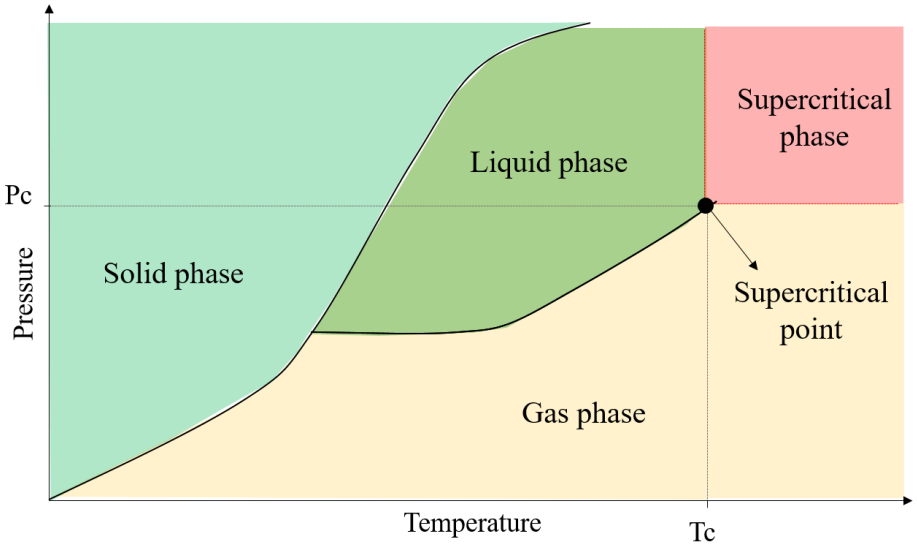

Figure I.6 - Typical phase diagram illustrating the possible physical states of substances under different temperatures and pressures. The critical point is reached at specific critical temperature and pressure values (Tc and Pc, respectively).

Carbon dioxide (CO_2) has been the most widely used gas as a supercritical fluid, owing to its advantageous properties such as non-toxicity, low flammability, and cost-effectiveness. Another significant benefit is that the critical points of CO_2

are easily attainable, with a critical pressure (Pc) of approximately 7.3 MPa and a critical temperature (Tc) of around 31ºC, enabling processing at room temperature and,thereby preventing the thermal degradation of other compounds [26,27]. These benefits have led to the widespread adoption of supercritical CO_2 (sc-CO_2) in polymer process, with its application in foam production being particularly prominent [28].

Supercritical nitrogen can also be employed as a physical blowing agent [29–31]. However, as noted by Farhanmoghaddam [30], its use is less common due to its lower solubility in polymers compared to sc-CO_2, which results in a relatively high consumption of N_2.

1.1.2 Principle of foaming

The foaming process can be briefly described as the generation and stabilization of bubbles within a polymer matrix. According to Lee and Ramesh [20], this process involves three primary stages: gas introduction, expansion, and polymer stabilization. Similarly, Lee and Park [18] outline the foaming process as consisting of nucleation, bubble growth, and bubble stabilization. Banerjee and Ray [12] further elaborate by adding the dissolution of the gas into the polymer as the initial stage, as illustrated in Figure I.7.

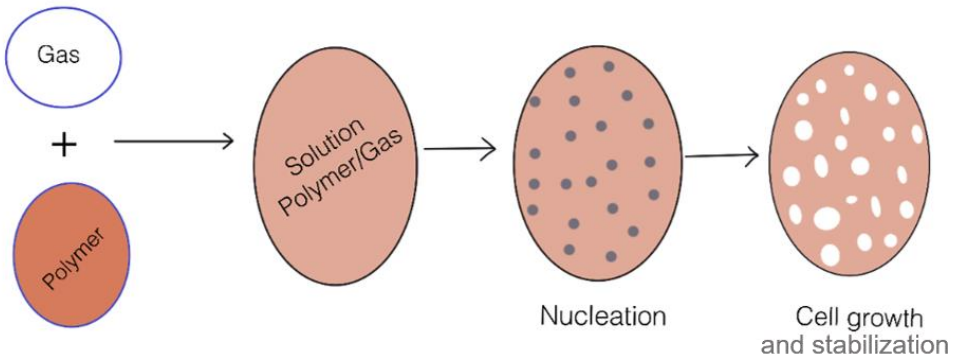

Figure I.7 – Main steps of foaming processing. Adapted from [12].

In the first stage, the gas is dissolved into the polymer matrix until saturation is achieved at a specific temperature and pressure, which must be above the gas critical point [12]. According to Gendron [32], ensuring the

complete dissolution of the physical blowing agent within the polymer matrix is crucial to producing a foam with a fine and uniform cell structure. Incomplete dissolution can lead to significant heterogeneity in the porous structures, resulting in surface defects in the material. Additionally, CO_2 can act as a lubricant in the polymer matrix, potentially altering its thermal and rheological properties [28].

In the subsequent stage, the system is brought to a supersaturated (and unstable) state, typically achieved through a change in pressure or temperature [12]. Due to the induced thermodynamic instability, the system naturally seeks to stabilize by phase separation between the gas and the molten polymer, aiming to minimize the system's free energy. This process leads to the formation of microcells, which is the beginning of nucleation [33,34]. Nucleation, therefore, refers to the formation of a new phase within the bulk material [18] , and in the foaming process, it specifically refers to the emergence of small bubbles within the polymeric system [20].

Nucleation can be classified as homogeneous or heterogeneous. In homogeneous nucleation, bubbles are generated from a single phase without second phase. In contrast, heterogeneous nucleation occurs in the presence of particles within the fluid, such as nucleating agents, crystals, or fillers, which facilitate cell formation by promoting nucleation at the solid-liquid interface [18,20].

Following nucleation, cell growth occurs due to the diffusion of excess gas within the polymer. This growth is influenced by several factors, including the polymer's viscosity, gas concentration, foaming process temperature, and, in certain cases, the quantity and nature of the nucleating agent [20]. The cells expand at a specific rate until they reach a sufficient size, leading to an increase in the overall volume of the material. The material is then cooled to preserve the generated cell structure [35].

Cooling solidifies the foam surface, increasing its resistance to further growth. Gas molecules near the surface may escape instead of contributing to additional cell growth. These factors collectively lead to the cessation of cell growth over time. The solidification of the molten or softened polymer enhances the material's strength, stabilizing the cell structure. After solidification, gas

exchange with atmospheric air occurs through diffusion. This mutual diffusion continues until the air completely replaces the gas within the cells. This final process, known as cell stabilization, marks the conclusion of the material expansion process [12].

1.1.3 Methods for foams production

The primary methods for producing thermoplastic polymeric foams include extrusion foaming, injection molding foaming, bead foaming, rotational molding foaming, compression molding foaming, oven heat foaming, and coextrusion foaming [12,36]. Among these, the main techniques utilizing supercritical CO_2 are batch foaming, extrusion foaming, and injection molding foaming. Table I.2 presents the key characteristics of these supercritical fluid foaming processes.

Table I.2 - Key characteristics of foam production processes using supercritical fluids. Adapted from [11,15].

Batch foaming	Extrusion foaming	Injection foaming
Necessary small amount of material (in g)	Necessary large amount of materials (in kg)	Necessary large amount of materials (in kg)
Yields uniform cell sizes and controlled cell shapes	Different cell sizes in the core and at the edges can happen	Difficult to obtain foam with uniform cells
Cell density 10^6-10^{16} cells/cm³	Cell density 10^4-10^{13} cells/cm³	Cell density 10^4-10^6 cells/cm³
Cheaper than the others	Expensive depending on machine capacity	Expensive depending on machine capacity and mold
Limited suitability for continuous production and commercial application	Continuous production, high output	It presents high mechanical costs compared to extrusion foaming.
	It can produce unrestricted product length.	Well-suited for the production of small and intricate parts in the industrial sector.

Although the batch process has the disadvantage of not being scalable for industrial production, it is crucial for the study and understanding of cellular structures. The batch process for producing microcellular materials was pioneered in the 1980s at the Massachusetts Institute of Technology, where the production of polystyrene foam in an autoclave using nitrogen as a blowing agent was patented [37,38].

This discontinuous process is typically conducted in an autoclave, where the sample is saturated at a specific pressure for a set period, and expansion is achieved by inducing thermodynamic instability in the system. Since the solubility of pressurized gases in polymers increases with pressure but decreases with temperature, thermodynamic instability can be induced either by an abrupt pressure drop or by a rise in temperature [37].

In temperature-induced foaming, the polymer sample is saturated at low temperatures and then transferred to a hot liquid (such as water, glycerin, or oil) heated above the polymer glass transition temperature (Tg). Under these conditions, the polymer chains gain mobility while the gas solubility decreases, leading to cell nucleation and growth, and consequently, the material expands [12]. Figure I.8 illustrates the process of temperature-induced foaming.

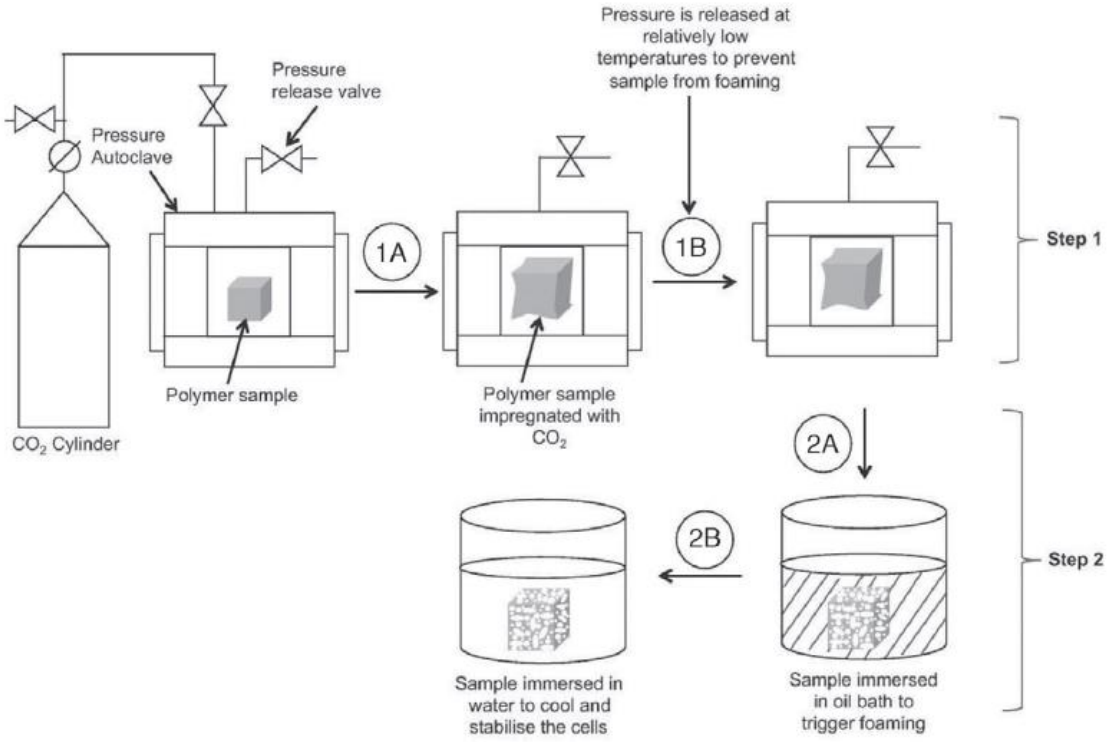

Figure I.8 - Two-stage, temperature-induced foaming process. Extracted from [12].

In the pressure-induced foaming method, the sample is placed in a high-pressure chamber, and expansion occurs due to the thermodynamic instability triggered by rapid depressurization. In this case, the polymer heated above its Tg becomes rapidly supersaturated, making it difficult for the polymer mass to retain the gas. This, in turn, induces phase separation, giving rise to cell nucleation and growth [39,40]. Figure I.9 illustrates the pressure-induced foaming process.

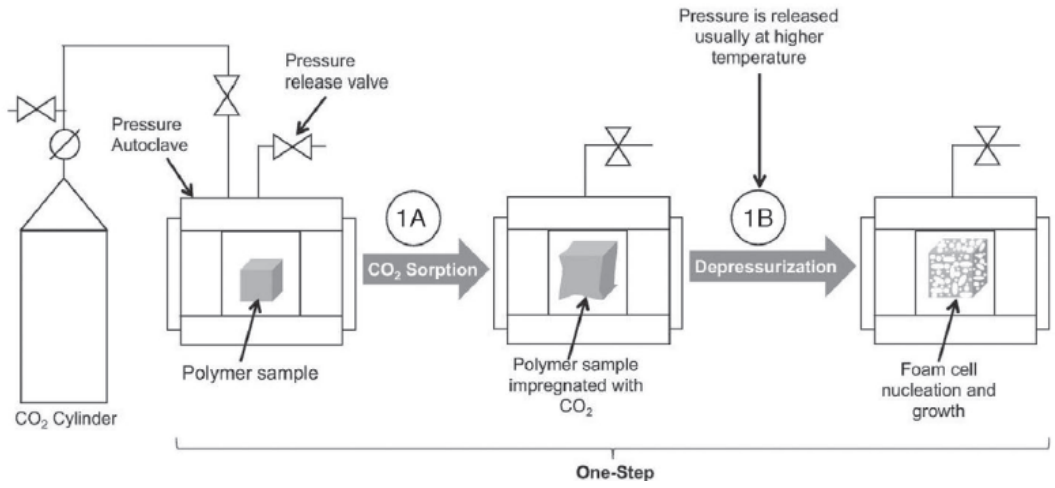

Figure I.9 - One-step foaming process induced by a pressure decrease. Extracted from [12].

It is important to note that in this method, the saturation and foaming temperatures can either be the same or different. When using the same temperature for both stages, it must be between the material's Tg and Tm. Gas saturation at temperatures equal to or above Tm requires a temperature reduction during foaming, as the material's viscosity is significantly low above Tm, which hinders foamability [41].

Thus, different foaming methods can produce varying characteristics that directly influence properties and quality of foams, such as cell density (number of cells per unit volume) [42], expansion ratio (ratio between non-foamed and foamed material density), cell size distribution, open cell content (porosity)) [43,44], and dimensional stability [12]. Additionally, several other factors can affect the final morphology of the material, as will be discussed below.

1.2 Factors influencing the foaming process using supercritical CO_2 as a blowing agent

Process parameters such as temperature, pressure, CO_2 concentration, and gas saturation time are crucial factors that significantly impact the

morphology of the cells. Additionally, the choice of blowing agent, modifications to the polymer matrix, and the inclusion of additives and fillers will also influence the final properties of the foams [11]. Figure I.10 summarizes the main characteristics of the materials that will influence polymer foaming.

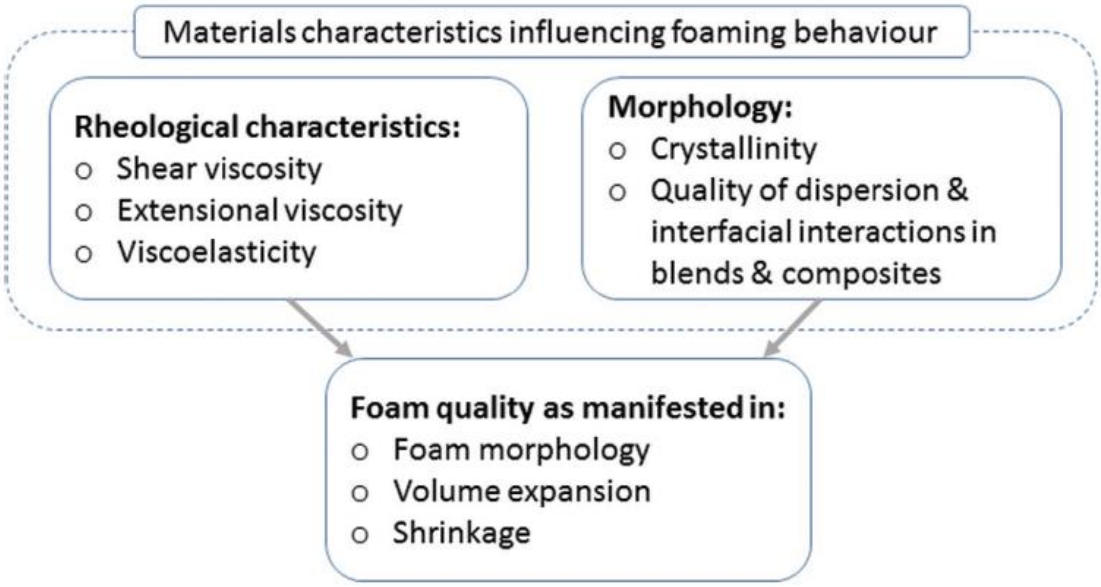

Figure I.10 - Main factors influencing the foaming ability of polymers [12].

As noted by Banerjee and Ray [12], the foamability of polymers is primarily governed by their rheological and morphological characteristics, processing conditions, and the type of blowing agent used.

1.2.1 Rheological characteristics

Extensional viscosity plays a critical role in the foamability of polymers. It is defined as the ratio between stress and strain rate during extensional deformation and is influenced by factors such as time, temperature, and strain rate. This property is essential for the foaming process since the deformation of the polymer occurs in extension. There are three types of extensional flow: uniaxial, planar, and biaxial, with biaxial flow being the primary deformation mode during foaming. Extensional viscosity can be measured through extensional deformation at a constant rate, where the resulting stress is observed [18].

Elasticity of the polymer melt is another crucial characteristic, particularly in the stabilization of growing bubbles during the foaming process. High first normal stress difference values during bubble growth are important to avoid cell coalescence [18]. However, elasticity is typically measured by the storage modulus (G') in shear, while the deformation during foaming processing is in extension. In this way, elasticity can be indirectly used to compare different behaviors. For instance, an increase in G' after chemical modification may suggest an increase in extensional viscosity. Castellón et al. [45] have noted that polymers with higher molar mass and higher complex viscosity at zero shear rates generally exhibit greater elasticity in the melt, which may also imply greater extensional viscosity.

Polymers with branched structures, like low-density polyethylene, exhibit a behavior known as strain hardening—a significant increase in viscosity with time and strain rate during extension. This property is crucial for stabilizing processes that involve primarily extensional deformations, such as blow molding, tubular film production, and foaming [46]. Figure I.11 illustrates the general behavior of polymers that exhibit strain hardening when analyzed by fixing different strain rates for the same sample.

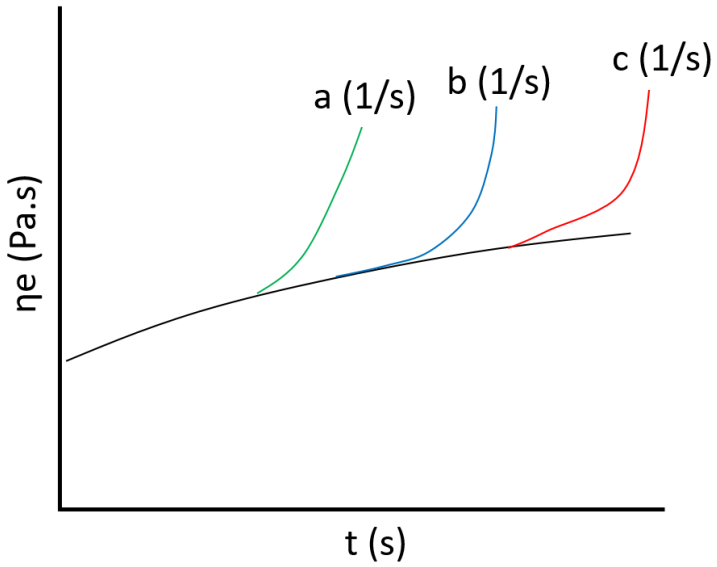

Figure I.11 – Representation of strain-hardening curves for the same sample at different strain rates, where a>b>c are different strain rates.

Strain hardening, commonly observed in branched polymers, is crucial in the formation of polymeric foams due to its self-healing mechanism. In materials with heterogeneity, such as regions of varying thickness, strain hardening leads to an increase in extensional viscosity and, consequently, material strength. This enhancement reduces the likelihood of cell wall rupture, resulting in more uniform cell sizes and a more homogeneous cell structure. This effect is attributed to the increased entanglement of macromolecules during extended deformation, which results in higher relaxation times. Therefore, rheological characteristics under extensional flow are essential for predicting the processability of the material during foaming [18,39].

1.2.2 Crystallinity

Another critical characteristic of materials is their crystallinity, which can significantly impact the rheological properties of polymers. Liu and coauthors [47] observed an increase in the elasticity of PLLA/PDLA blends compared to pure PLLA, attributing this enhancement to the presence of stereocomplex crystals in the polymer matrix. These stereocomplex crystals induced a high level of crosslinking between the chains. Additionally, the tan δ values were lower than those for the pure material, indicating an increase in the melt elasticity.

In general, amorphous materials tend to present a greater ability to foam compared to semicrystalline polymers [12]. This is because, during the saturation stage, the dissolution of CO_2 in the polymer matrix occurs mainly in the amorphous regions, and foaming will only occur where CO_2 is dissolved [48].

Thus, depending on the temperature at which CO_2 saturation is carried out, crystals may or may not be present in the PLA matrix. The presence of crystalline structures and the resulting reduction in the amorphous region lead to a lower concentration of dissolved CO_2, meaning that less gas will be available to enable the material expansion [49]. Additionally, the crystals act as barriers during saturation, which the gas molecules must overcome, potentially leading to gas escape and consequently reducing its availability in the system and the material’s ability to expand [48]. Besides influencing gas dissolution, the

presence or absence of crystals can make bubble nucleation either heterogeneous or homogeneous, as discussed by Liu and coauthors [47].

1.2.3 Blowing agents

For the foaming process to be successful, the gas must be efficiently dissolved, meaning the chosen gas must be highly soluble and distributed throughout the polymer matrix. Additionally, the dissolved gas imparts a lubricant effect, which decreases the material viscosity. This reduction in viscosity is a crucial factor, as the material viscosity plays a significant role in the foaming process [20].

1.2.4 Processing conditions

The conditions for batch processing include saturation temperature and time, foaming temperature, and pressure. Each of these conditions affects the gas solubility in the matrix, as well as the material rheology and crystallinity.

1.2.4.1 Influence of Pressure, Temperature, and Time on Gas Solubility During CO_2 Saturation

The time of gas saturation is crucial for ensuring that CO_2 is dissolved in substantial quantities within the polymer matrix. According to Li and collaborators [50], gas sorption in the polymer matrix increases until it reaches saturation, after which it stabilizes. In tests conducted on PLA, the saturation time was found to be 50 minutes across all temperatures studied. However, increasing the temperature from 125 to 143°C led to higher gas sorption, attributed to the reduction in crystalline content at higher temperatures, facilitating gas absorption. It is important to note that while increased temperature can enhance gas dissolution by reducing crystal content, it may also promote gas escape, thereby influencing the outcome in various ways.

Regarding pressure, Wang and collaborators [49] investigated CO_2 solubility in the PLA matrix and observed an increase in solubility with high pressure. This is because elevated pressure enhances the density of CO_2, leading to a greater concentration of CO_2 molecules within the polymer matrix. Conversely, CO_2 solubility decreased almost linearly with increasing temperature, consistent with Henry's Law. The temperature rise softens the PLA chains, increasing the free volume of the mixture and thereby facilitating the escape of gas, resulting in lower gas concentration available for solubilization [49].

Additionally, the presence of crystals in the matrix also impacts gas solubility, influenced by the pressure and saturation temperature. Chen and coauthors [51], noted that crystallization during foaming is primarily induced during the saturation phase with sc-CO_2. Thus, the temperature and pressure during saturation will lead to varying outcomes.

1.2.4.2 Effects of foaming temperature

The foaming temperature significantly impacts the final morphologies of foams. At low temperatures, the high melt viscosity results in strong resistance to cell growth, leading to smaller cell sizes and spherical morphologies. At medium temperatures, reduced resistance to cell growth allows for greater cell expansion, resulting in polyhedral morphologies. Conversely, at very high temperatures, the low melt viscosity facilitates the formation of open cell structures [49,52].

Foams with smaller cell sizes generally exhibit a low number of open cell content and tend to have superior mechanical properties, such as compressive strength and elastic modulus, compared to open cell foams. However, open cell foams possess capillaries that enhance fluid absorption properties and contribute to noise attenuation [36]. Figure I.12 illustrates a comparison between open and closed cell structures.

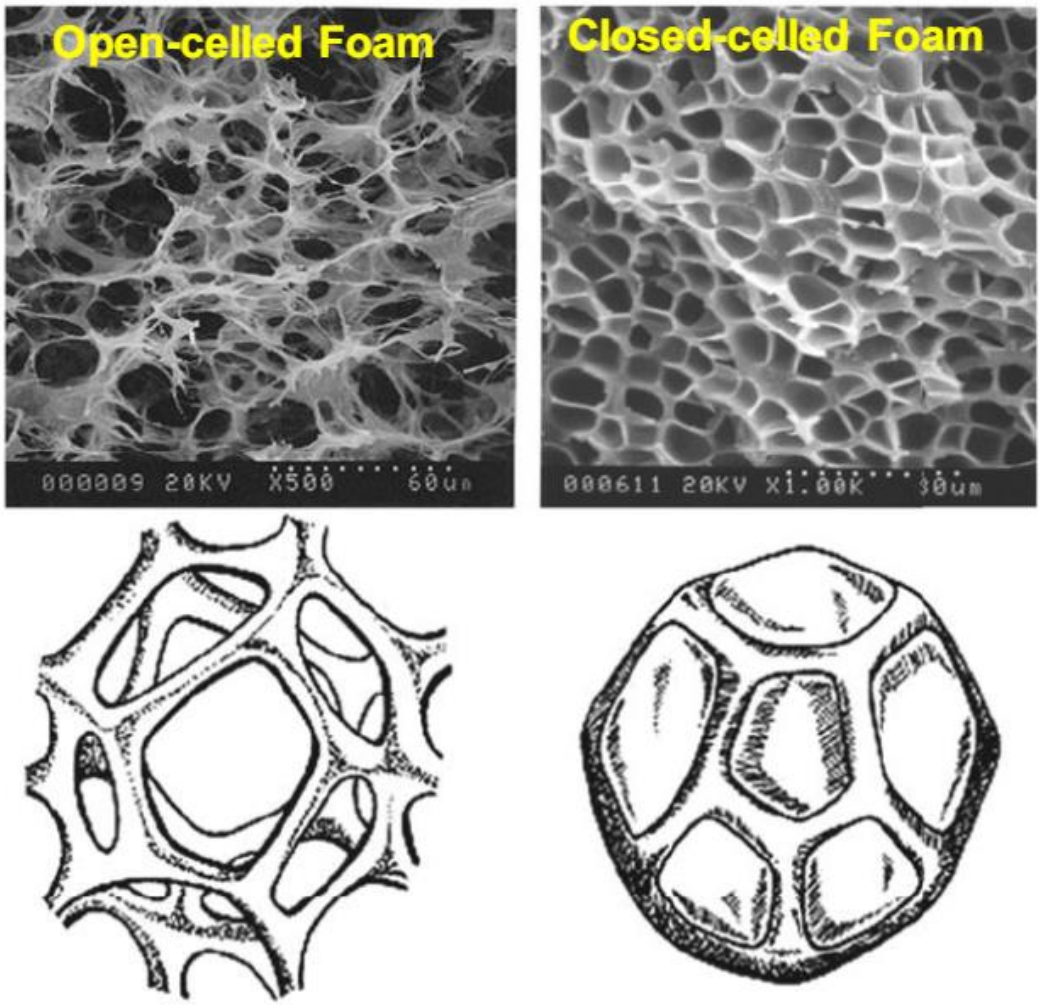

Figure I.12 - Typical SEM images and schematic representation of open and closed cellular structures in foams [53].

Additionally, the lubricant effect of CO_2 can shift the material crystallization temperature, leading to crystallization even at foaming temperatures below the crystallization temperature (Tc). Conversely, at higher foaming temperatures, crystallization can be hindered due to the increased mobility of the polymer chains [49].

Temperature also affects the morphology of the crystals formed. High temperatures, combined with the lubricant effect of CO_2, can result in the formation of less perfect crystals [51].

This variation in crystallization influences cell structures directly. In a study on PLA foaming, samples containing crystals exhibited an average cell diameter

of 1.7 μm and a cell density of approximately 10^{13} cells/cm³, typical of microcellular foams. In contrast, samples without crystals showed cells with an average diameter of 199 μm and a cell density of 10^{8} cells/cm³, indicative of homogeneous cell nucleation. The study concluded that crystals facilitated heterogeneous cell nucleation, thereby enhancing cell nucleation and restricting cell growth. The absence of crystals, on the other hand, led to fewer nucleation sites, allowing the few formed nuclei to grow into larger cells. Additionally, the presence of crystals increased the melt strength of PLA, further limiting cell expansion [41].

Thus, by adjusting the foaming temperature, it is possible to control both the material viscosity and the mode of bubble nucleation, whether heterogeneous in the presence of crystals or homogeneous in their absence.

1.2.4.3 Influence of the presence of fillers in the polymer matrix

Reinforcing agents generally alter both the cell structure and mechanical properties of foams, with each type of filler affecting the material differently based on its characteristics. Adding nanoparticles to the polymer matrix can enhance heterogeneous nucleation during foaming and reduce cell coalescence, leading to more stable growth with higher cell densities and expansion ratios due to increased viscosity [35,54].

Moreover, the compatibility between the filler and the matrix affects the material morphological and rheological properties, impacting foam production [12].

The following sections will explore nanocomposites in more detail.

1.3 Final considerations on polymeric foams

Despite advances in research and technology aimed at producing polymeric foams, achieving small cell structures (smaller than 100 μm), uniform size distribution, and homogeneous cell distribution remains challenging. Various

strategies have been employed to control cell morphology and distribution, including the incorporation of nanoparticles, block copolymers, and chemical modifications [12].

Another significant issue with foams is their reliance on fossil-based polymers and their limited recyclability due to logistical and economic challenges [4]. Consequently, some countries have implemented or are considering to implement legislation to restrict the use of foams in certain applications. By 2019, more than 60 countries had introduced or planned to ban single-use plastics [55]. For instance, expanded polystyrene (EPS) food packaging has been gradually banned in various parts of the United States since 1990 [46]. In Europe, Article 5 of the EU Directive from 2019 prohibits Member States from placing single-use plastics and products made from oxy-degradable plastics on the market. This includes EPS cups, drink containers, lids, and food containers [56].

By 2022, 108 bills were identified at the federal level in Brazil aiming at restricting, regulating, or banning single-use plastics. However, none have been approved. At the state and municipal levels, 25 out of 27 states have regulations for plastic items, including straws, cups, and bags [57]. None of these regulations specifically target foams.

Currently, Brazil is debating a bill that establishes rules for the circular economy of plastics. This bill proposes banning the manufacture, import, distribution, use, and marketing of certain single-use products, such as plates, cups, lids, trays, and bowls made from EPS [58].

It is important to note that the problem of polymeric foams derived from non-renewable sources primarily affects single-use applications and the depletion of fossil resources. Given the extensive application of polymeric foams across various sectors, addressing this issue involves exploring alternatives to conventional polymers. Studies increasingly suggest that biodegradable polymers and those from renewable sources could mitigate plastic pollution and resource depletion. However, these materials present their own processing challenges, underscoring the need for ongoing research in this area [44].

2 Biobased polymers contextualization

Many of the environmental issues currently under debate are linked to conventional polymers - synthetic materials made from fossil sources that are durable and have a low degradation rate - resulting in resource depletion and waste accumulation when not properly managed [59].

Bioplastics have been gaining attention in both academic and industrial fields as an alternative to non-renewable materials. According to the definition provided by European Bioplastics, bioplastics can be categorized as biodegradable, biobased, or both [60]. Figure I.13 illustrates these classifications and the polymers associated with each type of bioplastic.

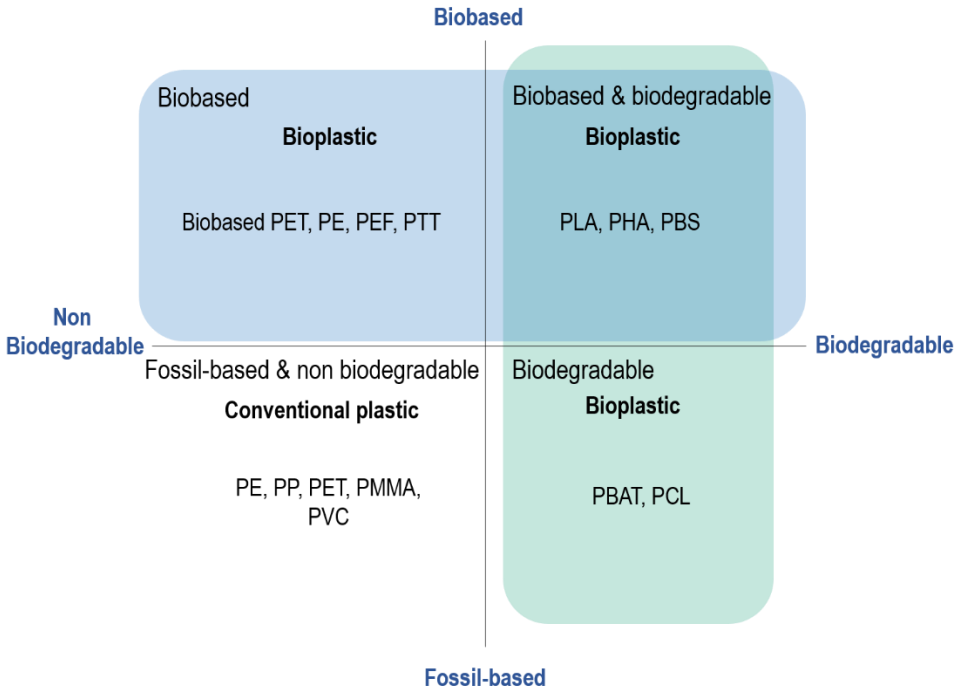

Figure I.13- Classifications of bioplastics. Adapted from [60].

However, the terminology surrounding these materials can be confusing. Biobased polymers are those obtained either fully or partially from renewable carbon sources. They can be natural, such as starch, alginate, cellulose, chitosan, and proteins, or synthetic polymers derived from renewable sources, such as PLA and PHB. Biopolymers, as defined by IUPAC [61], are polymers formed by living organisms (including proteins, nucleic acid and

polysaccharides). Biocompatible polymers are those that are compatible with the human body and its fluids [62]. Biodegradable polymers are susceptible to degradation by biological activity, with the degradation process resulting in a reduction in molar mass [63].

Bioplastics find applications in various sectors, including packaging (both rigid and flexible), consumer goods, electronics, construction, and agriculture [64]. They are also suitable for biomedical applications when they exhibit biocompatibility [65].

Additionally, nanoparticles can be incorporated into bioplastics to enhance their mechanical, thermal, water resistance, barrier, and antimicrobial properties. Various agents, such as clays, carbon nanotubes, cellulose nanofibers, and crystals, can be used for this purpose [66]. Figure I.14 illustrates common nanoparticles used as reinforcements and the properties they can improve upon incorporation.

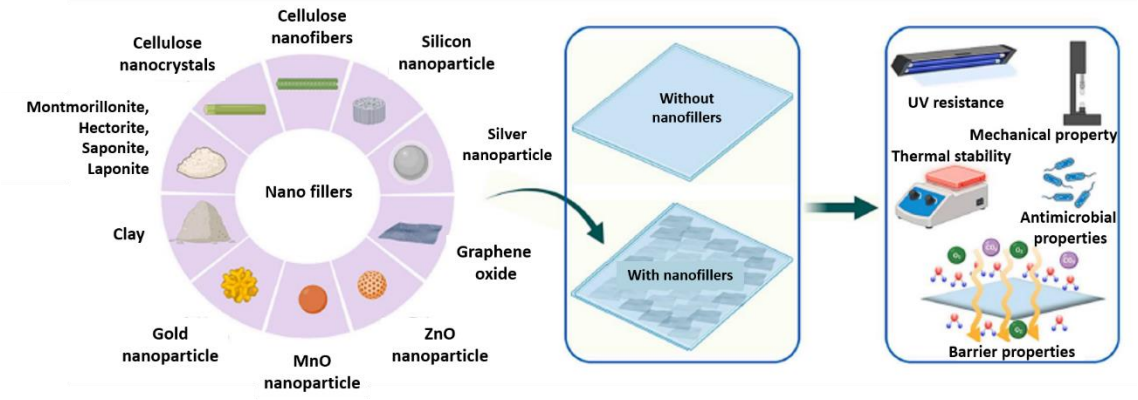

Figure I.14 - Nanoparticles commonly used to improve the properties of bioplastic nanocomposites. Extracted from [66].

Currently, reinforced bioplastics are available in several countries, including Canada, Mexico, Brazil, Italy, Germany, Thailand, Japan, and Australia [66].

Among commercially available bioplastics, PLA (polylactic acid) has the largest global production capacity, as shown in Figure I.15. Additionally, cellulose, a renewable resource and the most abundant polymer on Earth

emerges as a promising alternative to conventional polymers. The combination of PLA and cellulose holds significant potential for developing advanced composites and nanocomposites, which will be explored in the following sections.

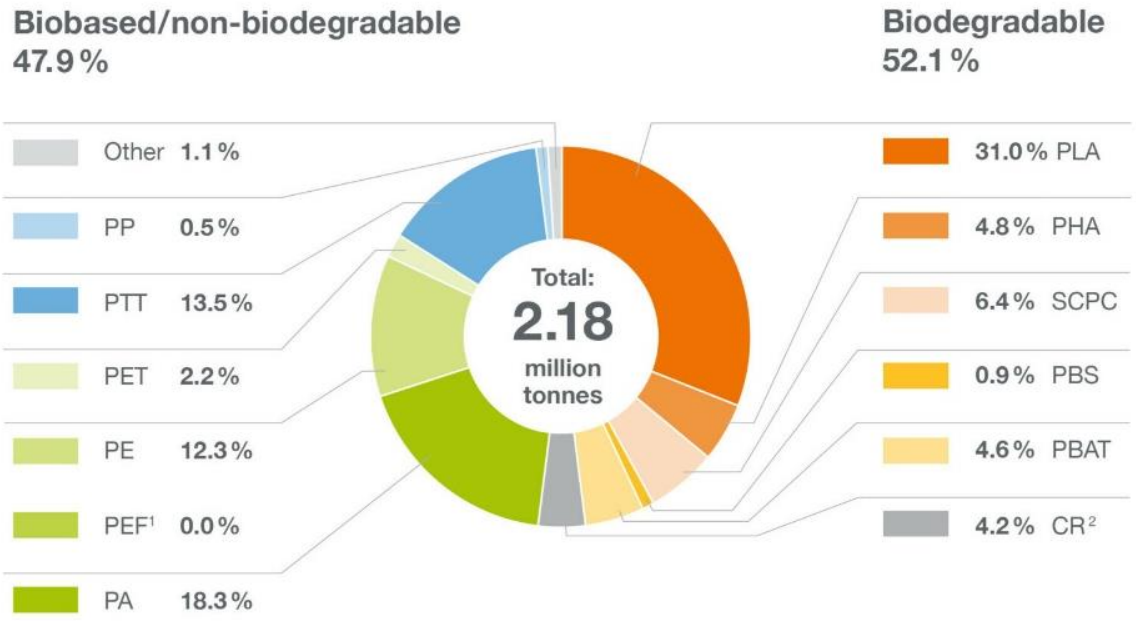

Figure I.15 - Global production capacity of bioplastics in 2023. Extracted from [64].

Therefore, the use of renewable, compostable, and biodegradable polymers as alternatives for applications where the disposal and recyclability of conventional plastics are challenging can help mitigate the negative externalities associated with these materials [67].

Given PLA increasing prominence in industrial-scale production and its properties that are comparable to some conventional polymers, this study will focus on PLA and will discuss it in greater detail in the following sections.

3 Poly(Lactic Acid)

Among the various polymers derived from renewable sources, poly(lactic acid) (PLA), also known as polylactide, stands out for its compostability and biocompatibility. It is produced on a large scale and available in various grades, allowing for diverse processing methods such as extrusion, injection molding, and additive manufacturing [68].

In the early 1930s, Wallace Hume Carothers produced low-molecular-weight PLA for the first time by heating lactic acid under vacuum and removing water through condensation. This process was later patented by DuPont [69].

Today, PLA is produced in significant volumes by various industries, predominantly in Asia, as illustrated in Table I.3.

Table I.3 - List of the largest PLA producers [70].

Company	Country
Futerro (Galactic/Total)	Belgium
Nantong JiudingBiologic	China
Shenzhen Bright China	China
Shanhai Tong-Jie-Liang	China
Zhejiang Hisun	China
Purac / Corbion	EU/ Thailand
NatureWorks LLC	USA / Thailand
Pyramid	Germany
Teijin	Japan

With advancements in the understanding of PLA crystallization, rheology, and processing technologies, the material is now available in various forms such as foams, fibers, films, containers, among others. These products are utilized across various applications, including biomedical, packaging, textiles, environmental, electronics, agro-industrial, automotive, and consumer goods

sectors [71,72]. Among these, flexible and rigid packaging applications are currently the most prominent [64]. Figure I.16 provides an overview of PLA applications across different sectors.

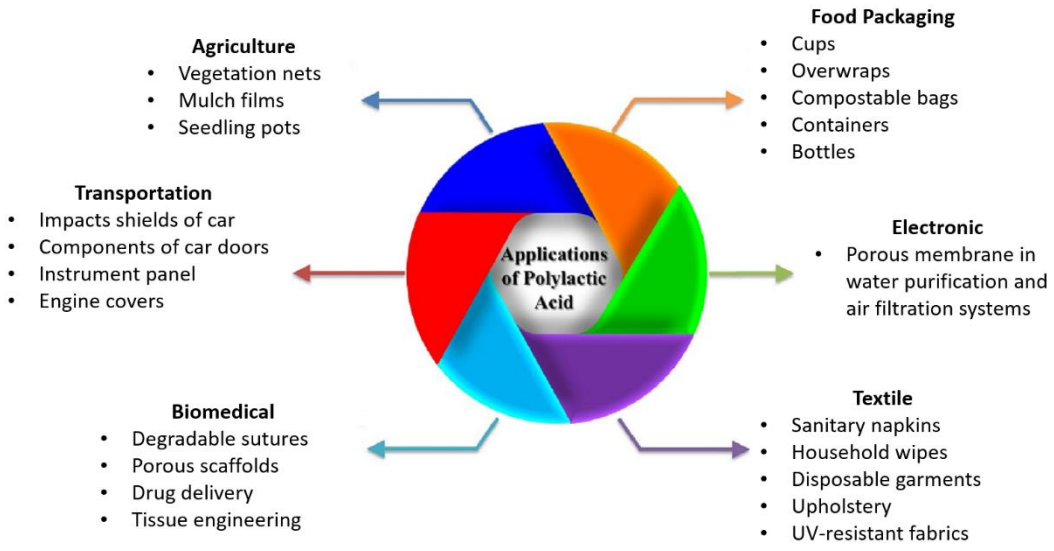

Figure I.16 - PLA applications in different areas. Adapted from [73].

Among the applications listed, PLA foams are particularly promising as alternatives to polystyrene foams in areas such as packaging, protection, construction, thermal and acoustic insulation, and general plastic utensils. Additionally, PLA foams find potential use in biomedical applications, including scaffolds and tissue engineering, due to their biocompatibility [53].

A notable feature of PLA foams is their ability to be used at temperatures above the glass transition temperature (Tg). Solid PLA often has low crystallinity, which restricts its use at higher temperatures. However, PLA foams can exhibit increased crystallinity due to the effect of gas dissolution in the polymer, thereby extending their usability at temperatures above Tg [53].

3.1 Structure and production

PLA is an aliphatic, linear polyester, produced from lactic acid units (2-hydroxy propionic acid), which is obtained through bacterial fermentation of carbohydrates, or can be chemically synthesized [46]. Figure I.17 illustrates the PLA repeated unit.

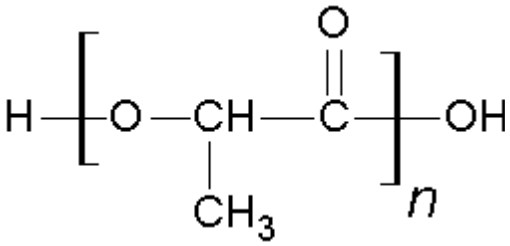

Figure I.17 - Repeating unit of poly(lactic acid).

On an industrial scale, lactic acid is predominantly produced through bacterial fermentation due to limitations associated with chemical synthesis, such as high costs and the difficulty of selectively producing only L-lactic acid stereoisomers [69].

Renewable sources that provide simple sugars for the fermentation process include corn, potatoes, sugar cane, and others [46]. Additionally, carbohydrates can be sourced from food waste, including both cooking by-products (tea leaves, vegetable and fruit peelings) and food waste (milk, rice, bread, etc) [72].

Lactic acid contains a chiral carbon, resulting in two stereoisomers: D-lactic acid (D-LA) and L-lactic acid (L-LA), with the L-isomer being the most commonly used commercially. The ratio of these isomers significantly affects the properties of the polymer, particularly its crystallization behavior [46]. Figure I.18 shows the enantiomers of lactic acid.

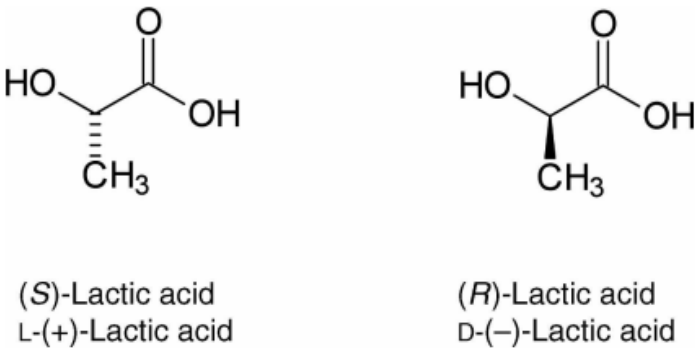

Figure I.18 – Lactic acid enantiomers. Extracted from [46].

From the monomer produced, PLA synthesis can be carried out in four main ways: polycondensation, azeotropic dehydration, and ring-opening polymerization.

Direct polycondensation of lactic acid results in a glassy, brittle polymer with a low molar mass (Mw from 1000-5000 Da), limiting its application [74]. Azeotropic dehydration involves the use of solvents and yields PLA with a high molar mass without the need for additional additives or chain extenders; however, it requires high concentrations of catalysts, leading to significant waste. Ring-opening polymerization is the most common method for producing high molar mass PLA (Mw > 100,000 Da). This method uses the cyclic dimer of lactic acid, known as lactide, which undergoes ring-opening polymerization in the presence of a catalyst [73].

Lactide is obtained from the depolymerization of low molar mass PLA under reduced pressure [75]. Depending on its stereoisomerism, lactide can have different structures [72]. Figure I.19 illustrates the isomers of lactide.

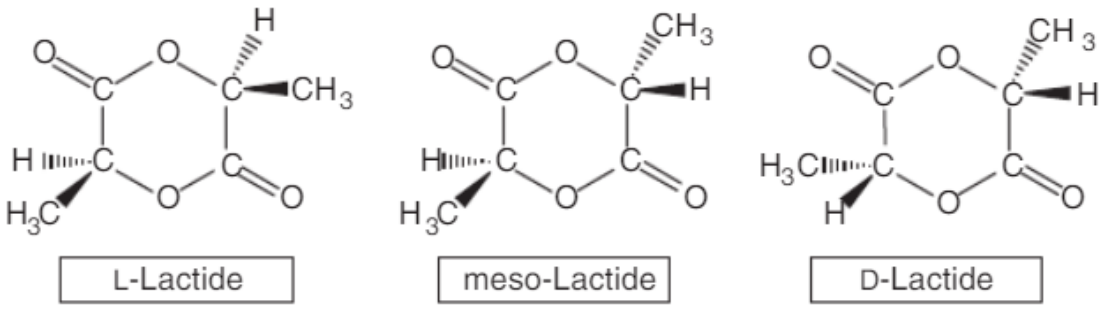

Figure I.19 – Isomers of lactide. Extraced from [76].

Once obtained the lactide, it is purified and then undergoes ring-opening polymerization (ROP) to produce high molar mass PLA. Stannous octoate ($Sn(Oct)_2$) is frequently used as a catalyst in modern PLA polymerization processes [73].

Figure I.20 shows a summary of the main PLA polymerization routes.

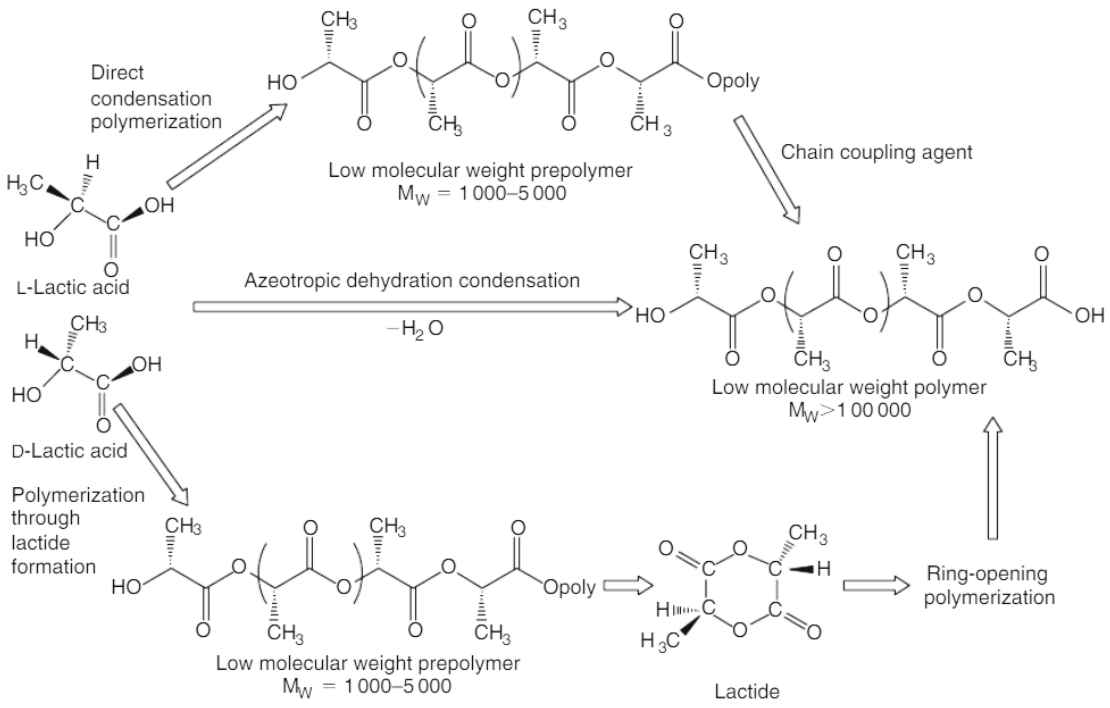

Figure I.20 - Scheme of the three main PLA production routes. Extracted from [76].

Depending on the isomer used, different types of PLA can be produced, such as PLLA, PDLA, and PDLLA, with distinct characteristics [72]. For biomedical applications, it is important to note that the human body can only metabolize L-lactic acid. Therefore, for applications requiring biocompatibility, only L-lactide and PLLA are suitable [77].

3.1.1 Degradation and biodegradation

Several factors can influence the degradation of PLA, including enzymes, water, UV radiation, and microorganisms [73]. Hydrolysis is the primary degradation mechanism of PLA, wherein water molecules penetrate the matrix, breaking the ester bonds and leading to the formation of smaller chains. Hydrolysis can occur both on the surface and within the polymer bulk and can be influenced by environmental factors such as temperature, pH, and time [78].

PLA can also experience thermal degradation. The material begins to degrade at temperatures above 200ºC through processes such as hydrolysis, oxidative chain scission, and inter/intra molecular transesterification reactions [79]. Degradation is also influenced by time, the presence of impurities, and catalysts. Catalysts and oligomers can lower the degradation temperature and increase the degradation rate of PLA, which affects its rheological and mechanical properties, among others [74].

The ASTM D883-20b standard [9] defines the degradation of biodegradable plastic as the result of the action of naturally occurring microorganisms, including fungi, bacteria, and algae. Lucas and collaborators [80] emphasize that, besides abiotic factors, the biodegradation process involves three main stages leading to the material decomposition: biodeterioration, biofragmentation, and assimilation.

Biodeterioration is the initial stage, where microorganisms grow on the material's surface, causing mechanical, chemical, and/or enzymatic degradation. This activity leads to fissures, cracks, and a reduction in the material's resistance

and durability. Biofragmentation is the process in which microorganisms break down the polymer chains into smaller oligomers and/or monomers. These small molecules are essential for the subsequent stage, as they must be small enough to pass through the cell wall or cytoplasmic membrane of the microorganisms during the assimilation stage. Finally, assimilation is the final stage, where the low-molecular-weight molecules diffuse through the microbial cellular plasma membrane. Inside the cell, these molecules are metabolized, producing energy that supports the growth and reproduction of the microorganisms. This process also results in the elimination of metabolites such as water, carbon dioxide, methane, nitrate, ammonium, salts, minerals, and biomass [80,81].

The biodegradability of PLA depends on the environment in which it is exposed [39] and its structural characteristics, including molar mass, degree of crystallinity [71], and porosity [49]. Under natural conditions, PLA has a relatively slow biodegradation rate, taking long period to decompose than other biodegradable polymers [71]. This slow rate is primarily due to its high glass transition temperature (Tg), approximately 57°C, which is above room temperature. Additionally, the literature presents that few soil microorganisms can assimilate PLA oligomers, further slowing their biodegradation rate [39,71].

However, PLA biodegradation rate can be significantly improved under composting conditions, where the environment can be controlled [71]. Composting is a natural process that decomposes organic materials into humus, an organic compound found in soil. This process is mainly driven by microorganisms, with additional influence from small insects, earthworms, and other soil organisms. The composting process requires the presence of carbon, oxygen, nitrogen, water, and heat [78].

The ASTM D6400 standard specifies that for a polymer to be considered biodegradable under composting conditions, 90% of the carbon in the polymer must be converted into CO_2 within 180 days [82].

In a study investigating PLA biodegradation, PLA cups were subjected to composting conditions at 58°C. The results showed that in the first 25-30 days, only disintegration and biofragmentation occurred. Mineralization began after 70-

90 days, particularly in samples with ratios of 1:40 (w/w) and 1:20 (w/w) – PLA mass/compost mass [83].

3.1.2 PLA properties

Regarding the thermal transitions of PLA, its glass transition temperature (Tg) for a commercial grade is around 57ºC. This relatively low Tg limits its use in some applications unless the crystallinity of the final product reaches an adequate level [46]. The melting temperature (Tm) and Tg of PLA are sensitive to the ratio between the D and L isomers. PLA composed solely of L-LA units exhibits a maximum Tm between 175ºC and 180ºC [46,84,85]. However, an increase in the proportion of D units generally results in a decrease in Tm [46].

In general, PLA typically presents a high Tg and low Tm than other thermoplastics, leading to a narrow processing window [71]. PLA thermal degradation temperature starts at approximately 200ºC, especially in the presence of moisture [79]. To address this issue, the incorporation of D enantiomers can lower the Tm by generating less perfect crystals. This adjustment helps to broaden the processing window and mitigate thermal and hydrolytic degradation [71].

PLA exhibits a slow crystallization rate similar to that of polyethylene terephthalate (PET) [46]. The highest crystallization rates are observed at temperatures between 100ºC and 130ºC and are primarily influenced by the molar mass and the content of D isomer. An increase in D isomer decreases the degree of crystallinity, once the isomer acts as a comonomer. Concentrations above 10% of the D unit result in an amorphous polymer [85]. A significant consequence of the stereoisomerism of lactic acid is that PLA can form stereocomplex crystals, which present a melting temperature approximately 50°C higher than the respective homopolymer [85].

Crystallinity plays a crucial role in determining several properties of PLA, including its mechanical properties, permeability, and biodegradation rate [46]. The mechanical properties of PLA are significantly influenced by the molar mass and stereochemical structure of the polymer chains [74]. PLA exhibits high rigidity

[71], tensile strength and modulus compared to other biodegradable polyesters. However, its low elongation at break compared to conventional polymers limits its use in flexible applications [46].

Regarding rheology, PLA displays Newtonian behavior at low shear rates, characterized by a plateau. As shear rates increase, typical of extrusion processing, PLA exhibits pseudoplastic behavior, which can be described using the Power Law equation [46,78].

A notable disadvantage of PLA is its low resistance in the molten state, a common behavior of linear polymers. The lack of branching in its structure prevents strain hardening from occurring during elongational deformations, a phenomenon observed in branched polymers like low-density polyethylene. As previously discussed, high resistance in the molten state and strain hardening are crucial for processes such as foaming and blown film [46].

Strategies such as chemical modifications or the introduction of reinforcing agents are employed to address these processing challenges. The following sections will explore these strategies in detail.

3.2 PLA reactive processing for production of foams

As previously mentioned, chemical modification can be an effective strategy for enhancing certain characteristics of PLA and enabling its processing for specific applications.

Reactive processing is employed for various purposes, including polymer modification, compatibilization of immiscible blends, in-situ polymerization, and polymer crosslinking. This method is attractive due to its advantages, such as low cost, high efficiency (with fewer process steps), and solvent-free operation [86].

Reactive processing can be performed using mixing equipment that fits as a chemical reactor. This can be carried out through both continuous and discontinuous processes [87].

Discontinuous mixing equipment is commonly used because it offers benefits such as adjustable residence time, power control, and precise control

over screw geometry and rotation speed. However, challenges associated with discontinuous processing include temperature and pressure control during mixing, continuous feeding of liquids or volatile products, and material extraction [88].

In literature, most of studies on reactive processing had employed the reactive extrusion process, a continuous method. Conversely, using an internal mixer (torque rheometer) for chemical modifications in the molten state has also been used. This method is favored for its simplicity and cost-effectiveness and is often used in preliminary stages before reactive extrusion to study the variables involved [89].

Reactive processing can generally be categorized into five main strategies: mass polymerization, grafting reactions, copolymer formation, coupling reactions, and polymer functionalization [90,91]. Additionally, extensive research has been conducted on controlling molar mass and incorporating long branches into polyolefins. Adjustments in molar mass are made to develop new grades, while the introduction of long branches enhances the resistance of polymers in the molten state, facilitating the production of tubular films and foams.

In grafting reactions, the polymer is reacted with a monomer, typically in the presence of an initiator. The outcome of these reactions, including the size of the grafts, depends on the reactivity of the system and the processing conditions [90].

Peroxides are frequently used as initiators in chemical modifications. At process temperatures, the scission of the ROOR bond generates peroxyl radicals (RO●), which are highly reactive and can abstract a hydrogen atom from the polymer chain, resulting macroradicals [92]. The efficiency of grafting and the properties of the melt are influenced by the tendency of the initiator to abstract hydrogen from the polymer chain. This reactivity is related to the structure of the peroxide and is quantified by its half-life time (t1/2), which represents the time required for 50% of the peroxide to decompose at a specific temperature. Ensuring that nearly all of the peroxide is consumed during reactive processing is also crucial [93].

Standau and co-authors [39] reviewed various chain extenders used for the chemical modification of PLA, focusing on their reactive functional groups. They identified extenders with epoxy, isocyanate, anhydride, oxazoline, carbodiimide, and phosphite groups. Among these, extenders containing epoxy groups were the most commonly used for modifying PLA to produce branching, which enhances elongational viscosities necessary for effective foaming.

Epoxy groups can react with the carbonyl and hydroxyl groups in PLA through a ring-opening reaction [39,71,94]. Joncryl® is a widely used product from BASF, characterized as a random multifunctional oligomer with styrene-acrylic-epoxy groups (Figure I.21). Joncryl® is common in PLA modifications due to its high functionality and effectiveness in increasing molar mass [95]. Its multiple reactive sites allow numerous PLA chains to be connected from a single molecule, resulting in chain extension, branching, and/or crosslinking [96]. For foam production using NatureWorks 8052D PLA grade, the manufacturer recommends adding 0.7 wt% of Joncryl® 4368C.

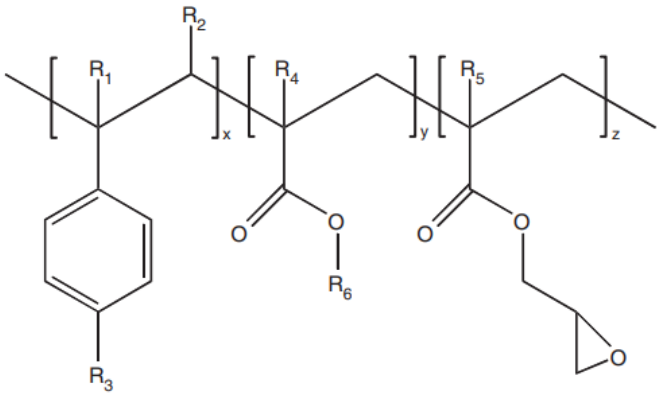

Figure I.21 - General molecular structure of the multifunctional chain extender Joncryl®, where R1-R5 can be H, CH3, long alkyl chains, or combinations thereof; R6 represents an alkyl group, and x, y, z range from 1 to 20 units [97].

Among the available monomers, glycidyl methacrylate (GMA) stands out as a bifunctional monomer possessing both epoxy and acrylic groups. In the presence of peroxide, the secondary hydrogen of PLA can be abstracted, generating a radical that can react with the double bond of the acrylic group in

GMA. Additionally, the epoxy group in GMA can react with other functional groups, such as hydroxyls and carbonyls [98].

Other chain extenders used for the chemical modification of PLA include BDDA (1,4-butylene diacrylate), TMPTA (trimethylolpropane triacrylate), and PET4A (pentaerythritol tetraacrylate) [99], styrenic maleic anhydride copolymers; isocyanurate and diisocyanate combinations; and bisoxazoline with diisocyanate [100–102]. Additionally, random copolymers of ethylene and glycidyl methacrylate are also utilized [103].

These options illustrate that various strategies for chemically modifying PLA through reactive processing can be employed to tailor its properties. Another approach for property adjustment is the incorporation of reinforcing agents, which will be discussed in the following section.

3.3 PLA nanocomposites for foams

The development of PLA nanocomposites is an efficient strategy for improving materials foamability, either by adjusting rheological properties or by acting as nucleating agents [104]. Nanocomposites are a class of composites in which the filler has at least one of its dimensions on a nanometric scale [105].

Different reinforcing agents are used in the literature to produce PLA foams, including minerals such as metals, clays, and silicates, as well as lignocellulose [104,106]. In general, the presence of fillers in the production of PLA foams can be linked to their rheological properties, degree of crystallinity, and role as cell nucleants.

In terms of rheological properties, depending on the concentration and dispersion quality of the nanoparticles in the polymer matrix, a percolation network can be formed in which the material properties undergo significant changes. Rheological percolation can be identified by dynamic rheological analysis, by observing the storage modulus (G') and loss modulus (G'') curves as a function of the oscillation frequency (ω). Figure I.22 illustrates a typical dynamic rheological behavior of melting polymers.

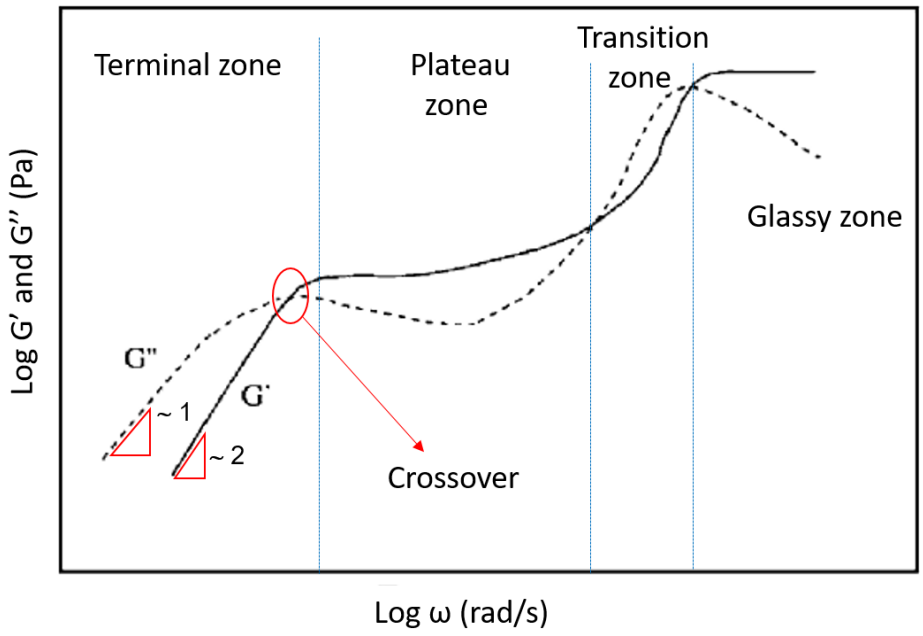

Figure I.22 – Typical behavior of melting polymers under rheological dynamic analysis. Adapted from [107].

As can be seen, at low frequencies the loss modulus of molten polymers is high, in which the terminal slope is close to 1 for G" and 2 for G'. In this case, the low frequency allows the molecules to entangle and disentangle. The crossover is the point at which the elastic component becomes more pronounced than the viscous component. As the frequency increases, the material enters the plateau zone, where the observation time is too short to detect the movements of entanglement and disentanglement. Therefore, the behavior is governed mainly by the entanglements between the polymer chains, where the magnitude of G' becomes greater than that of G". Increasing the frequency can lead to the release of entanglements, which results in the transition zone. Finally, at very high frequencies, the response time becomes very short and the material behaves like a glassy material [107,108].

Zhao and co-authors [109] carried out an empirical study and developed a model to represent the changes in G' and G" at low frequencies as a function of the concentration of nanoclays added to the polystyrene matrix, considering a good dispersion and interaction between the particles and the matrix. The model, represented by Figure I.23, shows that the addition of particles results in high G'

and G'' and a decrease in the terminal slope of the G' curve. As the addition of particles approaches the minimum value required for forming a percolated network (ϕv), a behavior with two crossovers between the G' and G'' curves is observed. Finally, when the concentration of particles is higher than ϕv, the movement of the chains is very restricted due to the network formed between the polymer and the particles, which results in a behavior where G' is higher than G''. This shows that the elastomeric plateau is brought forward to lower frequencies due to the high rigidity of the polymer mass, caused by the percolated network.

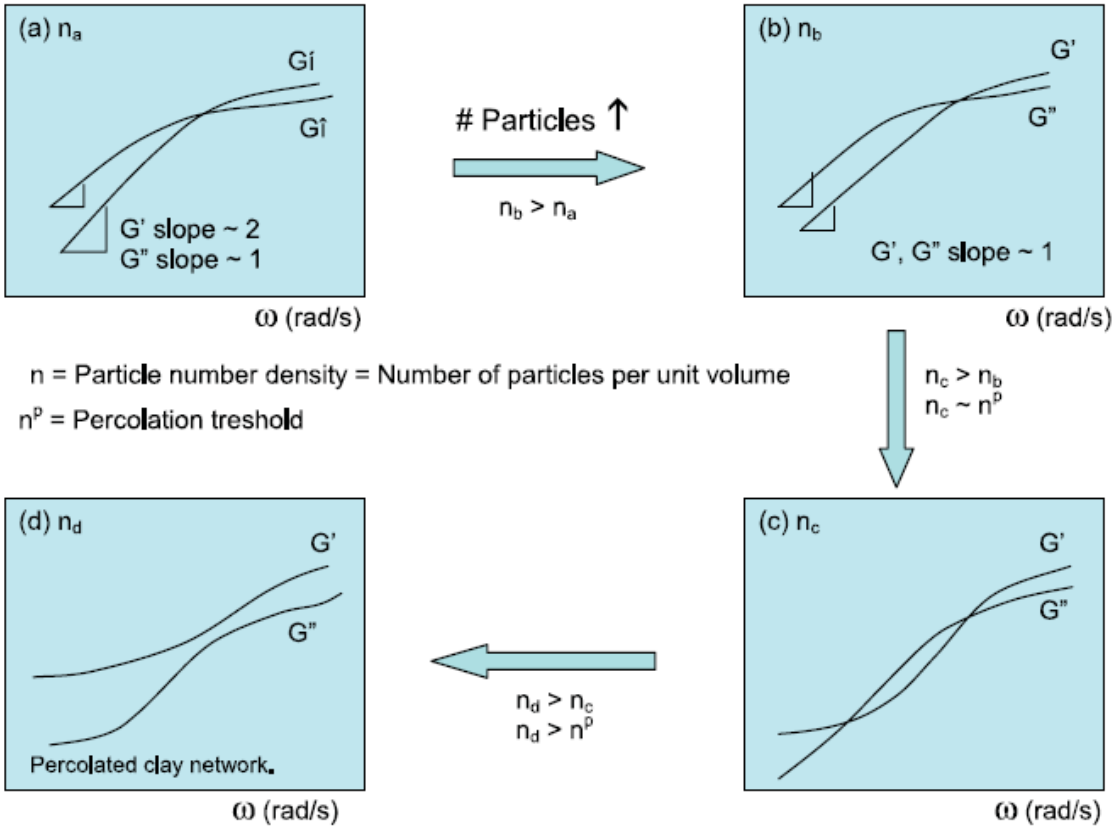

Figure I.23 – Proposed model for the dynamic rheological response of polymeric matrix filled with nanoclays, where $n_a<n_b<n_c<n_d$ are the number of particles per unit volume Extracted from [109].

Investigations on PP and CNC nanocomposites also resulted in similar findings: i) a shorter terminal zone compared to the neat polymer; ii) an increase in viscosity at low frequencies; iii) G′ higher than G″ over the entire frequency

range; iv) tan δ less than 1 over the frequency range [110]. All these behaviors were related to the rheological percolation.

However, in general, increasing the concentration of reinforcement in the PLA matrix tends to decrease the expansion ratio of the foams. This can be attributed to the number of nucleated cells and gas molecules dissolved in the material, which is lower in the presence of particles and crystals [104]. Therefore, nanoparticles can influence the foaming of polymeric materials in various ways.

In this context, cellulose is widely used as a component, fiber, or process additive in PLA composites. Many properties of PLA can be adjusted with the addition of various types of cellulose, such as cellulose fibers, microfibrillated cellulose, and cellulose nanocrystals [111].

To maintain the biodegradability and biocompatibility characteristics of PLA, one strategy is to use nanocellulose as a reinforcing agent. The next topic will focus on understanding cellulose.

4 Nanocellulose

4.1 From cellulose to nanocellulose

As the name suggests, natural fibers are originated from natural sources such as plants, animals, or minerals. Plant-derived fibers consist of various components, including lignin, hemicellulose, pectin, and cellulose, which confer rigidity and structural stability to the plant cell wall. These fibers are known as lignocellulosic fibers and may be sourced from both wood and non-wood materials. Non-wood lignocellulosic fibers can be obtained from stems, straws, leaves, seeds, fruits, and other parts of the plant. Wood-derived fibers, on the other hand, can be extracted from both hardwoods and softwoods [112–114].

Cellulose, the most abundant renewable polymer on the planet, produces approximately 1.5 x 10^{12} tons of biomass annually, representing a significant renewable and biodegradable resource that can be used as a raw material. In 1938, Anselme Payen and coauthors discovered and isolated cellulose for the first time. During this investigation, they determined its molecular formula, $(C_6H_{10}O_5)_n$. The term "cellulose", however, was first introduced in 1839 [115].

Nevertheless, the polymeric nature of cellulose, was only elucidated in 1920 through the work of Hermann Staudinger [116], who identified its structure as consisting of long molecular chains. Figure I.24 illustrates the molecular structure of cellulose, a carbohydrate composed of D-anhydroglucopyranose units (commonly referred to as glucose). These units are covalently linked by β-glycosidic bonds between carbons 1 and 4, forming an extended linear chain with three hydroxyl groups per anhydroglucose unit (AGU). The linkage of two AGUs produces cellobiose, which is the repeating unit of cellulose. The degree of polymerization of cellulose is determined by the number of AGUs and can vary depending on the source material [115,117,118]. For instance, cellulose derived from wood typically exhibits a degree of polymerization ranging from 300 to 3300, whereas in cotton fibers, it can range from 10000 to 15000 [119].

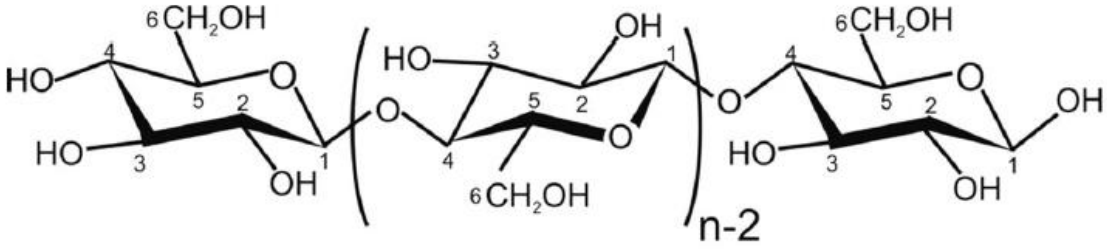

Figure I.24 - Molecular structure of cellulose (where n represents the degree of polymerization). Extracted from [120].

Due to its molecular structure, cellulose exhibits properties such as hydrophilicity, chirality, and biodegradability. Additionally, the abundance of hydroxyl groups in each AGU enables various chemical reactions initiated by this reactive group. It also facilitates the formation of hydrogen bonds between molecules, leading to partially crystalline structures [114,115,121].

Cellulose crystalline structures can be organized in multiple configurations, imparting polymorphism to the material. Each configuration is referred to as a polymorph. Cellulose exists in four distinct polymorphs: Cellulose I, II, III, and IV. Cellulose I is the most crystalline, occurring in its native form, and can be further classified into Iα and Iβ types. The other polymorphs are derived through transformations of Cellulose I [117,122,123].

Figure I.25 illustrates the various polymorphs and the transformations of cellulose.

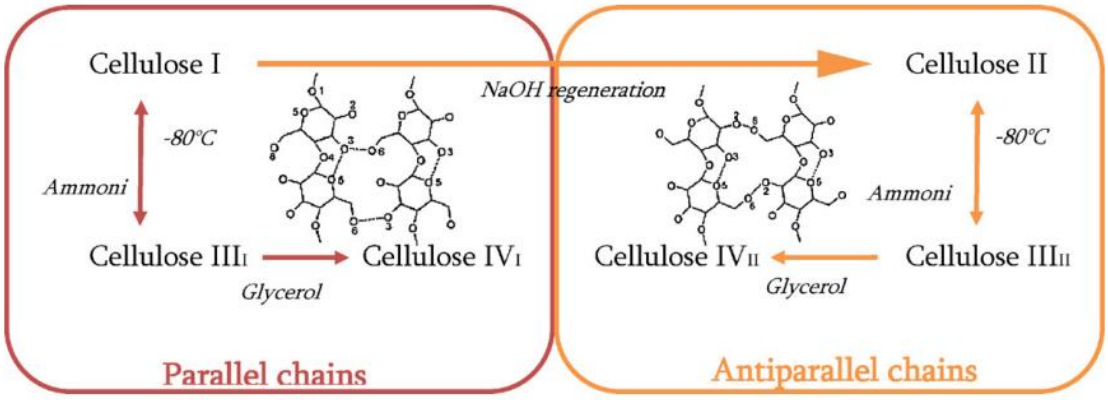

Figure I.25 - Cellulose polymorphs and the main steps involved in their formation [124].

These crystalline structures are key to understanding the hierarchical organization of cellulose, as depicted in Figure I.26. The molecular chains, composed of alternating crystalline and amorphous regions form elementary fibrils. These fibrils are further organized into microfibrils, which aggregate into microfibril bundles. The assembly of these hierarchical structures ultimately forms cellulose fibers [125].

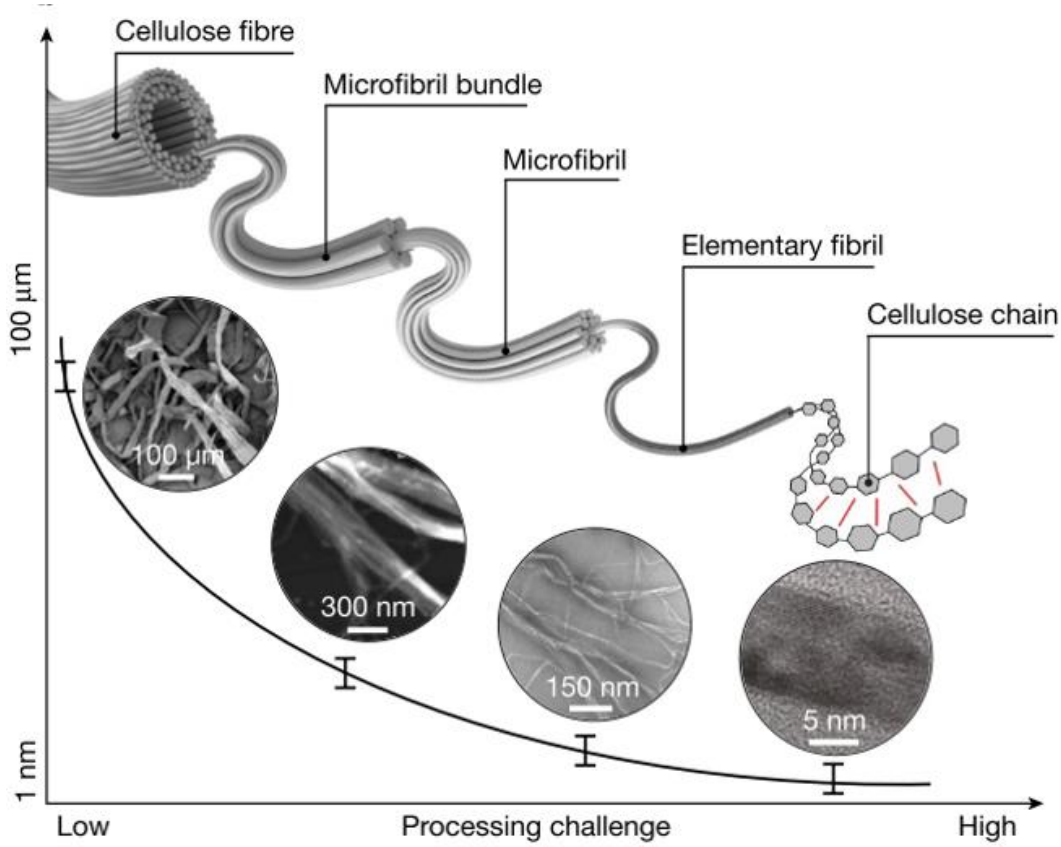

Figure I.26 - Hierarchical organization of cellulose fiber. Extracted from [126].

Due to their hierarchical organization and semi-crystalline nature, cellulose fibers can be deconstructed into nanoparticles using a top-down mechanical approach or chemically induced deconstruction [127]. In the mid-1980s [128], nanocellulose emerged as a novel class of cellulose [127,129], with researchers successfully extracting cellulose nanofibers from eucalyptus pulp using a high-pressure homogenizer [127,130]. It is classified as nanocellulose if at least one of its dimensions falls within the nanometer range [130–133].

Nanocelluloses are widely used across various industries, including packaging, energy-based applications, and environmental remediation. On a smaller scale, it finds use in sectors such as electronics, food, construction, and cosmetics [134].

Three main types of nanocellulose can be produced through two distinct strategies: the top-down approach, which yields cellulose nanofibers (CNF) and cellulose nanocrystals (CNC), and the bottom-up approach, associated with bacterial nanocellulose production [130,132,133]. Figure I.27 outlines the primary differences between these three types of nanocellulose. However, since the focus of this thesis includes CNF and CNC, only these two types will be discussed in detail.

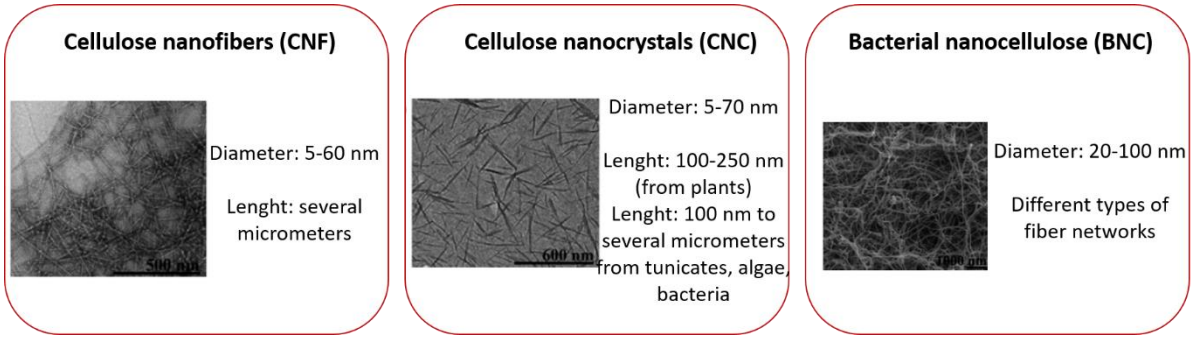

Figure I.27 – Different types of nanocelluloses. Adapted from [130].

4.2 Nanocelluloses productions and application

4.2.1 Cellulose nanofibers (CNF)

Cellulose nanofibers was first documented in the literature in 1983 by Turbak [135] and Herrick [136], who processed an aqueous suspension of softwood pulp through a high-pressure homogenizer multiple times, resulting in cellulose with nanometric dimensions. Today, a range of mechanical treatments, both conventional and unconventional, can be employed to produce nanofibrillated cellulose [118]. Figure I.28 illustrates the various types of mechanical treatments reported in the literature.

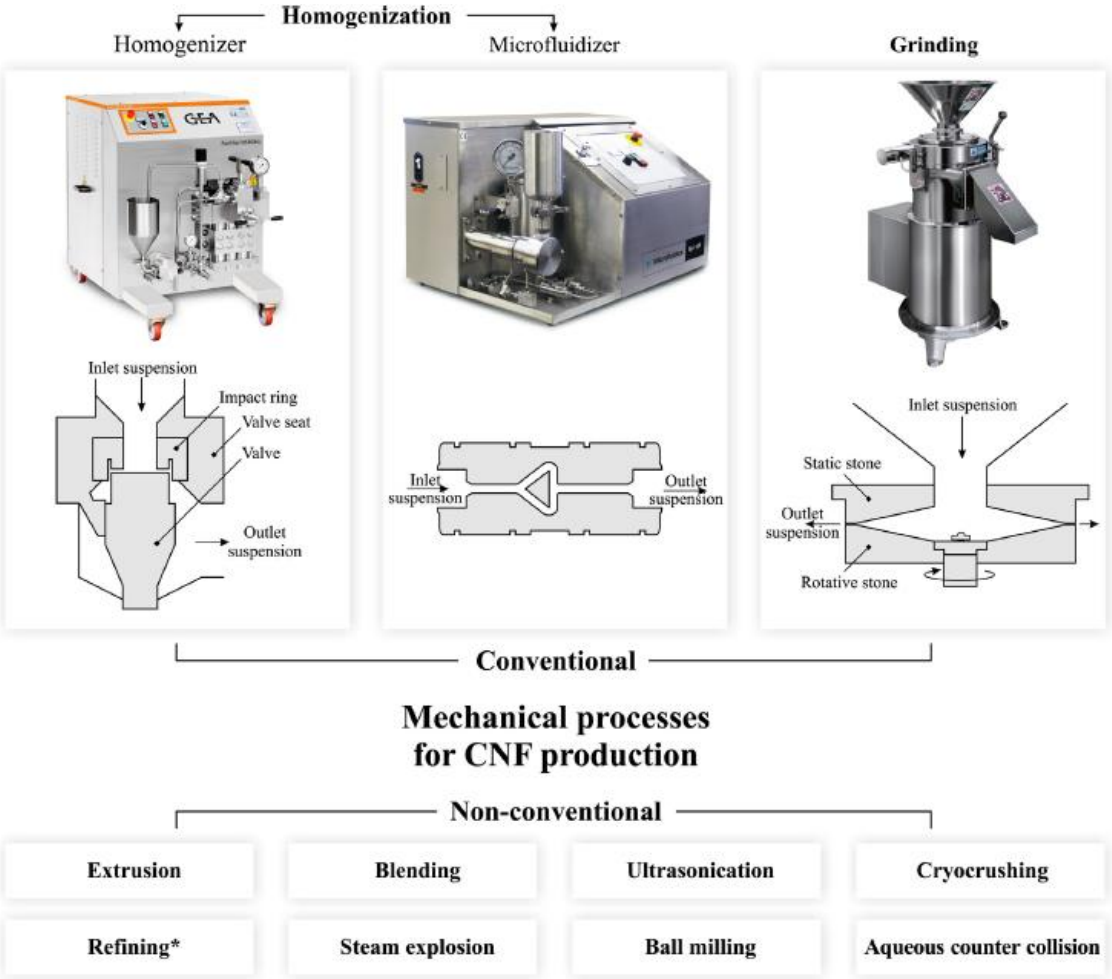

Figure I.28 - Mechanical processes for producing CNF. Extracted from [118].

Conventional processes are the most widely used for producing cellulose nanofibers (CNF) [137]. Techniques such as the Homogenizer and Microfluidizer [138] employ high shear and impact forces to induce fibrillation of the cellulose fibers. In these processes, the cellulose suspension is pumped through the equipment under high pressure. Conversely, the Grinder [139] processes cellulose slurry between fixed and rotating stones, and the shear forces generated between the discs and the cellulose fibers progressively reduce fiber size with each pass [137].

Mechanical methods offer advantages, including simplicity of operation, high material output, and lower emissions of toxic substances. However, these processes consume a lot of energy. To mitigate energy consumption, pre-treatment strategies can be employed to facilitate the fibrillation of cellulose

during mechanical processing [137,140]. Enzymatic and chemical treatments are commonly used to weaken the hydrogen bonds in cellulose fibers, thereby enhancing fibrillation efficiency and reducing the energy required to produce CNF. Each pre-treatment method imparts distinct characteristics to the final nanofibers [137].

The most common chemical pre-treatment for reducing energy consumption is TEMPO-mediated oxidation. Beyond lowering energy requirements, this method can be combined with other reagents to introduce reactive groups or functionalize the surface of the nanofibers [141].

Once cellulose nanofibers (CNF) are obtained, they can be used in several applications. However, the abundance of hydroxyl groups in their structure imparts high hydrophilicity, which can limit their use. Various modifications can be employed to overcome this limitation and enhance their hydrophobic character [142].

Among the available strategies are modifications through adsorption or grafting of molecules and polymers [137,142]. Figure I.29 provides an overview of the CNF production process and the potential post-treatments that can be applied.

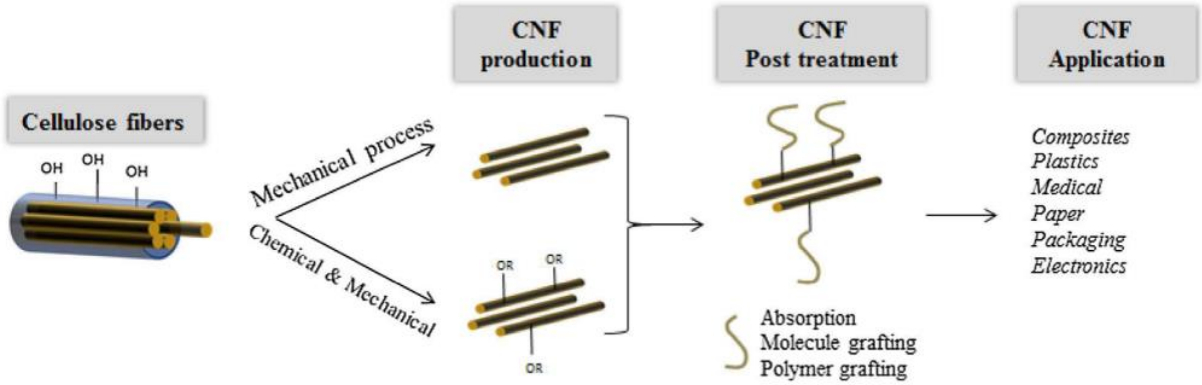

Figure I.29 - Representative scheme for obtaining CNFs from cellulose fibers. Extracted from [137].

Depending on the form in which CNFs are produced and their resulting properties, they can be applied in various fields, including antimicrobial

packaging, corrosion inhibitor carriers, gels, conductive films, 3D printing, composites, biomedicine, among others [124,142].

In some of these applications, the material features a porous structure. Porous CNF-based materials are being investigated for use across multiple sectors and can be produced using different methods, as will be discussed in the following sections.

4.2.1.1 CNF-based porous materials

As one of the topics explored in this thesis are cryogels, this section will focus on this class of porous material.

According to IUPAC classification, porous materials are categorized based on pore size as follows: micropores (<2 nm), mesopores (2-50 nm), and macropores (>50 nm) [143–145]. Aerogels and cryogels are types of porous materials that can be derived from nanocellulose. Their high porosity imparts desirable properties such as low density and high specific surface area, making them suitable for a range of applications including absorbent materials, templates for inorganic or carbon-based porous materials, gas membranes/filters, packaging materials, and biomedical applications [146,147].

Lavoine and Bergström [147] summarize that the production of nanocellulose-based porous materials involves two key phases: (i) gel preparation and (ii) solvent removal. The method of solvent removal significantly affects the properties of the final material.

In the first phase, gel preparation can be achieved by increasing the concentration of solid content in the dispersion or by destabilizing the colloidal suspension, such as by altering the pH [147].

The second phase involves solvent removal from the gel, which determines the final characteristics of porous material. Solvent removal through evaporative methods, either in a vacuum or at ambient pressure, generally causes pore collapse due to the capillary pressure. This results in materials with

reduced porosity and increased density, often leading to warping or cracking. Such materials are referred to as "xerogels" [148,149].

However, alternative drying methods, such as supercritical drying and freeze drying, can result in materials with high porosity and low density. These methods avoid meniscus formation, rendering capillary pressure insignificant [129,147,148,150].

In the literature, porous nanocellulose-based materials are commonly classified as aerogels or cryogels. Aerogels are typically defined as materials exhibiting high porosity, high specific surface area (at least 100 m^2/g), and low density, which can be produced by either supercritical drying or freeze-drying [129,147,151–153]. However, in this work, the term "aerogels" will refer to porous materials produced by supercritical drying, while "cryogels" will denote porous materials obtained through freeze-drying [146,148–150]. Figure I.30 summarizes the types of porous materials that can be produced from different methods.

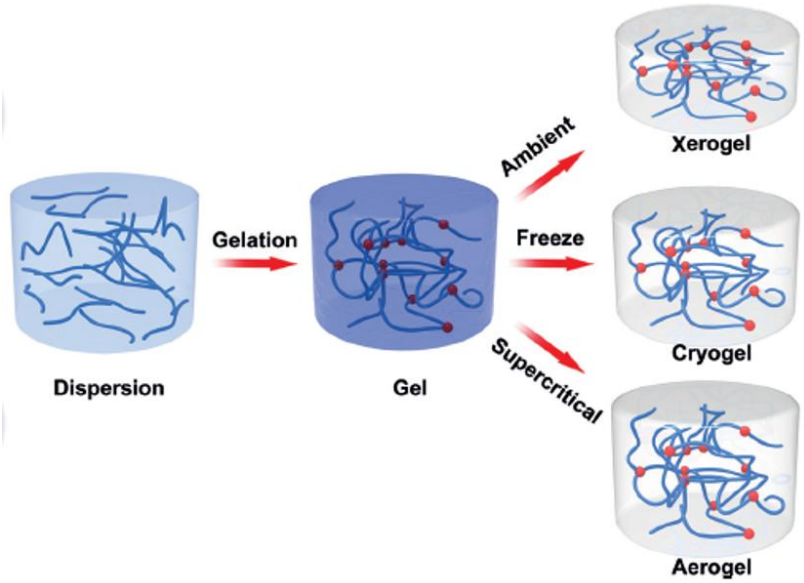

Figure I.30 – Different methods to produce porous materials. Adapted from [154].

In the production of aerogels, the solvent is removed through supercritical drying. Initially, the original solvent (typically water) is replaced with a solvent in which the supercritical fluid is miscible, such as acetone or ethanol. The gel is then placed in a system where temperature and pressure are controlled to exceed

the critical point of the chosen supercritical fluid. After the system is saturated with the supercritical fluid, the pressure is gradually reduced to atmospheric levels while the solvent is vented out of the system at a constant temperature. The presence of the supercritical fluid prevents the formation of a liquid/vapor interface during the drying process, thereby avoiding meniscus formation and capillary pressure during solvent removal [149,155,156].

Cryogels are produced by lyophilization of the gels. This process involves first freezing the gel so that ice crystals can be sublimated, resulting in porous structures. The system must be maintained at conditions where the solvent is at a temperature and pressure below the triple point of its phase diagram. This approach bypasses the liquid-gas interface, thereby preventing capillary pressure that could compromise the pore structure [154,155]. Figure I.31 illustrates the formation of pores in this process.

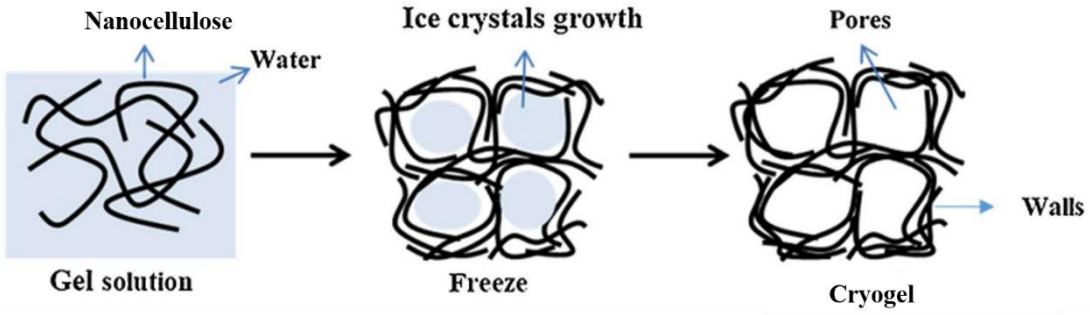

Figure I.31 – Formation of porous structures from ice crystals sublimation. Adapted from [155].

In cryogel production, the characteristics of the pores are directly influenced by the freezing process, including factors such as the direction of freezing and the relationship between the freezing front velocity (V) and the critical freezing front velocity (Vcr). When the freezing rate is very slow ($V \ll Vcr$), no pores are formed (Figure I.32 i). At slower freezing rates ($V < Vcr$), lamellar walls are formed (Figure I.32 ii). When $V > Vcr$, nanocellulose can become entrapped between the forming ice crystals, resulting in distinct porous structures compared to those observed at slower rates (Figure I.32 iii). At very high freezing

rates (V≫Vcr), the nanocellulose can become encapsulated within the ice crystals (Figure I.32 iv). Additionally, the temperature gradient between the mold and the material also affects the pore structure. Unidirectional and radial freezing can produce ice crystals with lamellar structures, while pore sizes are influenced by the solidification rate [157]. Figure I.32 illustrates these effects on pore formation.

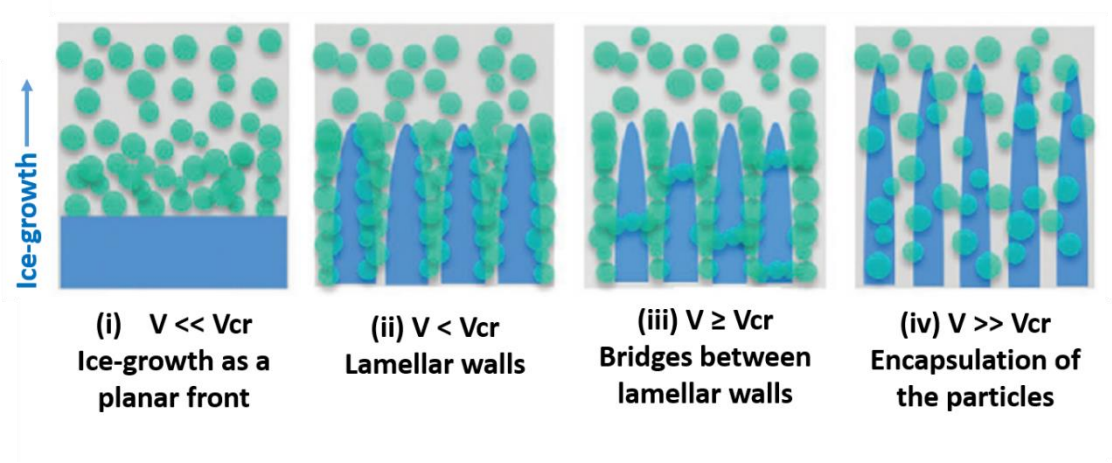

Figure I.32 – Different ice crystals structures during freezing for cryogels production. Extracted from [157].

As a result of the different drying methods, aerogels and cryogels exhibit distinct porous structures. Cryogels typically form macroporous structures, leading to a lower specific surface area compared to aerogels. Aerogels, on the other hand, possess pores that range from tens of nanometers to a few microns, resulting in a significantly higher specific surface area [148]. Figure I.33 compares aerogels, cryogels, and xerogels produced from a 7 wt% concentration microcrystalline cellulose aquagel.



Figure I.33 – Aerogel, cryogel and xerogel produced from microcrystalline cellulose. Extracted from [148].

The use of alternative methods to conventional polymer processing techniques enables the production of materials with a high nanocellulose content. This innovation facilitates their application across various sectors, as previously mentioned.

4.2.2 Cellulose nanocrystals (CNC)

Cellulose nanocrystals (CNCs) were first described by Ranby in 1949, who employed acid hydrolysis to disperse cellulose fibers in water, resulting in nanocrystals. This method involves using sulfuric acid to degrade the amorphous regions of cellulose, thereby preserving the crystalline regions. The outcome is a rigid CNC with a rod-like shape and sulfate groups on its surface [118].

CNCs are also find in the literature as nanowhiskers, whiskers, or nanocrystalline cellulose. They are elongated crystalline particles with rod- or needle-like shapes, typically measuring 5-20 nm in width, 50-350 nm in length, and having an aspect ratio of 5-30 [158].

The most commonly reported method for producing CNCs is through the acid hydrolysis of cellulose fibers [159], with mineral acid hydrolysis being the predominant technique [160]. This process can be divided into five stages, as illustrated in Figure I.34.

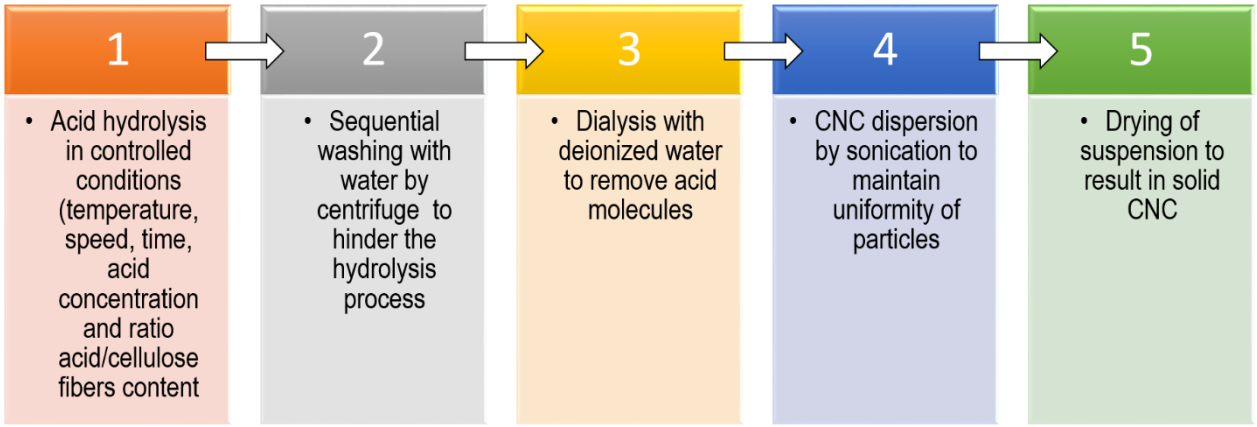

Figure I.34 – Steps for obtaining CNC from acid hydrolysis [161–163].

According to the literature, the most commonly used mineral acids for this purpose are sulfuric acid (H_2SO_4), hydrochloric acid (HCl), phosphoric acid (H_3PO_4), and hydrobromic acid (HBr) [164]. From these, sulfuric acid is the most widely used because it forms a stable suspension of CNCs, as well as it produces a negative surface charge on the particles [165,166].

In the presence of a mineral acid, protonated hydrogens (H^+) and hydronium ions (H_3O^+) facilitate the hydrolysis process by breaking the glycoside bonds present in the amorphous regions. The crystalline regions, which are less accessible due to their ordered structure, resist acid attack, while the amorphous regions are partially depolymerized [159]. Figure I.35 illustrates a summary of how CNC is obtained from cellulose fibers.

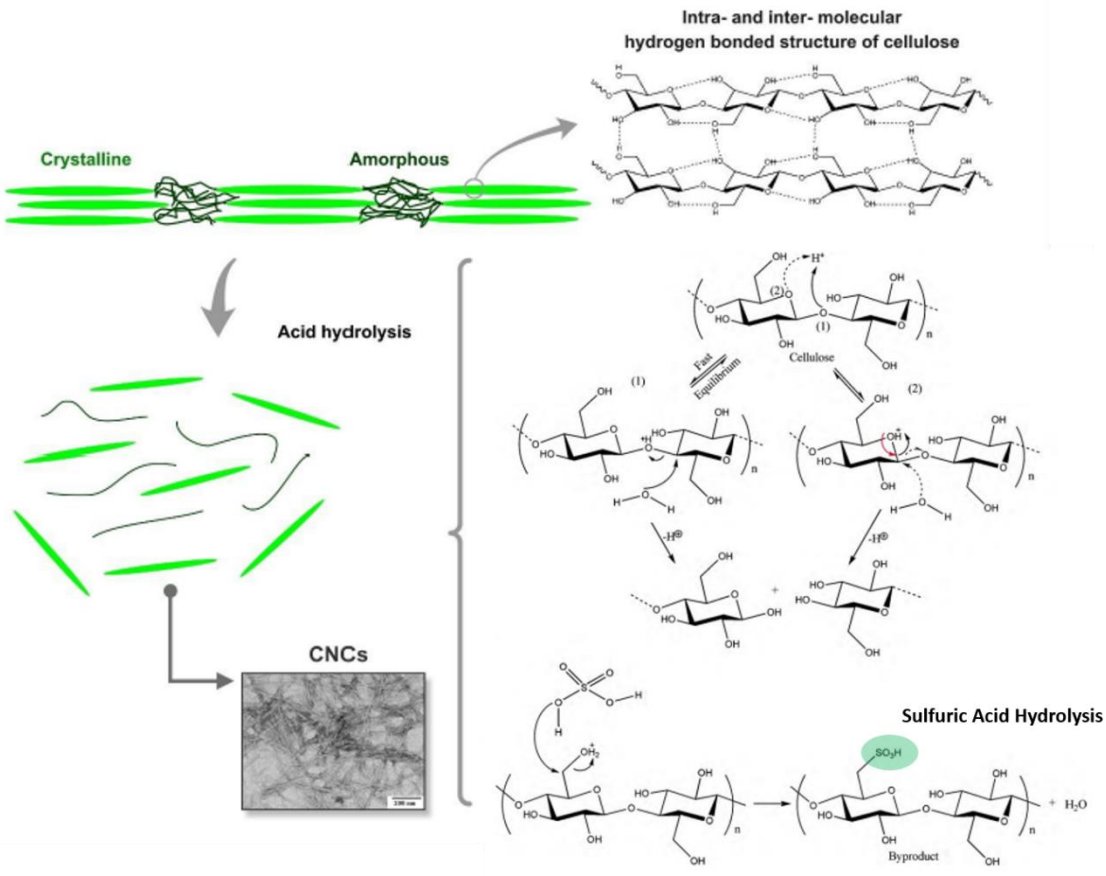

Figure I.35 - Representative scheme for obtaining CNC from acid hydrolysis by sulfuric acid, resulting in sulfate half-ester surface groups. Extracted from [167].

Other CNC extraction methods can be employed, such as enzymatic hydrolysis, or by using ionic liquids, and deep eutectic solvents, which are well described in literature reviews [159,164,165]. However, each method will yield CNCs with different properties (e.g., colloidal stability, aspect ratio, crystallinity percentage), so the extraction method must be considered for each specific application [165].

Once extracted, CNCs can be used in several applications, including medical, paper, packaging, and electronics [137]. Due to their low density and high mechanical strength, CNCs are often used as reinforcements in nanocomposites, serving as oxygen and moisture barrier agents, coatings in photonic applications, and electronic materials, packaging, and the food industry [159,165]. For this reason, CNC-based nanocomposites will be discussed in the next section.

4.2.2.1 CNC-based nanocomposites

PLA has been widely used as a matrix in preparing nanocomposites with CNC, primarily due to its favorable mechanical properties and biodegradability [168]. However, achieving good dispersion of CNC within hydrophobic matrices remains a significant challenge [131] primarily because of the strong hydrogen bonds inherent in CNC, which impede homogeneous filler dispersion [169].

Functionalizing the surface of the CNC to make it less hydrophilic is a suitable strategy to enhance the compatibility between the filler and the matrix. This approach is common because CNC contains numerous hydroxyl groups on its surface that can be modified through chemical, physical, or enzymatic reactions [170,171], as Figure I.36 illustrates.

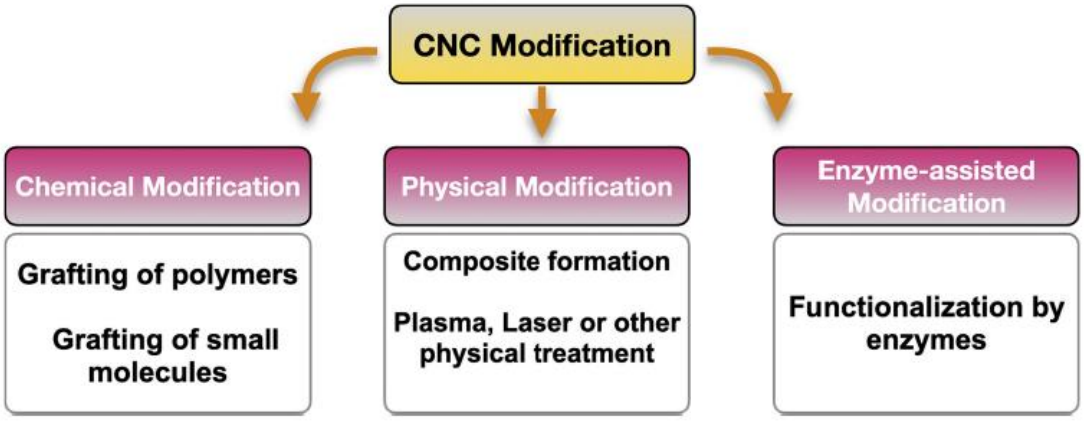

Figure I.36 – Representation of modification methods of CNC. Extracted from [171].

Since part of the doctoral research will focus on the chemical modification of CNC using small molecules, this strategy will be elaborated upon in more detail. However, several literature reviews present other functionalization methods [171–173].

4.2.2.2 CNC funcionalization

The literature reports two main strategies for functionalizing CNC by chemical reaction: cellulose modified by small molecules - such as esterification, oxidation/amination, carbamate, and silanization - and cellulose grafted with polymers [170,171]. Figure I.37 presents the main chemical modifications performed on CNC.

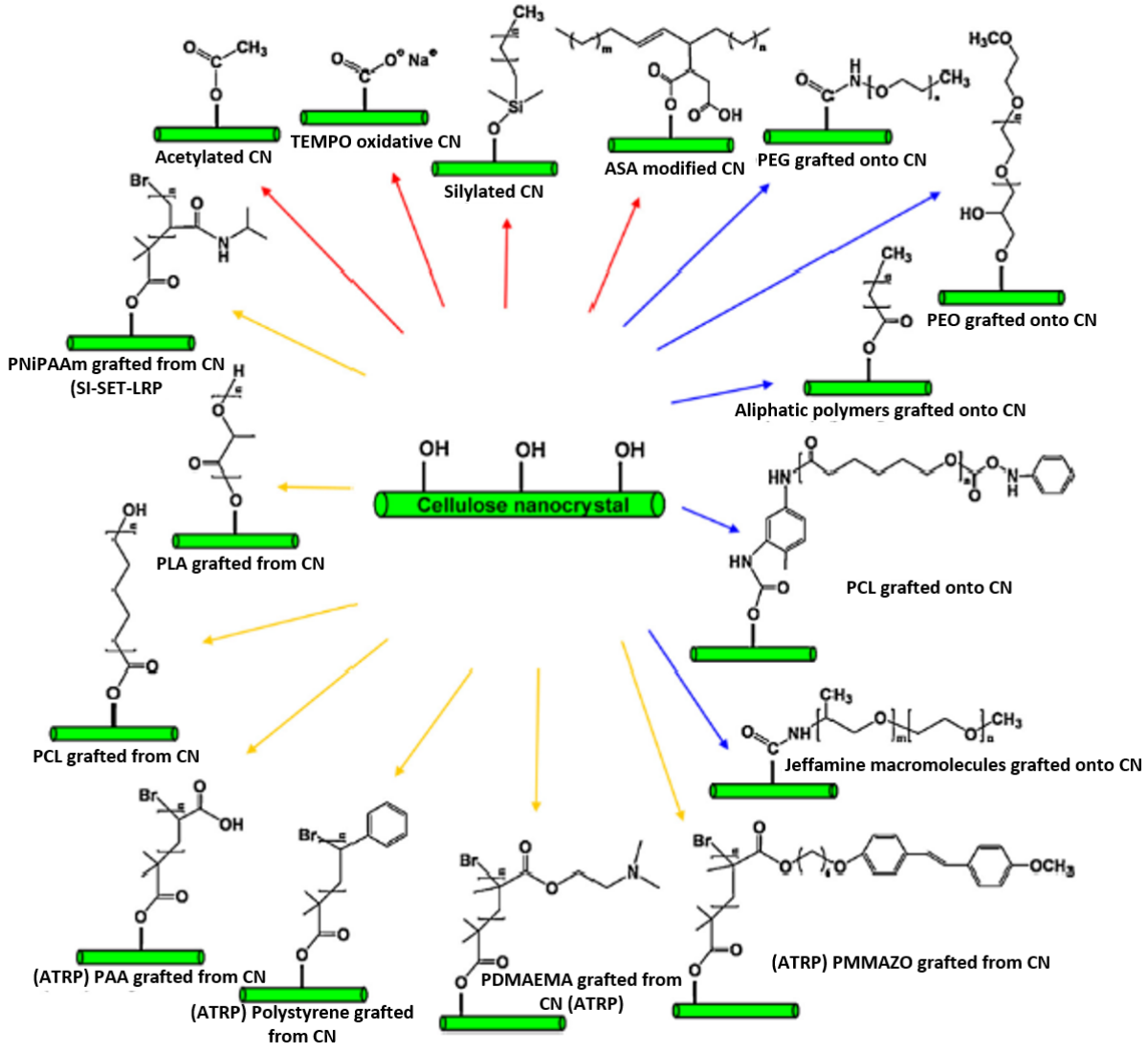

Figure I.37 – Common chemical modifications of CNC, where PEG: poly(ethylene glycol); PEO: poly(ethylene oxide); PLA: poly(lactic acid); PAA: poly(acrylic acid); PNiPAAm: poly(N-isopropylacrylamide); and PDMAEMA: poly(N,N-dimethylaminoethyl methacrylate). Extracted from [174].

Among the various modifiers used in CNC, aliphatic and aromatic isocyanates have garnered attention in recent years for the modification of nanocellulose [175], although their use with cellulose dates back to the 1920s [176]. Isocyanates offer some advantages in nanocellulose modification, including a relatively high reaction rate (compared to esterification, for example),

and the chemical stability of the resulting urethane [177]. Figure I.38Figure I.38 illustrates the main isocyanates used in the modification of nanocellulose.

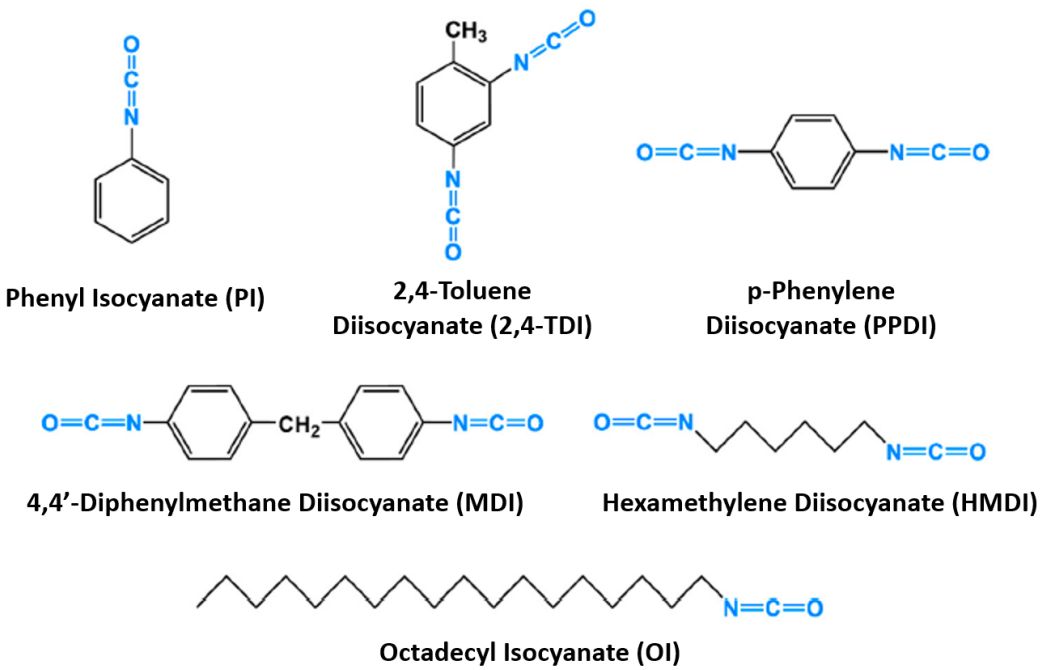

Figure I.38- Mono- and di-isocyanates, aliphatic and aromatics, most commonly used in nanocellulose functionalization [175].

Among these modifiers, n-octadecyl isocyanate (n-OI) and phenyl isocyanate are the most commonly used to modify nanocellulose, primarily to reduce its hydrophilic character [175]. n-OI is particularly attractive due to its long aliphatic chain, composed of 18 carbon atoms.

Figure I.39 illustrates the reaction between n-octadecyl isocyanate and the CNC surface.

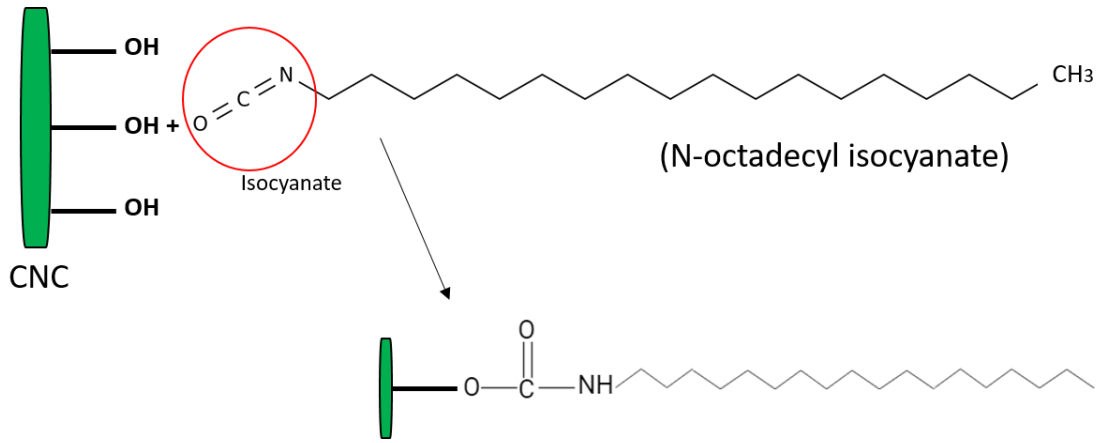

Figure I.39 – Chemical reaction between n-OI and hydroxyl group from CNC.

When an excess of isocyanate groups is present in the reaction medium, they can also react with the already formed urethane groups, leading to the formation of allophanate groups, as illustrated in Figure I.40.

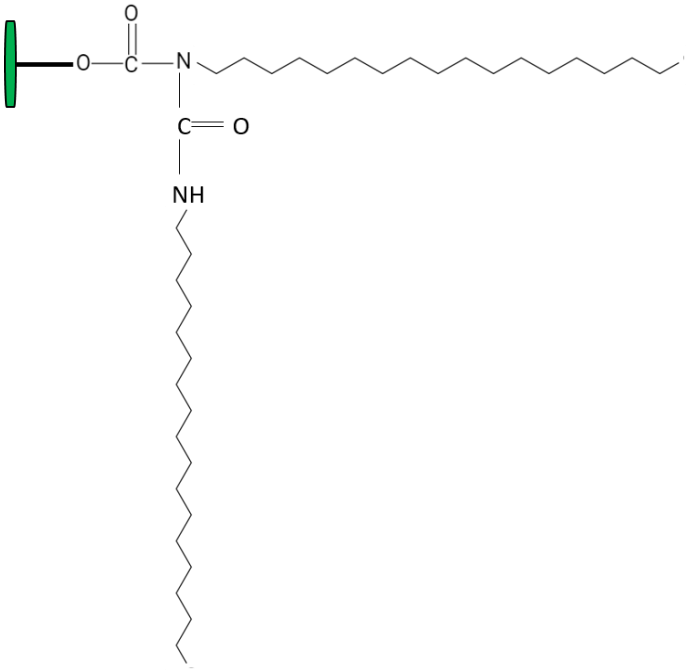

Figure I.40 - Formation of the allophanate group when excess isocyanate is present in the reaction medium, reacting with the urethane group formed. Adapted from [178].

Additionally, in the presence of moisture, isocyanates can react with water, producing amines ($R\text{-}NH_2$). If amine groups are in excess, they can further react

with another isocyanate group to form di-substituted urea, which is considered a by-product of the reaction [177]. Figure I.41 illustrates the reactions that occur in the presence of water.

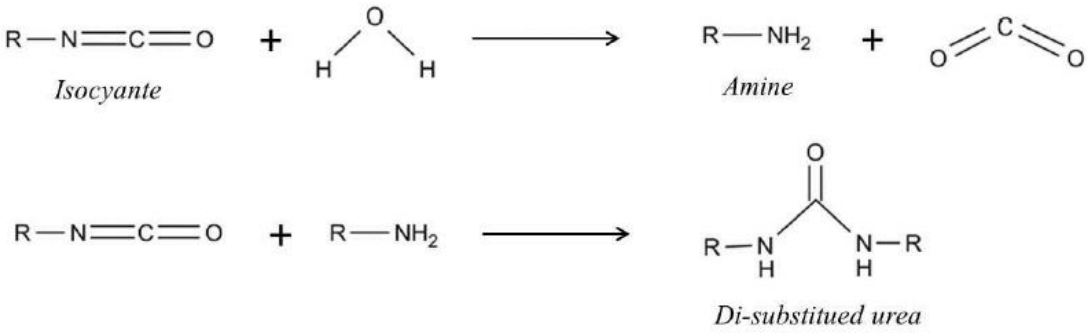

Figure I.41 - By-products produced in the reaction between isocyanate and water. Extracted from [179].

The functionalization of CNC and CNF with n-octadecyl isocyanate (n-OI) was first reported in 2010 [177], where two solvent exchange methods were studied. Figure I.42 illustrates the methodologies that were investigated.

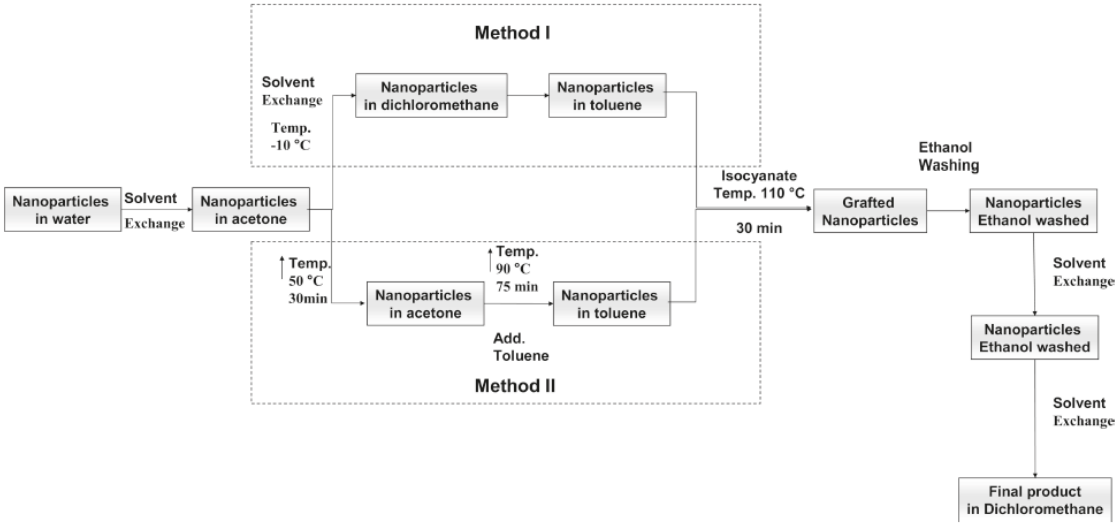

Figure I.42 – Methods studied for functionalizing CNC using n-OI. Extracted from [177].

The modification of CNC using both methods was effective, with degrees of substitution (DS) - representing the number of n-OI chains per anhydroglucose unit (AGU) - ranging from 0.6 to 0.7. However, for CNF, method I resulted in poor dispersion and a low level of grafting, making it impossible to calculate the DS. In contrast, method II achieved a DS of 0.09. The authors note that these DS values indicate that the reaction primarily occurred on the surface of the CNCs and CNFs. Despite the relatively low amount of grafting, it significantly altered the material's surface energy, as evidenced by contact angle measurements.

Since the initial study in 2010, other researches have adapted this CNC functionalization method. These adaptations have led to various applications, including the production of nanocomposites and improvements in barrier properties [180–183].

However, the original method presents some drawbacks that includes the use of large amount of organic and toxic solvents, high temperatures, and extended reaction times. Therefore, alternative methods are being explored to achieve chemical modification more efficiently.

One promising alternative is mechanochemistry, which enables chemical reactions between solids and with minimal or no solvent use [184]. According to IUPAC, a mechano-chemical reaction is a chemical reaction induced by the direct absorption of mechanical energy, typically achieved through processes like shearing, stretching, and grinding [185].

Among the various techniques, ball milling has gained particular attention in chemistry. This grinding method applies mechanical shear in the presence of chemical agents, which can be used to functionalize CNC [186]. It also offers several advantages, as outlined in Table I.4.

Table I.4 – Advantages and drawbacks of ball milling [186].

Advantages	Drawbacks
Fast	Possibility of contamination
Solvent-free	Changing in shape and size
Easy to handle	Produce noise
Cost-effective	Long cleaning times
Reproducible	
Applied in wet and dry conditions	

Different types of ball milling tools can be found, as illustrated in Figure I.43.

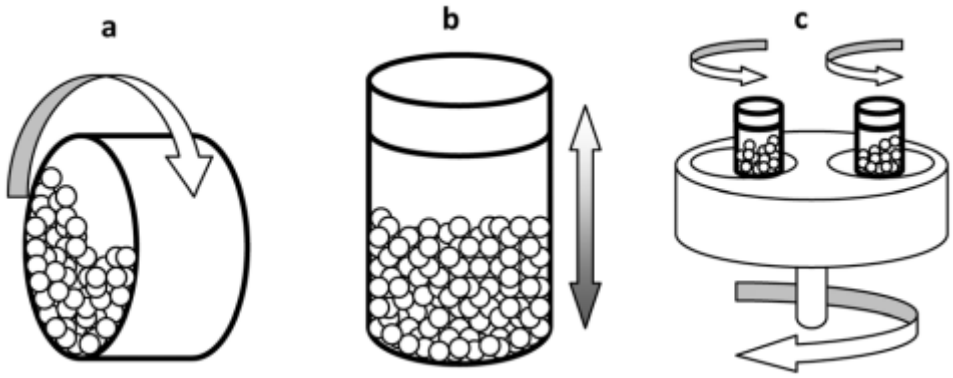

Figure I.43 – Different types of instruments used to the ball milling process: a) tumbler ball mill; b) vibratory mill; c) planetary ball mill. Extracted from [187]

Several parameters can influence the milling process, including the type of milling device, the amount of material in the chamber, the number and size of balls, the milling speed, the conditions (dry or wet), the temperature and the duration of the process [187]. According to the authors, time may be the most important variable because significant reductions in particle size occur over time.

4.2.2.3 Methods for CNC nanocomposites production

In addition to the functionalization of CNC, the composite method of production directly influences the filler dispersion and, consequently, the nanocomposite performance. Numerous challenges persist in processing polymer composites with CNC, particularly concerning agglomeration, interfacial compatibility, non-homogeneous dispersion, and degradation during processing [169].

The literature highlights three primary methods for producing nanocomposites: solvent casting, continuous melt extrusion, and batch processing. The solvent casting method involves dissolving a polymer in a volatile solvent, followed by incorporating CNCs. Once a stable colloidal suspension of the polymer and CNCs is achieved, the solution is poured into a mold of the desired shape, allowing the solvent to evaporate and forming a thin film of controlled thickness. Despite its effectiveness in producing nanocomposites, this method is limited by small-scale production and the use of volatile and often toxic solvents such as DMF, THF, and chloroform, among others [169,188].

The other two methods prevalent in the literature are melt mixing, which can be performed continuously (melt extrusion) or in batch processing. Melt processing of polymer nanocomposites is a key method due to its capacity to handle high volumes, affordability, speed, and industrial and economic viability while solvent-free [131].

However, processing in the molten state presents challenges, particularly in achieving adequate dispersion of the CNCs [169]. To address these challenges, some studies have employed a two-step dispersion technique, starting with producing masterbatches. In this method, a masterbatch with a high concentration of CNCs can be produced as a film, freeze-dried suspension, or pellets [169,189–191], which are subsequently incorporated into the matrix.

Thus, similar to CNFs, CNCs can be used in various applications and can have their properties tailored through appropriate chemical modifications, thereby extending their range of use.

4.3 Market of nanocellulose

Considering these factors, numerous opportunities for utilizing nanocellulose emerge, particularly as a reinforcement material. However, one critical consideration when evaluating these opportunities is the feasibility of production on an industrial scale.

In 2022, the global nanocellulose market was valued at USD 0.4 billion, with projections indicating a growth to USD 2 billion by 2030, largely driven by escalating environmental concerns and the increasing demand for biobased materials [192].

Brazil, endowed with abundant biomass resources, has entered the nanocellulose production market and has initiated industrial-scale manufacturing of microfibrillated cellulose (MFC), primarily for the textile industry [193].

Therefore, although there are significant challenges associated with scaling up nanocellulose production, ongoing efforts are being made to improve this scenario in the coming years, bringing nanocellulose as a versatile class of materials with potential applications across various sectors and as a sustainable alternative to conventional polymers.

Conclusion Chapter I

In light of environmental concerns, the exploration of materials derived from renewable sources that are biodegradable or compostable is crucial for generating data and insights that can facilitate the development or enhancement of products, particularly those that pose challenges throughout their life cycle, such as polymeric foams.

However, these materials present significant processing challenges. For instance, neat PLA exhibits limited foamability due to its low viscosity and elasticity in the melt state, a consequence of its linear chemical structure. Strategies such as chemical modification and the incorporation of reinforcing agents have been proposed to address this issue.

Nanocellulose, in its various forms, presents a promising option as a filler due to its renewable origin and biodegradability. Nevertheless, it exhibits low compatibility with PLA, which leads to the need of functionalization processes to enhance interfacial adhesion. Literature presents that the method of functionalization of nanocellulose, commonly use several toxic solvents. Therefore, the investigation on different methods that can be solvent-free, are an opportunity to new studies.

Additionally, porous materials can be derived from nanocellulose; however, the production methodologies for these materials differ from those used for polymeric foams. They also present a very high hydrophilic character, which can be a challenge for specific applications.

In this context, the primary topics related to the objectives of this thesis were presented: the chemical modification of PLA and the incorporation of CNC, both neat and chemically modified, into the PLA matrix to tailor its properties for foam production. Furthermore, the development of an alternative porous material, wherein nanocellulose serves as the matrix, is also explored.

To address these objectives, Chapters II, III and IV will present investigations to overcome the main challenges presented in this literature review, as illustrated in Figure I.43.

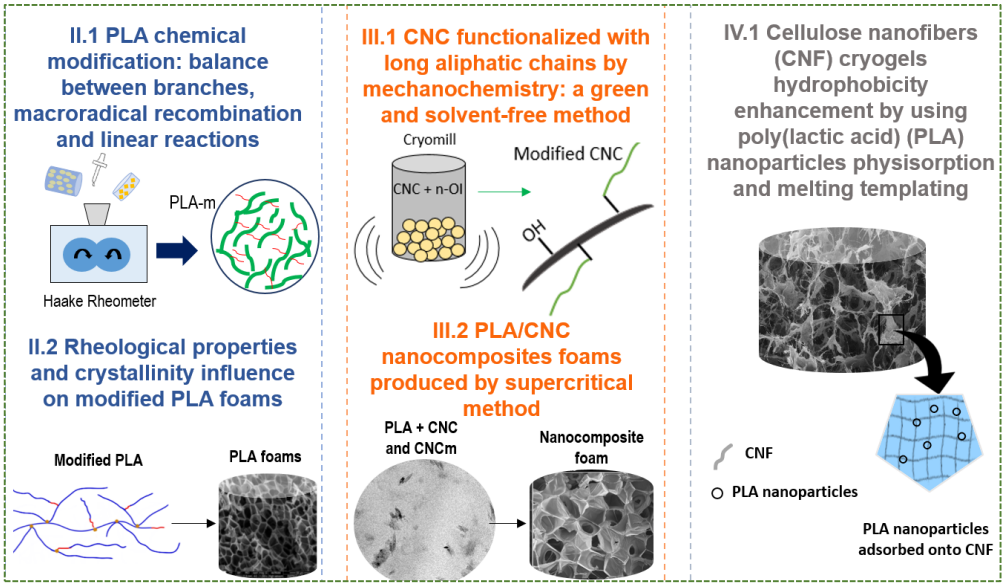

Figure I.43 – Main investigations conducted in this thesis.

Chapter II

PLA chemical modification and foams

CHAPTER II – PLA CHEMICAL MODIFICATION AND FOAMS

Introduction to Chapter II

As discussed in **Chapter I**, PLA possesses intrinsic characteristics in its molecular structure that make it challenging to process for certain specific applications, such as the production of foams. It was also mentioned that several strategies can be adopted to adjust the material properties, including chemical modification.

Section II.1 will focus on the chemical modification of PLA, using a 2^2 factorial experimental design with glycidyl methacrylate (GMA) as the modifying agent, and peroxide as the initiator. GMA was chosen primarily due to the presence of the epoxy reactive group in its structure, which can react with the acid chain ends of PLA, leading to chain extension through long branches. The study explored the relationship between the concentrations of GMA and peroxide to understand the structures of the formed chains.

Subsequently, **Section II.2** will present the foaming process on the modified PLA to investigate the relationship between the properties and structures formed from the chemical modification of PLA and the cellular structures of the foams.

Therefore, **Chapter II** aims to contribute to the understanding of the chemical modification of PLA and how the properties obtained through this modification impact the final cellular structures of the foams.

II.1 The role of chemical modification in producing different PLA chain structures: balance between branches, macroradical recombination, and liner reaction.

This section is adapted from the paper "SUQUISAQUI, A.B.V.; GONÇALVES, L.V.G.; POSSALI, L.T.; SILVA, E.A.; LIMA NETO, B.S.; BRETAS, R.E.S; ROSA, P.T.V.; BETTINI, S.H.P. The role of chemical modification in producing PLA foams: balance between branches, macroradical recombination, and linear reaction." Submitted in July 2024 to the journal ACS Applied Polymer Materials.

1 Introduction

The environmental impact generated by the improper disposal of plastic materials has been the subject of academic and industrial concerns [194–196]. One of the alternatives to this problem is the development and improvement of biobased materials that can minimize the depletion of non-renewable sources and also can biodegrade under compost conditions, minimizing negative impacts on the environment, microbiota, and population [197].

Among the various known biodegradable polymers, PLA, which comes from renewable sources, stands out for being produced on a large scale, allowing its processing in different ways, such as extrusion, injection, and additive manufacturing, among others [68]. One of the main disadvantages of PLA, however, is its low melt strength, related to its linear chain structure, which, as a consequence, avoids strain hardening, an essential property during the foaming process of semi-crystalline polymers [46].

However, the literature reports that, with appropriate modifications, it is possible to improve some characteristics of PLA to allow its foaming. Dirlam et al. [198] used mono-, tri-, and tetrafunctional initiators in the polymerization of PLA in order to synthesize 3- and 4-arm star PLA. Compared to linear PLA, 3- and 4-arm star PLA resulted in homogeneous foams, presenting lower density than linear PLA, which was a result from the complex structures formed and consequent increase in melt strength.

Li et al. [99] also modified PLA in the presence of peroxide and different co-agents such as 4-butylene diacrylate (BDDA), trimethylolpropane tri-acrylate (TMPTA), and pentaerythritol tetra acrylate (PET4A). They identified an increase in molar masses for all formulations, even when compared to the modification using only peroxide. The authors affirm that the presence of co-agents improves the insertion of long branches, which results in higher molar masses and also improves rheological properties, leading to PLA foams with thin cell walls and a high expansion ratio. In contrast, the neat PLA foam modified only with peroxide had thick cell walls and a low expansion ratio.

Standau et al. [39] conducted a literature review and evaluated different types of chain extenders most commonly used for the chemical modification of PLA based on their reactive functional groups. The authors highlighted extenders containing epoxy, isocyanate, anhydride, oxazoline, carbodiimide, and phosphate groups. Among these extenders, those with the epoxy group were the most used for chemical modification of PLA to improve characteristics and enable the foaming process. [39,71,94].

One of those extenders was glycidyl methacrylate (GMA), a bifunctional monomer with epoxy and acrylic groups. The epoxy group of GMA can react with other groups, such as hydroxyls and carbonyls while the acrylic group can graft GMA into the polymeric chain via free radicals [98]. Those radicals can be obtained by using peroxides as initiators, where at processing temperatures, the ROOR bond splits, generating peroxyl radicals (RO●), which abstract an H atom from the polymeric chain, creating a macroradical [92]. In this way, the stability or relative reactivity of the radicals is related to the peroxide structure, and its decomposition rate can be measured through its half-life time ($t_{1/2}$).

Some works have highlighted the chemical modification of PLA as an alternative to chain extension. Rigolin et al. [199] modified PLA using GMA in the presence of peroxide and observed an increase in molar masses depending on the concentration of both chemicals. The authors observed that increasing the concentration of GMA did not enhance the molar mass at the same proportion, probably because the high concentration of monomer enabled the formation of a second phase (monomer) into the PLA phase. However, this investigation did not perform foaming of modified PLA.

For the PLA foaming purpose, studies are concentrated in using GMA as chain extender in the form of random copolymers such as polystyrene/poly(glycidyl methacrylate) (by sc-CO_2) [200], ethylene/glycidil methacrylate (sc-CO_2) [103,201], ethylene/acrylic ester/glycidicl methacrylate (azodicarbonamide) [202], styrene/cryolinitrile/GMA (by sc-CO_2) [203]. Other strategy is the grafting of GMA in other polymers to process with PLA and produce foams, e.g. poly(ethylene octane) grafted with GMA by sc-CO_2 [204,205] or by azodicarbonamide [206]. These strategies are also improving rheological properties to produce foams.

Li et al. [103], for example, modified PLA using an ethylene glycidyl methacrylate random copolymer at several concentrations without an initiator; by Soxhlet extractor the presence of crosslinking in the modified samples was observed, which, they concluded was essential to the improvement of elasticity in the melt state and thus, to the ability to expand the material. According to the authors, the higher the concentration of chain extender, the higher the percentage of crosslinking and the complex viscosity, which led to a limitation of the cell growth because the increase in viscosity also increases the resistance to material expansion.

By this, it can be concluded that the control of the chemical structure of PLA can lead to structural modification and the promotion of the material´s expansion. In this sense, this section aimed to chemically modify PLA using GMA and dicumyl peroxide as an initiator. A 2^2 experimental design was used to evaluate the influence of the ratio peroxide/GMA on the PLA chain extension (by linear extension, branching, or crosslinking). These results will be important for the next section on the foaming process of modified PLA.

Nevertheless, the chemical modification of PLA only modified with GMA monomers in the presence of peroxide, with the aim of the production of foams, is still not well explored in the literature.

2 Materials and Methods

2.1 Materials

PLA Ingeo Biopolymer 4043D was purchased from NatureWorks LLC (MRF 6 g/10 min, 210°C, 2.16 kg), with a melting temperature T_m between 145 and 160°C. The manufacturer did not inform the % of D content (considered medium D content) but it was assured that it was free of additives and hydrolysis stabilizers (which could influence the chain extension reactions). The GMA and dicumyl peroxide (DCP, half-life time 30 s at 180°C) were purchased from Sigma-Aldrich (both structures are presented in Figure II.1); both materials were used as received.

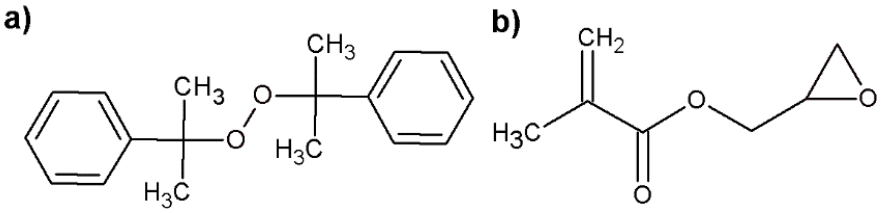

Figure II.1 – Chemical structure: (a) DCP; (b) GMA.

2.2 Chemical Modification of PLA

Chemical modification of PLA was conducted by reactive processing in a Haake torque rheometer, model Rheomix 600, equipped with roller rotors, following a 2^2 factorial design; the GMA and DCP concentrations, (C_{GMA}) and (C_{DCP}), respectively, were varied at 2 levels and measured in parts per hundred of resin (phr), as shown in Table II.1. This experimental design was based on work by Rigolin and collaborators [199], whose results showed that the modification using 1 phr of DCP and 2 phr of GMA was more efficient in increasing the molar mass of neat PLA. Thus, this formulation was used as a reference, shifting the peroxide levels by 0.5 phr and reducing the GMA concentration since high concentrations generated a second phase, reducing the interface for

reactions. Process conditions were as follows: temperature of 180°C, rotation of 50 rpm, reaction time of 6.5 minutes, under nitrogen atmosphere. The addition of DCP and GMA was carried out between 80 and 90 seconds. PLA was dried in a vacuum oven at 70°C for 4 h before processing. Table II.1 presents the nomenclature of the samples.

Table II.1 – Nomenclature of samples with different DCP and GMA concentrations.

Identification	C_{DCP} (phr)	C_{GMA} (phr)
PLA_0.5_1	0.5	1
PLA_0.5_3	0.5	3
PLA_1.5_1	1.5	1
PLA_1.5_3	1.5	3

Code: PLA_per_gma

2.3 Characterization

2.3.1 Size Exclusion Chromatography (SEC)

The molar mass was obtained in a Viscotek_HT-GPC size exclusion chromatograph with a refractive index detector. The samples were solubilized in tetrahydrofuran (THF) at 45°C; the injection volume was 200 µL, at a concentration of 5 mg/ml. All samples were previously purified to remove residual monomers and/or unreacted oligomers, by previously drying them for 4 h in a vacuum oven at 70°C, dissolving in HPLC grade chloroform at room temperature for 24 h, and then precipitating in HPLC grade ethyl alcohol.

2.3.2 Determination of acids groups

Purified samples were dried in a vacuum oven (4 hours at 70°C); the percentage of acid groups was determined by titration. PLA (0.5 g) was dissolved in chloroform (50 ml) at room temperature and titrated using ethanolic KOH

solution, with a concentration of 0.04 M. The reverse titration was done in isopropanol HCL solution at a concentration of 0.04M. Phenolphthalein was used as the indicator. The percentage of acid groups (% acidity) was calculated from:

$$\% \text{ acidity} = \left(\frac{\mathbf{V_e} \times \mathbf{C_{KOH}} \times \boldsymbol{M_{g.a}}}{\mathbf{m_a}}\right) \qquad \text{Equation II.1}$$

Where V_e is the equivalent volume of KOH added ($V_{KOH}+V_{excess}-V_{HCl}$), C_{KOH} is the molar mass concentration of KOH, M_{ga} is the molar mass of the PLA acid group (45 g/mol), and m_a is the mass of the sample.

2.3.3 Rheological analysis

Rheological data was obtained using a tension-controlled TA Instruments AR-G2 rheometer with parallel plates geometry (d = 25 mm, gap between plates = 1 mm). The steady-state (between shear rates of 0.01 and 100 s^{-1}) and the small amplitude oscillatory shear properties (between angular frequency of 0.05 and 500 rad/s), at 180°C and under nitrogen atmosphere were measured. Unpurified samples were used for this characterization, being vacuum-dried before the experiment (4 hours at 70°C).

2.3.4 DSC

Differential scanning calorimetry (DSC) was performed in a TA Q2000 DSC. A first heating cycle at a heating rate of 10°C/min, between 0°C and 200°C, under nitrogen gas flow was applied to dried samples (4 hours at 70°C); after attaining 200ºC, the samples were kept at that temperature for 1 min and then were cooled down to 25ºC. A second heating cycle was applied at 10°C/min, between 0°C and 200°C. The crystallinity index (Xc) was calculated by using Equation II.2:

$$Xc = \frac{[\Delta H_m - \Delta H_{cc}]}{[\Delta H_m^o]} \times 100$$ Equation II.2

Where ΔH_m is the melting enthalpy, ΔH_{cc} is the crystallization enthalpy during the heating and ΔH_f^o is the melting enthapy for a hypothetically 100% crystalline polymer. For PLA, the value adopted was 93 kJ/g [207,208].

2.3.5 Crosslinking content

The crosslinking of the unpurified samples was determined by extracting the soluble fraction with boiling chloroform and using a Soxhlet extractor for 6 h. All samples and filters were vacuum-dried (4 hours at 70°C) and weighed before extraction. Finally, all samples were left for solvent evaporation and vacuum-dried at 70°C for 5 hours. The calculation of the crosslinking percentage was obtained as follows:

$$\%\, Crosslinking = \frac{m_f - m_{filter}}{m_{PLA_i}}$$ Equation II.3

Where m_f is the mass of the remaining PLA and the filter (both dried) after extraction, m_{filter} is the mass of the dried filter before the extraction, and m_{PLA_i} is the mass of dried PLA before the extraction.

2.3.6 NMR analysis

^{1}H, ^{13}C, and HSQC (500 MHz) NMR analysis were performed on an Agilent Technologies, model 500/54 premium shielded. In order to identify the functional groups involved in the branching reaction and for mechanistic studies. Spectra were obtained at 26°C in $CDCl_3$.

2.3.7 Statistical analysis

When appropriate, statistical tests ANOVA, followed by Tukey's multiple comparisons test, were conducted with a 95% confidence level ($p < 0.05$ = significance level).

3 Results

3.1 Torque results during chemical modification of PLA

As torque rheometry was used for reactive processing, the process was evaluated as a function of the reaction time (which was set to be higher than five times the half-life of the peroxide – 30 s at 180°C [209]). The torque *versus* time curves of the formulations produced from the experimental design are shown in Figure II.2.

For all the curves shown, it is possible to observe a discontinuity near 1.5 minutes, when the reagents were added to the mixture. The addition of GMA to PLA (Figure II.2.a), in the absence of peroxide, did not modify the torque of the PLA. This can be explained by the fact that the GMA cannot be grafted onto the PLA chain in the absence of peroxide. However, a reaction between the epoxy group of the GMA and the carboxyl or hydroxyl groups of the PLA chain ends can occur, as illustrated in Figure II.3. On the other hand, the GMA that did not react during processing can remain present in the polymer mass, behaving like a lubricant, which can explain the slight decrease in the viscosity of the material and, consequently, the lower torque of the formulation with 3 phr of GMA.

Regarding the addition of peroxide to PLA, in the absence of GMA, it is observed that unlike the addition of GMA, the presence of peroxide resulted in a significant increase in torque compared to pure PLA (Figure II.2.a), even at the lowest level of the experimental design (0.5 phr). This suggests that an extension of the PLA chain occurred by branching and/or crosslinking, promoted by this initiator, which led to an increase in the viscosity of the medium and, consequently, an increase in the torque.

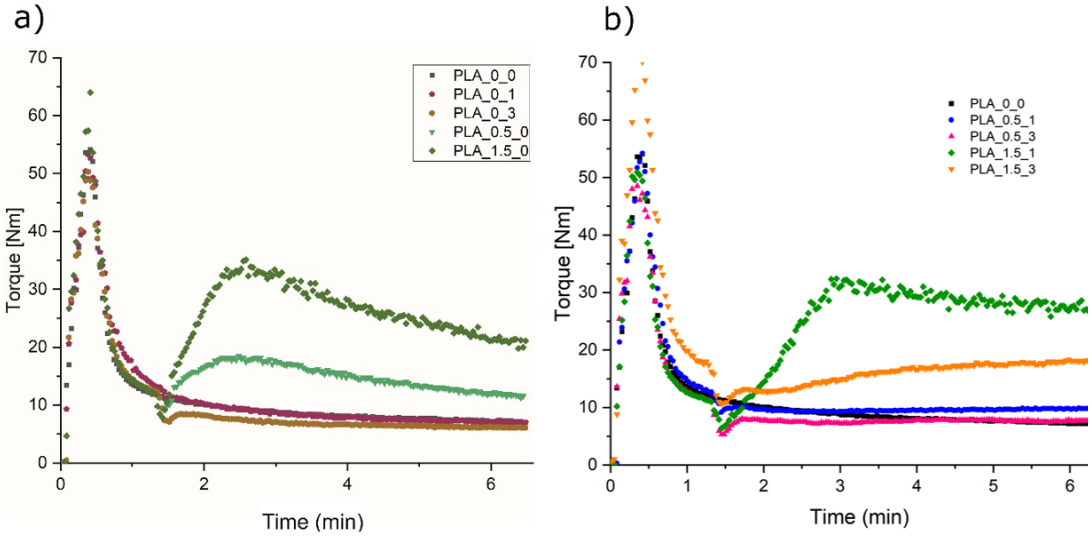

Figure II.2: Reactive processing of the formulations: (a) reference formulations (b) experimental design 2^2. Code: PLA_C_{DCP}_C_{GMA}.

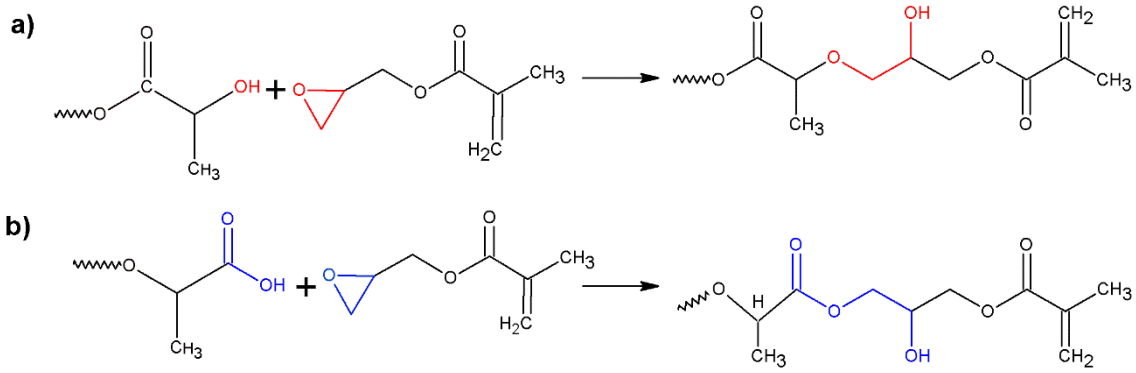

Figure II.3 - Possible reactions between the epoxy group present in PLA-g-GMA and the a) hydroxyl group at the end of the chain of another PLA molecule and b) carboxylic acid group at the end of the chain of another PLA molecule.

Figure II.2b shows the graphs for PLA modified with peroxide and GMA at lower and upper levels. It is observed that, within the experimental error, the lower-level formulations of DCP (PLA_0.5_1 and PLA_0.5_3) had similar torque to those of the pure PLA sample (PLA_0_0). However, the 1.5 phr peroxide and 1 phr GMA formulation (PLA_1.5_1) displayed an increasing torque during processing with a maximum of 30 N.m. Removing that material from the torque rheometer was difficult due to its solidification, which may indicate chain extension with a predominance of crosslinking. When the concentrations of

peroxide and GMA concentration were maximum (PLA_1.5_3), an increase in torque with processing was also observed, but at a lower level than the PLA_1.5_1 formulation. It can be highlighted that large structural variations can also display similar torques. Therefore, SEC analysis, acid group titration, and Soxhlet extraction were carried out to investigate possible changes in the modified structures.

3.2 Influence of chemical modification on final chemical structures

Degradation can also occur during reactive processing. As can be observed in Table II.2 – Results of SEC and titration of acid groups., processed PLA presents a lower molar mass than PLA pellets. This degradation results from high temperatures, shear stresses, oxygen presence, and hydrolysis (small water concentrations in PLA can be present even after drying). All these factors can lead to a decrease in molar mass during processing. In addition, it is possible to observe that the acidity of processed PLA is much higher than that of the PLA pellets since the hydrolysis of ester bonds during processing can produce more acid groups.

Table II.2 – Results of SEC and titration of acid groups.

Sample	Peroxide concen-tration (phr)	GMA concen-tration (phr)	$\bar{M}_n$ (SEC_RI) (g/mol)	$\bar{M}_w$ (SEC_RI) (g/mol)	PDI	% acidity
4043D_pellet	0	0	127,462	202,946	1.5	0.001 ± 0.192[b,c]
PLA_0_0	0	0	117,421	180,267	1.5	0.107 ± 0.43[a]
PLA_0_1	0	1	95,329	167,904	1.8	0.009 ± 0.177[b,c,d]
PLA_0_3	0	3	108,003	183,003	1.7	0.008 ± 0.077[d, e]
PLA_0.5_0	0.5	0	104,671*	268,643*	2.6	0.018 ± 0.223*[b]
PLA_1.5_0	1.5	0	-	-	-	-
PLA _0.5_1	0.5	1	127,790	218,030	1.7	0.013 ± 0.115[b,c,d,e]
PLA _0.5_3	0.5	3	123,580	223,141	1.8	0.004 ± 0.086[c,d,e]
PLA _1.5_1	1.5	1	-	-	-	-
PLA _1.5_3	1.5	3	188,280	487,090	2.6	0.001 ± 0.066[e]

*Soluble phase of the formulation. Same letters are statistically similar.

To understand the possible reactions occurring during the reactive process, Figure II.4 shows reaction mechanisms that may happen during the chemical modification. When the reactions are carried out in the presence of peroxide, its dissociation forms two peroxyl radicals (Figure II.4, R1), which abstract hydrogens from the secondary carbon of the PLA chain [199], resulting in PLA macroradicals (Figure II.4, R2). These macroradicals can be stabilized by two routes: i) PLA chain scission (Figure II.4, R3), which decreases molar masses; ii) recombination between PLA macroradicals (Figure II.4, R4), which can lead to a decrease in the free volume of chains and depending on the intensity of recombination, it can lead to a crosslinked structure. When PLA, peroxide, and GMA are present, other reactions can also occur: iii) grafting of GMA molecules onto PLA (Figure II.4, R5'), resulting in short, branched

structures. As GMA presents an epoxy group, GMA epoxy groups likely react to both hydroxyls and carboxylic end groups of PLA [39,71,94]. However, reactivity with carboxylic groups is higher than with hydroxyls. This last reaction can result in long chain branches (Figure II.4, R5''). All the mentioned reactions are competitive, and the intensity of each reaction will depend on the concentration of peroxide and GMA [199].

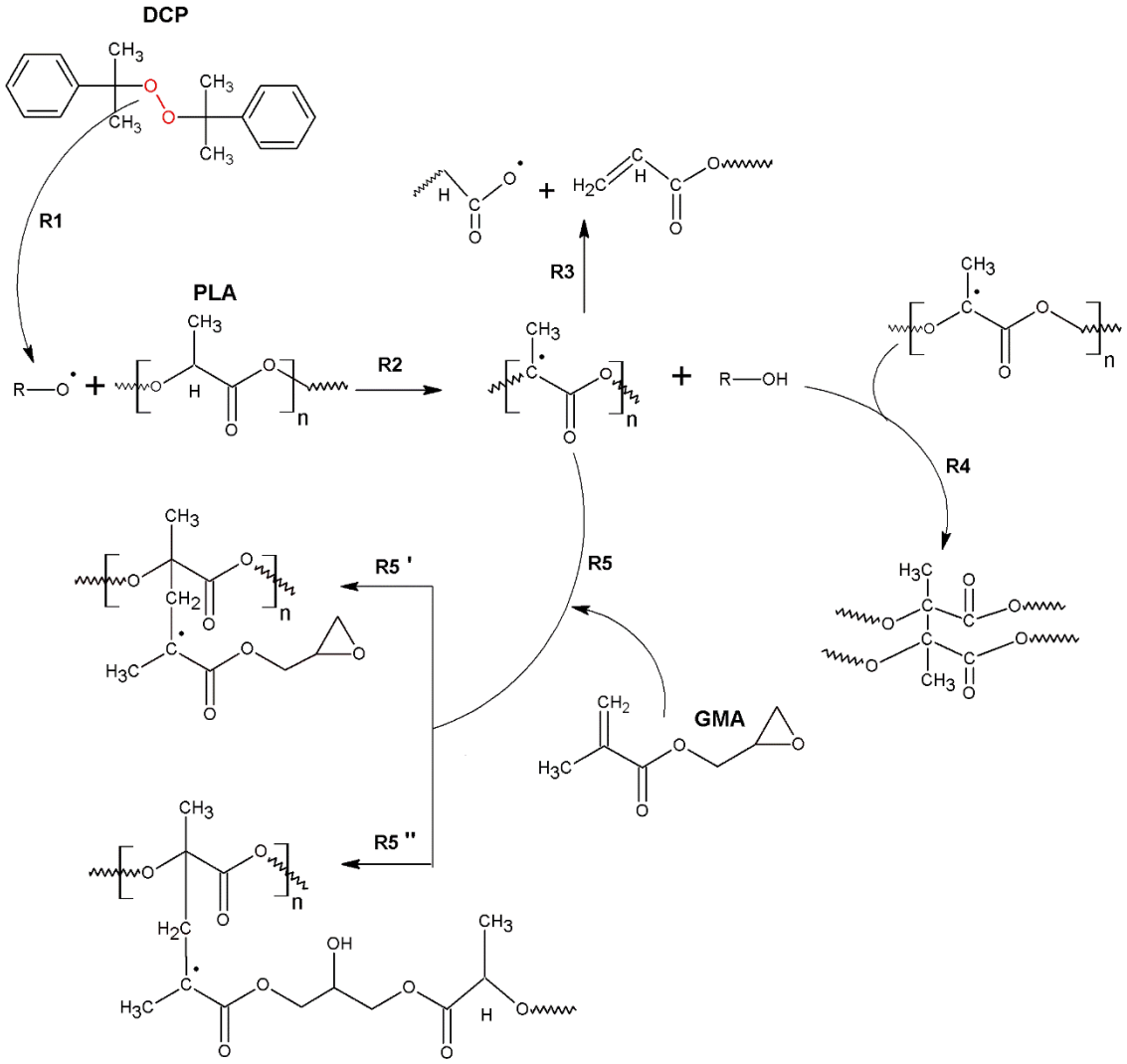

Figure II.4: Reaction mechanisms for PLA chemical modification, where: R1: Decomposition of DCP into two peroxyl radicals; R2- Formation of PLA radical in the presence of a peroxide; R3- Stabilization of PLA radical by chain scission; R4- Stabilization of PLA radical by recombination between different PLA radicals; R5' – Stabilization of PLA radical by insertion of GMA monomer; R5'' – Linear chain extension of GMA branched after reaction between epoxy group from GMA and carboxylic group from PLA.

From Table II.2, it is possible to note that the analysis of formulation PLA_1.5_0 (upper level of peroxide) and PLA_1.5_1 (upper level of peroxide and lower level of GMA) was not done since both were insoluble in chloroform or THF. For those samples, a gel behavior was observed when in solution, suggesting possible crosslinking reactions. The occurrence of crosslinking in PLA in the presence of peroxide has already been reported in the literature. Li et al. [210] explain that linear peroxides form crosslinked structures, while cyclic peroxides form mainly branched structures. Södergård et al. [211] also stated that the use of linear peroxides in concentrations between 0.1 % and 0.25 % promotes branched reactions; however, above 0.25%, it is possible to observe crosslinking reactions. To confirm this statement, Soxhlet extraction was performed for 6 hours; Figure II.5 presents the effect caused by the chemical modification using only peroxide in PLA.

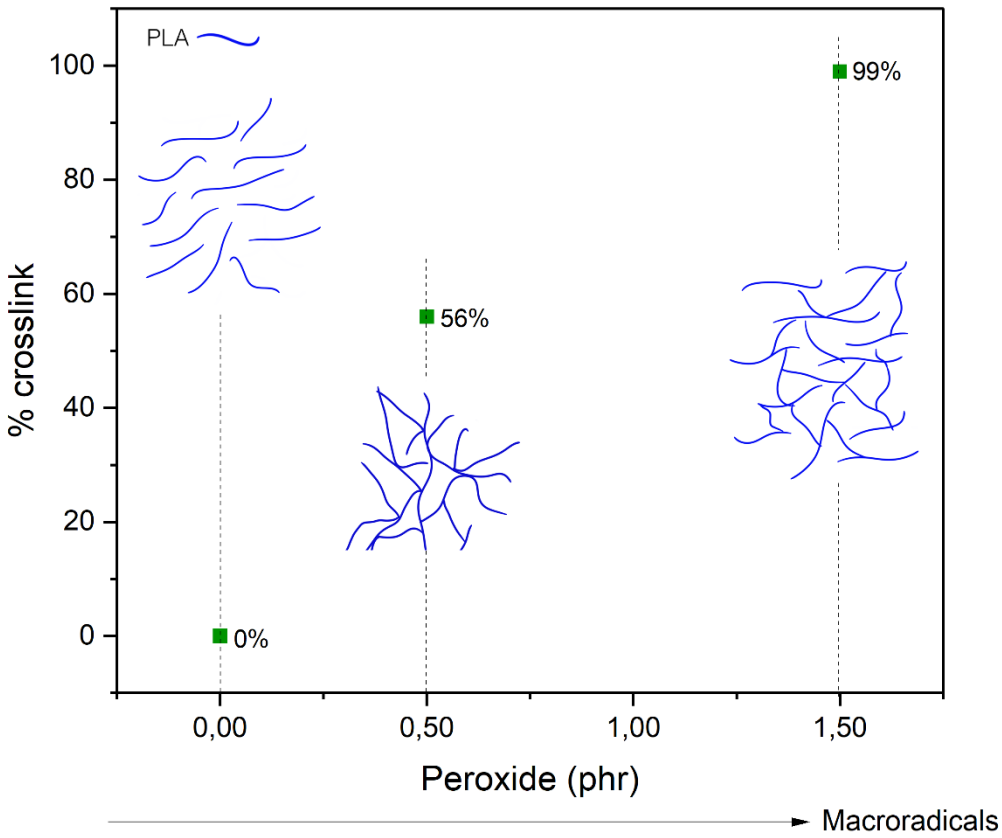

Figure II.5 – Percentage of crosslinking structures obtained by Soxhlet extraction during 6 hours at two concentrations of peroxide (0.5 and 1phr).

As shown in Figure II.5, the higher the peroxide concentration, the higher the level of PLA crosslinking (for 0.5 phr and 1.5 phr, the crosslinking percentage was 56.2% and 99.3%, respectively). This result is mainly due to the increase in the concentration of PLA macroradicals formed as the concentration of peroxide increases. The higher the concentration of PLA macroradicals, the greater the degree of recombination between those macroradicals, which leads to the formation of a crosslinked network of PLA chains. Due to the high level of crosslinking, sample 1.5_0 was not analyzed. Sample 0.5_0, on the other hand, was analyzed by filtering out the crosslinked portion.

When GMA is added to the reaction medium, there is a competition between the recombination of PLA macroradicals and the grafting of GMA onto the PLA macroradical. The preferential reaction will result from the relative concentrations of peroxide and monomers in the reaction medium. Table II.3 shows the occurrence of crosslinking for the samples.

Table II.3 – Crosslinking percentage of the samples.

		Crosslinking percentage		
		GMA (phr)		
		0 (absense)	**1 (low level)**	**3 (high level)**
Peroxide (phr)	**0 (absense)**	0%[c]	-	-
	0.5 (low level)	56%[b]	0.1%[c]	0.2%[c]
	1.5 (high level)	99%[a]	100%[a]	0.3%[c]

For the lowest peroxide level (0.5phr), adding GMA at both the upper and lower levels reduced the crosslinking percentage from 56% to values close to 0%. Furthermore, as observed in Table II.2, both formulations had an increase in molar mass compared to pure PLA, indicating that chain extension occurred mainly through the insertion of branches (Figure II.4, R5) and the reaction between PLA and GMA chain ends (Figure II.3). In addition, it can be seen that the increase in GMA concentration from 1 phr to 3 phr increased $\bar{M}_w$ by approximately 8% and $\bar{M}_n$ by 18% suggesting that, for this amount of macroradicals, the higher monomer concentration increased the likelihood of grafting occurring on the PLA macroradicals, in addition to the reactions between

the PLA and GMA chain ends. This result can be validated by the acidity content of the samples since GMA will react preferentially with the acid groups of PLA. Sample 0.5_3 had the greatest increase in molar mass and the lowest percentage of acidity among the samples with a low peroxide level, indicating the effectiveness of the reaction between PLA and GMA. Under these conditions, recombination reactions between macroradicals are less likely to occur. Contrarily, when the concentration of GMA in the medium is low, the predominant reactions will be recombination between PLA macroradicals, concomitantly with GMA grafting reactions, in which the latter will occur to a lesser extent.

For the higher peroxide level (1.5 phr) the concentration of GMA was decisive for the balance between crosslinking and branching reactions. As can be seen in Table II.3, the addition of 1 phr of GMA led to complete crosslinking of the sample (100%), while the addition of 3 phr of GMA produced the same crosslinking content as the samples with the lower level of peroxide (0.3%). This result suggests that the amount of PLA macroradicals formed was very high when the GMA concentration was at its lowest level (1 phr), which may have further favored crosslinking formation in the sample as a result of macroradicals recombination. On the other hand, the addition of GMA at a higher concentration (3 phr) was enough for the monomer to be grafted onto the PLA macroradicals, leading to the insertion of branches and, therefore, reducing the recombination between macroradicals that lead to the crosslinking of the material. For this formulation (1.5_3), the increase in $\bar{M}_w$ compared to pure processed PLA was approximately 170%, and the acidity content was the lowest among the modified samples.

To synthesize the correlations between concentrations of DCP and GMA, Figure II.6 shows possible structures formed due to the reactive process.

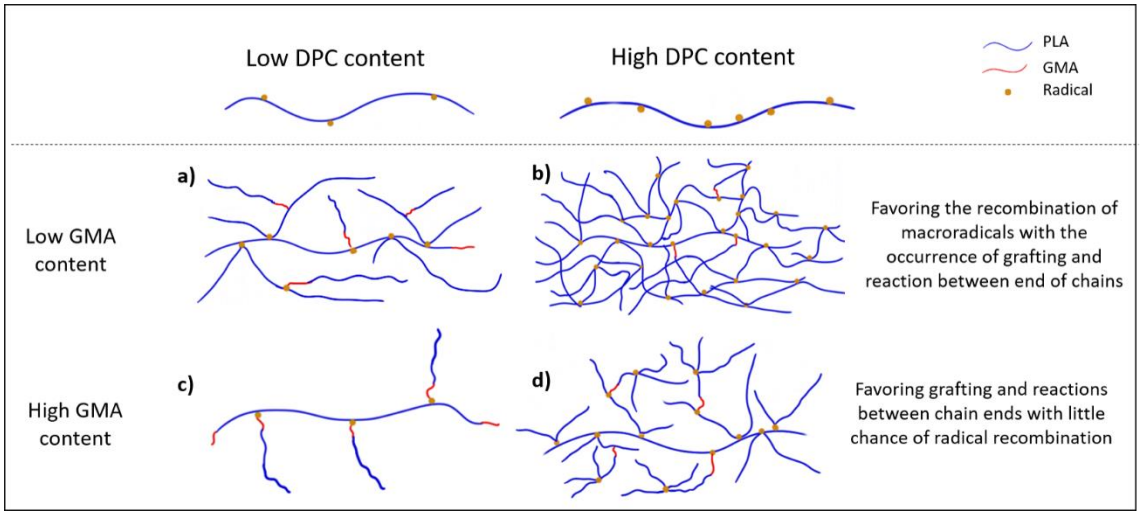

Figure II.6 – Possible chain structures formed as a result of variation of DCP and GMA concentration during the reactive process, where: a) represents sample 0.5_1; b) sample 1.5_1 which presented crosslinked structure; c) sample 0.5_3 and; d) sample 1.5_3.

FTIR and Nuclear magnetic resonance (NMR) analyses were carried out to confirm the reaction assumptions and the spectra are presented in the Appendix 1 and 2, respectively. However, by FTIR analysis no difference could be observed. On the other hand, the chemical modification was observed by NMR. As the analyses were carried out in solution and the abundance of ^{13}C is 1.1% and that of ^{1}H is 99%, changes can be observed in the chemical shifts of the secondary hydrogens of PLA and those of GMA. It can be inferred from comparing the PLA and modified PLA's spectra that in different proportions of peroxide and GMA, different products are formed. Analysis of sample PLA_0.5_1 indicates the production grafting of GMA onto PLA macroradicals, followed by chain extension by reaction with carboxylic end groups. This product is present in all formulations. The differences between the formulations are due to the presence of other products. In the case of sample PLA_0.5_3, unreacted GMA is present in the formulation, confirming the excess of GMA, which may have lubricated the system. In the case of PLA_1.5_3, in addition to the grafted PLA, the PLA chain is terminated with two isomers. The entire discussion of chemical shifts and proposed mechanisms is presented in Appendix 2.

Thermal analyses with DSC were performed to better understand chemical modification, and the results are presented in

Table II.4. The curves of second heating are presented in Appendix 3. For all modified samples, Tg was shifted to lower temperatures, as well as Tm. Furthermore, it was possible to observe that the crystallinity also decreased, mainly for formulation PLA_1.5_3, which presented a higher increase in molar mass, according to SEC results. Although small differences in Tg and Tm, these results can confirm structural modifications, with the possible insertion of branches, which could increase free volume and, as a consequence, result in lower Tg values, less structural organization, less perfect crystals, and lower crystallinity, compared to neat PLA.

Table II.4 – Thermal results from second heating curves by DSC analysis, from 0°C to 200°C, at 10°C/min.

Samples	**T_g**	**T_{cc}**	**T_m**	**ΔH_{cc} (J/g)**	**ΔH_m (J/g)**	**% crystallinity**	**% maximum crystallinity potential**
PLA_0_0	60.7	113.7	150.0	23.8	24.8	1.10	23.1
PLA_0.5_1	59.3	116.9	147.4	18.3	18.9	0.95	18.9
PLA_0.5_3	57.3	117.4	148.2	20.0	20.3	0.89	20.5
PLA_1.5_3	57.5	121.8	145.5	9.5	9.3	0.81	9.4

Although the $\bar{M}_w$ and $\bar{M}_n$ values were very similar for the reactions conducted at the lower peroxide level (PLA_0.5_1 and PLA_0.5_3), the percentage of acid groups was higher for the PLA_0.5_1, and also the torque values. Therefore, rheological analyses were carried out in the steady state and oscillatory regimes to better understand these differences.

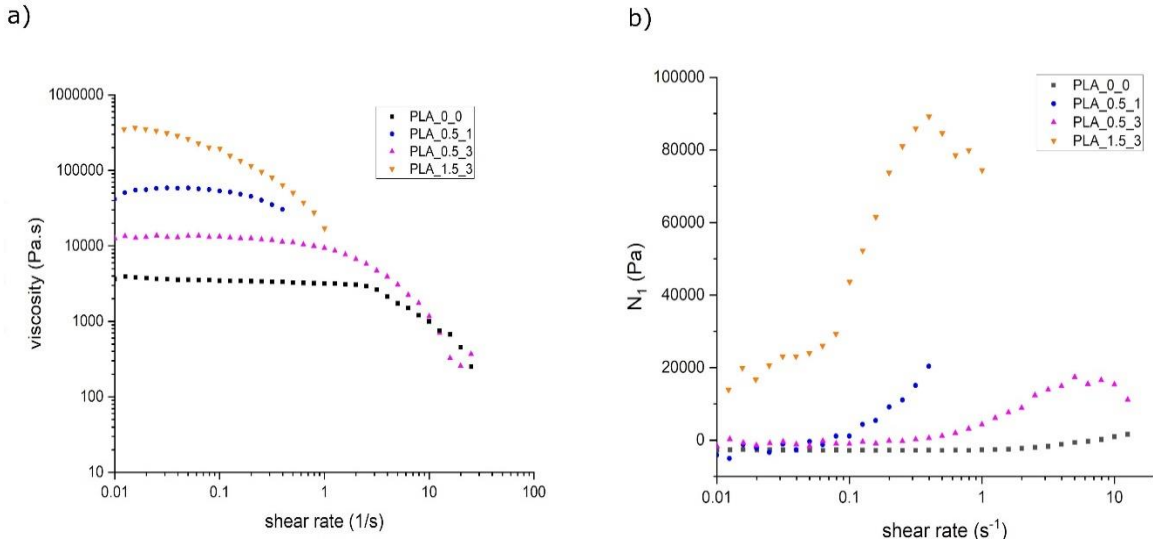

Figure II.7: Steady-state shear at T=180°C: (a) Viscosity *versus* shear rate (b) First normal stress difference (N_1) *versus* shear rate.

As can be seen from Figure II.7, the PLA_1.5_3 formulation had a higher viscosity and a higher first normal stress difference (N_1) than the other formulations at all shear rates; however, it attained a pseudoplastic behavior at lower shear rates. It is worthwhile to point out that long-chain branching (LCB) can increase both viscosity and elasticity [212] due to the formation of further entanglements. The earlier attainment of pseudoplastic behavior can be credited to its higher polydispersity. Therefore, long chain branches were probably formed by adding 1.5 phr of peroxide and 3 phr of GMA, as shown in Figure II.6. However, when comparing the PLA_0.5_1 and PLA_0.5_3 formulations, which presented very similar molar masses and polydispersity, it was observed that the viscosity at the Newtonian plateau (η_0) of the PLA_0.5_1 and the N_1 were much higher than the PLA_0.5_3 formulation. The difference between both formulations is the added amount of GMA. To be sure that residual GMA in the sample would not interfere with the analysis, purified samples were also studied and the results are presented in Appendix 4. No difference of behaviors was detected.

The molar masses of those two formulations were very similar. The molar mass of the PLA_0.5_1 was only 3% higher than the molar mass of the PLA_0.5_3 (within the experimental error); however, the η_0 of formulation

PLA_0.5_1 (approx. 5 X 10^4 Pa.s) was 416 % higher than the η_0 of formulation PLA_0.5_3 (approx. 1.2 X 10^4 Pa.s). A very slight increase in molar mass would not produce such a high increase in viscosity (recalling that for linear polymers, $\eta_0 \sim M^{3.4}$). Therefore, the increase in viscosity and elasticity of the PLA_0.5_1 was due to concurrent reactions between macroradical recombination and grafting of GMA onto PLA with subsequent reaction via epoxy group with PLA chain ends. When the concentration of GMA increased (PLA_0.5_3), the grafting reaction was predominant. In the latter case, greater free volume is associated with branching compared to recombination between macroradicals, which leads to higher viscosities.

To confirm the above-mentioned analyses, rheological analyses were performed in the oscillatory state, and Figure II.8a and Figure II.8b present graphics of tan δ vs. frequency and Cole-Cole, respectively.

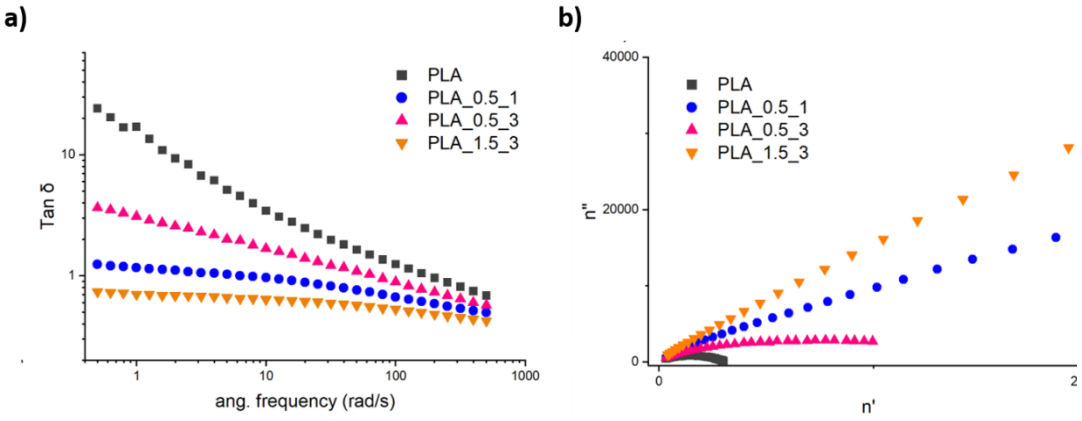

Figure II.8 – a) Rheological analysis in the oscillatory state for modified and neat PLA samples of tan δ *versus* frequency; b) Cole-Cole graphics for neat PLA and modified PLA. T=180°C.

As shown in Figure II.8a, PLA_0_0 presented a typical viscous fluid behavior in low frequencies in the terminal zone. For the modified samples, tan δ is lower but still presents a viscous fluid behavior for sample PLA_0.5_3. For samples PLA_0.5_1 and PLA_1.5_3, values of tan δ are low in low frequencies, decreasing to values near 1, forming a Plateau. These results indicate a likely formation of long chain branches for these formulations, with higher relaxation times.

Cole-Cole analysis (Figure II.8b) suggests the same interpretations, as it is possible to observe the formation of arcs for PLA_0_0, a typical behavior of linear polymers [99]. Sample PLA_0.5_3 also presents an arc form with a bigger diameter, indicating a higher molar mass. For formulations PLA_0.5_1 and PLA_1.5_3, it is not possible to observe the complete formation of arcs due to their very high relaxation times, suggesting the formation of long chain branches, making the material more elastic. Tian et al. also observed the same evidence for long-chain branch formation [213]. The authors evaluated the chain extension of PP during the reactive process with 2,5-dimethyl-2,5(tert-butylperoxy) hexane peroxide and pentaerythritol triacrylate (PETA).

4 Conclusions

This section presented the results obtained from the chemical modification of PLA by reactive processing, using GMA as the modifying monomer and DCP as the initiator. From the results and analysis found, it was possible to evaluate the influence of the reagents on the chain extension of PLA and the influence of the different concentrations on the chemical structures formed (linear extension, branching, cross-linking).

Concerning chemical modification, the study showed that there is competition between reactions during reactive processing, and depending on the concentrations of the reagents, this competition will favor the recombination of macroradicals, and/or the formation of branches, and/or linear reactions.

The presence of DCP isolated at the concentrations studied (0.5 phr and 1.5 phr) resulted in the crosslinking of the sample and the higher its concentration, the higher the crosslinking content. This result is due to the large number of macroradicals formed which recombine to create a complex network. However, for most of the samples, the crosslinking decreased to close to zero when GMA was added at different concentrations.

It is therefore clear that there is an optimum relationship between the concentrations of reagents in which the amount of macroradicals formed and the amount of GMA available in the medium will dictate the types of chemical structures that will be formed. Consequently, these relationships will result in different thermal and rheological properties.

II.2 Rheological properties and crystallinity influence on modified PLA foams

1 Introduction

Due to environmental concerns over the excessive use of fossil-based polymers, poly(lactic acid) has gained prominence because it is a material obtained from renewable sources, is biodegradable in compost conditions, biocompatible and produced on a large scale [68]. For this reason, it has been explored as an alternative in the production of polymeric foams that mostly use polymers from fossil sources [214]. In addition, recent literature has mainly investigated the behavior of the foaming process using supercritical carbon dioxide (sc-CO_2) as the physical agent, which presents non-toxicity, non-flammability, low cost, and chemically inert [26,27,214].

However, the low strength in the molten state and the slow crystallization rate of PLA makes the foaming process a challenge, as it generally results in foams with large, heterogeneous cell sizes, thick walls and low expansion ratios [99,210].

The literature has therefore explored various strategies to overcome these problems. The chemical modification of PLA using various chain extenders and/or peroxides is quite common [215–218], as is foaming by controlling crystallization [41,47,49,219,220].

In principle, factors that affect the viscoelastic properties of the molten polymer will affect the structure of the foams [221]. Li and coauthors [103] observed branching and cross-linking when modifying PLA with a random copolymer of ethylene and glycidyl methacrylate, which restricted cell growth due to the high viscosity, resulting in a decrease in cell size with increasing chain extender concentration. The same was observed by Venkatesan and colleagues [215], who used a multifunctional chain extender (Joncryl) as a modifying agent and linked the increase in molar mass and viscosity to the formation of branches. As a result, the modified PLA produced foams with homogeneous cell morphologies and an expansion ratio 8 times higher than pure PLA. Li and

colleagues [99] modified PLA with various chain extenders (1,4-butylene diacrylate (BDDA), trimethylolpropane triacrylate (TMPTA) and pentaerythritol tetraacrylate (PET4A)), in the presence of cyclic peroxide, and observed an increase in complex viscosity for all the samples. In addition, the authors identified through the vGP and cole-cole graphs a deviation in the modified sample's curves from pure PLA, which was linked to the presence of branched structures. These differences led to the production of foams with thin-walled cellular structures and an expansion ratio of up to 27, while pure PLA obtained 4.

However, rheological properties are not exclusive factors. Crystallization during the foaming process is crucial as it directly impacts the dissolution of CO_2 within the PLA matrix. CO_2 primarily dissolves in the amorphous phase, where the crystalline regions act as barriers to molecular diffusion. Furthermore, crystallization can influence cell nucleation, with crystals acting as nucleation sites, thereby controlling the foam's cellular structure [222].

During the gas saturation process with sc-CO_2, the gas molecules lubricate the system, allowing the polymer chains to be more mobile. This explains the fact that even at temperatures below the crystallization temperature of PLA, the material crystallizes in the presence of sc-CO_2 [223]. For the foaming process, this is important because the crystallization of the material during the CO_2 saturation phase will determine whether the expansion will take place in the presence or absence of crystals, thus characterizing the type of cell nucleation: as homogeneous or heterogeneous.

Li and collaborators [224] subjected a semi-crystalline PLA to isothermal pre-crystallization in order to regulate the structures of the PLA foam. They explained that increasing the number of crystals in the samples increased the viscoelasticity of the material, thereby reducing cell rupture. In the samples in which there was reduced crystallization, the expansion ratio was up to 10 times higher than in the PLA that did not crystallize, while as crystallinity increased, the expansion ratio tended to decrease, which the authors attributed to the fact that high amounts of crystals can limit cell growth. Yang and colleagues [52] carried out DSC analyses on the foams to understand whether crystallization occurred during the foaming process with sc-CO_2. They observed that at a high foaming temperature (120°C) the foams presented no melting peak, which showed that

there was no crystallization during gas saturation. For temperatures between 70 and 110°C, DSC analysis resulted in a melting peak with no crystallization peak, which was associated with the complete crystallization of the material during the foaming process.

Studying and understanding the factors that influence the cell structures of polymeric foams is important because they will affect the final properties of the foam. Small, closed cells with uniform distribution generally exhibit superior mechanical properties [12]. Thermal insulation can also be increased by increasing the expansion ratio since the thermal conductivity of the air is much lower than that of the matrix [225,226]. Foams with open cells, for example, have lower mechanical properties compared to closed cells, but present a high absorption and acoustic insulation capacity [12,36].

Therefore, this study aimed to understand the relationship between crystallinity and rheological properties in the cell structures of the foams produced. The findings may help to understand the formation of branched structures resulting from grafting or recombination of radicals, which consequently have different rheological properties and crystallinity, thus affecting the cellular structures of the foams produced.

2 Materials and Methods

2.1 Materials

The foams were produced using PLA modified with GMA in the presence of peroxide. A detailed description of these materials can be found in **section II.1**

2.2 Methods

2.2.1 Chemical modification

The chemical modification was carried out as described in section II.1. The experimental design was a 2^2 factorial one and the samples were modified in a torque rheometer for 6.5 minutes at 180°C in a nitrogen atmosphere. Table II.5 summarizes the formulations produced and the nomenclature for each one.

Table II.5 - Experimental design.

Identification	C_{DCP} (phr)	C_{GMA} (phr)
PLA_0.5_1	0.5	1
PLA_0.5_3	0.5	3
PLA_1.5_1*	1.5	1
PLA_1.5_3	1.5	3

Code of nomenclature: PLA_per_gma; *crosslinked sample

2.2.2 Batch foaming

The foaming process was done in an in-house device, in the melt state, using supercritical CO_2 as the blowing agent. The device consisted of a high-pressure pump of CO_2, an oven, and a hermetical cylinder, as shown in Figure II.9.

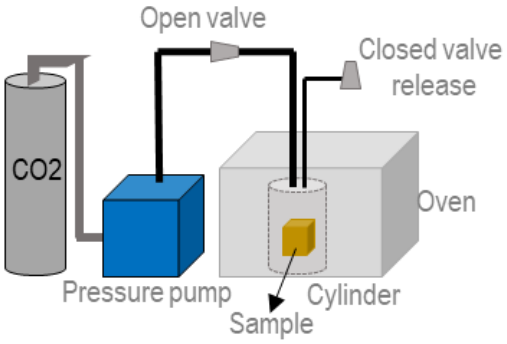

Figure II.9 – Scheme of the in-house made foaming device.

The process can be divided into 3 steps as shown in Figure II.10:

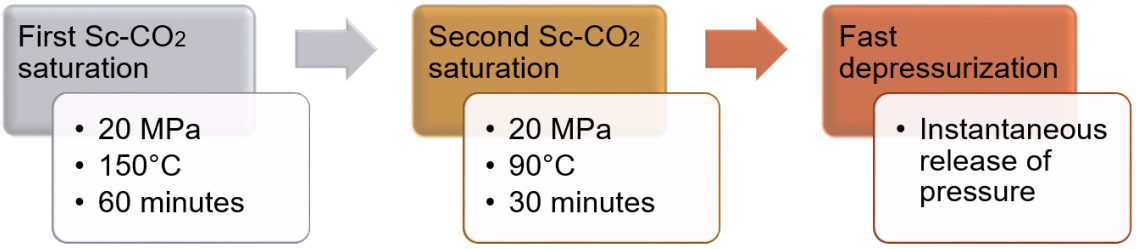

Figure II.10 – Steps for the foaming process with sc-CO_2.

The modified and neat PLA samples (approximately 0.4 g) were inserted in a cylindrical Teflon mold evolved by a hermetic cylindrical system; the sample was then saturated for 1 hour at 150°C and 20 MPa. The second step was lowering the temperature to 90°C for 30 minutes and 20 MPa. This decrease in temperature is necessary to increase the material viscosity, once in the first step, the high temperature (close to Tm) hinders the expansion due to the low viscosity. Finally, the pressure was quickly released by opening the valve. As mentioned in Chapter I, the rapid release of pressure allows the formation of cellular structures. The foamed samples were removed from the cylinder and left to cool at room temperature.

2.2.3 Rheological characterization

Rheological characterization was carried out using a tension-controlled TA Instruments AR-G2 rheometer with parallel plates geometry (d = 25 mm, gap between plates = 1 mm). The small amplitude oscillatory shear (SAOS) test was performed between angular frequency of 0.05 and 500 rad/s, at 180°C and under nitrogen atmosphere. All samples were vacuum-dried before the experiment (4 hours at 70°C).

2.2.4 Differential scanning calorimetry (DSC)

Differential scanning calorimetry (DSC) was performed in a TA Q2000 DSC. The foams were subjected to a heating cycle from 0ºC to 200ºC, at a rate of 10º/min. The samples were not dried before the analysis to preserve their thermal history. The crystallinity index (Xc) was calculated by using Equation II.4:

$$Xc = \frac{[\Delta H_m - \Delta H_{cc}]}{[\Delta H_m^o]} \times 100 \qquad \text{Equation II.4}$$

Where ΔH_m is the melting enthalpy, ΔH_{cc} is the crystallization enthalpy during the heating and ΔH_f^o is the melting enthalpy for a hypothetically 100% crystalline polymer. For PLA, the value adopted was 93 kJ/g [207,208].

2.2.5 Foam characterization

The densities of the foamed and non-foamed samples were determined using the water displacement method (ASTM D792-20), in triplicate, with each one measured five times. The volumetric expansion ratio (VER - φ) was calculated by the ratio between the density of the non-foamed material and the density of the foamed material.

A FEI Magellan 400L scanning electron microscope (SEM) was used for the morphological analysis. The foam samples were cryofractured using liquid nitrogen and then coated with gold. The cell structures (cell size and cell density) were characterized using the ImageJ program. Cell density (N) was calculated using Equation II.5, with at least 100 cells measured for each sample.

$$N = \left(\frac{n}{A}\right)^{3/2} \times \phi \qquad \text{Equation II.5}$$

Where N is the cell density, n is the number of cells in a known area A and ϕ is the volume expansion ratio.

2.2.6 Statistical analysis

When appropriate, statistical tests ANOVA, followed by Tukey's multiple comparisons test, were conducted with a 95% confidence level ($p < 0.05$ = significance level).

3 Results

As presented in section II.1, the experimental design for the chemical modification of PLA faced limitations, as the PLA_1.5_1 sample showed a high degree of cross-linking, as indicated by the Soxhlet extraction. Consequently, it was not possible to melt or solubilize this sample, making its rheological characterization and foam production impossible. Therefore, three of the four experimental design formulations will be studied in this section.

3.1 Rheological properties

In order to understand the cell structures from rheological data, a Small Amplitude Shear Oscillation (SAOS) analysis was carried out on the non-foamed samples. Figure II.11 shows the complex viscosity of the different formulations.

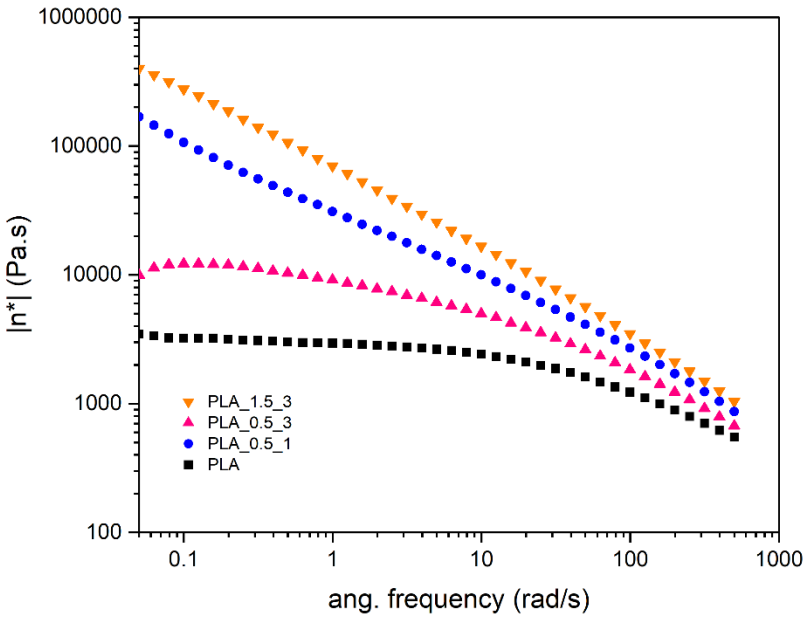

Figure II.11 – Complex viscosity obtained from 0.05 to 500 rad/s, at 180°C.

As detailed in section II.1, the properties of modified PLA indicate the presence of branching, evidenced by high viscosities and elastic properties such as the first normal stress difference (N1) and Cole-Cole plots that deviate from those of linear polymers. The complex viscosity and elastic modulus can indicate

a relationship between polymer chain structures and their rheological responses. Figure II.11 illustrates that the chemical modification of PLA leads to distinct rheological behaviors. Notably, the modified samples exhibit higher complex viscosities compared to pure PLA, with samples 0.5_1 and 1.5_3 demonstrating particularly high viscosity at shear rates approaching zero η_0 (as shown in Table II.6) and a pseudoplastic behavior observable from low frequencies, distinguishing them from the other samples.

This behavior aligns with the findings of Nouri and collaborators [227], who studied various branched structures such as 4-arms star, comb-like, and hyperbranched PLA. With the addition of a 5% initiator, all the samples exhibited similar behavior, with η_0^* in the order of 10^4 Pa.s (at 0.1 rad/s).

The melt elasticity also has a direct impact on the foamability of polymers. Figure II.12 illustrates the G' and G'' curves for the samples studied. From these results, it was possible to calculate the cross-over where G' becomes higher than G'' (Table II.6).

Table II.6 – Terminal slope, cross-over, and η_0^* values obtained from the graphs presented.

	Terminal Slope	**Cross-over (rad/s)**	**η_0^* (Pa.s) (at 0.05 rad/s)**
PLA	1.3	158.1	$3x10^3$
PLA_0.5_1	0.5	6.3	$1x10^6$
PLA_0.5_3	1.4	63	$1x10^4$
PLA_1.5_3	0.4	0.05	$4x10^6$

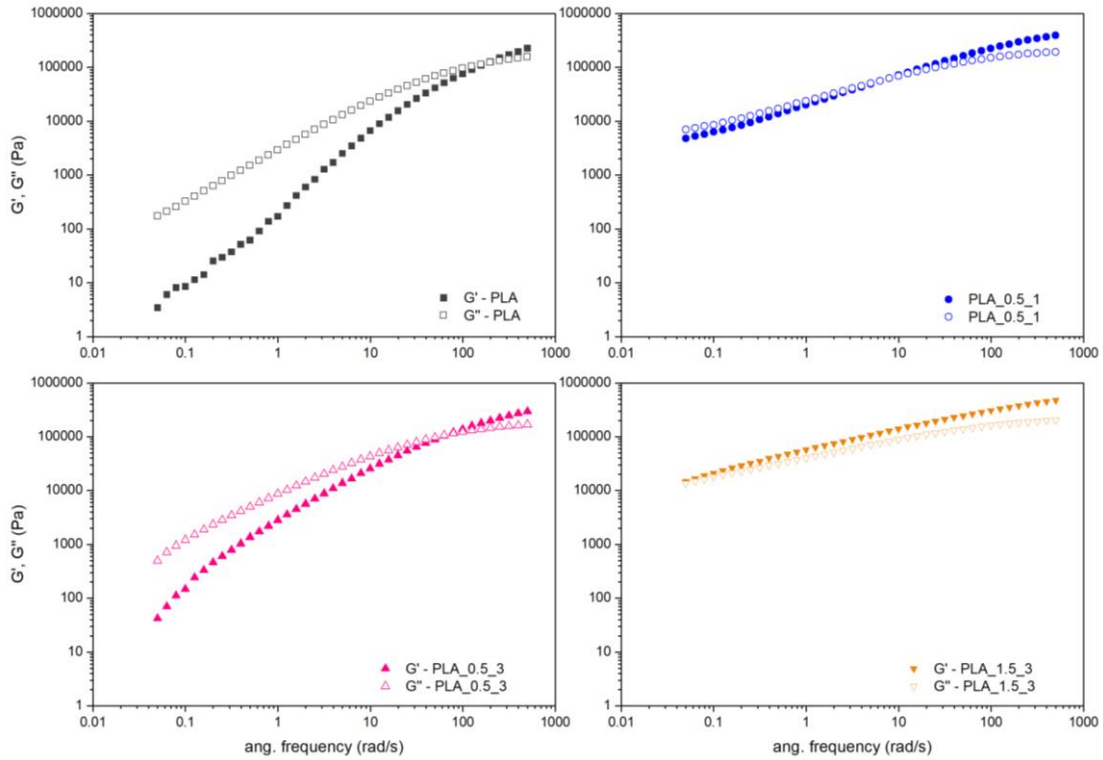

Figure II.12 – Plots of log G' and G'' *versus* log angular frequency from 0.05 to 500 rad/s, at 180ºC.

As illustrated in the figures, the loss modulus (G″) for the formulations PLA_0.5_1 and PLA_1.5_3, is lower across a broad range of frequencies. For these samples, the crossover has shifted to lower frequencies, with the latter exhibiting a crossover at the beginning of the test. This indicates that the elastic component of the material is more pronounced than the viscous component, resulting from the increased chain entanglement and consequent increased relaxation times.

To elucidate these differences in the elastic modulus, Figure II.13 displays the G′ curves for the studied samples, enabling a comparative analysis of the different curve behaviors. According to the literature, linear polymers exhibit a G′ proportional to approximately ω^2 at low rates on a log-log graph [108]. As shown in Table II.6, the terminal slope at low rates for neat PLA was 1.3, while for the PLA_0.5_3 sample, it was 1.4. These results indicate minimal branching in the structure of the latter sample, suggesting that its chain structure is closer to that of neat PLA. Conversely, the other modified samples demonstrated slopes

between 0.4 and 0.5. Terminal slopes between 1.03 and 1.39 have been reported in the literature for PLA and have been directly associated with the branched nature of the materials [227], indicating that these samples possess more complex structures.

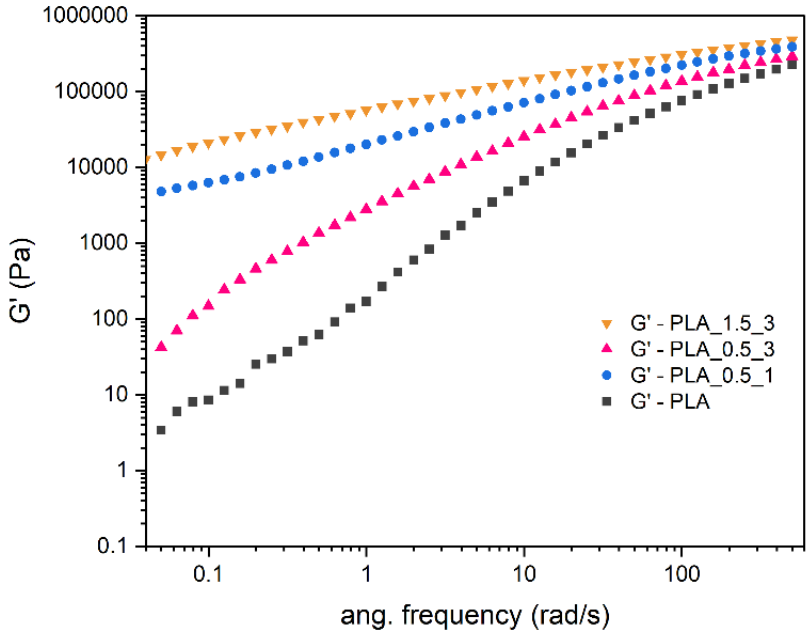

Figure II.13 – Log G' *versus* log angular frequency performed at 180°C, from 0.05 to 500 rad/s.

Ultimately, the van Gurp-Palmen (vGP) plot is utilized to distinguish between linear and branched polymer structures [228]. The behavior of linear polymers is characterized by a phase angle δ close to 90° at low |G∗| values, which is typical of linear polyethylenes. The extent of deviation from this behavior is indicative of the presence of branched structures [229].

Figure II.14 presents the vGP plot for the samples analyzed. The graph illustrates that neat PLA exhibits behavior consistent with linear polymers, displaying a well-defined terminal zone near the 90° phase angle. However, the modified samples demonstrate a noticeable deviation from this pattern, particularly evident in the PLA_1.5_3 and PLA_0.5_1 samples, suggesting the presence of branching. At equivalent values of the complex modulus, these samples exhibit a reduced phase angle, indicating a less viscous behavior

compared to neat PLA. Similar deviations from the behavior of neat PLA have been observed by other researchers [210,216,217].

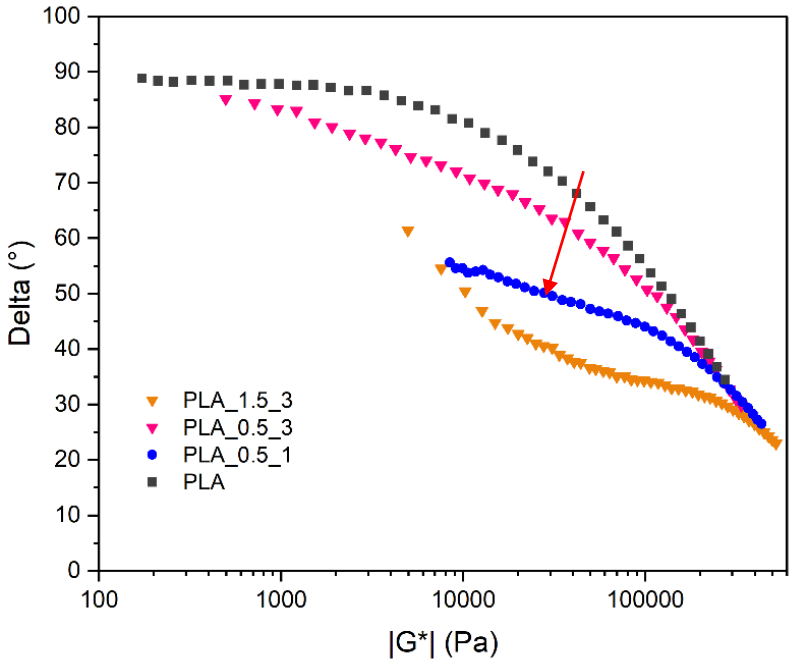

Figure II.14 - van Gurp-Palmen (vGP) graph for the samples studied

This analysis allows the correlation of the observed rheological properties with the tested concentrations of glycidyl methacrylate (GMA) and dicumyl peroxide (DCP). Given that all modified samples exhibited higher viscosity and elasticity than pure PLA, comparisons will be focused only on the modified samples. Three distinct relationships can be identified between the concentrations of GMA and DCP to elucidate their respective influences:

- **Influence 1 –** Increasing in peroxide (PLA_**0.5**_3 vs. PLA_**1.5**_3)**:** There is a significant increase in both complex viscosity and storage modulus. The substantial deviation observed in the vGP graph indicates the presence of branching structures.
- **Influence 2 –** Increasing in GMA (PLA_0.5_**1** vs. PLA_0.5_**3**): A notable decrease in complex viscosity and storage modulus is observed, with the behavior approaching that of linear polymers, as depicted in the vGP graph.

- **Influence 3 –** Increasing in peroxide and GMA (PLA_**0.5_1** vs. PLA_**1.5_3**): There is an increase in complex viscosity, with a predominance of storage modulus over loss modulus, suggesting high elasticity. The behavior in the vGP graph is similar for both samples, yet both exhibit significant deviations from the behavior of linear polymers. This suggests the presence of long chain branches and recombination between macroradicals without the formation of crosslinks.

Understanding the influence of GMA and DCP on the structure of PLA and, consequently, the rheological properties of the material, provides valuable insights into how these factors will impact the cellular structures of the resulting foams.

3.2 Foamability of modified PLA

In general, the literature shows that the chemical modification of PLA with various chain extenders and/or peroxides results in foams with more controlled structures due to the increase in melt strength [215,217].

As can be seen in Figure II.15 (at low magnification), unmodified PLA has large cells with heterogeneous shapes and misshapen regions where thick cell walls can be seen (identified by the red circles). The modified samples, on the other hand, show smaller cell sizes, in which sample PLA_0.5_3 has a more heterogeneous morphology when compared to the other two, with ruptured structures, that lead to large voids, as identified by the red arrows. Less obviously, sample PLA_1.5_3 also shows heterogeneity in its cell structures, with larger ruptured cells. In general, sample PLA_0.5_1 shows smaller cell sizes with greater homogeneity.

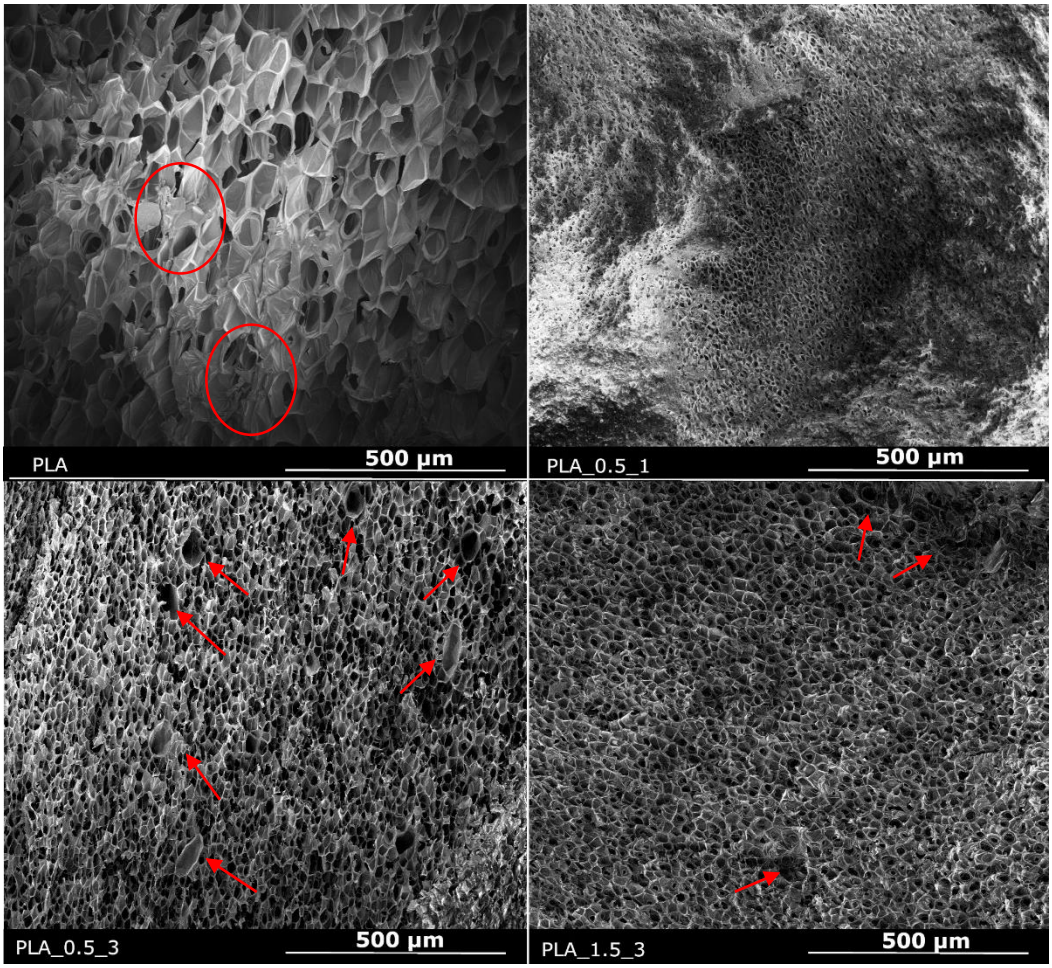

Figure II.15 – SEM images of neat and modified PLA at a magnification of 250x.

These observations were confirmed by the characterization of the structures. Figure II.16 and Figure II.17 illustrate, respectively, higher magnification images (1200x) as well as their respective cell size distributions and the foam density, cell density values, volume expansion ratio and average cell size.

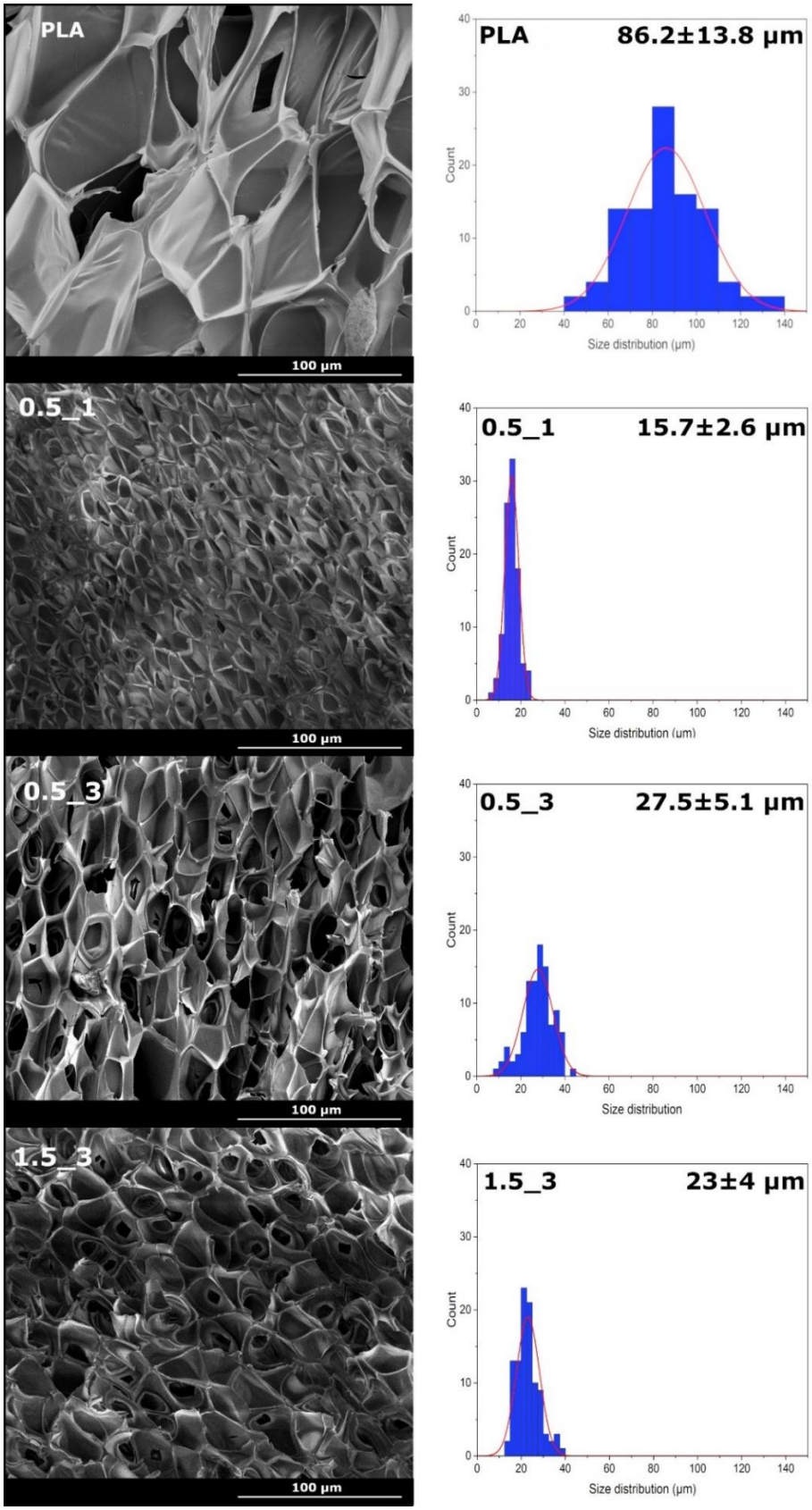

Figure II.16 – Morphologies of cell structures obtained by SEM at 1200x magnification, with graphs of the respective cell size distributions.

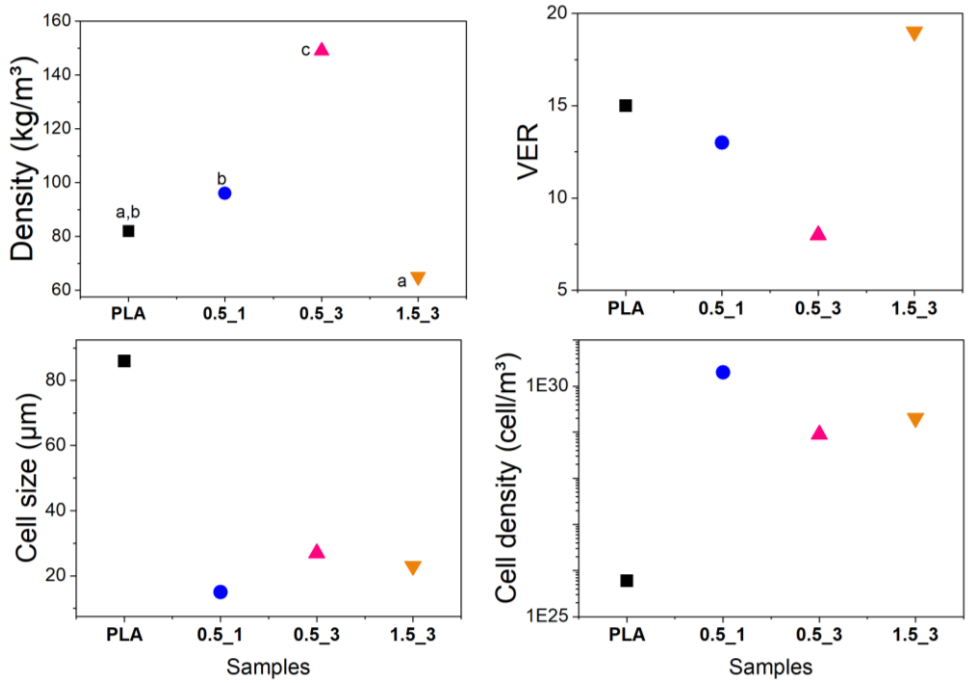

Figure II.17 - Density, volume expansion ratio (VER), cell size and cell density values. Equal letters correspond to statistically similar samples.

As can be seen, the modified PLA was able to produce microcellular foams, with average sizes of around 15 and 20 µm. According to the statistical test, all the samples showed a significant difference in size, including neat PLA.

According to the cell size distribution graphs, it is clear that neat PLA resulted in cells with larger sizes and a wide distribution, which is a result of the heterogeneity of the structures. With the addition of the modifiers, the cells presented a decrease in size, in which sample PLA_0.5_1 resulted in the smallest average and narrowest distribution.

The statistical test showed that the significant difference between the densities of the samples is mainly between the modified ones. Following the same idea as before, it is possible to correlate the structures achieved to the concentrations of peroxide and GMA.

- **Influence 1** - Increase in peroxide (PLA_**0.5**_3 vs. PLA_**1.5**_3): increase in VER, decrease in cell size and increase in cell density.

- **Influence 2** - Increase in GMA (PLA_0.5_**1** vs. PLA_0.5_**3**): decrease in VER, increase in cell size and decrease in cell density.
- **Influence 3** - Increase in peroxide and GMA (PLA_**0.5_1** vs. PLA_**1.5_3**): Increase in VER, increase in cell size and decrease in cell density.

It is therefore understood that in Influence 1, the expressive increase in viscosity and elasticity resulted in an increase in VER and a decrease in cell size, which increased cell density. Therefore, cell density was decisive in the material's foamability. Influence 2, on the other hand, caused a decrease in VER, which must be the result of the decrease in viscosity and elasticity of the material, which did not have enough resistance to prevent the cells from coalescing. As a result, the decrease in cell density resulted in a decrease in VER. Finally, Influence 3, as well as Influence 1, also increased VER, but with an increase in cell size, which must be the result of the increased elasticity of the samples and the lower degree of heterogeneous nucleation of cells, due to their lower crystallinity [230].

However, for semi-crystalline polymers, it is known in the literature that crystallization can occur during the gas saturation phase, which will have a direct influence on the structures formed. It is therefore essential to investigate the presence of crystals during the foaming of the material.

3.3 Crystallinity influence on foams

In order to understand the role of crystals during the foaming process, a DSC analysis of the foams was carried out. The results can be found in Figure II.18.

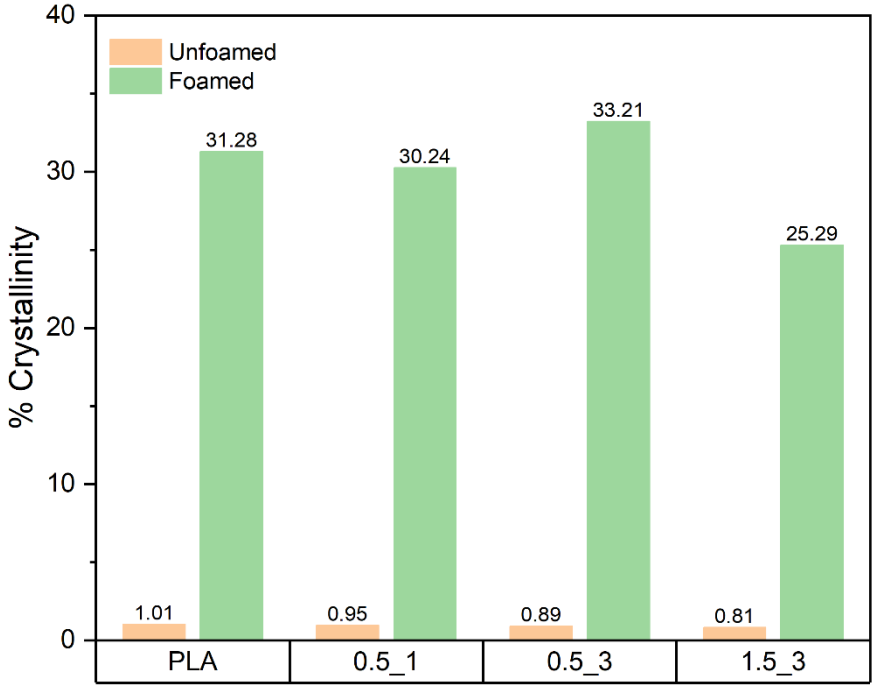

Figure II.18 - Differences in the crystallinity percentages of the foamed and non-foamed samples (Following Equation II.4).

As can be seen, all the foamed samples, including neat PLA, showed an increase in the percentage of crystallinity after the foaming process. The PLA_1.5_3 sample showed the smallest increase in crystallinity, which can be explained by the complex branched structure due to grafting and possible recombination of radicals, which, even with the lubricating effect of sc-CO_2, was unable to organize itself at the same level as the other samples. However, it is possible to state that, even if in different magnitudes, all the samples had a heterogeneous cell nucleation process. This may explain, for example, why neat PLA was able to expand, even though it had low elasticity in the melt. According to Li and colleagues [224], increasing the number of crystals can increase the elastic nature of the material, reducing cell rupture. For the other modified samples, other factors influence foaming due to changes in the structure of the material, which was not the case for neat PLA.

Another observation is that even though the PLA_1.5_3 sample had the highest storage modulus and viscosity values, the resulting structures did not have the smallest cell sizes or the narrowest distribution. This can be explained

by the smaller number of crystals present during saturation with sc-CO_2. The smaller the amount of crystals, the smaller the nucleation, so the cells can grow more, which explains the lower cell density for this sample when compared to PLA_0.5_1.

In general, with the observations made, the difference in crystallinity between the PLA_0.5_1 and PLA_1.5_3 samples seems to have been the decisive factor in determining the cell structures formed, since the experiments were all carried out under the same conditions. The two samples showed the greatest elasticity and viscosity, but the higher percentage of crystallinity in the PLA_0.5_1 sample may have been the reason why the cells showed smaller sizes and a more homogeneous distribution.

For sample PLA_0.5_3, crystallinity was the highest among the samples, which helped with cell nucleation and increased melt strength. However, the strength was not enough to prevent the cells from coalescing.

This shows that the foaming of polymeric materials is complex and depends on several factors. The same factors will not always have the same magnitude of contribution [230]. For the present study, a relationship could be established between the complex viscosity of the material and the percentage of crystallinity achieved during saturation with sc-CO_2, as can be seen in Figure II.19.

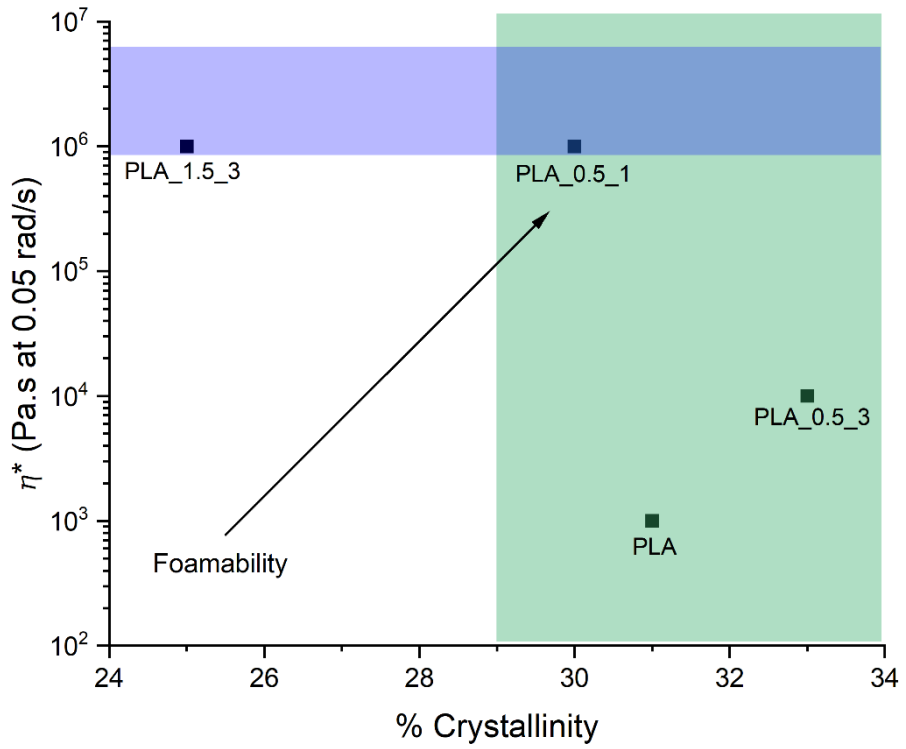

Figure II.19 - Relationship between crystallinity and complex viscosity for the production of foams with controlled and uniform sizes.

As can be seen, crystallinity close to 30% with a complex viscosity of around 10^6 Pa resulted in homogeneous structures with small cells and closed pores. Chen and collaborators [51] analyzed PLA with different levels of D-isomer to understand the role of crystallinity in foams. The authors also observed that a minimum crystallinity limit resulted in closed and homogeneous pore structures, where for the low crystallinity grade it was between 18 and 24% and for the more crystalline grade the values were between 32 and 39%.

This relationship shows that the increase in complex viscosity with the increase in crystallinity led to the production of suitable structures. However, it is known that this ratio can only increase up to an optimum condition, as very high viscosities can make the melt strength too high for the material to expand [103] and very high crystallinity can make it difficult for CO_2 to dissolve in the material [48], reducing foamability.

4 Conclusion

This study aimed to understand the influence of the rheological properties and degree of crystallinity of modified PLA samples on the final cell structures of their respective foams.

The properties resulting from modification with GMA and DCP cannot be directly related to the final cell structures formed, as the crystallization of the material during the CO_2 saturation stage will also influence the process.

The increase in the expansion ratio will be determined either by the increase in cell size or by the increase in cell density, both of which can be determined by the crystallinity of the material.

It can be concluded that crystallinity can favor the formation of small, homogeneous structures at a given viscosity, since high crystallinity at low viscosities resulted in large structures with many coalesced cells.

On the other hand, high viscosities hinder the formation of crystals, which reduces the nucleation of bubbles, resulting in larger cells.

Other factors influence the process, such as temperature, time and pressure, among others. It is important to highlight that the structures were achieved without the use nucleating agents, which can also influence the process.

Therefore, this study showed that there is an optimum conditions window that combines viscosity *versus* crystallinity to achieve cells with uniform structures. Understanding the relationship between polymer properties and the cell structures formed is essential for determining the properties of the final foam products, which can be applied in various sectors. In addition, the fact that the material comes from renewable sources and can biodegrade under composting conditions also helps to mitigate the problems currently faced by the excessive use of conventional plastic products.

Conclusion Chapter II

The aim of Chapter II was to investigate the chemical modification of PLA as a strategy to enable the production of foams with controlled cell structures.

The chemical modification of PLA with GMA in the presence of DCP showed that there is an optimum relationship between the concentrations of reagents, which will dictate the types of structures that will be formed (branching, crosslinking, radical recombination, and linear extension).

In the two formulations in which viscosity and elasticity were higher, there was a direct effect on the foams produced, which resulted in smaller cells sizes and a more homogeneous distribution. However, among these two formulations, the one with the lowest viscosity and elasticity had even smaller cells, which was associated to its higher crystallinity.

Therefore, this investigation has shown that controlling the rheological properties of the material to be foamed is essential in order to achieve small and homogeneous cells, although crystallinity can be decisive. Thus, for this study, there is an optimum ratio between viscosity and crystallinity that resulted in higher cell density and smaller cell sizes (approximately 15 µm).

Chapter III

CNC functionalization and nanocomposites foams

CHAPTER III CNC FUNCTIONALIZATION AND NANOCOMPOSITES FOAMS

Introduction to Chapter III

The aim of **Chapter III** was to study a second strategy to achieve smaller and more homogeneous cell structures in PLA foams, by foaming nanocomposites with CNC.

Therefore, **Section III.1** will present the functionalization of CNC, by mechanochemistry, using n-octadecyl isocyanate as a reagent, in order to increase the hydrophobic character of the nanocrystals and thus check the compatibility with the matrix. In literature, the process of CNC functionalization are mainly using different solvents and time-consuming reactions. This section will propose a solvent-free and fast method, using low concentration of reactant to functionalize CNC.

Subsequently, in **Section III.2**, the production and characterization of PLA nanocomposites incorporated with neat and modified CNC will be explored, to investigate whether the introduction, concentration, and type of CNC affected the cellular structures of the nanocomposites foams. The incorporation of CNC in PLA matrix is already know in literature, as well as the role of functionalization in improving compatibility with polymer. However, investigations on PLA/CNC nanocomposites foams are still not as explored as the foaming of PLA incorporated with fiber and nanofiber.

Therefore, this Chapter intend to provide new insights on more sustainable methods to functionalize CNC, as well as the role of CNC in PLA foams structures.

III.1 CNC functionalized with long aliphatic chains by mechanochemistry: a green and solvent-free method

1 Introduction

Cellulose nanocrystals have been attracting attention not only because of their renewability, sustainability, and abundance but also because of their lightweight, nanoscale dimension, unique morphology, and so on [231]. CNCs exhibit properties such as high stiffness, high specific surface area and low density, characteristics that lead to a good candidate for advanced polymeric nanocomposites [131].

However, because of the high specific surface area and the large number of hydroxyl groups (OH) on the CNC surface, the material presents an intrinsic hydrophilicity character, which leads to a strong self-aggregation because of the strong inter/intramolecular hydrogen bonds of OH groups [232]. As a result, the uniform dispersion of CNC in a hydrophobic polymeric matrix becomes a challenge. This leads to the necessity of finding a match between the surface character of the matrix and filler. The most common strategy adopt to solve this problem is the CNC surface functionalization by using surfactant or covalently grafted hydrophobic materials [131].

In this context, it is common to observe studies performing chemical modification on CNC surfaces, thanks to the high availability of hydroxyl groups. Some examples are the use of materials such as cinnamate [233], succinic anhydride [234], tannic acid, octadecyl amine [235], lauric acid, stearic acid, poly(glycidyl methacrylate) [236], n-octadecyl [177,181,237], among others.

As a result, CNC has been used in several applications as a reinforcing agent in nanocomposites [169], biomedical engineering (antibacterial/antiviral agents, tissue engineering, scaffolds, sensors, drug delivery vehicles, etc [132,238]), wastewater treatment [238–240], energy and electronic sectors [238,241], smart polymers and hybrid systems [242] and so on.

In general, CNC chemical modification evolves chemicals and solvents in its procedure, in addition to the fact that can take several hours for the reaction to be concluded. For this reason, a strategy is mechanochemistry, which performs chemical modifications in substances by applying mechanical action, inducing chemical and physical changes [243]. Ball milling is an efficient technique to perform mechanochemistry, which allows the process to be performed without the use of organic solvents [186].

Kuga and Wu [244] present in their review several works adopting mechanochemistry as the method for modification of cellulose fibers, such as esterification and saccharification. However, the study of cellulose nanocrystal functionalization by mechanochemistry is more restricted. The literature presents several works on CNC extraction by mechanochemistry using different strategies and solvents [243,245,246], however, the functionalization process is rare. In 2015, Lu and collaborators [247] extracted CNC from bamboo pulp by mechanochemistry using acetic acid and 4-dimethylaminopyridine (DMAP) to perform extraction and esterification in one step. From 1 to 2 hours of milling the degree of substitution (DS) was increased, while in 3 hours the DS decreased, probably because of the destruction of crystalline regions. Tang and co-authors [248] also extracted CNC and functionalized them by mechanochemistry combined with ultrasonication, using maleic anhydride and sulphuric acid, varying the time between 0.5 and 2 hours. As a result, was observed that at 2 hours of milling, the crystalline structure was destructed, and the degree of substitution was decreased.

In this context, this section aimed to investigate CNC functionalization by mechanochemistry method using n-octadecyl isocyanate as a reactant, in a low concentration, to enhance their surface hydrophobicity character to produce polymer nanocomposites.

2 Materials and Methods

2.1 Materials

CNC used was purchased from CelluForce Canada, which is produced from cellulose wood fibers by sulfuric acid treatment. n-Octadecyl Isocyanate (n-OI) was purchased from Sigma-Aldrich and was used as received. Acetone was purchased from Carl Roth. Figure III.1 shows the chemical structures of n-OI.

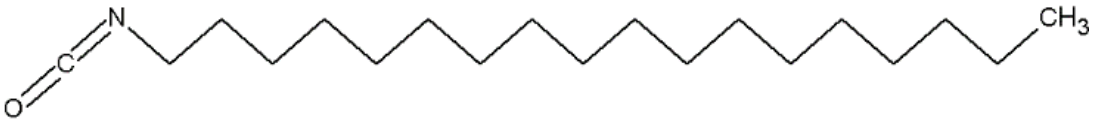

Figure III.1– Chemical structure of n-octadecyl Isocyanate.

2.2 CNC chemical modification

CNC chemical modification was performed using ball milling, a vibratory device Cryomill from Retsch. The grinding jar has a volume of 20 mL and it is made of zirconium dioxide (ZrO_2), as well as the balls used, which presented a diameter of 5 mm and were 50 in number. According to the manufacturer, the jar should be loaded with a ratio of 1/3 for reagents, 1/3 for balls, and 1/3 for air.

Dried CNC (105°C for 18 hours) was added into the ball milling reactor, along with n-OI, in a proportion of 1:1 molar ratio between anydroglucose unit (AGU) and n-OI. The reaction was performed for 15 minutes, at 30 Hz and room temperature. The resulting CNC was recovered and washed with acetone by 3 centrifuging cycles at 20°C, 10000 rpm (16211 G), and for 15 minutes. Modified CNC was left to dry at room temperature during the night and then was dried in the oven at 105°C for 18 hours. Figure III.2 shows the jar filled with zirconium dioxide balls.



Figure III.2 – Grinding jar made of zirconium dioxide filled with 50 zirconium dioxide balls.

2.3 CNC characterization

2.3.1 Fourier-transform infrared (FTIR) spectroscopy

FTIR spectra of neat CNC and modified CNC_n-OI were acquired on a Perkin Elmer Spectrum 65 spectrometer by ATR method. The powder was gently smashed in a mortar and pestle and deposited on the device. The absorbance spectra were recorded between 4000 cm^{-1} and 600 cm^{-1} with a resolution of 4 cm^{-1} and 64 scans. Measurements were done at least in duplicate for each sample.

2.3.2 X-ray photoelectron spectroscopy (XPS)

Surface chemical analysis has been carried out using X-Ray Photoelectron Spectrophotometer (XPS), the analyzed depth is inferior to 10nm. The XPS K-Alpha device (Thermofisher) was used. The substrates were positioned at an angle of 90° under an ultrahigh vacuum of less than 10^{-7} Pa. Samples were pressed at 6 tons for 5 minutes and then were dried in the oven for 24 hours before the measurements. At least two measurements were done for each sample.

2.3.3 Elemental Analysis

Elemental analyses of CNCs samples were carried out on a Thermoscientific FlashSmart elemental analyzer, equipped with a 32-sample autosampler and 2 chromatographic columns. The elements measured were C, H, N, S, and O. The results were provided with an absolute precision of ± 0.2% and were validated by at least 2 tests.

2.3.4 X-ray diffraction (XRD)

XRD acquisitions were performed with an X'Pert Pro MPD X-ray diffractometer from the PANalytical company. Measurements were collected in reflection mode using the Bragg-Brentano geometry. The x-ray source was a copper anode with the associated wavelength from the Cu Ka transition (1.5418 Angström). Samples in the powder were added into the small cavity of a Zero Diffraction Plate (diameter 16mm, cavity deepness 200µm) and smoothed with a glass slab. The crystallinity index (CI) was calculated according to the Segal height peak method [249], as shown in Equation 3.1:

$$CI = \frac{1 - I_{am}}{I_{002}} \times 100 \qquad \text{Equation III.1}$$

Where I_{am} is the intensity at the minimum between peaks 002 and 001, and I_{002} corresponds to the crystalline peak.

2.3.5 Transmission electron microscopy (TEM)

Images were recorded with a JEOL JEM-2100-Plus microscope operating at 200 kV and equipped with a Gatan Rio 16 digital camera. Droplets of dilute CNC suspensions in water (neat CNC) or ethanol (modified CNC) were deposited onto glow-discharged carbon-coated TEM grids. After 2 min, the liquid in excess was blotted with filter paper, and before drying, a droplet of 2 wt% uranyl acetate

negative stain was deposited. The stain in excess was wicked off and the specimen was allowed to dry. The characterization of CNC was made by digital image analysis, thought Software *ImageJ.*

2.3.6 Dynamic light scattering (DLS)

CNC size distribution was estimated by DLS (Dynamic Light Scattering) using a VASCO particle size analyzer, in which a diluted suspension of neat CNC (in water) and modified CNC (in acetone) at around 10^{-2}-10^{-3} wt% was introduced. At least ten measurements at 15-second time steps and a limit noise ratio of 0.7 were carried out for samples and averages were used for discussion. It is known that CNC particles are rod-like in shape and the model to calculate the diameter by DLS considers the hydrodynamic radius. Because of this, the diameter is not well represented, the reason why only the distribution is being considered.

2.3.7 Contact Angle

Contact angle analysis was performed using the Attension Optical Tensiometer, model Theta Flex, from Biolin Scientific, equipped with a digital camera with zoom, CMOS 2/3" USB 3.0, with a maximum resolution of 1984x1264 pixels and a maximum image measurement speed of 3009 fps. A 5 µl droplet of distilled water was deposited on CNC films or modified CNC pellets, at room temperature. The acquisition of measurements was recorded for 30 seconds. For all samples, at least five measurements were repeated, and the biggest and smallest values were discarded for the average calculation used in the discussion.

3 Results

3.1 CNC chemical modification

After chemical modification with n-OI, was expected that the OH groups from CNC and the isocyanate group from n-OI would react forming the grafting with a long aliphatic chain, as can be observed in Figure III.3.

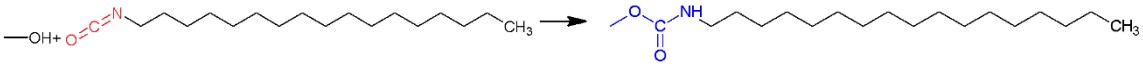

Figure III.3 – Chemical reaction between the OH group from CNC and isocyanate groups from n-OI.

To confirm chemical modification, FTIR was performed (Figure III.4) and it is possible to observe intense bands at 1615 cm^{-1} and 1574 cm^{-1}, assigned to amide I and amide II vibrations, respectively, which means the presence of ureic linkage formed during the reaction. A small shoulder at 3400 cm^{-1} is observed for amine stretching. It is also possible to note an increase in band characteristics of the grafted alkyl chain (-CH3 and -CH2 groups) at 2848 and 2915, which corresponds to the long chain grafted. The absence of bands at 2260 cm^{-1} is indicative that no more isocyanate functions were present after 3 cycles of washing in acetone [177].

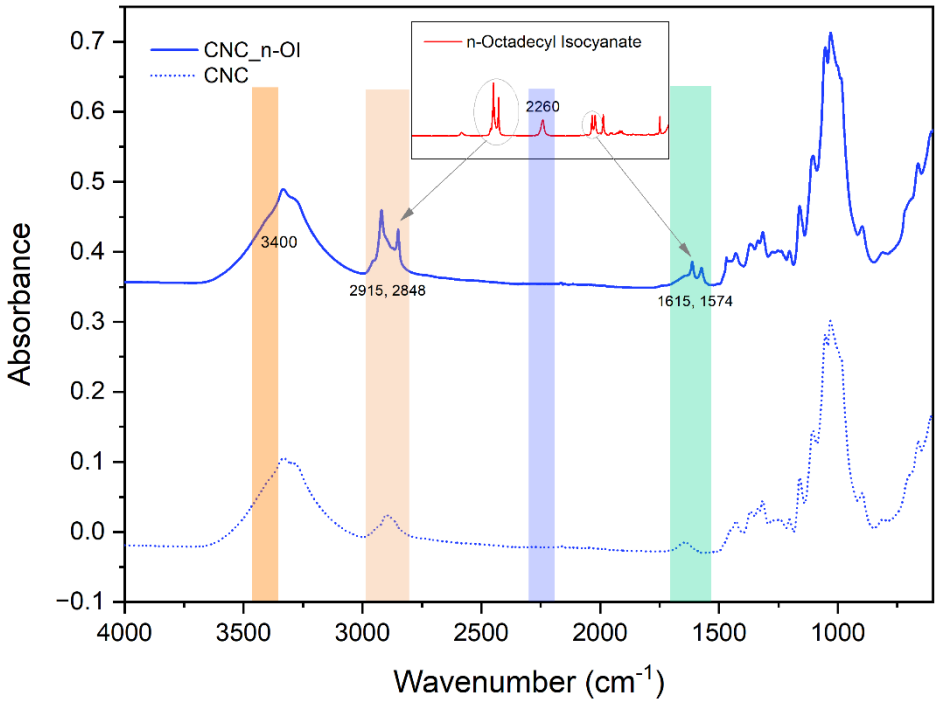

Figure III.4 – FTIR curves of neat CNC and CNC modified with n-OI.

To be sure that surface grafting occurred at the surface, XPS analysis was performed, and curves are present in Figure III.5.

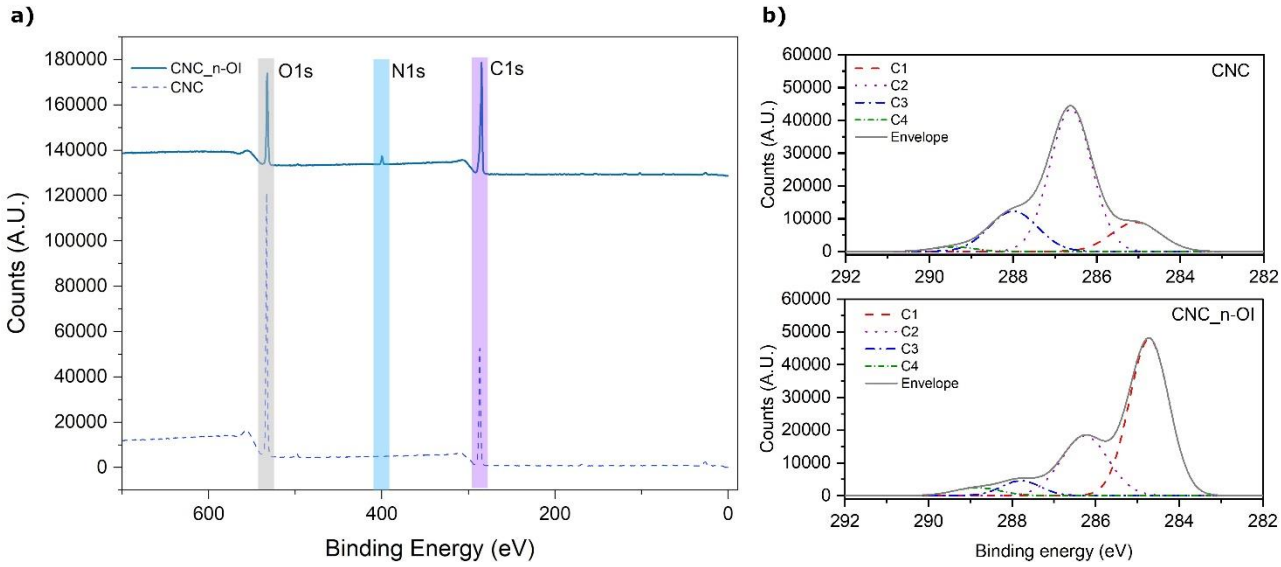

Figure III.5 – XPS results a) peaks b) Deconvolution of carbon peaks for neat and modified CNC.

According to Figure III.5a) it is possible to observe that neat cellulose presents two characteristic peaks related to the presence of oxygen (around 532 eV) and carbon (around 285 eV). For modified CNC, it is also possible to observe the presence of a peak at 400 eV, corresponding to the presence of nitrogen, proving the success of n-OI grafting onto the CNC surface.

To compare the elementary surface composition, the following Equation III.2 was used:

$$O/C = \frac{I_1}{I_2} \times \frac{S_1}{S_2} \qquad \text{Equation III.2}$$

Where I_i is the intensity of signal i (carbon, oxygen or nitrogen) and S_i is the atomic sensitivity factor from which values were calculated:

$$S_i = \frac{T_i \gamma_i \sigma_i}{4\pi} \qquad \text{Equation III.3}$$

Where T_i, γ_i, σ_i are transmission energy, electron inelastic mean free path and photoionization cross section for the X-ray source, respectively. T_i depends on the atomic Kinect energy E_i^{kin} (eV) as shown:

$$T_i = \frac{1}{(E_i^{kin})^{0.7}} \qquad \text{Equation III.4}$$

Where $E_C^{kin} = 1202\ eV$, $E_O^{kin} = 956\ eV$ and $E_N^{kin} = 1089\ eV$.

It is possible also to evaluate, quantitatively, differences in peaks after grafting. Table III.1 shows the mass concentration of each element for neat and modified CNC samples, as well as the deconvolution values for C1s curves (Figure III.5b).

Table III.1 – Experimental values of XPS and values of decomposition peaks of C1s curve.

Samples	Experimental values				Decomposition of C1s						DSS
	C%	O%	N%	O/C	C1	C2	C3	C4	C1/C3	C4/C3	
CNC	62.3	37.6	-	0,6	14.9	62.6	20.4	1,9	0,7	0.9	-
CNC_n-OI	75.8	20.0	3.1	0.2	62.4	28.2	5.7	3.6	10.9	0.6	**1.08**

Experimental values (Table III.1) for C1s signal increases after grafting due to the presence of long aliphatic chains from n-OI, which also corroborates the ratio O/C decreasing after chemical modification. The deconvolution of the C1s signal is important to quantify the occurrence of grafting at the surface. For both neat CNC and CNC_n-OI, four peaks were found. C1 is attributed to C-H, C2 to C-O, C3 to O-C-O and/or C=O and C4 to O-C=O, as shown in Figure III.5b

It can be seen that C1 notable increases after modification, from 14.9% to 62.4%. The ratio C1/C3 represents the number of aliphatic carbons per glucose unit, once each glucose moiety presents one C3 carbon. In this away, after chemical modification, the ratio increased from 0.7 to 10.9, which is a result of the very big C18 aliphatic chain presented in n-OI. The same analysis can be done to C4/C3, in which is possible to note that ratio increases from 0.09 to 0.6 after chemical modification.

To determine the degree of substitution at the surface (DSS), Equation III.5 was used based on the amount of nitrogen present [250]:

$$DSS = \frac{M_{AGU} \times x}{(100 \times M_N) - (M_{graftedGroup} \times x)} \qquad \text{Equation III.5}$$

Where M_{AGU} is the molecular weight of one anydroglucose unit (162.14 g/mol), M_N is the molar weight of one atom of nitrogen (14 g/mol), $M_{graftedGroup}$ is the molecular mass of grafted moieties (295.51 g/mol) and x is the mass concentration of nitrogen.

As can be observed in Table III.2, the DSS for CNC after chemical modification was found to be 1.08. It is important to note that this value represents only the substitution at the surface.

To compare, elemental analysis was performed, and the experimental values can be found in Table III.2.

Table III.2 – Elemental analysis results of experimental values and corrected values

Samples	Experimental values					Corrected Values		DS
	C	H	N	S	O	C	O	
CNC	40.4	6.2	0	0	53.1	44.4	49.4	-
CNC_n-OI	43.1	62.5	0	0	50.4	47.3	46.8	**0.05**

In theory, the weight ratio between oxygen and carbon atoms, from anhydroglucose, is 1.11, corresponding to 49.4% of oxygen and 44.4% of carbon. However, it is possible to observe in Table 4 that the ratio O/C of experimental values is 1.31, resulting from 53.1% of oxygen and 40.4% of carbon atoms. Due to this difference, it is necessary to correct experimental values, by multiplying experimental value by the ratio between theoretical and experimental value of oxygen and carbon of ungrafted CNC.

From this, corrected values were applied to Equation III.6, which led to the degree of substitution (DS) value.

$$DS = \frac{(72.07 - C) \times 162.14}{295.51 \times (C - 228.19)} \qquad \text{Equation III.6}$$

where C is the relative carbon content in the sample; 72.07 is the carbon mass of anhydroglucose unit, 162.14 is the mass of anydroglucose, 295.51 is the mass

of n-OI and 228.19 is the carbon mass of n-OI. As results show, the degree of substitution on the surface is higher than when considering all bulk samples.

The milling process tends to amorphize cellulose [243], therefore XRD analysis was performed in neat CNC, CNC after 15 minutes of the milling process and CNC modified with n-OI. Figure III.6 shows the curves comparing all samples studied. By applying the Segal method of calculation (by the difference between picks (110) and (200) of cellulose I), results show that there is no significant difference between crystallinity index comparing neat CNC (86%), milled and modified ones.

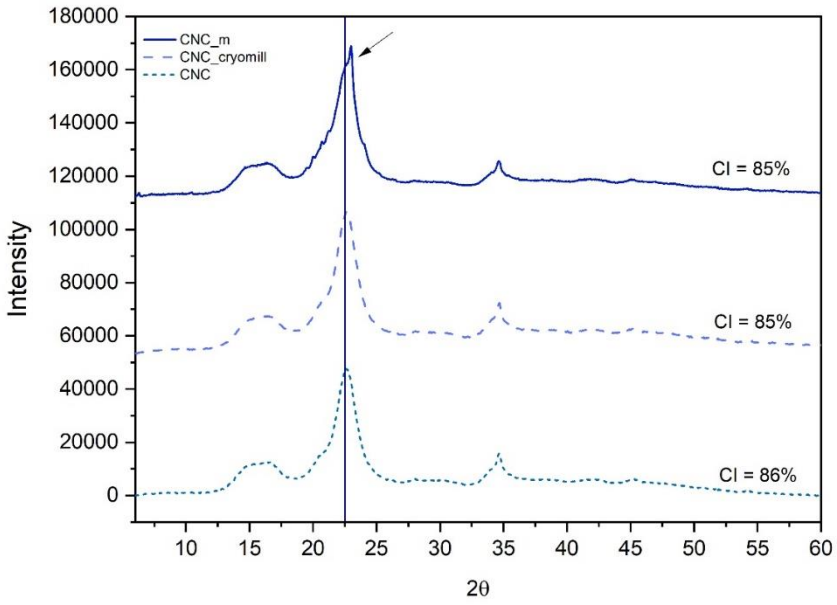

Figure III.6 – XRD curves for all neat CNC, neat CNC after milling and modified CNC.

In another hand, it is possible to observe that for modified CNC, a new peak around 2θ=23° is present. It is known that for crystalline structure of cellulose, two main values are observed. The amorphous part can be identified by 2θ=18.5°and the crystalline part by 2θ =22.5°. After chemical modification, the peak at 2θ=23° is related to the crystalline organization of the C18 aliphatic chain of n-OI, that is identified as a second reflection order. It is important to highlight that the presence of this new peak is also related to the efficiency of grafting,

once, Missoum et al. [250] observed that for lower grafting surface density, was not possible to observe the presence of this new crystalline phase.

Regarding the morphology of the studied CNC, by DLS (Figure III.7) was possible to note that the milling process by itself, resulted in two different peaks of sizes, with a high PDI. The modified CNC presented a very high PDI, which means a very broad size distribution when compared to the neat CNC. This can be a result of agglomeration of particles formed after process and modification. These results were also confirmed by TEM images (Figure III.8).

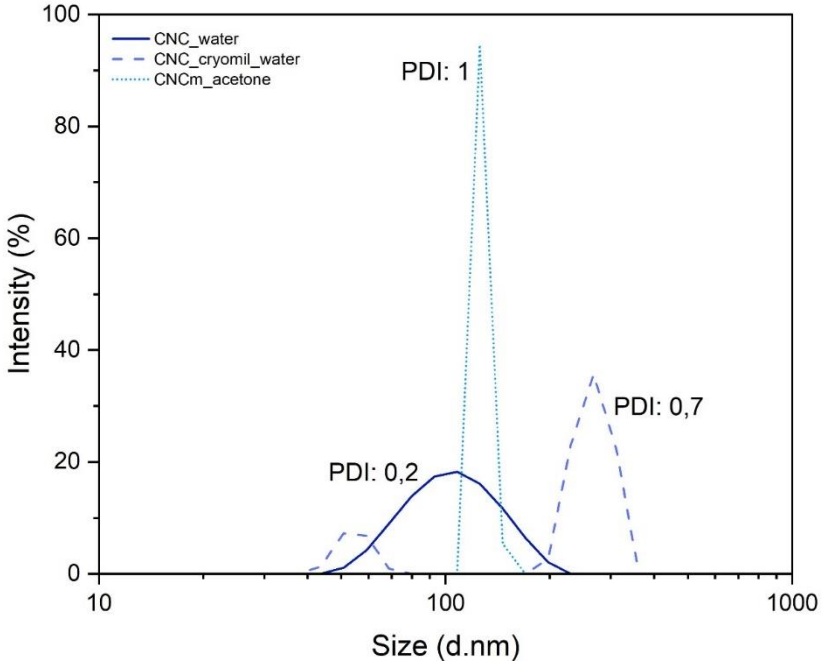

Figure III.7 – DLS of neat CNC, milled CNC, and modified CNC.

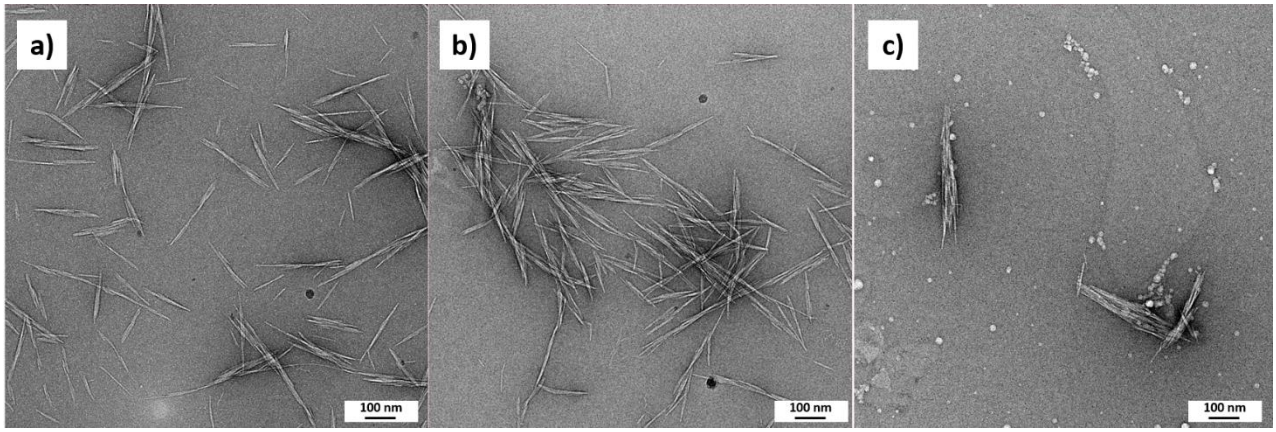

Figure III.8 – TEM of a) neat CNC in water; b) neat milled CNC in water; c) modified CNC in ethanol.

As it can be seen, neat CNC presented a very homogeneous distribution with a rod-like shape, as already presented in the literature [131]. After the mechanical treatment, neat milled CNC (Figure III.8b), presented the same shape but with a more agglomerated distribution when compared to neat CNC. Figure III.9 presents a comparison between neat CNC and neat CNC milled, where it is possible to observe some agglomerations signed by the arrow (Figure III.9b). After chemical modification, it is possible to observe that this aggregation was even more pronounced.

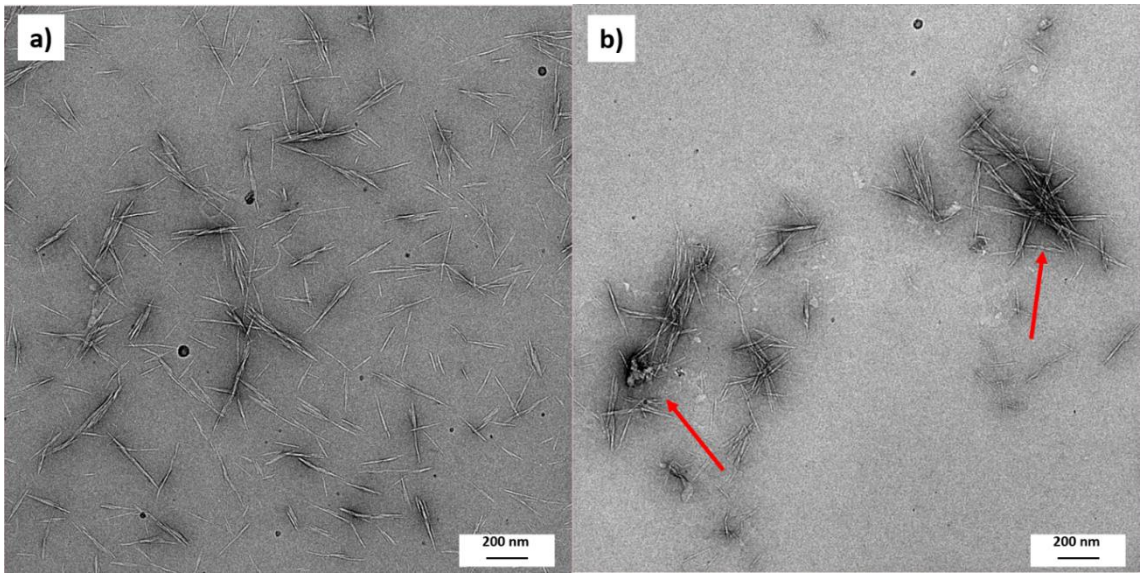

Figure III.9 – Comparison between a) neat CNC and; b) neat cryomilled CNC, at the same magnification. Arrows show some agglomeration after cryomilling process.

From TEM images was possible to calculate the length and diameter of CNC particles, as shown in Table III.3. The neat CNC had a rod-like shape and 136±28 nm and 9.2±3 nm in length and diameter, respectively. When the same neat CNC was subjected to the milling process under the same conditions used for the material modification, the length and diameter increased to 164.7±43 nm and 13.7±3 nm, respectively. Douard [251] studied the effect of milling for 3 hours on neat CNC at 30 Hz and also observed the formation of aggregates of various sizes, in which the largest agglomerate reached a diameter of approximately 80 µm. Structures with preserved morphologies were also observed, as in the present study. The author explains that this was probably the result of the intense mechanical shearing during the 3-hour experiment, but as far as is known, there are no studies investigating the morphological change of milling treatment under these conditions.

Table III.3 - Length and diameter of neat CNC and neat CNC cryomilled for 15 minutes.

	Length	Diameter	Aspect ratio
CNC	136±28	9.2±3	14±4.2
CNC_cryomilled	164.7±43	13.7±3	14±4.4

However, for the modified CNC sample, the formation of agglomerates was observed, with diameters ranging from 80 nm to 350 nm, as can be seen in Figure III.10.

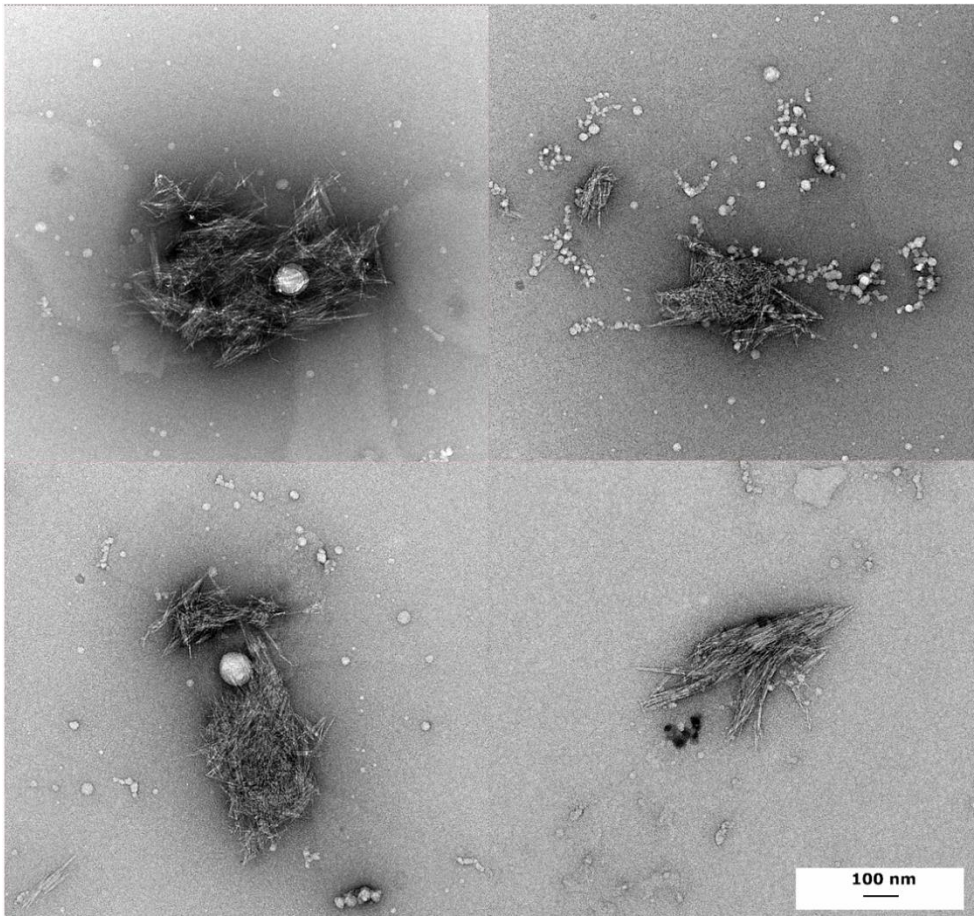

Figure III.10 – Different aggregates obtained after CNC chemical modification with n-OI.

As the main purpose of this chemical modification is to improve interactions between hydrophilic CNC and the hydrophobic character of the

polymeric matrix, contact angle measurements were carried out to state if surface interaction with water was increased (Figure III.11).

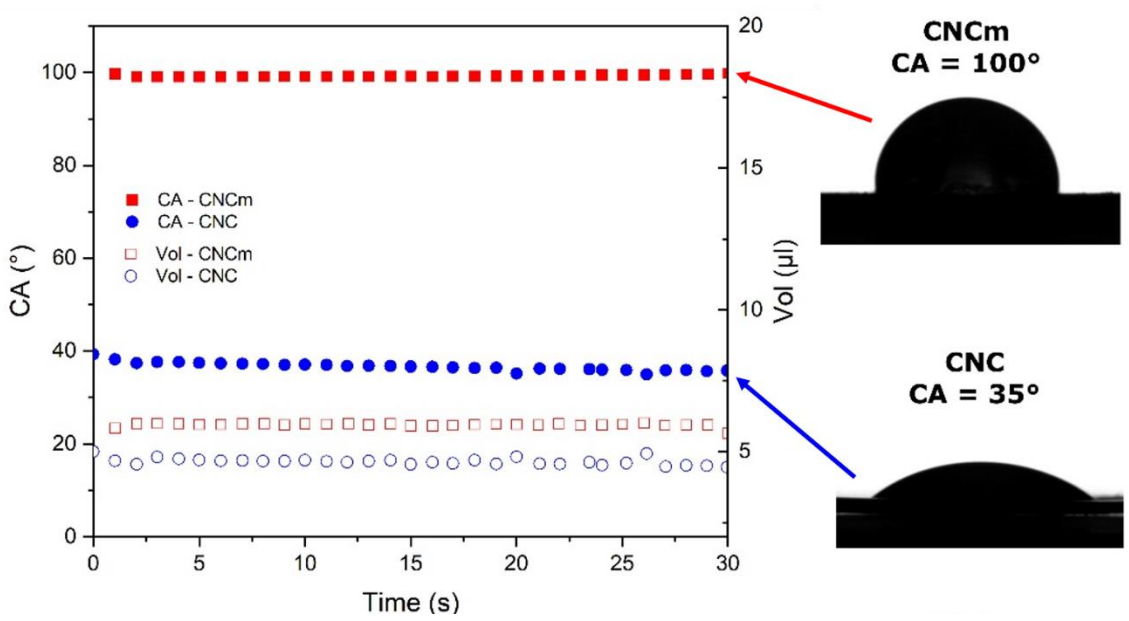

Figure III.11 – Contact angle for neat and modified CNC, for 30 seconds.

As can be seen, the contact angle for the pure CNC was around 40°, while for the modified CNC the average was increased to 100°, showing that the functionalization of the CNC increased the hydrophobic character of the samples. The volume of the droplets was also measured over time, and it can be seen that for the modified CNC sample the volume remained more stable during the analysis time. However, for both samples studied, the volume was constant, indicating that no water was absorbed by the sample.

As a matter of comparison, Table III.4 will present a summary of the results from this research and previous results found in the literature regarding the chemical modification of CNC with n-octadecyl isocyanate. Is important to note there are also some studies on the chemical modification of cellulose nanofibers with n-OI [250], however because of their morphological differences, de comparison will be done only between modifications with CNC.

As can be seen, all the other studies were carried out using the method developed by Siqueira and co-authors [177], which consists of solvent exchange

CNC to acetone and toluene (in some cases other solvents such as chloroform, dichloromethane) and add the n-OI, in high temperature (approximately 110°C) for 60 minutes. No relevant differences were found when comparing the characteristics of reported results and the results presented in this research, although the time of processing and the ratio between CNC and n-OI were smaller for the present investigation.

Table III.4 – Comparison between results found in the literature of CNC modification using n-OI.

Procedure						Characteristics							Reference
Source of CNC	**Method**	**Duration**	**n-OI: OH groups concentration**	**Solvents used during chemical modification**	**Temperature**	**Length**	**Diameter**	**DS**	**DSS**	**CI (%)**	**Contact Angle (°)**	**Objective**	
Wood fiber (CelluForce)	Mechanochemistry	15min	1:1	-	Room temperature	Neat: 136 nm Modified:-	Neat: 9 nm Modified:-	0.05	1.08	Neat: 86 Modified: 85	Neat:35 Modified: 100	Nanocomposites((PLA/CNC) by melt mixing	This work
Acid hydrolysis from bleached sisal fibers	In situ Solvent exchange	60min	1:10	Toluene and Dichloromethane	50, 90 and 110°C	Neat: 215±67 nm Modified: 130±38 nm	Neat: 5±1.5nm Modified: 7.1±1.6	0.06	-	Neat: 95 Modified: 86.4	Neat:44.6 Modified: 67.4	Nanocomposites (PCL/CNC) by solvent casting	Siqueira et al., 2010 [177]
Acid hydrolysis from MCC	In situ Solvent exchange	60 min	1:10	Toluene and Dibutyl dilauryl	110°C	Neat: 243±48 Modified: -	Neat: 9.4±2.5 Modified: -	-	-	Neat: 87.2 Modified: 73.3	Neat:66 Modified: 89	Nanocomposites (PLA/CNC) by solvent casting	Espino-Perez et al., 2013 [252]
Acid hydrolysis from MCC	In situ Solvent Exchange	60 min	1:10	Acetone and Toluene	110°C	Neat: 250±80 Modified: -	Neat: - Modified: -	-	-	Neat: - Modified: -	Neat: - Modified: -	Nanocomposites PLA/NR*/CNC by solvent casting and extrusion	Bitinis et al., 2013 [183]
Acid hydrolysis from MCC	In situ Solvent Exchange	60min	1 :10	Toluene and Dichloromethane	50, 90 and 110°C	Neat: 143±71 Modified: -	Neat: 11±4 Modified: -	0.23	-	Neat : 84 Modified: 80	Neat: 59 Modified: 94	Nanocomposites (PBAT/CNC) by solvent casting	Morelli et al., 2016 [180]
Acid hydrolysis from MCC	In situ Solvent Exchange	60 min	1:10	Toluene, acetone and chloroform	110°C	Neat: 155 nm Modified: 176 nm;	Neat: 17 nm Modified: 9nm	3	-	Neat: 84 Modified: 73	Neat: 57 Modified: 95	Water and volatile organic molecules physisorption on CNC	Espino-Perez et al., 2016 [181]
Acid hydrolysis from Munguba fibers	In situ Solvent Exchange	60 min	1:10	Toluene	100ºC	Neat: 131±34 Modified: -	Neat: 11±2 Modified: -	-	-	Neat: - Modified:-	Neat: - Modified:-	Nanocomposites (PBAT/CNC) by meting mixing	Pinheiro et al., 2019 [182]
Acid hydrolysis from MCC	In situ solvent exchange	30 minutes	1:10	Acetone and toluene	90 and 110°C	Neat: - Modified:-	Neat: 10-20 nm Modified:-	-	-	Neat: - Modified:-	Neat: - Modified:-	Nanocomposites PCL/CNC by solvent casting	Celebi et al, 2022 [253]

4 Conclusion

This section aimed to modify cellulose nanocrystals in order to increase their hydrophobic character and improve their compatibility in nanocomposites with an apolar matrix.

The mechanochemistry strategy used for modification is not so explored in the literature to modify CNC. Mechanochemistry is very interesting because the process can be done in a shorter time and does not need the involvement of organic solvents during the reaction.

Compared to other studies in the literature, this study used a low concentration of reactant, and the reaction was carried out for only 15 minutes. Likewise, the results showed success in modifying CNC, conserving their crystalline structure and increasing their hydrophobicity (proved by contact angle).

However, the final morphology of modified CNC presents some aggregation compared to the neat and neat-milled CNC. From the literature, is known that the milling process can result in aggregation of CNC after long periods of the milling process, however, this subject has not yet been explored in depth.

III.2 PLA/CNC nanocomposites foams produced by supercritical method

1 Introduction

According to Gonçalves and co-authors [214], in the last 10 years, studies involving polymeric foams have focused mainly on biodegradable polymers and their mixtures or composites, in which PLA has been the most prevalent in recent studies, followed by starch, PBS, and PCL.

One of the many reasons for studying and developing PLA composites is their low resistance in the molten state. This characteristic is important for several processes, as in the case of the production of polymeric foams.

Developing nanocomposites is proving to be an efficient and sustainable way of improving the foamability of PLA, resulting in foams with more homogeneous cell morphologies than those obtained by neat PLA. This strategy is versatile due to the wide range of fillers that can be used (lignocellulose and minerals, for example) and the fact that they can be combined with additives, chain extenders, and surface treatment of the fillers [37].

In the literature, it is possible to find studies that have carried out the foaming of PLA from composites and nanocomposites using various reinforcing agents by the supercritical method, such as organoclays [254], halloysite [255], calcium carbonate [256], silica [257], cellulose nanocrystals [258,259], cellulose fibers, and nanofibers [260–263], among others. However, few studies still deepen the understanding of the influence of particles on the cell morphologies produced [37].

Among the many options, cellulose-based nanocomposites attract attention because they are biodegradable and from renewable sources, in which cellulose is considered to be the most abundant polymer on the planet. Cellulose nanocrystals (CNC) have characteristics such as high stiffness, high specific surface area and low density, which make them a suitable option for the production of nanocomposites [131].

However, there are still many challenges in processing polymer composites with CNC, mainly related to aggregation, interfacial compatibility, and non-homogeneous dispersion [169]. These factors can directly influence the quality of the foams produced.

Among the most common methods of producing PLA and CNC nanocomposites are solvent casting and melt compounding. Solvent casting is a solution mixing method that results in less CNC agglomeration compared to other methods, however, it requires the use of a large quantity of solvents and the generation of waste makes this method economically unfeasible. Melt processing of polymer nanocomposites is a key method once it is possible to process high-volume products, it is cheap, fast, industrially and economically suitable, and solvent-free. However, direct mixing of CNC into molten PLA can result in high agglomeration, which hinders the formation of a percolated network [131,264].

Despite the extensive study of PLA/CNC nanocomposites, research into the foaming of these materials by the supercritical method is scarce. The literature mainly presents work on foaming PLA with cellulose nanofibers [104,260,261,263,265,266]. Qiu and collaborators [258] are among the few cases in which CNC was used as a filler. They produced PLA/CNC foams with supercritical CO_2, containing 3 wt% of reinforcing agent. CNC was added pure or acetylated at two different levels of substitution. The nanocomposites were prepared by film casting followed by melt mixing. The authors observed that the introduction of CNC, both pure and modified, resulted in a higher expansion ratio, smaller cell sizes, and higher cell density when compared to neat PLA. However, the foams produced with acetylated CNC at a higher degree of substitution had a higher modulus of elasticity and tensile strength than neat PLA foams. In comparison, foams containing neat CNC and acetylated CNC at a lower degree of substitution had lower mechanical properties than neat PLA foams.

Other methods of producing nanocomposite foams have been found. Boruvka and co-authors studied the addition of CNC to the PLA/PDLA blend modified with maleic anhydride in the presence of peroxide, to compare with the cell structures achieved in the pure PLA and pure blend samples, in which the method of obtaining the foam was carried out in injection molding equipment

using supercritical N_2 as the blowing agent [267]. In addition to this, studies of PLA/CNC composite foam using the casting/leaching method were also found in the literature [268,269], in which spherical particles are used to produce cast films, that are afterward dried and washed in an appropriate solvent that will dissolve the incorporated particles, thus giving rise to cellular structures.

Observing the above, it is clear that the strategy of using CNC to control the cellular structures of PLA foams produced by the supercritical CO_2 method has been little explored. Thus, this section aimed to study the rheological and morphological properties of PLA incorporated with neat and modified CNC and their influence on the final cellular structures of foams produced by supercritical CO_2.

2 Material and Methods

2.1 Materials

CNC used was purchased from CelluForce Canada, and modified CNC was obtained as presented in Section III.1. PLA Ingeo Biopolymer 4043D was purchased from NatureWorks LLC (MRF 6 g/10min - at 210°C), melting temperature between 145 and 160°C, % of D content (not informed) – considered medium content.

2.2 Methods

2.2.1 CNC functionalization

CNC functionalization was achieved using n-octadecyl isocyanate by mechanochemistry. Section III. 1 presents the description of all procedures and the characterization of CNC.

2.2.2 Nanocomposite foams production

Nanocomposites were produced in a Haake torque rheometer, model Rheomix 600, equipped with roller rotors, in which the concentration of neat CNC and modified CNC were varied, as shown in Table III.5. Process conditions were as follows: the temperature at 180°C, rotation of 50 rpm, and processing time of 6.5 minutes. The addition of neat or modified CNC was carried out between 80 and 90 seconds. PLA was dried in a vacuum oven at 70ºC for 4 hours before the process, and CNCs were dried for 24 hours at 70°C in a vacuum oven.

Table III.5 – Nanocomposites formulations and nomenclature.

Sample	Neat CNC (wt%)	Modified CNC (wt%)
PLA	-	-
PLA_CNC$_2$	2	-
PLA_CNC$_5$	5	-
PLA_CNC$_{10}$	10	-
PLA_CNC$_{m2}$	-	2
PLA_CNC$_{m5}$	-	5
PLA_CNC$_{m10}$	-	10

For the production of nanocomposite foam, an in-house device was used, and supercritical CO_2 was adopted as a blowing agent. The device consisted of a high-pressure CO_2 pump, an oven, a hermetical cylinder and Teflon mold, as shown in Figure III.12.

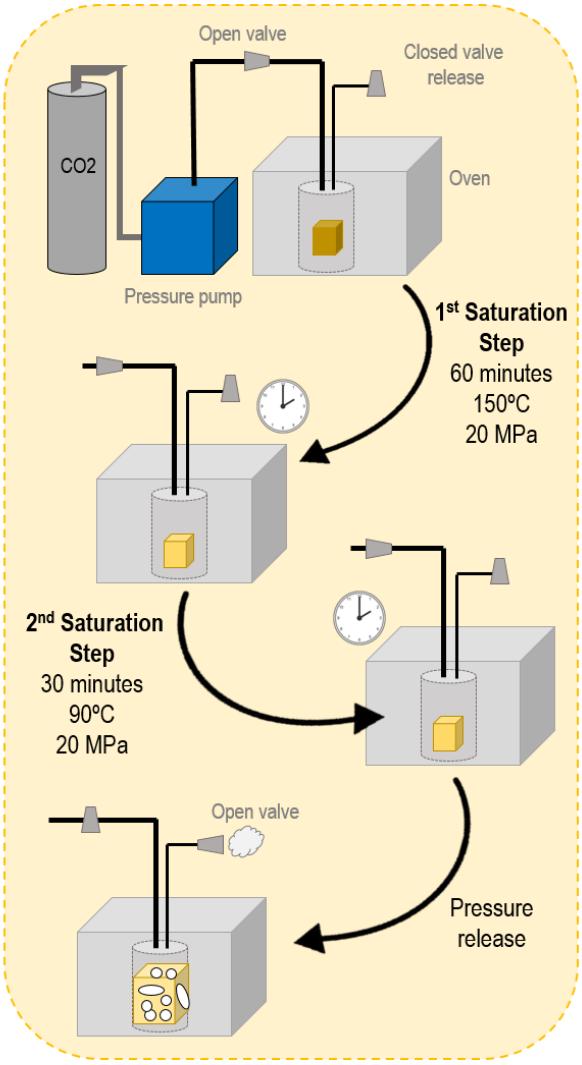

Figure III.12 – Scheme of the in-house made foaming device and the steps of the foaming process.

The entire system, including the mold and the hermetic cylinder, was placed inside the oven to allow temperature control. High-pressure CO_2 was then introduced into the hermetically sealed system containing the sample mold.

The foaming procedure consisted of three stages, as illustrated in Figure III.12. Throughout the process, the saturation pressure was maintained at 20 MPa. In the first stage, CO_2 saturation was conducted for 1 hour at 150°C, a temperature close to the melting temperature of the samples. Immediately following this stage, the system temperature was reduced to 90°C and held for 30 minutes. After this second stage, the system was manually and rapidly depressurized to induce sample expansion.

2.2.3 Fourier-transform infrared spectroscopy (FTIR)

The nanocomposites were characterized by FTIR using ThermoScientific equipment, model Nicolet 6700 in ATR mode. The absorbance spectra were recorded between 4000 cm^{-1} and 400 cm^{-1} with a resolution of 4 cm^{-1} and 64 scans. Measurements were made at least in duplicate for each sample.

2.2.4 Nanocomposites rheological analysis

Rheological data for unfoamed nanocomposites was obtained using a tension-controlled TA Instruments AR-G2 rheometer with parallel plates geometry (d = 25 mm, gap between plates = 1 mm). The steady-state (between shear rates of 0.01 and 100 s^{-1}) and the small amplitude oscillatory shear properties (between angular frequency of 0.05 and 500 rad/s), at 180°C and under nitrogen atmosphere were measured. Samples were vacuum-dried before the experiment (4 hours at 70°C).

2.2.5 Differential Scanning Calorimetry (DSC)

Differential scanning calorimetry (DSC) was performed in a TA Q2000 DSC, for both foamed and unfoamed nanocomposites. A first heating cycle at a heating rate of 10°C/min, between 0°C and 200°C, under nitrogen gas flow was applied to samples; after attaining 200ºC, the samples were kept at that temperature for 1 minute and then were cooled down to 25ºC. A second heating cycle was applied at 10°C/min, between 0°C and 200°C.

Unfoamed samples were vacuum dried for 4 hours, at 70°C before measurements. Foamed samples were not dried to preserve the thermal history of foams.

The crystallinity index (Xc) of samples was calculated by using Equation III.7:

$$Xc = \frac{[\Delta H_m - \Delta H_{cc}]}{(1 - \phi) \times [\Delta H_m^o]} \times 100 \qquad \text{Equation III.7}$$

Where ΔH_m is the melting enthalpy, ΔH_{cc} is the crystallization enthalpy during the heating, ϕ is the mass fraction of CNC incorporated in PLA, and ΔH_f^o is the melting enthalpy for a hypothetically 100% crystalline polymer. For PLA, the value adopted was 93 kJ/g [207,208].

2.2.6 Transmission Electron Microscopy TEM

Nanocomposites samples were trimmed on a RMC Ultra MT-7000 microtome, using a glass knife. After trimming, samples were sectioned with feeding lengths of 50 nm at 1 mm/s in an ultramicrotome LEICA Reicher Ultracuts FC S. The cuts were carried out at room temperature. The nanometric films were

deposited in a copper grid and analyzed in a Transmission Electron Microscope FEI TECNAI G²F20 HRTEM 200 kV.

2.2.7 Foam characterization

The foam expansion was evaluated by calculating the Volume Expansion Ratio (VER, φ), which is the ratio between the density of the non-foamed and the foamed material. Densities for all samples were determined using the water displacement method (ASTM D792-13), where the mass of the sample in air and in water was used to perform the calculation. It was assumed that no water was absorbed by the foams, as the mass remained stable during the measurements. Three different samples per formulation were analyzed, with each piece measured at least five times. The highest and lowest values were discarded to calculate the mean and standard deviation.

Morphological characterization of the cellular structures was performed using images obtained from a scanning electron microscope (SEM, FEI Magellan 400L). The samples were cryofractured using liquid nitrogen, followed by gold sputtering. The resulting images were analyzed using ImageJ software, enabling the determination of cell density (N) and cell size. To calculate N, two different images for each sample were analyzed, and the following equation was used [270]:

$$N = \left(\frac{n}{A}\right)^{3/2} \times \Phi \qquad \text{Equation III.8}$$

Where N is the cell density, *n* is the number of cells in a given area *A* and ϕ is the volume expansion ratio (VER).

To determine the cell size, at least 100 cells were measured.

2.2.8 Statistical analysis

When appropriate, statistical tests ANOVA, followed by Tukey's multiple comparisons test, were conducted with a 95% confidence level ($p < 0.05$ = significance level).

3 Results

3.1 Properties of nanocomposites

Once the purpose of the surface functionalization of CNC, presented in Section III.1, was to improve its compatibility with the PLA matrix, nanocomposites PLA/CNC and PLA/CNCm were prepared at different concentrations, by melting mixture in a torque rheometer. By FTIR it was possible to observe that for all samples, the spectra seem to be the same. However, the range close to 3000 cm^{-1} presents different picks, as shown in Figure III.13a and b.

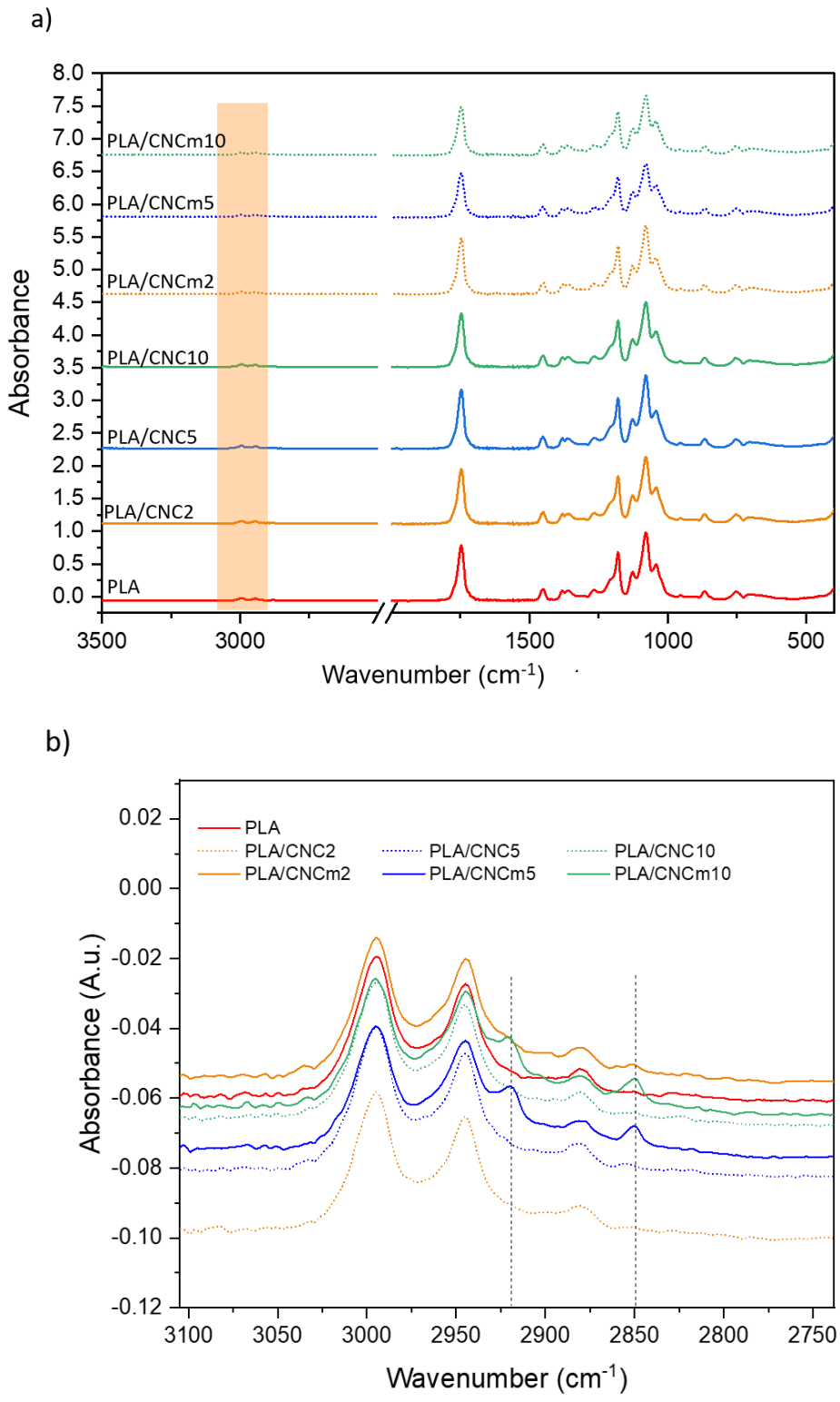

Figure III.13 – FTIR spectra for PLA and PLA/CNC nanocomposites: a) full spectra and; b) Zoom at region of 3000 cm^{-1} showing the presence of long aliphatic chains present in n-OI.

These additional picks are present in samples with modified CNC, and they are correlated to the CH_2 bonds. The wavenumber 2850 cm^{-1} corresponds to the symmetric axial stretching of CH_2, while 2920 cm^{-1} corresponds to the asymmetric axial deformation [271]. This is evidence of long aliphatic chains in the n-octadecyl isocyanate grafted onto the CNC surface, showing that the functionalization was stable during the melting mixture.

Figure III.14 presents the rheological results in the steady-state regime for the produced composites. As shown, the apparent viscosities of all samples exhibit Newtonian behavior at low shear rates, with an extensive plateau until the onset of pseudoplastic behavior at higher rates. This behavior is characteristic of molten polymers [272]. However, the apparent viscosity at zero shear rates (η_0) was varied with the introduction of CNC.

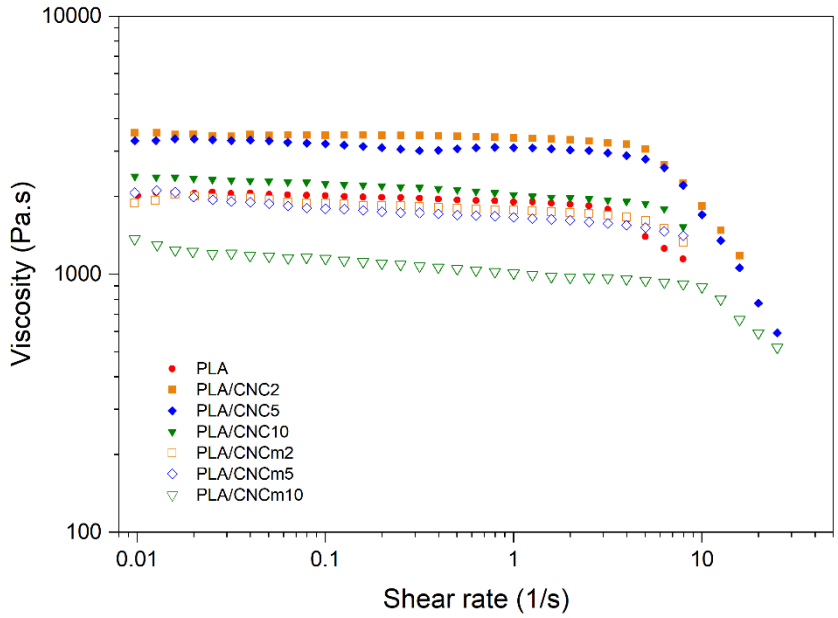

Figure III.14 – Apparent viscosity of PLA and PLA/CNC nanocomposites, at 180°C.

For all samples containing neat CNC, the zero-shear viscosity (η_0) was close to or higher than that of neat PLA, with the formulations containing 2 wt% and 5 wt% CNC exhibiting the highest viscosities. This increase in viscosity is likely due to the dispersion of nanocrystals within the polymer matrix. Since these

formulations had a low CNC concentration, fewer nanocrystals were present to agglomerate, resulting in greater flow restriction.

Conversely, the sample containing 10 wt% CNC showed a viscosity closer to that of pure PLA, which may be attributed to increased agglomeration, as a higher concentration of nanocrystals was available. A similar trend was observed by [25], where the viscosity was higher for samples containing 6 wt% CNC than for those with 7 wt% CNC.

For samples containing modified CNC, the opposite trend was observed: viscosities were close to or lower than that of neat PLA. This can be explained by the presence of long aliphatic chains grafted onto the CNC surface, which acted as lubricants, thereby reducing the material viscosity. The greater the concentration of modified CNC, the more pronounced the lubricating effect on the matrix.

The apparent viscosity data is crucial as it can be correlated with extensional viscosity (η_e), which is a decisive factor in the foaming process, where deformation during expansion is extensional and directly influences the final cell structures. This relationship indicates that as the elongation rate approaches zero, the extensional viscosity (η_e) approaches three times the apparent viscosity ($3\eta_0$) [108]. Therefore, since the elongation deformation rates during foaming are low [18], the extensional viscosity will be approximately three times the apparent viscosity at low elongation rates.

However, rheological data obtained in the oscillatory regime are more effective in characterizing the morphology and dispersion of nanocomposites. According to Vatansever et al. [273], the concentration at which cellulose nanocrystals form a network can be identified as the rheological percolation threshold. At these concentrations, long-range polymer chain relaxation can be restrained, potentially leading to a significant increase in viscosity and storage modulus at low frequencies. Figure III.15 presents the G' curves as a function of angular frequency, while Figure III.16 displays the G' and G'' curves as a function of angular frequency.

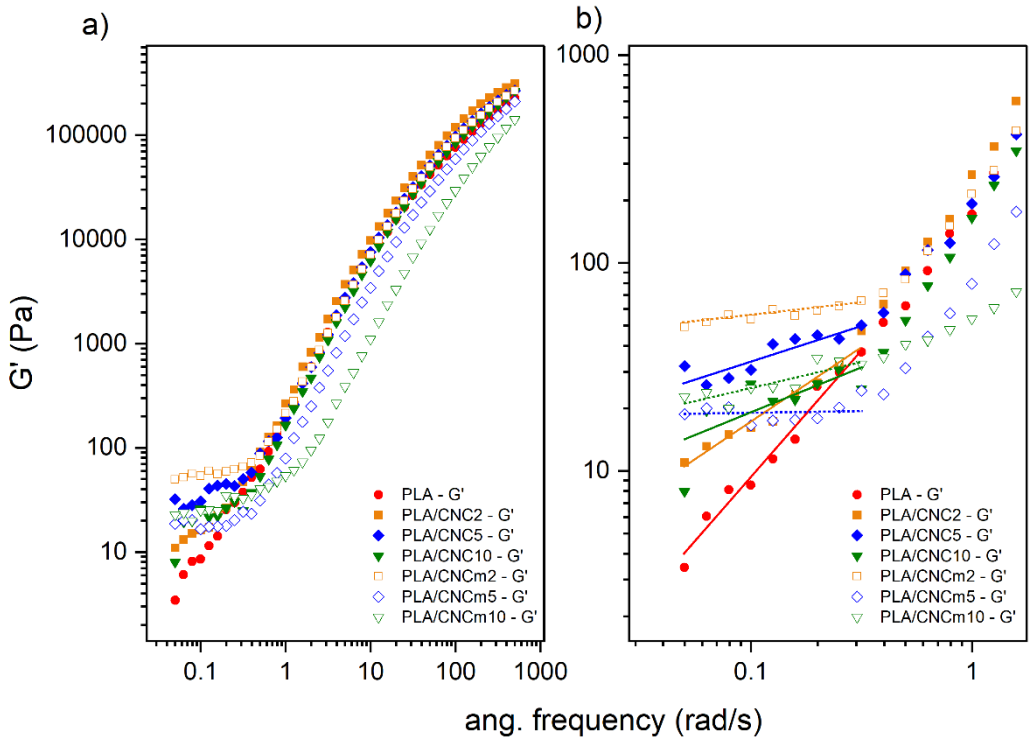

Figure III.15 – Log G' *versus* log angular frequency of nanocomposites performed at 180°C from a) 0.05 a 500 rad/s and; b) 0.05 a 0.3 rad/s.

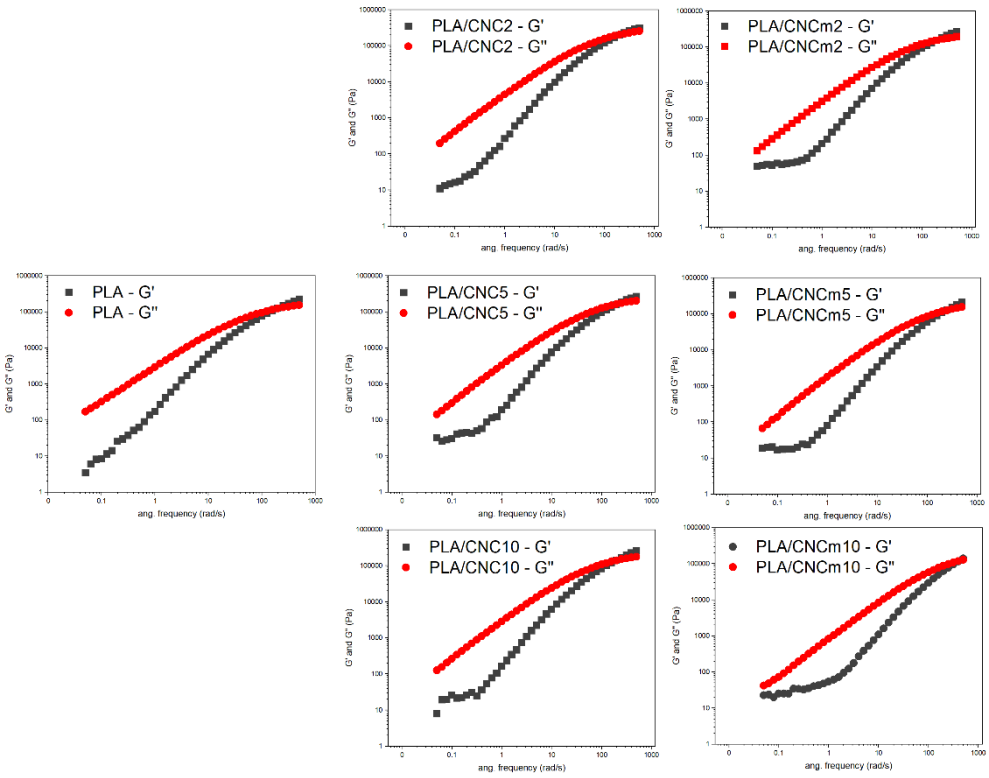

Figure III.16 – Log G' and G'' *versus* log angular frequency of nanocomposites performed at 180°C from 0.05 to 500 rad/s.

As illustrated in Figure III.15, the storage modulus (G') did not show expressive differences at frequencies above 1 rad/s, and the shape of the curves remained similar to that of neat PLA. However, at lower frequencies, a plateau was observed in the nanocomposite samples, with this effect being more pronounced in the CNC-modified ones, as shown in Figure III.15b.

To validate this observation, the terminal slope values were calculated, as presented in Table III.6. Homopolymers typically exhibit a G' with a terminal slope close to 2 in a log-log plot of G' versus ω [274], which was indeed observed for neat PLA. In contrast, at low frequencies, the nanocomposites exhibited a terminal slope of less than 1. This phenomenon was similarly observed by Zhao and coauthors [109], which, at filler concentrations near the percolation threshold, the G' and G'' curves presented crossover at low frequencies, with G' showing terminal slopes less than 1.

Table III.6 – Values of terminal slope (measured between 0.05-0.3 rad/s) and crossover for all samples.

Samples	Terminal slope G’	Crossover (rad/s)
PLA	1.2	158.1
PLA/CNC2	0.7	199.1
PLACNC5	0.3	199.1
PLA/CNC10	0.5	158.1
PLA/CNCm2	0.1	199.1
PLA/CNCm5	0.1	199.1
PLA/CNCm10	0.3	397.2

As discussed earlier in Chapter I, one of the consequences of rheological percolation is a G' curve surpassing G'' at low frequencies. However, as shown in Figure III.16, none of the studied formulations exhibited this behavior. Instead, the curves displayed typical molten polymer characteristics, with the loss modulus (G'') being higher across most of the frequency range, and crossover occurring only at higher frequencies (Table III.6 provides the frequencies at which crossover occurred for each sample). Notably, for the CNC-modified samples, G' shows a tendency to crossover at lower frequencies, a behavior also reported by Zhao, who linked this phenomenon to proximity to the percolation threshold [109].

Given that this same behavior was observed in samples containing both low and high concentrations of CNC, it is likely that the limiting factor for achieving rheological percolation was the inadequate dispersion of the filler within the matrix. Additionally, the samples containing neat CNC demonstrated a less pronounced tendency for crossover at low rates, particularly the sample with 2 wt% CNC. This suggests that the chemical modification of CNC may have improved its interaction with the matrix.

Finally, a thermal analysis of the nanocomposites was conducted to determine the glass transition, melting, and crystallization temperatures, as well as their respective enthalpy and crystallinity values (Figure III.17 and Table III.7). Thermal analysis of neat and modified CNC was also performed, as depicted in Figure III.18.

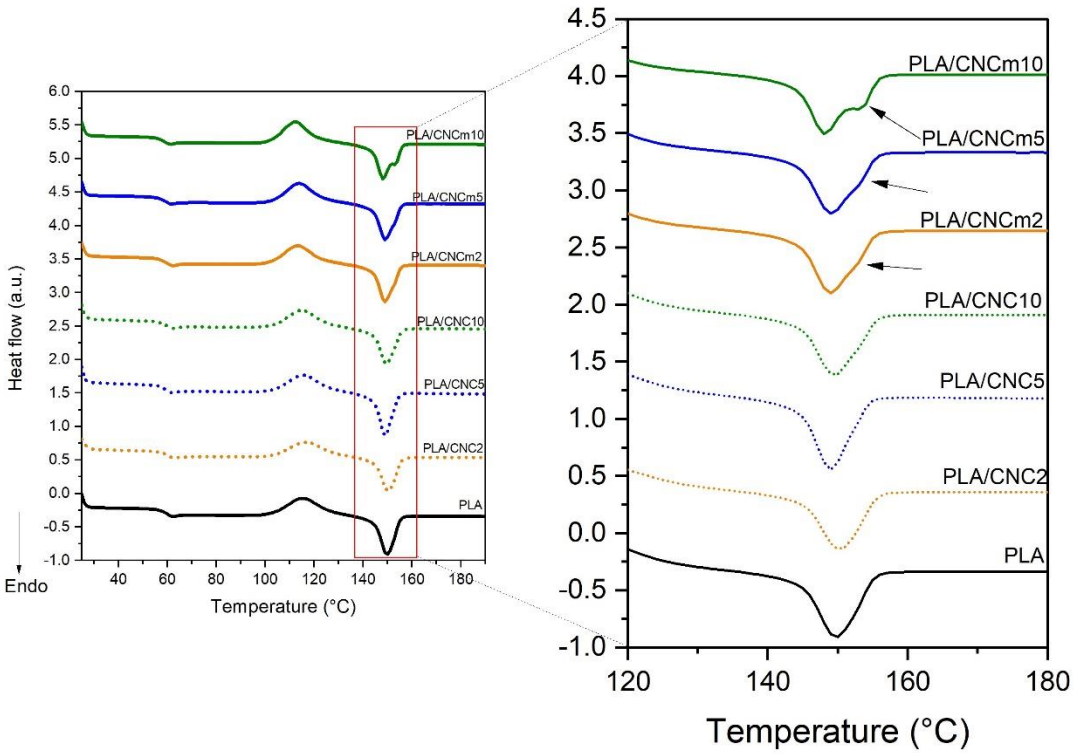

Figure III.17 – DSC second heating curves for all studied nanocomposites formulations.

Table III.7 – DSC results for all nanocomposites formulations.

Sample	T_g (°C)	ΔH_{cc} (J/g)	T_{cc} (°C)	ΔH_m (J/g)	T_m (°C)	Crystallinity (%)	Maximum Crystallinity Potential (%)
PLA	60.0	25.0	115.8	25.2	149.7	0.2	26,9
PLA/CNC2	60.5	22.1	117.0	22.6	150.0	0.5	24.3
PLA/CNC5	60.1	24.4	116.1	25.3	149.0	1	27.7
PLA/CNC10	60.0	23.9	115.3	24.6	149.5	0.8	28.5
PLA/CNCm2	59.7	24.7	113.7	25.2	148.9	0.6	27.1
PLA/CNCm5	59.7	25.1	114.1	25.4	149.0	0.4	28.4
PLA/CNCm10	59.1	25.5	112.5	26.0	148.1	0.2	30.5

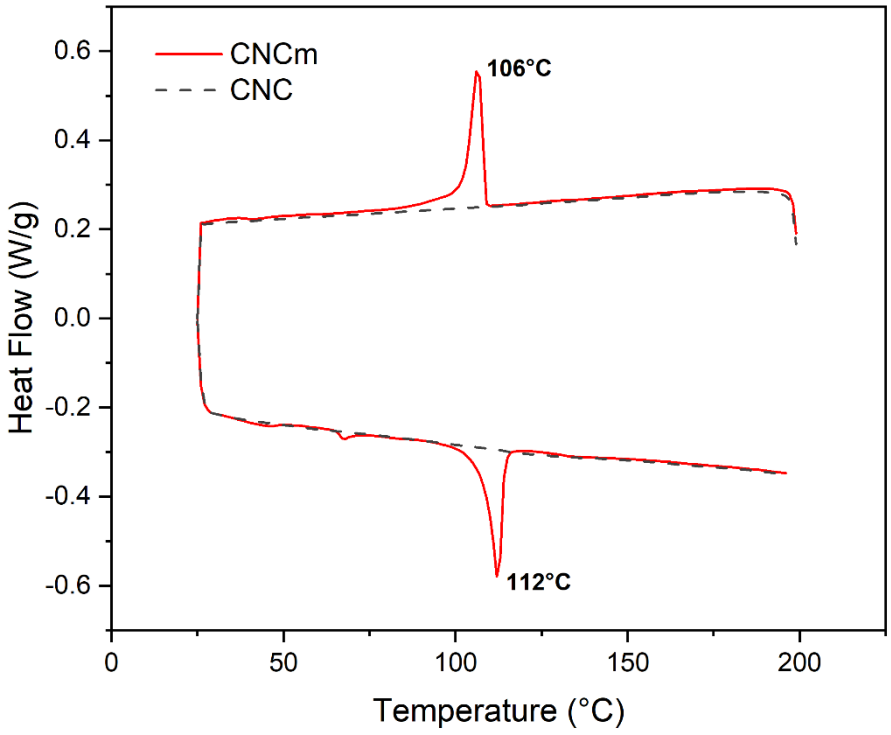

Figure III.18 –CNC and CNCm DSC curves, from 25°C to 200°C, at 10°C/min.

The results indicate that there were no expressive differences in glass transition temperatures between PLA and the nanocomposites. Similar

observations have been reported [275] in studies involving PEO with tunicate CNC [276], PVA with CNF [277], and cellulose acetate butyrate with CNC [278].

Regarding the crystallization temperature (Tc), a slight decrease was observed in the samples containing modified CNCs. This decrease may be attributed to the presence of long grafted aliphatic chains, which crystallize during cooling, as shown in Figure III.18. These crystals may act as nucleating agents for the PLA matrix, thereby shifting the Tc to slightly lower temperatures. In this case, the nanocomposites itself can act as nucleating agents.

Additionally, the crystallization of the n-OI chains also influenced the melting temperature (Tm) of the nanocomposites. Figure III.17 shows a second melting peak at 153°C for the sample containing 10 wt% modified CNC, and a shoulder at similar temperatures for the samples with 2 and 5 wt% modified CNC. As illustrated in Figure III.18, neat CNC does not exhibit any significant thermal events, unlike modified CNC, which shows a crystallization peak at 106°C during cooling and a melting peak at 112°C. This indicates that the long aliphatic chains grafted onto the CNC form crystalline structures. The melting temperature of these structures is very close to the crystallization temperature of the nanocomposites, which might lead to the reorganization of PLA chains during heating, along with the grafted CNC chains, resulting in cocrystallization. The sample with 10 wt% CNC, presenting a higher concentration of grafted chains, exhibited a more pronounced cocrystallization, as evidenced by the second melting peak.

PLA is known for its slow crystallization rate, which generally occurs during heating. As shown in Table III.7, the crystallinity values during cooling ranged from 0.2 to 1%, indicating that the material did not crystallize significantly during cooling. However, during heating, the samples exhibited crystallinity between 24% and 30%, with the modified CNC nanocomposites showing slightly higher values than those containing pure CNC. This suggests that the increase in crystallinity may be due to the cocrystallization of PLA with the grafted CNC chains.

Based on the information presented so far, there are indications that the CNC was not adequately dispersed within the PLA matrix. To confirm this, morphological analysis using transmission electron microscopy (TEM) was performed, as shown in Figure III.19.

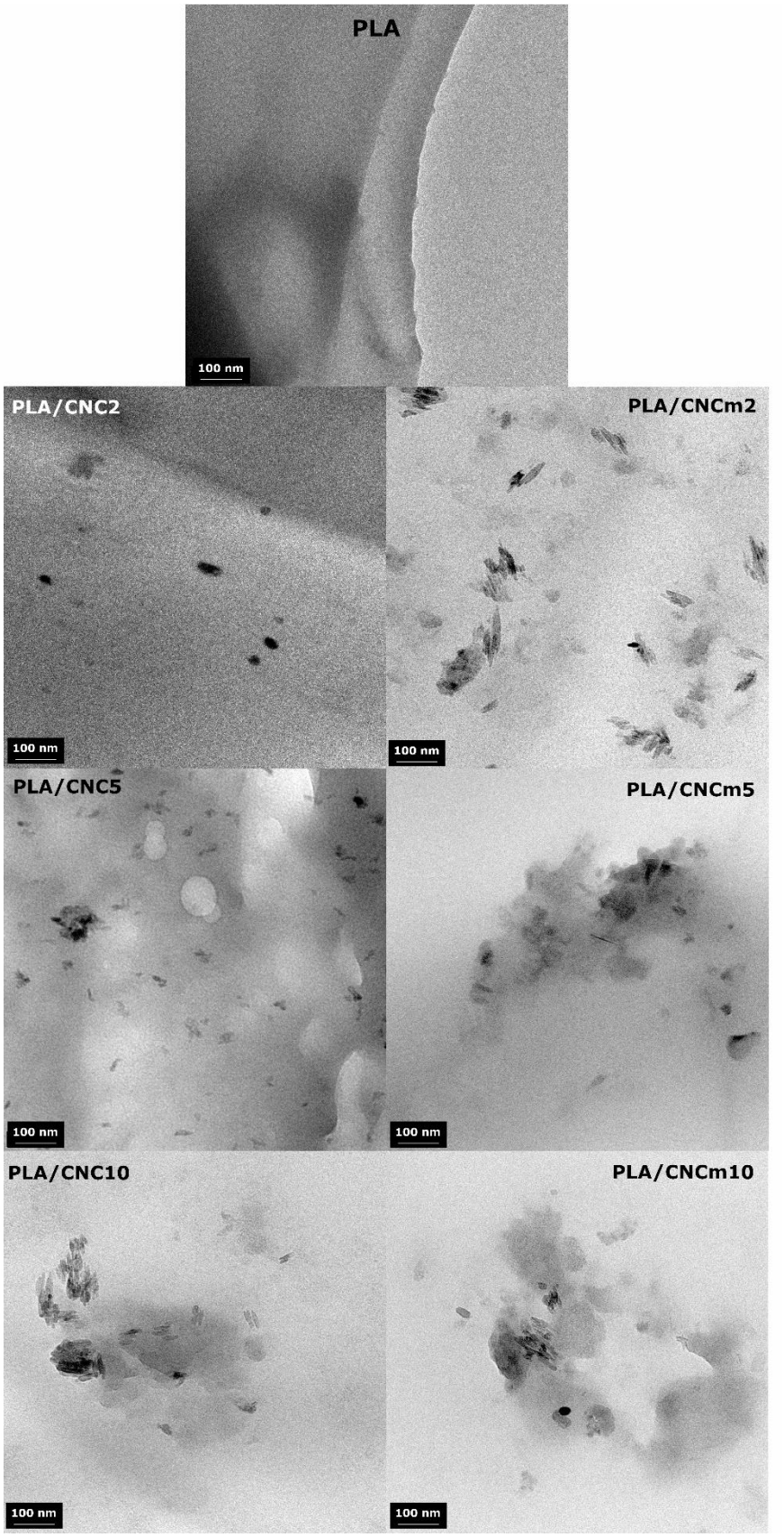

Figure III.19 – TEM images of nanocomposites at a magnification of 45000 x.

Figure III.19 shows that all samples exhibited low CNC dispersion, consistent with the rheological data. However, as discussed in Section III.1, the method used for chemically modifying the CNC resulted in agglomerated structures. Consequently, the low dispersion of the modified CNC is likely due not only to the nanocomposite production method but also to the morphology resulting from the chemical modification.

Furthermore, contrary to what is commonly found in the literature, the agglomerates formed in both the pure and modified CNC samples remained on the nanometer scale. For instance, Bagheriasl and coauthors [274] observed agglomerates of pure CNC in the PLA matrix within the 1-3 µm range, and Espino-Pérez reported similar findings in nanocomposites prepared by film casting [252].

This research aimed to explore the simplest method of incorporating CNC, focusing on understanding the effects of CNC modified with n-octadecyl isocyanate, which, to our knowledge, had not previously been incorporated into PLA via the melt mixing method.

The next section will detail the characteristics of the foams produced from the nanocomposite.

3.2 Foams characterization

DSC was performed on the nanocomposite foams to assess whether the samples crystallized during the CO_2 saturation period. As explained in Chapter I, at temperatures below Tc, CO_2 can act as a lubricant, facilitating crystallization and crystals growth.

In the first saturation stage, the PLA remained at 150ºC for 1 hour. Under these conditions, the molecules have high mobility, inhibiting crystallization. However, the second saturation stage was conducted at 90ºC for 30 minutes. This temperature is closer to the crystallization temperature of the nanocomposites, which is around 114ºC according to the DSC results. With the

lubricating effect of CO_2, the chains gained more mobility, which facilitated crystals growth. Figure III.20 illustrates the first heating curves of the foams.

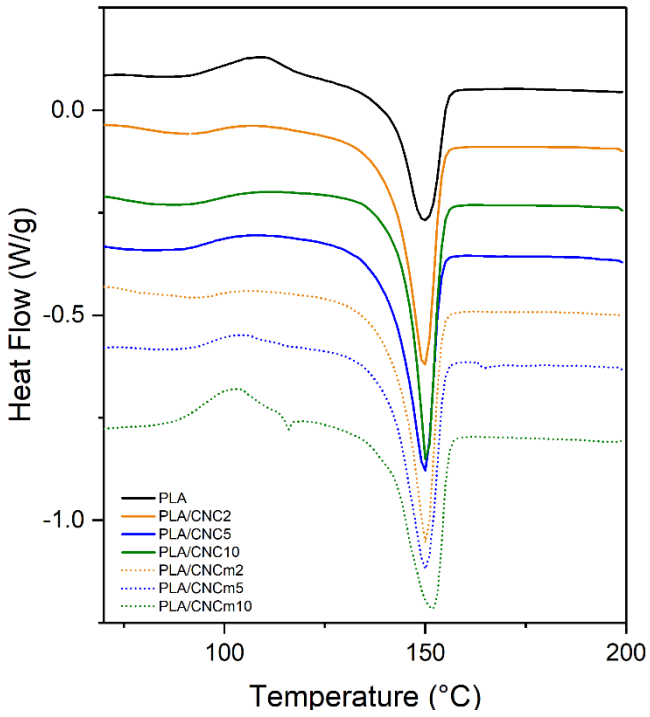

Figure III.20 - First heating curves in the DSC analysis of the foams produced.

As can be seen, the crystallization peak is much lower for most of the foamed samples, indicating that they either did not crystallize or crystallized very little during the DSC analysis, as they had already undergone significant crystallization during the foaming process. Figure III.21 highlights the differences in crystallinity percentages between the foamed samples.

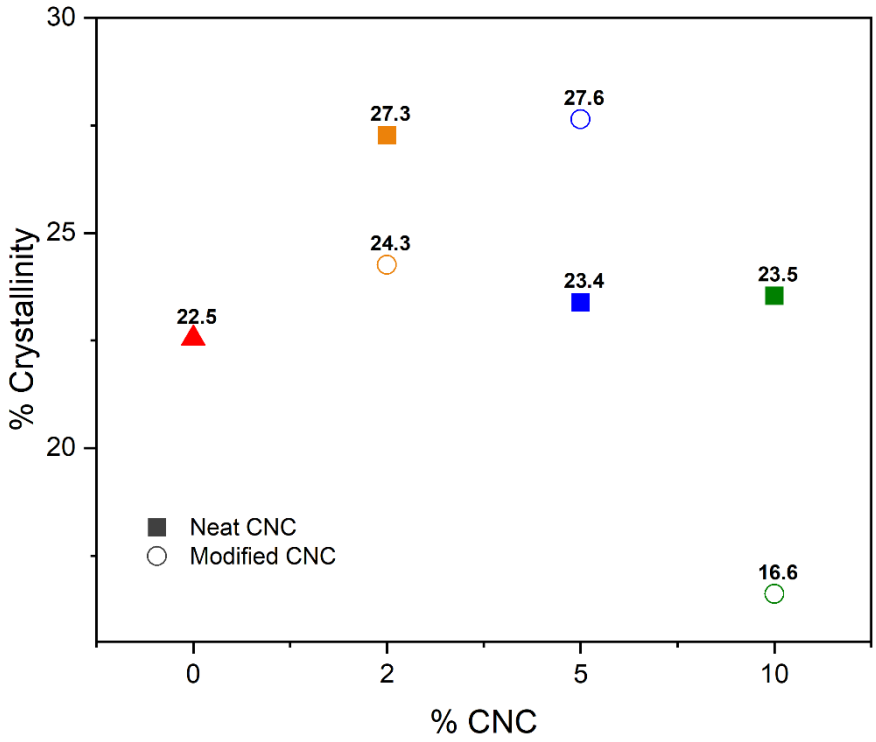

Figure III.21 – Crystallinity percentage of the foams obtained in the first DSC heating, at 10°C/min, representing the percentage of crystallization during the foaming process.

It can be observed that, except for the sample containing 10 wt% modified CNC, all other samples exhibited a crystallinity percentage equal to or higher than that of neat PLA, proving that crystallization can occur below Tc when sc-CO_2 is acting as lubricant in the system. However, the sample PLA/CNCm10 showed the lowest degree of crystallization, indicating that the high concentration of modified CNC significantly influenced the viscosity of the material. The lubricating effect of the grafted aliphatic chains onto the PLA likely hindered crystallization.

SEM images were acquired (Figure III.22), and the cellular structures were analyzed by cell size distribution, foam density, cell density, and expansion ratio (Figure III.23).

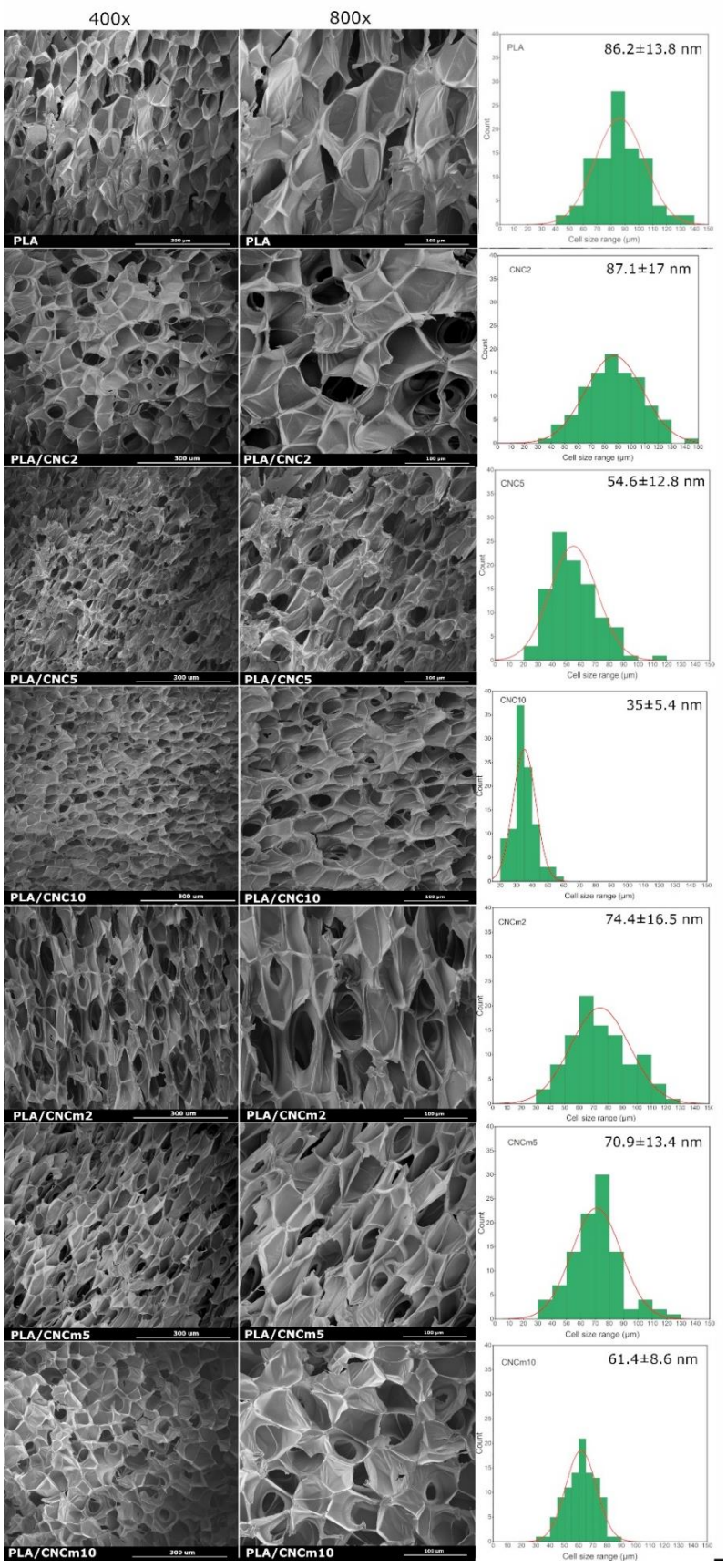

Figure III.22 – SEM images in two different magnifications (400x and 800x) for all nanocomposites formulations and its size distribution.

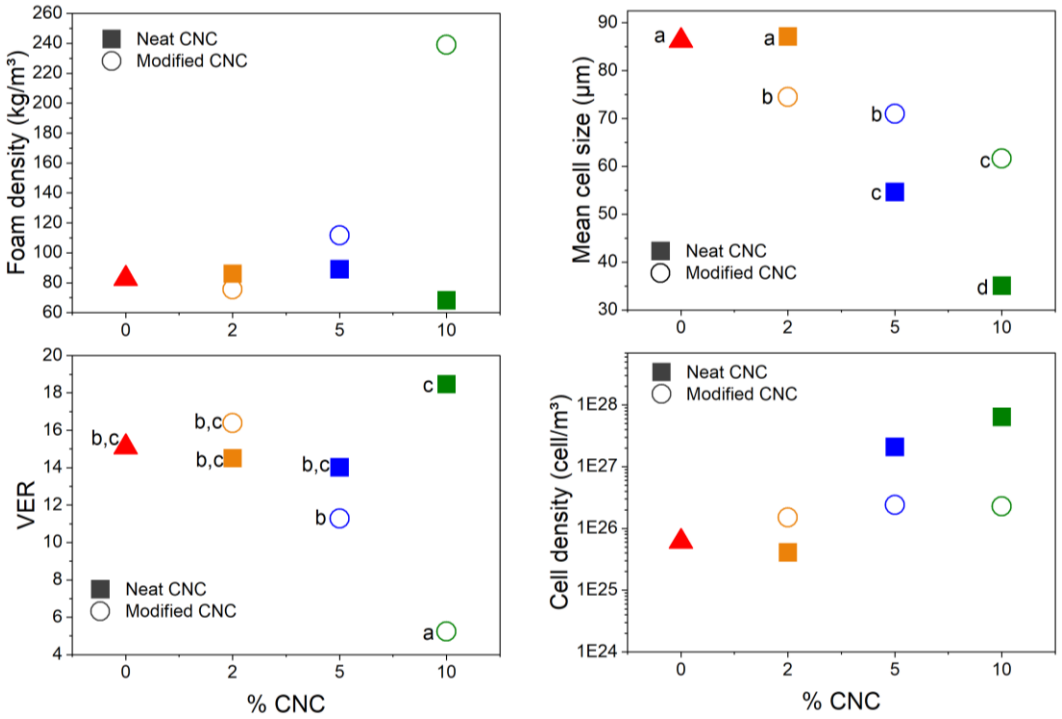

Figure III.23 – Cell morphology characterization. Different letters are statistically different.

As statistical analysis showed, cell sizes are statistically different comparing concentrations within CNC and modified CNC groups. Furthermore, except for the sample with 2 wt% of neat CNC, all the others presented a significant decrease in cell size compared to neat PLA. This can be attributed to the fact the 2 wt% of neat CNC with poor distribution in the matrix would not result in significant differences.

Furthermore, it was observed that increasing CNC concentration led to a reduction in cell size and a narrowing in size distribution within each group. This can be attributed to the higher particle concentration, which facilitated cell nucleation and led to higher cell density and smaller cell sizes.

At the same time, percentage of crystallinity did not show a pattern within the groups. For neat CNC samples at 5 and 10 wt%, crystallinity during foaming was approximately 23%. Decreasing CNC to 2 wt% led to an increase in crystallinity to 27%. It is known that crystals can play an important role in cell nucleation during foaming, where generally the higher degree of crystallinity results in higher cell density and smaller cell sizes. However, from the results

obtained, it can be inferred that, in this case, the factor that was decisive for the decrease in cell size was the concentration of CNC added, which facilitated cell nucleation. This can also be observed from the rheological results, in which even though the formulation containing 10 wt% CNC presented an apparent viscosity very close to that of pure PLA, it resulted in the smallest cell size. As a consequence, this formulation showed a significant increase in VER, which was a result of the high cell density.

A similar behavior was observed for the samples with modified CNC. The increase in concentration resulted in a decrease in cell size, but not as significant as for the samples with neat CNC. At concentrations of 2 and 5 wt% of modified CNC, the cells resulted in statistically equal sizes. The significant difference was only for the introduction of 10 wt% of CNCm. Making the same comparison, the decrease in cell size for this sample occurred even though it presented lower crystallinity and viscosity than the other two samples, evidencing that the decisive factor for the decrease in cell size was the concentration of CNC added.

Regarding the type of CNC introduced, except for the sample containing 2 wt%, the other concentrations obtained smaller cells with the introduction of pure CNC. In these cases, the samples with modified CNC present lower viscosities than the respective concentrations with pure CNC. This can lead to greater cell coalescence during growth, resulting in larger cell sizes.

As for the expansion ratio, it was only significantly different for the samples containing 10 wt% of CNC. In this case, neat CNC resulted in a VER of approximately 19 while modified CNC resulted in a VER of 5. These effects may be due to the low crystallinity that the sample presented during foaming. Comparatively, although both samples presented a high concentration of CNC that can act as a nucleant, the sample with modified CNC presented low crystallinity, which may have restricted cell nucleation, resulting in the difference of cell size and VER between the samples.

Therefore, it is clear that the nanocomposite foaming process is complex and involves several factors that can directly influence the structures formed. Furthermore, depending on the formulation, the same factors can influence in

different ways and magnitudes. Nevertheless, the functionalization of the CNC is also a factor that will influence the process.

4 Conclusion

The objective of this section was to produce foams from PLA/CNC nanocomposites, both neat and chemically modified, and to assess their influence on the foaming process. The results indicated that despite the success in increasing the hydrophobic character of CNC (as presented in Section III.1), the formation of agglomerates during the modification process may have hindered the material's dispersion during nanocomposite production.

Moreover, the nanocomposite production method used in this study was kept as simple as possible, involving direct melt mixing, which proved inefficient in dispersing both pure and modified CNC. However, unlike other studies found in the literature, the CNC agglomerates observed here were on a nanometric scale. The low dispersion prevented the samples from achieving rheological percolation, a factor that could have significantly enhanced the foamability of the samples.

Thus, the most significant variable was the CNC concentration in the samples. The two formulations containing 10 wt% CNC exhibited the most distinct effects. The addition of pure CNC at this concentration led to smaller cells and a high VER, while the modified CNC, which exhibited the lowest viscosity and storage modulus, resulted in the lowest VER. The impact of the grafted chains on CNC was also evident during crystallization, particularly in the 10 wt% formulation. Therefore, it is concluded that for the foaming process, the presence of CNC modified with n-OI in high concentrations can be detrimental to achieving small, well-distributed cellular structures.

In this investigation, the formulation containing 10 wt% pure CNC was the most effective in producing small, homogeneous structures with a higher VER than pure PLA.

Moreover, further studies must be done to deeper understand the effects of n-OI chains grafted onto CNC in the morphological crystallinity of nanocomposites, once this can be a decisive factor influencing in the foams strucutures.

Conclusion Chapter III

This chapter aimed to produce PLA/CNC nanocomposite foams and investigate the resulting cellular structures of their foams. The modification of CNC with n-OI effectively increased the hydrophobicity of the material. However, the ball milling process led to the formation of agglomerated structures, which significantly impacted composite production.

The melt mixing method used for producing nanocomposites resulted in poor dispersion within the PLA matrix, thereby preventing rheological percolation. As a consequence, there was no substantial increase in the viscosity of the nanocomposites, which limited the ability to correlate these properties with the foam structures produced.

Furthermore, the high concentration of modified CNC caused a reduction in viscosity and storage modulus (G'), resulting in the formulation with the lowest Volume Expansion Ratio (VER) among all those studied. This indicates that the functionalization of CNC plays a critical role in the foaming process of nanocomposites.

Future research should explore the achievement of functionalized CNC without aggregated structures, as well as alternative methods for producing nanocomposites, focusing on well dispersion of CNC. Such studies could provide further insight into how improved dispersion may influence the properties and structures of the resulting foams.

Chapter IV

Cellulose nanofibers (CNF) as a matrix for porous materials

CHAPTER IV CELLULOSE NANOFIBERS (CNF) AS A MATRIX FOR POROUS MATERIALS

Introduction to Chapter IV

Chapters II and **III** presented two strategies for producing PLA foams. However, PLA biodegrades slowly compared to other biodegradable polymers, as discussed in **Chapter I**. As an alternative to PLA foams, it is proposed to produce a porous material in which the matrix is cellulose nanofibers (CNF).

However, CNF cannot be melted, which makes it unfeasible to produce it using the same method used to produce PLA foams. As an alternative, by freeze-drying process is possible to produce a low-density and highly porous cellulose cryogel. However, cellulose-based cryogels present a high hydrophilicity character, which can be a drawback depending on the application desired. In literature, several alternatives are explored to overcome this challenge. Most of them use chemical methods, which involve chemicals and solvents.

Therefore, this chapter focused on studying how to improve the hydrophobic character of CNF cryogels without using chemical modifications, crosslinking agents or other methods based on chemicals and reagents.

IV.1 Cellulose nanofibers (CNF) cryogels hydrophobicity enhancement by using poly(lactic acid) (PLA) nanoparticles physisorption and melting templating

This section is adapted from the paper "SUQUISAQUI, A.B.V.; BETTINI, S.H.P ; BRAS, J. Cellulose nanofibers (CNF) cryogels hydrophobicity enhancement by using poly(lactic acid) (PLA) nanoparticles physisorption and melting templating." submitted to ACS Applied Biomaterials in June 2024.

1 Introduction

Cellulose-based materials have been used for thousands of years as engineering materials [151]. It is of great interest as they are biodegradable, non-toxic, and the most abundant polymer on Earth [127,129]. The main challenges aim at adjusting its properties, functionality, and durability to meet the requirements for high-performance materials, resulting in a sustainable and non-fossil source alternative.

Because of its hierarchical and semicrystalline structure, it is possible to extract cellulose nanoparticles by using a top-down mechanical or chemical deconstruction strategy [127] in which the resulting material will be called nanocellulose if at least one of its dimensions is in the nanometer range [130,132,133].

Among these nanocellulose materials, CNF is produced industrially since the last decade with several different applications as edible coating films for food application [279], barrier coating in packaging [280], wastewater treatment [281], pickering emulsifiers [282], biomedical [283], electronic device [284], among others. For some special applications, CNF is also used to produce cryogels, a porous material obtained by the freeze-drying method (also called lyophilization) [148,149,285–288]. Cryogels are interesting once they present several advantages, such as low density, high porosity, low thermal conductivity, large specific surface area, and high adsorption capacity [289]. CNF cryogels can be used in different applications such as biomedical (tissue engineering [146,157],

skin wounds [290,291]), water purification [289,292], sound and thermal insulation [293,294], and even to produce an ecology-drone [295].

Besides all the advantages, for some applications, cellulose-based materials present the drawback of being hydrophilic because of the high concentration of hydroxyl groups in cellulose structure, which leads to very low resistance in the presence of water. Therefore, studies look for pathways to make cellulose cryogels more hydrophobic. Several surface chemical grafting methods can be applied to this end, such as esterification, oxidation, silanization, etherification, etc [295,296]. Another drawback presented in literature about cellulose cryogels is their weakness regarding mechanical properties [297].

Lazzari and collaborators [296] produced a hydrophobic cellulose cryogel for petroleum sorption by comparing two methods of surface chemical modification: one, adding organosilane to the cellulose suspension and the other, adding organosilane vapor deposition. Results showed that cellulose cryogel surfaces were successfully modified with both methods, but vapor deposition was more efficient. In another study, cellulose cryogels were cross-linked by tethraethylenepentamine (TEPA) and functionalized by methyltrimethoxysilane (MTMS) aiming at wastewater treatment. Results showed that modified cryogels presented reduced shrinkage, high specific surface area, and high oil and Cr^{3+} adsorption.

However, the process of producing modified cryogel involves several steps and the use of different chemicals such as NaOH and urea [289]. Juan and collaborators [298] produced a thermally induced shape-memory cryogel with potential biomedical applications, in which TEMPO-oxidized CNF was functionalized by periodate oxidation to produce multifunctional CNF crosslinkers. Subsequently, chitosan glycol was reacted with the multifunctional CNF crosslinkers to produce cryogels, which presented macroporous structures, high water absorption and high compressibility.

The aforementioned studies use several steps and chemicals that can be potential pollutants to the environment. As environmental concerns are increasing more and more, it is important to seek less aggressive alternatives, such as the use of polymers instead of chemical processes. In literature, the use

of resins as reinforcement to enhance the mechanical properties of cellulose cryogels has already been tested. Yousefi and collaborators [297] synthesized three types of polyamide resins that were introduced into cellulose nanofiber gel, followed by the freeze-drying step. Results showed that the introduction of resins led to the formation of cross-linking between CNFs and resins. Consequently, compressive modulus and yield strength were more than 3 and 9 times higher than neat cellulose cryogel, respectively. The authors also observed that the morphology of pores influenced final properties; once the wall was thicker, the mechanical properties were higher. However, they used solvents, and the quantity of polymers was high. In addition, the polymer used is fossil-based and not biodegradable.

The use of biodegradable polymers as reinforcement is more difficult to find, although it could be a good alternative to improve cellulose-based cryogels properties. Among several biodegradable materials available, poly(lactic acid) (PLA) is produced from renewable sources, is biodegradable in industrial compost conditions, and is highlighted for being produced on a large scale, with a wide range of grades. Some of its main properties are high rigidity, transparency similar to polystyrene and poly(ethylene terephthalate), high tensile strength, and higher modulus than other biodegradable polyester [68,71].

Recently, a study explored the production of a ternary cryogel, in which CNF and nanochitin complex was used to stabilize a water-pickering emulsion of PLA in chloroform, for later cryogel production. The presence of nanochitin increased the interfacial activity leading to an increase in the adsorption of CNF on the surface of the PLA droplet. As a result, the ternary cryogels showed an increase in compressive strength and an increase in water resistance [299].

As far as it is known, no study produced a CNF cryogel only with the incorporation of a low amount of neat PLA to improve properties. In this context, the present study proposes, for the first time, a simple method for producing a CNF cryogel incorporated with PLA nanoparticles followed by a thermal treatment. The hypothesis is that the rigid and hydrophobic character of PLA nanoparticles physically adsorbed onto the CNF surface and then melted would improve CNF cryogels resistance to water. To this end, this study details the

introduction of PLA nanoemulsion into CNF suspension, enabling PLA nanoparticles to be adsorbed onto cellulose nanofibers. The influence of PLA melting by a drying post-treatment was performed, and the influence on morphology was discussed.

2 Materials and Methods

2.1 Materials

PLA Ingeo Biopolymer 4043D was purchased from NatureWorks LLC (MRF 6 g/10min - at 210°C), melting temperature between 145°C and 160°C, % of D content (not informed) – considered medium content. Cellulose nanofibers (CNF) suspension was purchased from Sappi, grade Valida® at 3 wt% of dry content in water. Dichloromethane was purchased from Carls Roth and used as received. The non-ionic surfactant used to produce the nanoemulsion was Glucopon® 215UP from BASF, a biodegradable surfactant based on alkyl polyglycoside that was diluted in distilled water to reach the desired concentration.

2.2 Methods

2.2.1 PLA nanoemulsion preparation

PLA nanoemulsion was first produced to be later dispersed into the cellulose nanofiber matrix. PLA was solubilized in dichloromethane for 1 hour at room temperature and mixed using magnetic stirring. Glucopon® 215UP was diluted in distilled water to obtain a concentration of 4.7 g/L, which corresponds to 10 times its critical micellar concentration (CMC).

After that, water and dichloromethane phases were mixed using an Ultraturrax at 7000 rpm, room temperature, and for 5 minutes, with a ratio of 70 wt% and 30 wt%, respectively. The prepared emulsion was submitted to an ultrasonic treatment (Sonifier S-250A – Branson, USA - equipped with a 0.5’’ diameter probe) for 2 minutes, with 20% energy capacity. It was later magnetically stirred for 2 hours in a water bath at 45°C to enable solvent evaporation. The last procedure was to carry out 3 cycles of recovery and water redispersion of PLA nanoemulsion in the centrifuge at 20°C, 10000 rpm (16211 G) for 15 min, to enable excess surfactant extraction. The final PLA nanoemulsion at 1.8 wt% solid

content was obtained and stored in the fridge for 6 months without sedimentation or aggregation.

2.2.2 CNF/PLA cryogel preparation

After PLA nanoemulsion preparation, the cryogels were produced by mixing CNF with PLA nanoemulsion in two different concentrations of PLA (10 wt% and 20 wt%) in comparison to the total weight of the final cryogel. First, the CNF (3 wt% dry nanofibers) was stirred using an Ultraturrax mixer, at 7000 rpm and room temperature, and the proper amount of PLA nanoemulsion was added to the suspension. For all cryogels, the nanoemulsion concentration was adjusted to reach, in the end, the same concentration of dried fibers, including the sample of neat CNF cryogel. The mixture was kept stirring for 5 minutes, and afterward, it was placed into the molds (24 places well plate) to be frozen using liquid nitrogen in a bottom-up flow for at least 15 minutes. Finally, the mold was placed into the freeze-drier to allow the sublimation of crystals ice for 72 hours, at 0.31 atm.

After freeze-drying, samples were recovered and thermally treated at 180°C for 20 minutes in an oven. Table IV.1 presents all formulations produced and their respective identification.

Table IV.1 – Identification of cryogel samples according to experimental design.

Identification	CNF (w:w%)	PLA (w:w%)	Thermal treatment 20 minutes (ºC)
CNF	100	0	0
CNF/PLA10	90	10	0
CNF/PLA20	80	20	0
CNF_180	100	0	180
CNF/PLA10_180	90	10	180
CNF/PLA20_180	80	20	180

2.2.3 Characterization

2.2.3.1 CNF Morphological analysis

CNF morphology was characterized by Transmission Electron Microscopy (TEM), Scanning Electron Microscopy (SEM), and Morphological Analysis (MorFi).

For TEM, a 0.1 wt% suspension of CNF was prepared in an Ultra Turrax for 5 minutes at 8000 rpm. The suspension was settled for 24 hours, and drops of the supernatant were deposited on a TEM carbon grid. The sample was stained with a 2 wt% uranyl acetate solution and dried. Images were taken with a Gatan Rio 16 camera equipped with a JEOL JEM 2100 Plus microscope at 200 kV. At least seven pictures were taken, and the most representative was selected.

For SEM, a suspension at 0.1 wt% was prepared, and then two drops were deposited onto a carbon substrate. The subsequent step involved evaporating the samples under high vacuum conditions (approximately 10 bar). Subsequently, all the samples underwent metallization with gold using a Rotary Pumped coating (Q150R ES Plus) equipped with a gold target, employing an

Argon plasma to deposit a thickness of 10 nm of gold. Finally, samples were analyzed using an ESEM Quanta 200, with a working distance of 10 mm and an accelerating voltage of 10 to 12.5 kV.

The morphology of TSE cellulosic material was analyzed using an optical image analysis, a MorFi Neo (Techpap, France). It analyzes a suspension of 25 mg/L for 5 minutes. Fine elements are considered below 50 µm; the repartition is done in 10 classes, the first being 5-10 µm and the last one fines superior to 50 µm. At least duplicates were done for a suspension and the average is presented.

2.2.3.2 Dynamic Light Scattering (DLS)

PLA nanoemulsion stability and diameter of particles were characterized by DLS (Dynamic Light Scattering) using a VASCO particle size analyzer, in which a diluted suspension of PLA nanoemulsion at around 10^{-2}-10^{-3} wt% was introduced. At least ten measurements at 15-second time steps and a limit noise ratio of 0.7 were carried out for PLA nanoemulsion, and averages were used for discussion.

2.2.3.3 Multi-SPR (Multi-Parameter Surface Plasmon Resonance)

PLA nanoemulsion interaction with CNF was analyzed by MP-SPR (Multi-Parameter Surface Plasmon Resonance) in a Navi 200 OTSO (Bionavis) device, and “full angular scan” curves were collected (40°-77°). First, the gold sensor was washed by preparing a solution of hydrogen peroxide, ammonium hydroxide, and distilled water in a proportion of 1:1:5 in volume. The solution was heated at 130°C, and the sensor was submerged for 20 minutes. After that, the sensor was recovered and washed with distilled water several times to make sure no more solution was present.

For the analysis, 0.5 mL of diluted poly(ethyleneimine) (PEI) suspension at 0.1 wt% was injected into the device at a rate of 50 µL/min. After injection, a washing step with distilled water was kept for 15 minutes. This layer allowed the

formation of a substrate to adsorb the CNF fiber. After ending of washing step with water, CNF was injected. TEMPO-oxidate CNF suspension at 0.1 wt% was used once the size of CNF Valida from Sappi was too large for the equipment capacity tube. We know the zeta potential of both CNFs is slightly different with respectively. But as the surfactant we have used is neutral, we consider TEMPO-CNF a good model surface to mimic cellulose surface in general, as it is admitted in the literature. An amount of 0.5 mL of CNF suspension was injected at a rate of 50 µL/min and then washed with distilled water for 15 minutes. Finally, PLA-NE was diluted at 0.1 wt% and, instead of performing the injection, the procedure was exchanged by a continuous flow with PLA-NE, which is the same procedure used for washing with water. After reaching a stabilization in the SPR angle, the washing step with distilled water was initiated for 15 minutes. The reason for this exchange was the fact that the volume of PLA NE injected was not enough to reach an SPR angle stabilization, as will be discussed in the Results section.

By data obtained from SPR analysis, it is also possible to estimate the thickness of particles adsorbed onto the substrate. For this, Equation IV.1 can be used as long as assumes that d (thickness of the layer) is a very small value:

$$d = \frac{ld}{2} \times \frac{\Delta SPRangle}{m(na - n0)} \qquad \text{Equation IV.1}$$

Where *ΔSPRangle* is the SPR angle change during adsorption, *ld* the characteristic evanescent electromagnetic field decay length, estimated as 0.37 of the light wavelength [300], *m* is sensor sensitivity factor (109.94° calculated by Gicquel[301]), *n0* and *na* are the refractive index of the bulk solution (estimated to be closed to water refractive index – 1.33) and adsorbed substance (PLA = 1.45), respectively. Once the thickness is calculated, the polymer mass per unit area (m) can be calculated using Equation IV.2 [302].

$$\Delta m = d \times \rho \qquad \text{Equation IV.2}$$

Where d is the thickness of adsorbed layer and ρ is the normal packing density of the adsorbed polymer, assuming that the adsorbent is spread uniformly. For PLA nanoparticles, ρ was estimated to be the density of the polymer 1.24 g/cm³, according to the supplier.

2.2.3.4 Cryogels characterization

Cryogels, with and without thermal treatment were characterized, using an electronic caliper and analytical scale, by measuring their apparent density (ρa), skeletal density (ρs), porosity (%) and shrinkage (vol%) [303], as it can be observed in Equations IV.3, IV.4, IV.5 and IV.6. At least five samples of each formulation was measured and the average value was used.

$$\rho a = \frac{m}{V} \qquad \text{Equation IV.3}$$

$$\rho s = \frac{1}{\left(\frac{wCNF}{\rho \mathrm{CNF}}\right) + \left(\frac{wPLA}{\rho \mathrm{PLA}}\right)} \qquad \text{Equation IV.4}$$

$$Porosity\ (\%) = 1 - \frac{\rho a}{\rho s} \qquad \text{Equation IV.5}$$

$$Shrinkage\ (vol\%) = 1 - \frac{Vm}{Vf} \qquad \text{Equation IV.6}$$

Where m and V are mass and volume of cryogels; $_{w}$CNF is weight fraction of CNF, $_{w}$PLA is the weight fraction of PLA, ρCNF is the density of CNF (cellulose density was considered 1.59 g/cm³ - perfect cellulose crystal of a beta polymorph [304]) and ρPLA is the density of PLA (1.24 g/m³ according to the material data

sheet); Vm and Vf are volume of the mold and the measured cryogel volume, respectively.

2.2.3.5 Fourier-transform infrared spectroscopy (FTIR)

For FTIR analysis an infra-red spectrometer by Fourier transform, model Nicolet 6700 from ThermoScientific was used. Cryogel samples without thermal treatment were analyzed in ATR mode, using a resolution of 4 cm^{-1} and 64 scans. The spectra were recorded between 4000 cm^{-1} and 400 cm^{-1}. For each sample, at least three spectra were obtained.

2.2.3.6 Specific surface area (SSA)

Surface specific area (SSA) was measured by nitrogen adsorption at 77K with a Quantachrome Nova 2200e device. Results were obtained by equation Brunauer-Emett-Teller (BET). Samples were previously vacuum degassed at 105°C for 16 hours. At least a duplicate was performed.

2.2.3.7 Contact angle

Contact angle analysis were performed using a contact angle meter OCA20 equipped with a CCD camera and SCA20 software. A 5 ml droplet of distilled water was deposited on cryogels, at room temperature, in both surface and cross-section. The acquisition of measurements was recorded for 60 seconds. For all samples, at least five measurements were repeated, and the biggest and smallest values were discarded for the average calculation used in the discussion.

2.2.3.8 Dynamic mechanical analysis (DMA)

Mechanical compression test was carried out in TA Instruments RSA 3 (New Castle, Delaware, USA) dynamic mechanical analyzer fitted with a 100 N load cell. Samples in a cylindrical shape (around 1.8 cm in diameter and 1.2 cm in height) were individually compressed at a rate of 0.1 mm/s and room temperature after storing the cryogels at 50%HR and 23°C conditioned room for at least 24 hours before any characterization. At least three measurements were performed for each sample.

2.2.3.9 Cryogel morphological analysis

Morphological and structural analysis was carried out by scanning electron microscopy (SEM). Samples were cut using a razor blade in cross-section at room temperature, pasted on a stub covered with double-sided carbon tape, and sputter coated with Au/Pd. Secondary electron images were recorded with an FEI Quanta 250 scanning electron microscope equipped with a field emission gun and operating at 2.5 kV in high vacuum mode or at 5 kV in low vacuum mode (50 Pa). At least ten images of two different samples from the same treatment were performed and the most representative images were selected and used for the discussion.

3 Results

3.1 CNF and PLA Nanoemulsion characterization

CNF grade Valida is obtained from a wood fiber source and offered as a suspension in water, at a concentration of 3 wt%, as presented in Figure IV.1a. CNF morphology can be observed by SEM (Figure IV.1b), TEM analysis (Figure IV.1c), and optical microscopy (Figure IV.1d). Results obtained by MorFi analysis are presented in Table IV.2, in which it is possible to observe the fiber content, the fines content (particles with length less than 200 µm [305]), the mean length-weighted length, and the mean fine area.

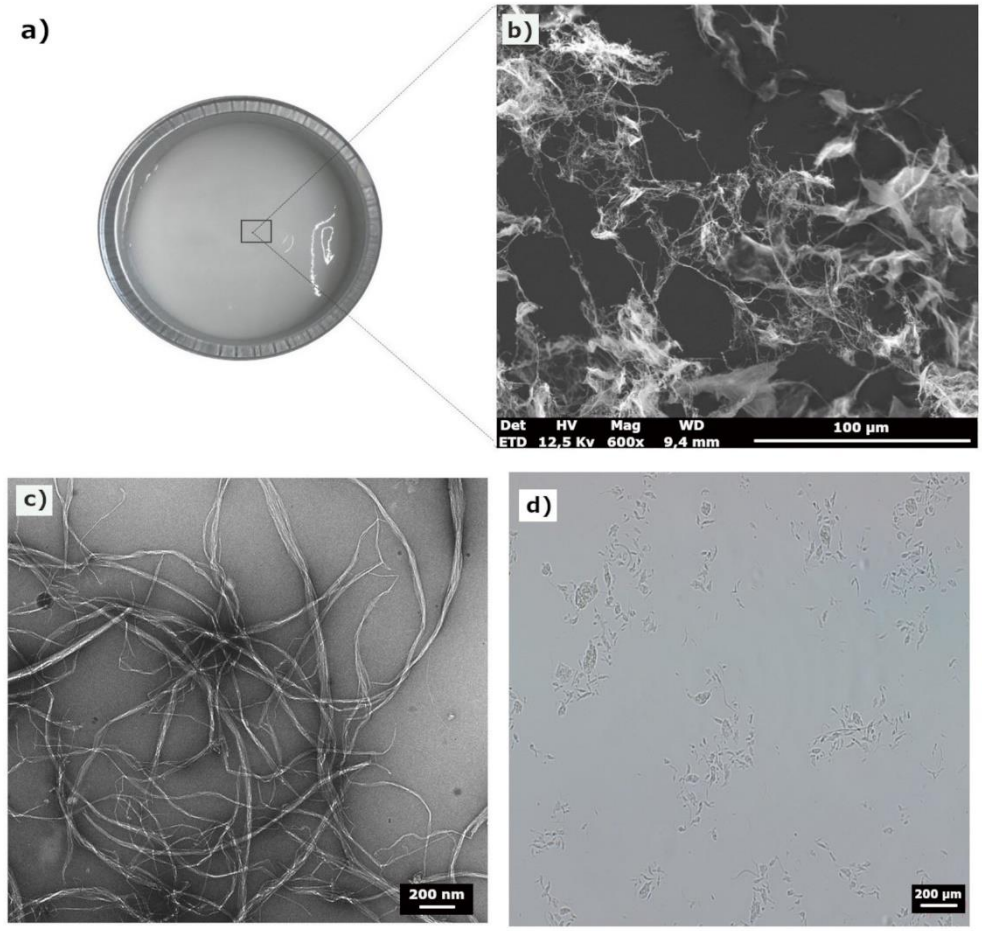

Figure IV.1 – a) CNF at 3 wt% dry content; b) SEM image of CNF at magnification of 600x; c) TEM image of CNF; d) optical microscopy of CNF.

Table IV.2 – MorFi analysis of CNF samples.

Fibers		Fines	
Fiber content. millions/g of pulp	74.6	Fine content. millions/g of pulp	8029.7
Mean length (weighted in length) (µm)	95	Mean fine area (µm²)	313

These are classical dimensions for CNF produced industrially with mechanical refining, as detailed by Desmaisons et al. [306] in their study of the quality index of cellulose nanofibril suspensions. This is quite a heterogeneous suspension with still some fibers (observed in optical microscopy), as well as microfibers and nanofibers, as shown by SEM and TEM.

PLA nanoemulsion was first prepared and characterized to observe nanoparticle size distribution. Figure IV.2 presents the prepared PLA nanoemulsion and its DLS analysis.

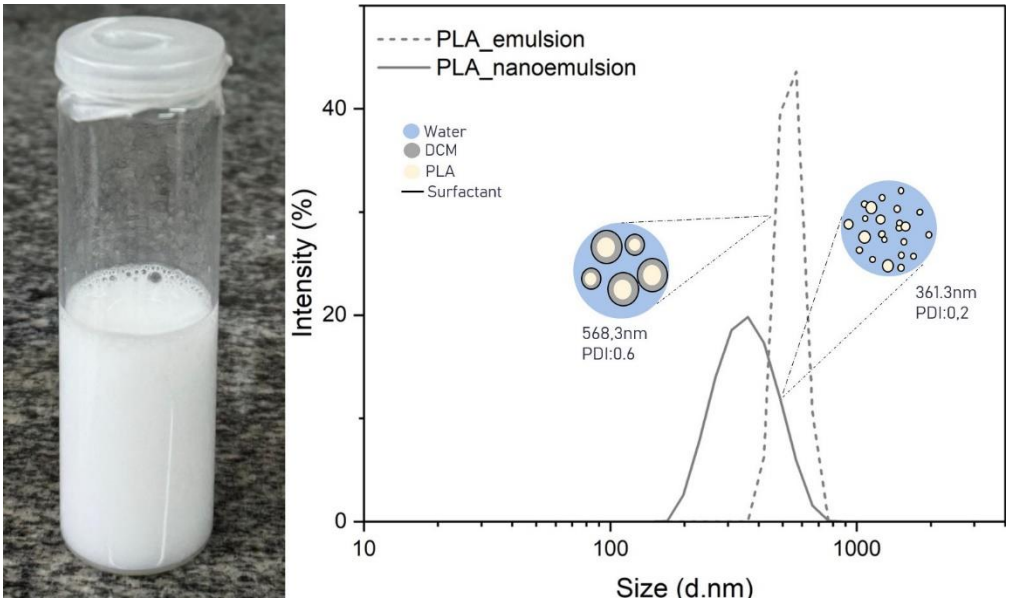

Figure IV.2 – Picture of PLA nanoemulsion 6 months after its preparation, at a concentration of 1.8 wt% and stored at room temperature, followed by characterization of PLA nanoparticles size and PDI before (emulsion) and after (nanoemulsion) ultrasonic treatment.

As can be seen, PLA nanoemulsion was homogeneous in a white color, without any presence of phase separation. Nanoemulsions are unique because

of their long-term physical stability without apparent flocculation or coalescence [307]. This is due to the high energy given by the ultrasonic treatment, which overcomes the surface-free energy necessary to increase the interfacial area between phases and disperse one phase into another [308]. According to Gupta and collaborators [309], droplets are in the range of 20-500 nm in nanoemulsions. The translucent aspect of nanoemulsions can be observed in systems with droplet radius below 100 nm; above this, systems become hazy and white due to multiple scattering [310]. This is confirmed by our PLA nanoemulsion whitish aspect and its stability observed visually for at least 6 months.

From DLS measurement, it is possible to observe two different curves, one representing the micro-emulsion without ultrasonication treatment and solvent evaporation and the other representing the nanoemulsion obtained after ultrasonication and solvent evaporation. It is possible to observe that, after ultrasonic treatment and solvent evaporation, PLA particle sizes have decreased (from 568 nm to 361 nm), and its PDI became smaller (from 0.6 to 0.2). This is a consequence of the ultrasonic treatment, which makes the PLA droplets smaller and more homogeneous. Also, it is a consequence of solvent evaporation. Once the solvent evaporates, only PLA stays in the droplet, and the size tends to decrease. As a result of this size decreasing, it is possible to reach a colloidally stable nanoemulsion, which can also be considered as a dispersion of PLA nanoparticles. For simplification, we will keep describing it as a PLA nanoemulsion (PLA NE) for the rest of the section.

Up to our knowledge, such PLA NE using anionic or cationic surfactants have already been produced [311], but this is the first time a biobased surfactant has been used. Similarly, it is worth noting that mixing polymer or molecule nanoemulsion with CNF has already been done in the literature to produce hydrophobic films [312] or coating layers [313], but in each case, they used cationic surfactant to favor interactions with anionic CNF. So, it was important to check if this glucose-based neutral surfactant was also adsorbed onto CNF.

3.2 PLA Nanoemulsion interaction with CNF

Once PLA nanoemulsion was prepared, it was important to investigate how PLA nanoparticles would behave on cellulose nanofibers surface.

Figure IV.3 presents an SPR sensogram and a scheme representing what happens during the injection of CNF and PLA.

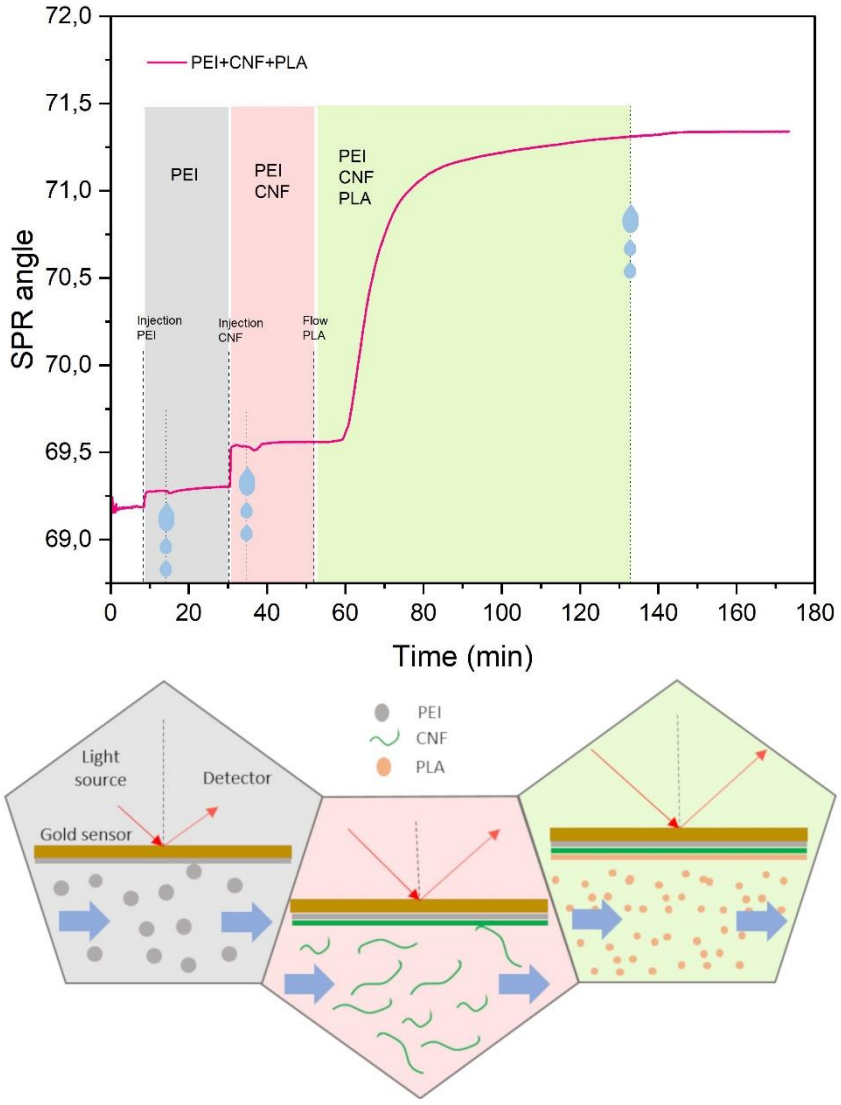

Figure IV.3 – SPR sensogram and a representation of what happens in each step of injection: 1) First layer with PEI as a substrate for CNF adsorption; 2) second layer with CNF; 3) third layer with PLA.

In a SPR sensogram, the change in the reflected angle (y) is proportional to the amount of material adsorbed at the surface, as shown by Equations IV.1 and IV.2 presented in section 2.2.3. In this way, it is possible to notice that after adding PEI, there is an instantaneous increase in SPR angle with the injection of CNF, followed by a small decay after some minutes, which is associated with the dissociation of some adsorbents [302]. After some minutes, the angle stabilization takes place, which means that CNF was adsorbed at the PEI surface. With PLA nanoparticle injection, it is possible to notice a very high increase in SPR angle, but at a lower rate than compared to PEI and CNF.

The first trials showed that the injection volume of PLA NE was insufficient to observe the stabilization of the SPR angle, meaning that the adsorption of PLA nanoparticles could still happen if we kept the flow of PLA nanoemulsion. For this reason, instead of performing the injection of PLA nanoemulsion, a continuous flow took place with the solution until a stabilization of the SPR angle was observed. When the stabilization was achieved, the washing procedure was exchanged for distilled water. As a consequence, since the change in the SPR angle is proportional to the mass of adsorbed material, it was possible to estimate the thickness and the mass per unit area of adsorbed PLA layer. According to Equation IV.1, the thickness was estimated to be 15.62 ± 1.75 nm, and by Equation IV.2, the mass per unit area of adsorbents was estimated to be 0.02 ± 0.002 g/cm^2.

It is important to clarify that, as far as we know, the study of PLA nanoparticle adsorption using the SPR method has never been reported before. The estimation made in this study used some approximations to get quantitative results but, for the objective proposed here, the most important fact was the observation of adsorption behavior for PLA nanoparticles onto the CNF surface, which was proven by the obtained sensogram, as it was shown by the changing in the SPR angle.

This is a very important response for the study, as PLA and CNF present different surface characters. The presence of surfactant enhances the interfacial surface activity between PLA nanoparticles and CNF, enabling an enhanced interaction between these materials. As a result, it is possible to observe by SPR measurements that PLA nanoparticles can be successfully adsorbed onto CNF.

3.3 Preparation of CNF/PLA nanoparticles Cryogel

Former trials showed that, due to the excess surfactant in PLA-NE, the mixture with CNF suspension produced air bubbles that were maintained during the freezing step, producing bigger crystals ice and resulting in a breakable material, as can be observed in Figure IV.4. For this reason, removing the excess surfactant by 3 centrifuging cycles was important to the process, which led to more stable samples.

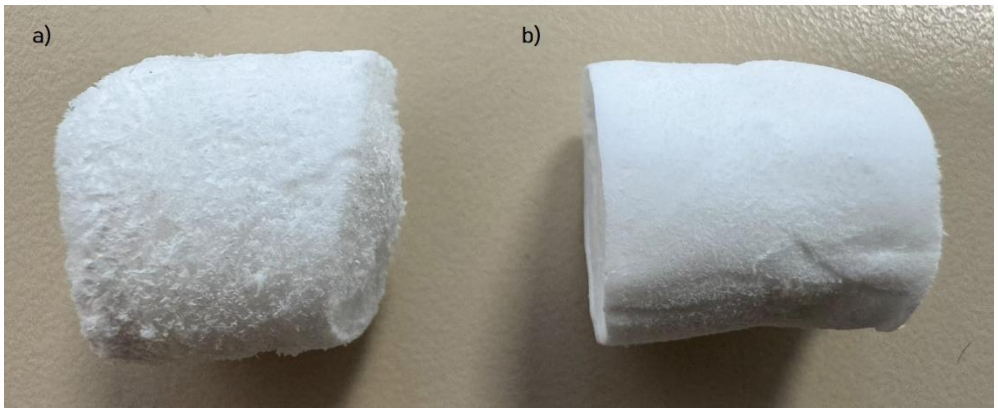

Figure IV.4 - Different structures formed in cryogels as a result of the a) presence of excess surfactant; b) absence of excess surfactant after several centrifuging cycles.

Other former tests were performed to choose a suitable temperature to enable PLA nanoparticle melting, in which samples were thermal treated at 150, 160, 170, and 180°C and then immersed in distilled water to observe their stability (Appendix 5). These were temperatures above melting temperature for the PLA grade, and at 180°C, cryogel samples proved to be more stable in water than treated in other temperatures.

Once PLA NE was prepared, CNF/PLA cryogels were freeze-dried. Produced cryogels can be observed in Figure IV.5.

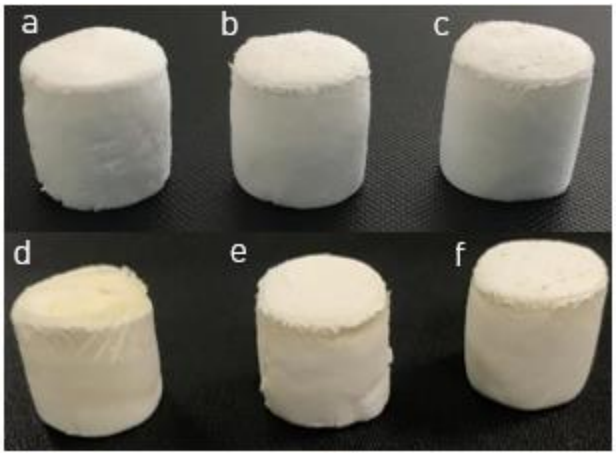

Figure IV.5 – Produced cryogels before and after thermal treatment: a) CNF; b) CNF/PLA10; c) CNF/PLA20; d) CNF_180; e) CNF/PLA10_180; f) CNF/PLA20_180.

As Figure IV.5 shows, cryogels neat or with PLA presented no visual differences, except for the brownish color observed in samples after thermal treatment.

FTIR analysis was performed to confirm the presence of PLA nanoparticles in CNF cryogel (Figure IV.6).

As can be observed in Figure IV.6, for neat CNF cryogel, typical peaks of pure cellulose are present, for example, at 1105 cm^{-1} and 3000-3600 cm^{-1}, corresponding to vibrations of C-O bonds and hydroxyl groups, respectively [179,314]. After the insertion of PLA nanoparticles, a new peak around 1750 cm^{-1} appears, corresponding to the ester bond (C=O) present in the chemical structure of PLA. Thus, it is clear that PLA nanoparticles are present in the CNF cryogel.

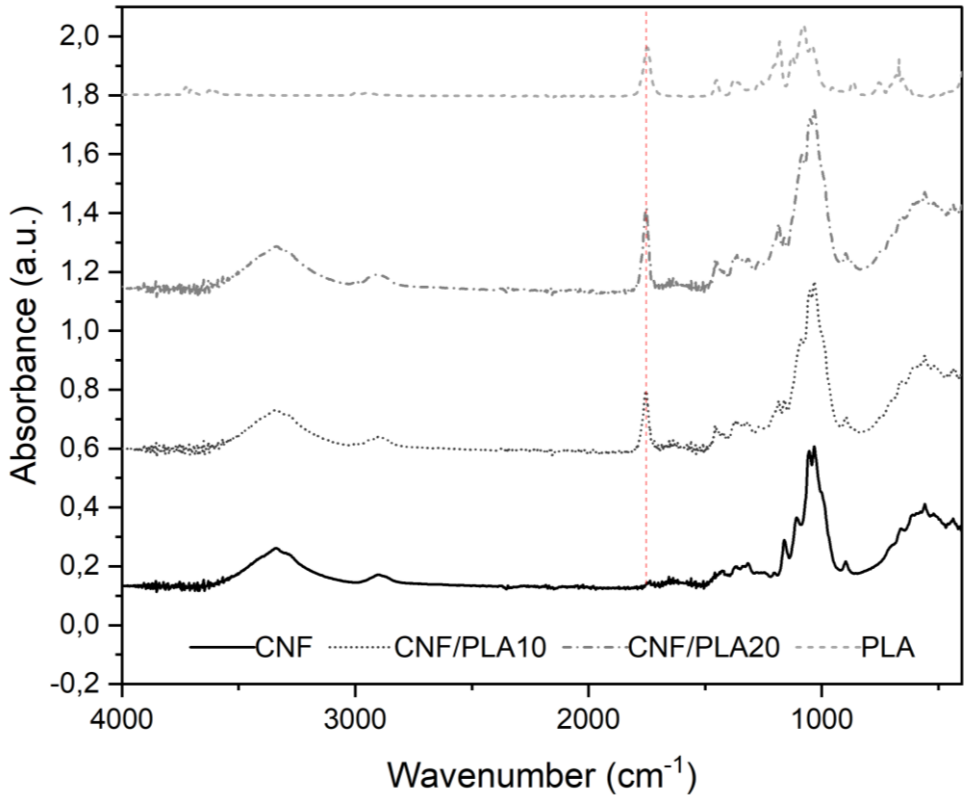

Figure IV.6 – Comparison between FTIR curves of neat PLA, CNF cryogel, and CNF/PLA cryogel with 10 and 20 wt% of PLA.

To understand the characteristics of produced cryogels, density, porosity, shrinkage, and SSA were calculated as explained in the methodology. No expressive difference could be seen regarding density and porosity. All the cryogels presented very low density, 0.02 g/cm³, as also stated in literature by Buchtová and Budtova [148], which produced microcrystalline cellulose cryogels at 3%, pre-frozen in unidirectional flow, density was found to be 0.05 g/cm³. No differences were observed for the densities of samples with and without thermal treatment. Regarding porosity, all samples were between 98 and 99%.

However, regarding shrinkage and SSA, some interesting differences were possible to note, as can be observed in Figure IV.7.

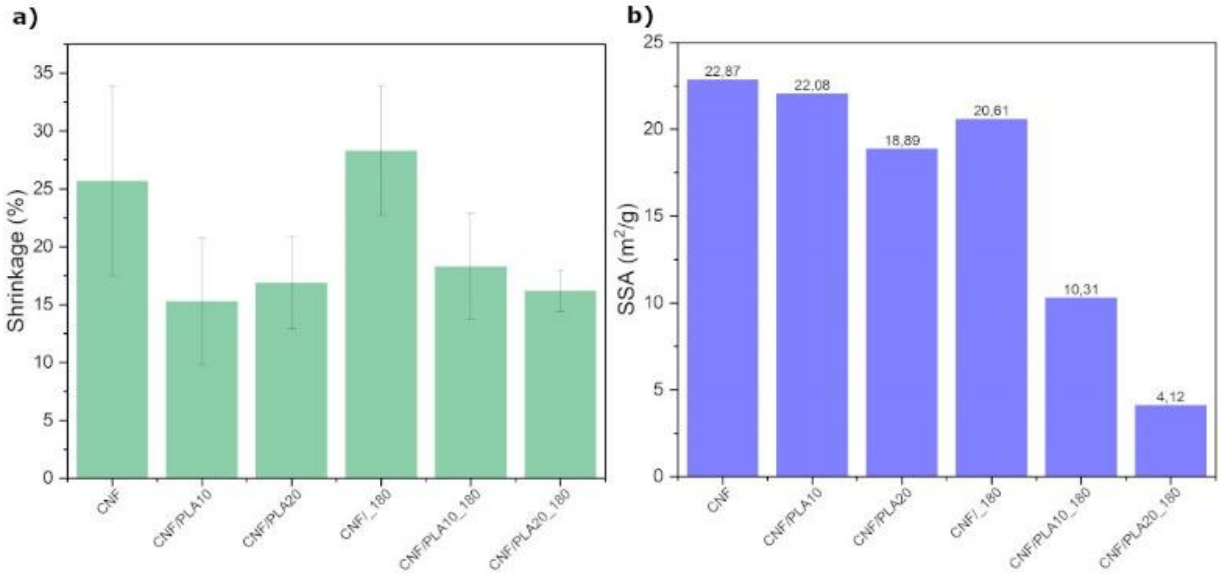

Figure IV.7 – Cryogel characterization: a) shrinkage; b) Specific Surface Area (SSA).

For neat CNF, shrinkage for samples both with and without thermal treatment presented higher percentages when compared to other formulations (around 25%), which corroborates the investigations carried out by Buchtová and Budtova [148], in which cellulose cryogels at 3 wt%, pre-frozen in unidirectional flow, the shrinkage was 19%. For samples with PLA nanoparticles, the shrinkage was slightly lower, which means that the addition of particles presented an influence during drying and coagulation. When water molecules are sublimated, fibers tend to coagulate, which results in volume shrinkage. As PLA nanoparticles are present, they can assist in the maintenance of structures, leading to lower shrinkage.

It is key to note that shrinkage was superior for samples after thermal treatment, which can be explained by the fact that the PLA melts on the surface decreasing the volume of spherical PLA nanoparticles between each CNF. At the same time, the drying process can cause the collapse of structure by the removing of water molecules, leading to a bigger attraction between fibers.

As observerd by Yousefi and collaborators [297], in general, cryogels present a SSA below 100 m²/g. As expected, with the incorporation of PLA nanoparticles, SSA tends to decrease. The difference is very subtle for neat CNF

and CNF/PLA10, probably because the amount of PLA was not high. After thermal treatment the SSA became very low for samples with PLA nanoparticles, which shows that the temperature was sufficient to melt these particles, forming a sort of coating on fibers, resulting in a decrease in SSA.

To understand the effects caused by the thermal treatment of cryogels, SEM images were performed in a cross-section direction, as can be observed in Figure IV.8. All images presented are at the same magnification (500 x) and samples with PLA nanoparticles are also presented at higher magnification (2500x).

The pore size in the micrometric scale is commonly observed for cryogels. Pure cellulose cryogels present a high amount of porous, regular structure, and thin walls, which leads to high porosity, low density, and low mechanical properties [297].

It is possible to observe that CNF and CNF/PLA10, both thermal treated or not, present similar porous structures with open cells, while samples CNF/PLA20 and CNF/PLA20_180 present more irregular structures. This can be due to the fact that for these samples, the percentage of fibers was 80%, which means that fewer fibers were present, leading to difficulty maintaining the pores' structures.

In higher magnification, it is possible to observe PLA nanoparticles distributed over CNF fibers in samples without thermal treatment. This corroborates results obtained by SPR measurements, which showed that PLA nanoparticles were well adsorbed onto CNF fibers. After thermal treatment, it is possible to observe that PLA nanoparticles were melted all over the fibers, which led to a kind of hydrophobic coating, as stated before. This means that a combination of the addition of PLA nanoparticles and thermal treatment can result in different properties for CNF cryogels.

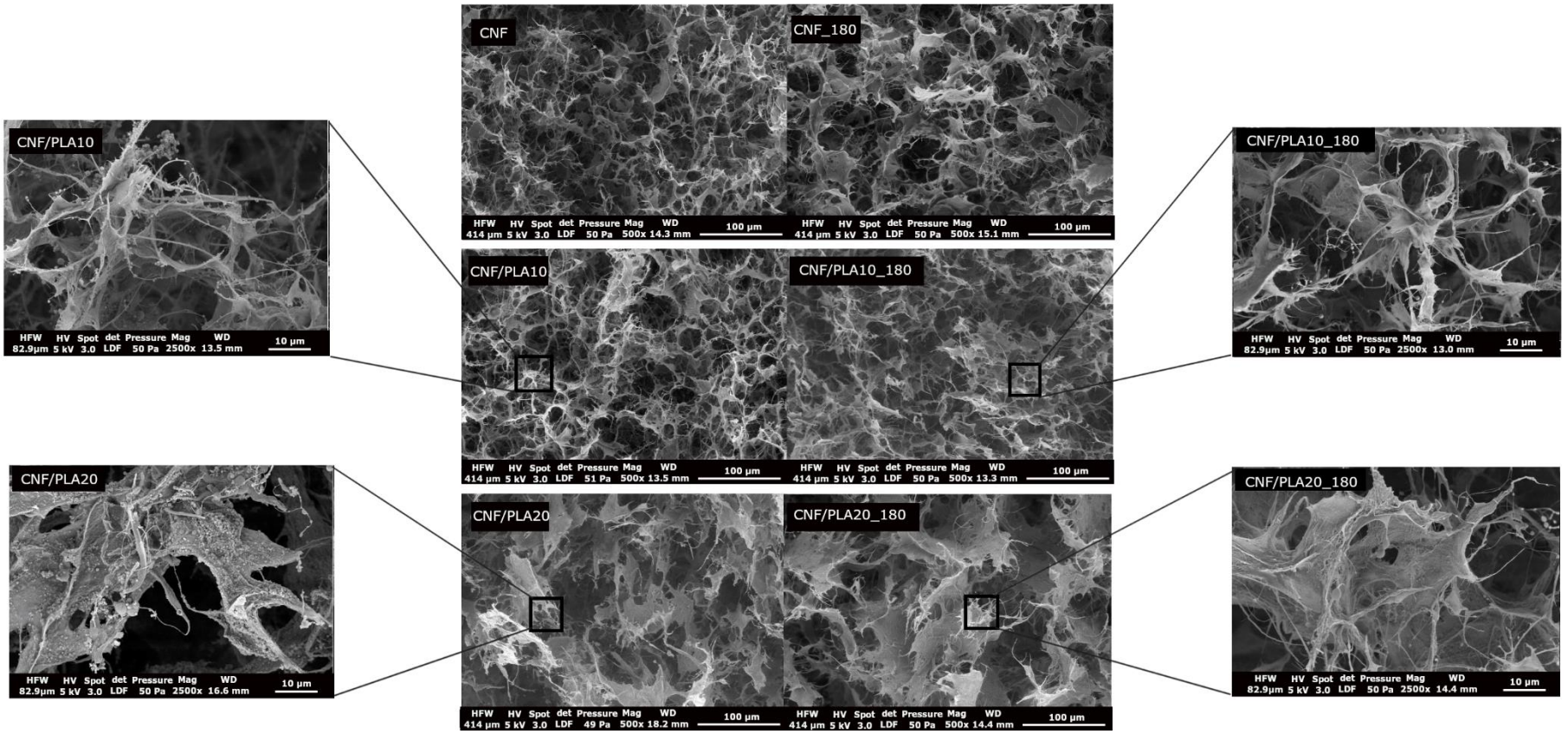

Figure IV.8 – SEM images of cryogels samples in cross-section direction.

3.4 Influence of PLA with or without thermal treatment in mechanical properties and water resistance of ensued cryogel

This effect was also analyzed in compression resistance. Figure IV.9 presents curves of compression stress for all samples studied. It is possible to observe that for all samples without thermal treatment and neat CNF with and without thermal treatment, curves did not present differences, even though PLA is a rigid polymer that could improve this behavior. However, when samples with PLA were thermally treated, it was possible to observe a slightly increase compression resistance, even in low strain. This result shows that the addition of PLA nanoparticles has not resulted in expressive effects or the thermal treatment by itself, once neat CNF with and without thermal treatment presented very similar behaviors.

Moreover, it is possible to notice that CNF/PLA20_180 presented slightly higher resistance all over the strain range until it reached 70% when the behavior became very similar to the sample CNF/PLA10_180. This can be explained by the fact that after receiving compression strain, porous materials suffer densification, which is due to the disappearance of porous structures (air), resulting only the solid material. As can be observed in Table IV.3, values for CNF before and after thermal treatment, in both 50% and 80% strain are very similar, however, it is possible to observe a slight increase in stress after thermal treatment for samples with PLA nanoparticles. At 50% of strain, the thermal treatment increased by 92% and 41% of stress for 10% and 20% of PLA nanoparticles, respectively, as well as in 80% of strain, in which the increase was around 57% and 24% of stress for 10% and 20% of PLA nanoparticles, respectively.

However, this increase is not expressive once, in general, very high porous materials present poor mechanical properties. The addition of 10 and 20% of PLA nanoparticles seems to be still low to result in expressive mechanical enhancement.

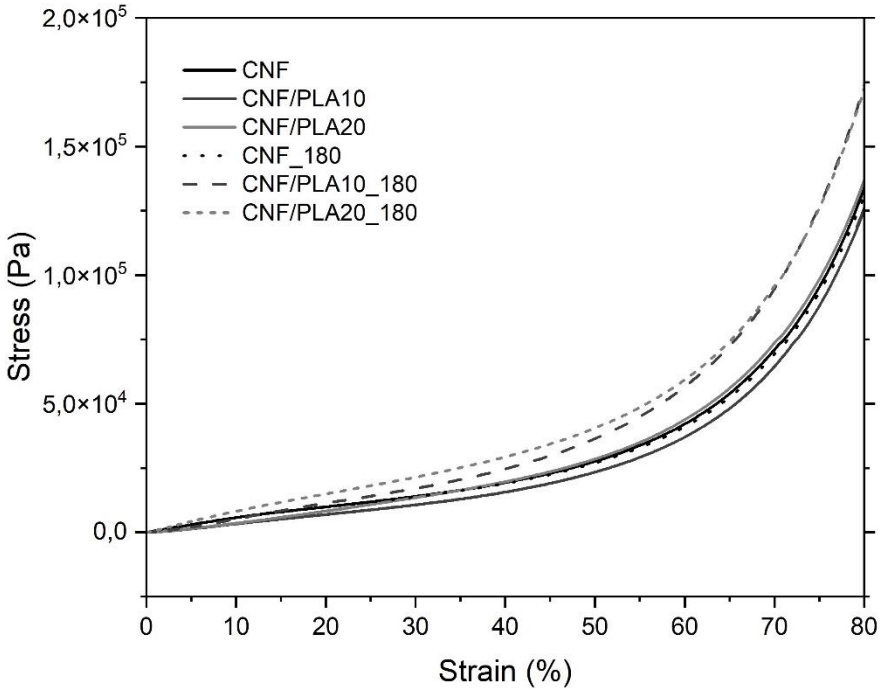

Figure IV.9 – Compressive resistance of cryogels samples in 50% HR, 23°C monitored room.

Table IV.3 – Stress values (Pa) for 50% and 80% of strain for all cryogels.

Sample	50% strain	80% strain
CNF	2.77 x 10^4 Pa	13.03 x 10^4 Pa
CNF/PLA10	1.90 x 10^4 Pa	10.95 x 10^4 Pa
CNF/PLA20	2.86 x 10^4 Pa	13.77 x 10^4 Pa
CNF_180	2.71 x 10^4 Pa	13.17 x 10^4 Pa
CNF/PLA10_180	3.65 x 10^4 Pa	17.20 x 10^4 Pa
CNF/PLA20_180	4.05 x 10^4 Pa	17.11 x 10^4 Pa

To study the influence of PLA nanoparticles and thermal treatment on water resistance, contact angle (CA) measurements were performed. However, for CNF/PLA cryogel samples without thermal treatment and for both neat CNF with and without thermal treatment, was not possible to be measured because the water droplet was instantaneously absorbed by the cryogel, forming a hole in the sample, making it impossible to be measured.

Regarding this behavior, neat CNF cryogels, with or without thermal treatment, were expected to not be resistant to water, once neat cellulose materials are very hydrophilic, as stated before [292]. The addition of PLA, a hydrophobic material, could improve the cryogel resistance to water, however, the same behavior was observed. Only after performing thermal treatment for both samples with 10% and 20% of PLA, at surface and cross-section, it was possible to note the improvement of water resistance, which reached contact angles higher than 100°, as shown in Figure IV.10 (contact angle of the surface is presented in Appendix 6). This means that temperature played a very important role once it made it possible for PLA nanoparticles to melt, creating a sort of hydrophobic coating.

It is possible to note that no big differences were observed for contact angle after 5 seconds, in which samples were obtained between 100° and 110° (CNF/PLA10_180 and CNF/PLA20_180, respectively). What is interesting to note is the behavior of samples across time. In the cross-section direction, it is possible to observe that the contact angle is slightly higher for samples with 20% of PLA. However, both samples presented very stable behavior during the 30 seconds of measurement. Regarding the volume of the droplet, as it is also stable, it is possible to conclude that the sample it is not absorbing the water, at least during this time.

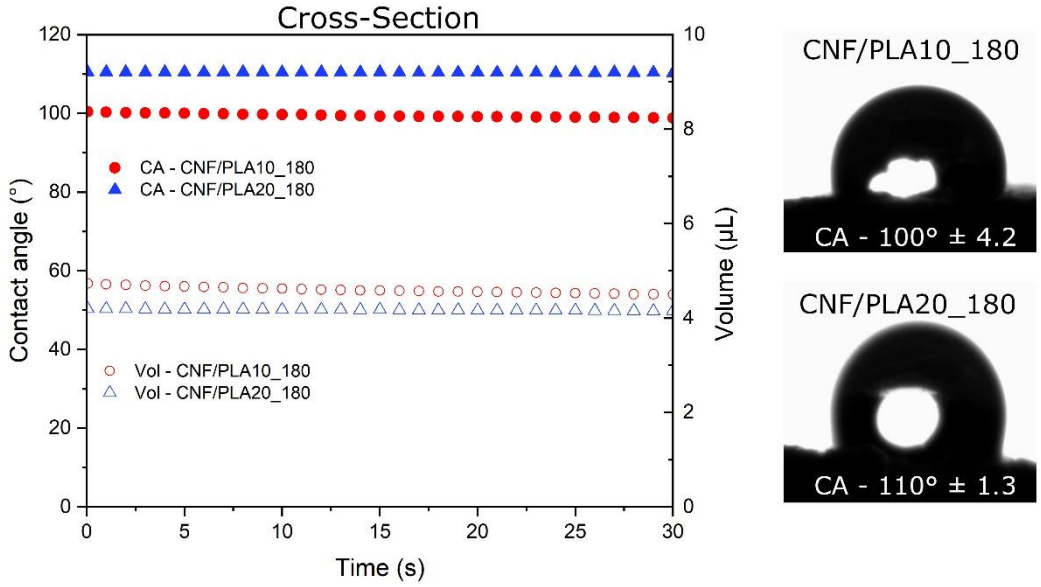

Figure IV.10 – Changes in contact angle and volume of water during 30 seconds and pictures of water droplets and their respective contact angle after 5 seconds.

This hydrophobic behavior was also observed when cryogels emerged in water. Figure IV.11 shows cryogels in water after 24 hours, where it is possible to note that samples thermally treated (at 180°C) presented resistance in the water.

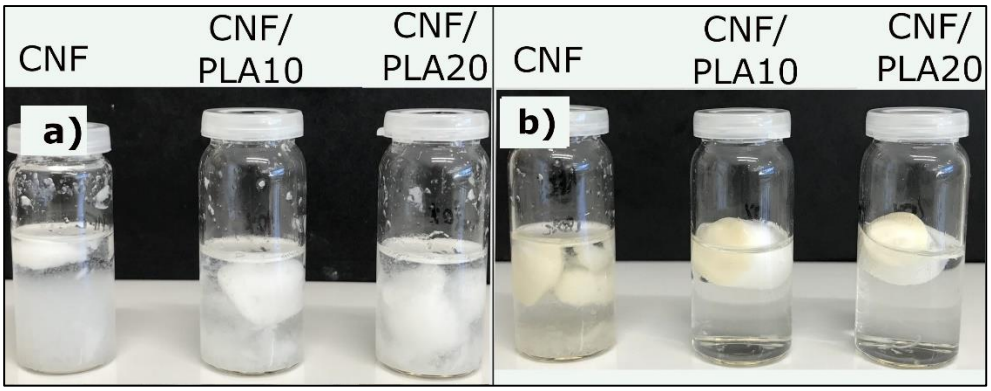

Figure IV.11– Water resistance of cryogels after 24 hours. a) Cryogels without thermal treatment; b) cryogels thermal treated at 180°C.

In Figure IV.11a it is possible to observe that cryogels are disintegrating in the water. However, with thermal treatment (Figure IV.11b), it is possible to note that samples with PLA nanoparticles do not present free fibers in the medium. This provides visual evidence of the role of molten PLA nanoparticles on the fibers acting as a hydrophobic coating.

4 Conclusion

This study aimed to produce, for the first time, a CNF cryogel with enhanced properties and hydrophobicity by adding PLA nanoparticles to the CNF suspension before freeze-drying. Results showed that the incorporation of PLA nanoparticles itself does not change properties, but the combined PLA addition and thermal treatment results in enhanced water resistance.

These results can be explained by the fact that after thermal treatment, PLA nanoparticles adsorbed onto CNF fiber can melt and produce a kind of PLA coating. As PLA is a rigid and hydrophobic polymer, cryogels present higher water resistance.

These results were only possible because of the successful production of PLA nanoemulsion, which provided enough stability to allow the mixture of PLA and CNF in water. Up to our knowledge, the PLA nanoemulsion produced using biodegradable surfactant has never been reported before. Besides, results from SPR were also important in proving that PLA nanoparticles were efficiently adsorbed onto CNF.

Two different concentrations of PLA nanoparticles were tested. Results show that incorporating only 10 wt% of PLA seems to be satisfactory once no big differences in contact angle were observed when compared to samples with 20 wt% of PLA. Actually, by morphological analysis, it was possible to observe that cryogels with 20% PLA resulted in non-homogeneous pore structures, probably because there were only 80% fibers in these samples, leading to the collapse of structures during the freeze-drying step.

Finally, this strategy can be an alternative to a more sustainable method of achieving cellulose cryogels with higher hydrophobic character, without the need to perform the chemical modification, cross-linking, vapor/atomic/metal/physical deposition, and without the need to use chemicals that can be a threat to the environment and human health.

General conclusion

General conclusion

This PhD research aimed to study the influence of chemical modification, by reactive processing, and the introduction of cellulose nanocrystals (CNC) on the properties of poly(lactic acid) (PLA) to produce foams using supercritical CO_2 as a foaming agent. In parallel, the study also proposes the production of a cellulose-based porous material with an enhanced hydrophobic character, without the need for chemical modifications.

In conclusion, the results showed that the different concentrations of GMA and DCP in the chemical modification of PLA led to different cell structures, in which an optimum condition relating to high viscosity and high crystallinity resulted in smaller and homogeneous cell structures. In comparison, the foams produced by the nanocomposites had larger sizes than the modified PLA foams, showing that the branched structures are more efficient in producing foams with more controlled structures. Furthermore, the low dispersion of the CNC in the PLA matrix limited the potential efficiency that the fillers could have in producing controlled structures.

Despite this, it was observed that CNC surface modification can directly influence cell structures. The long aliphatic chains of the n-OI lubricated the PLA chains, which decreased the viscosity of the material in general. This decrease in viscosity led to a foam with a low expansion ratio. In this sense, it is necessary to find an optimum concentration of CNC in the matrix so that it is high enough to form rheological percolation but low enough to avoid the lubricant effect of grafted chains in decreasing the material viscosity during the foaming process.

The work also aimed to study the enhancement of hydrophobic character on CNF cryogels, which is a contribution to the understanding of porous cellulose matrix materials. The introduction of 10 wt% PLA nanoparticles was enough to increase the contact angle without major changes to the porous structure of the material, compared to cryogels without nanoparticles. However, the introduction of 20 wt%, despite increasing the hydrophobic character, resulted in non-uniformed pores.

In this sense, this research is expected to have contributed to the understanding of the relationship between the properties of the polymer and its consequent foamed cell structure. This understanding is important because the structures formed will dictate the final properties of the foams. In addition, polymeric foams and porous cellulose matrix materials have a wide range of applications, and the results obtained in this research could contribute to the development of new materials or to improve their performance.

Perspectives and future works

As perspectives for future works, the following points are highlighted:

- Study of different foaming process variables such as temperature, pressure and saturation time, to investigate how these factors can influence the foam cell structures obtained by modified PLA and PLA/CNC nanocomposites;
- Investigating new methods of producing PLA/CNC nanocomposites to increase the dispersion of the reinforcement in the matrix as well as achieve non-aggregated structures after chemical modification;
- Study in depth the effect that n-OI chains have on the crystallization of PLA and its influence on the foaming process.
- Study other properties of the nanocomposites such as biodegradability, mechanical properties and barrier properties;
- Study the final properties of the foams such as mechanical, insulating and absorption properties.
- Study the introduction of CNC into PLA modified with GMA and DCP to investigate whether the nucleating effect of the fillers could reduce the size of the foam cells.
- Study of new techniques for heat-treating cryogels to avoid pore rupture.

Appendix

Appendix 1 – Supporting Information Chapter II

FTIR analysis in ATR mode was performed but no difference between neat and modified PLA was detected. The region of 910 cm^{-1} corresponds to the epoxy function, but as can be observed, nothing was detected.

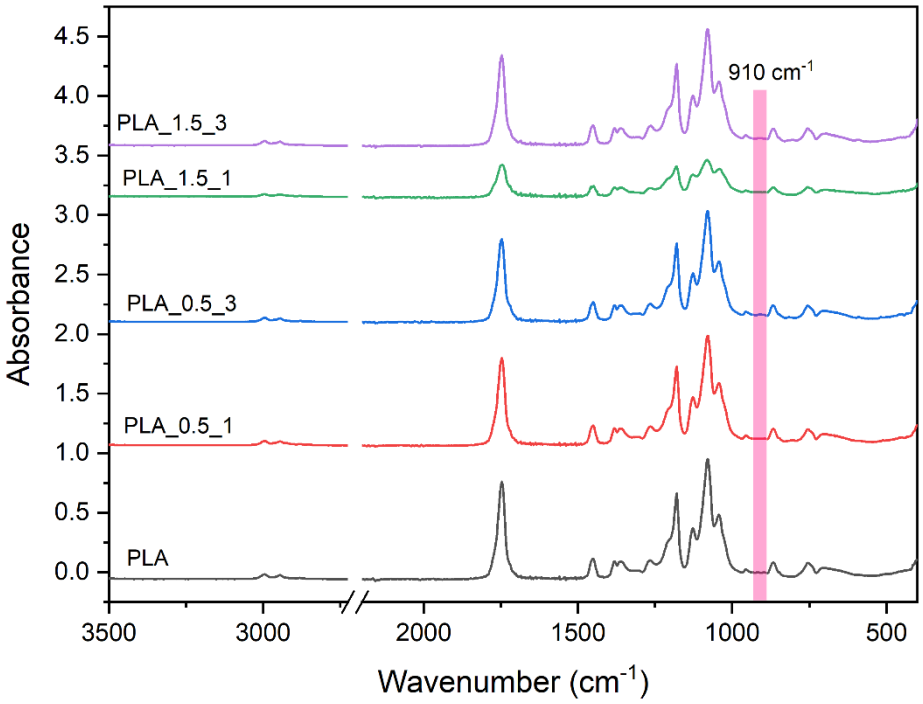

Figure II-SI.1 - FTIR curves for neat and modified PLA.

Appendix 2 - Supporting Information Chapter II

Proposed mechanism supported by NMR

In the ^{1}H NMR spectrum for the commercial PLA sample (Figure II-SI.2), it is possible to identify all the expected signals for the neat polymer: a doublet at 1.59 ppm with an area of 3 hydrogens referring to the methyl group, and a quartet of CH protons in the region of 5.17 ppm with doublet of CH_3 for ^{13}C NMR. The three signals referring to the carbons of the molecule are also identified in Figure II-SI.3. Figure II-SI.4 shows the HSQC spectrum of the PLA polymer**.**

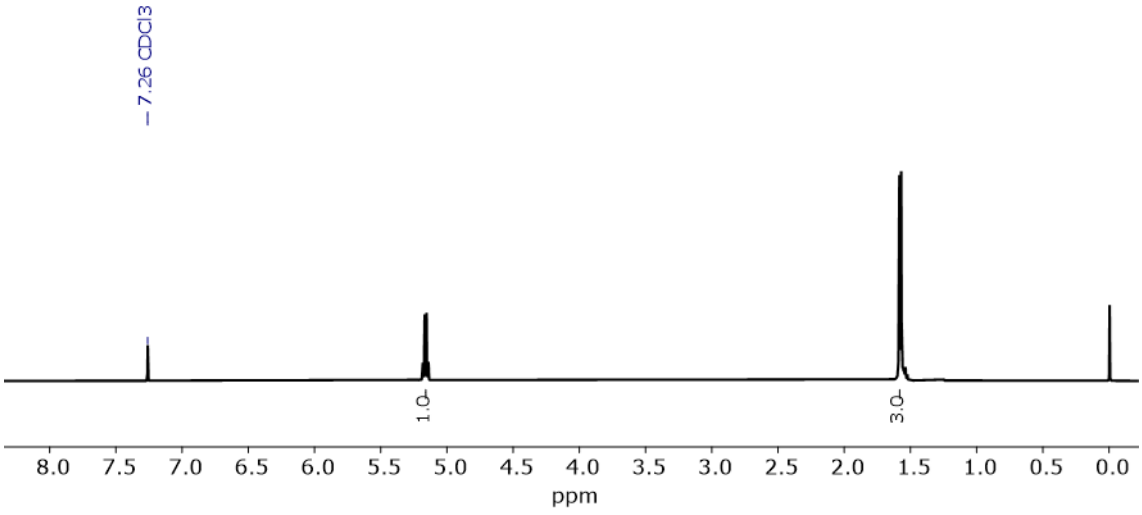

Figure II-SI.2: RMN 1H PLA

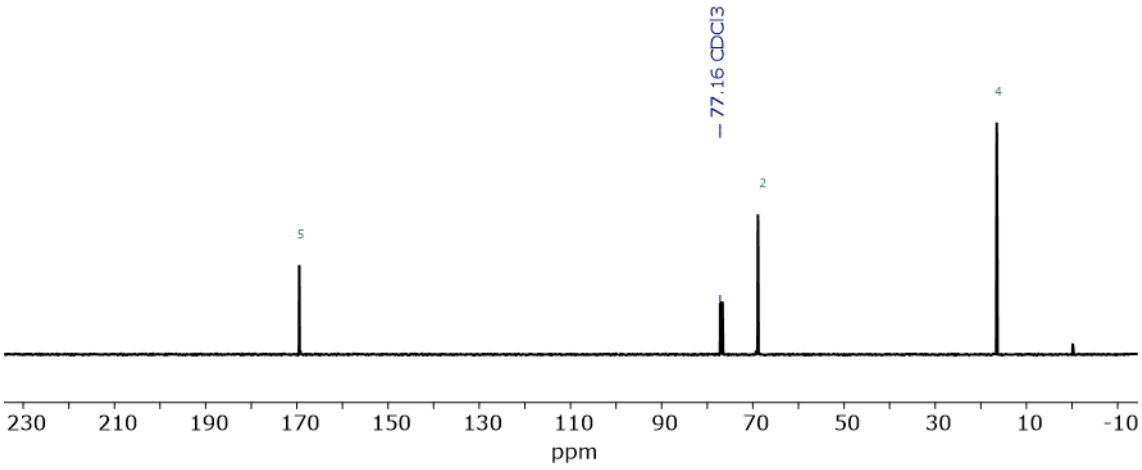

Figure II-S.3: RMN 13C PLA

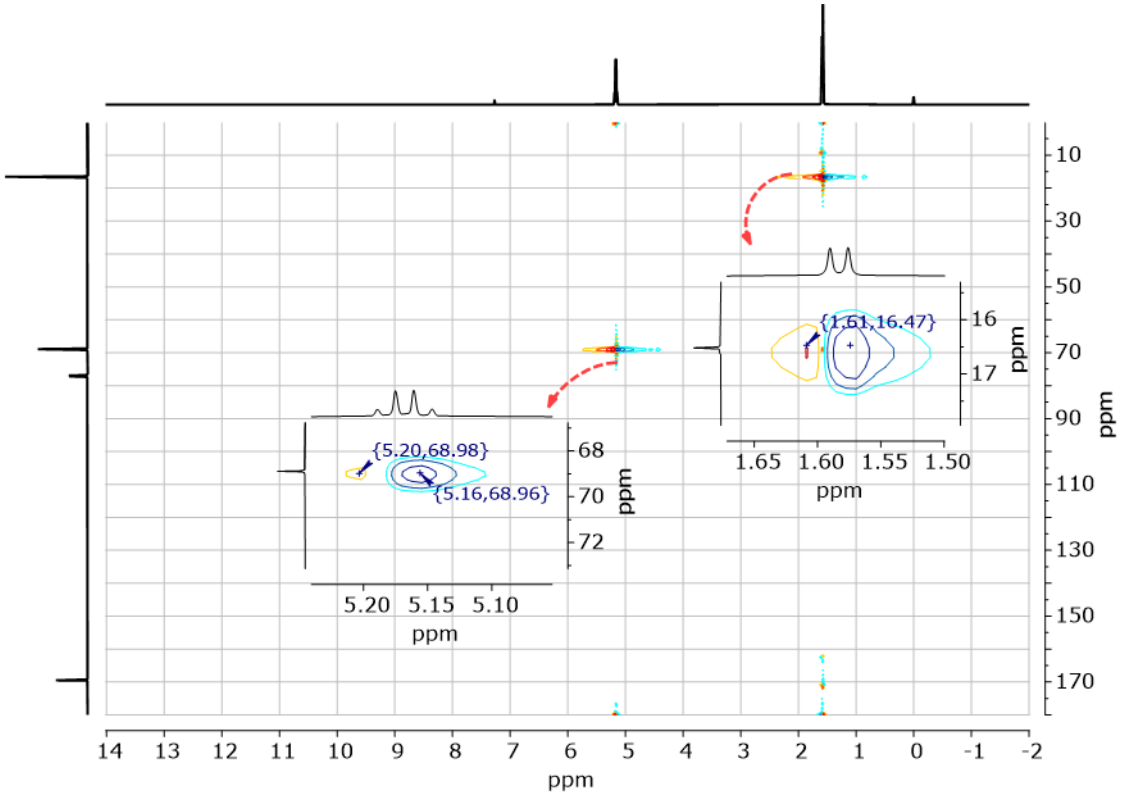

Figure II-SI.4: HSQC spectrum of the PLA polymer

The proton NMR spectra for GMA epoxide are found in Figure II- SI.5. The interpretations for this spectrum are that the CH_2 (hydrogens *6*) is not in the same chemical environment, each hydrogen was in a region: one in 4.00 ppm with an area of integration 1 and the double doublet multiplicity. The other hydrogen *6* is found in the 4.45 ppm region and has the same area of integration and multiplicity. Hydrogen *11* (5.61 ppm) and *12* (6.10 ppm) are also bonded to the same carbon and yet do not have the same chemical environment. The last two hydrogens mentioned are the ones that will be observed in the spectra of the branched polymer.

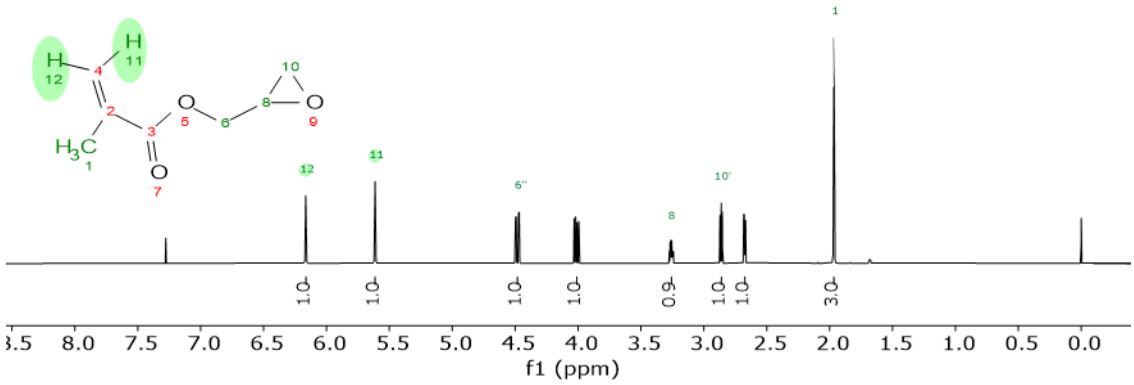

Figure II-SI.5: ^{1}H NMR spectrum of GMA EPOXIDE.

To study the reaction mechanism of epoxide branching in the PLA chain, nuclear magnetic resonance experiments were carried out with the reaction products. In Figure II-SI.6 there is a set of ^{1}H NMR spectra of GMA, PLA, PLA_0.5_1, PLA_0.5_3, and PLA_1.5_3.

In addition to the two characteristic signals of PLA at 1.54 and 5.15 ppm, in the spectrum of sample PLA_0.5_1 was also possible to identify GMA signals with chemical shifts, in the region of 4.35 ppm of CH_2 (*6*). Moreover, the hydrogens that previously had different chemical environments in the reactant appeared in the same environment in the product. The hydrogens H_2C=R11(5.61 ppm) and 12(6.10 ppm) are located in this region and are in the free GMA. In the spectrum, it is possible to observe that these signals “disappeared” and moved to the region of highest shielding as a singlet at 2.49 ppm in the R-CH_2-R1 structure. This shift of the signals to a field of greater shielding indicates the formation of branches in the polymer. In Figure II-SI.7 this is illustrated in step 5-PA02.

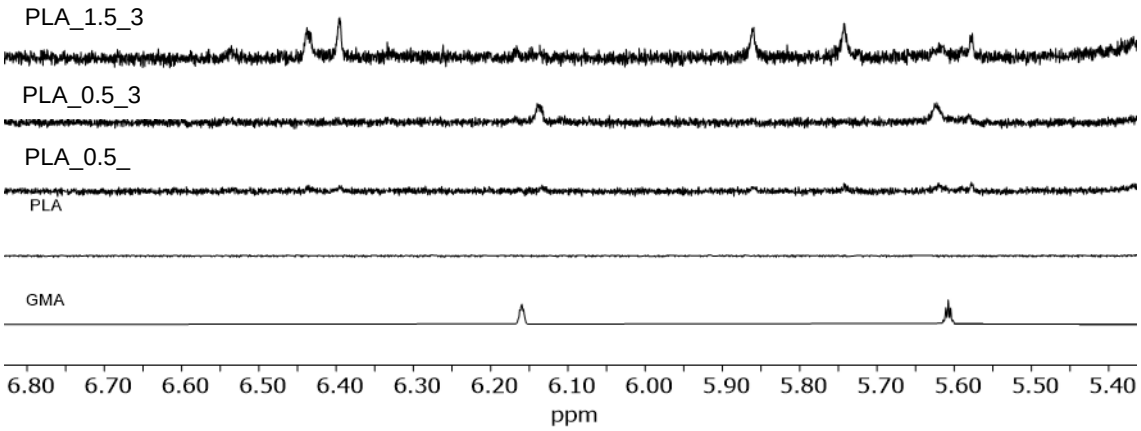

Figure II-SI.6: RMN de 1H

In the spectrum of sample PLA_0.5_3, the formation of the branch is observed, but also free GMA. This is because the proportion of GMA is much higher for this reaction compared to peroxide. This result is illustrated in step 5-P03.

Finally, sample PLA_1.5_3 presented, among its products, signs relating to PLA branching equal to the two other samples but presenting other signs in the region of 6.43, 6.40, 5.85, and 5.75 ppm. In the mechanistic illustration (step 5-P05), it is demonstrated that parallel reactions occur between GMA and PLA. Instead of forming a branch, GMA binds to PLA in two possible ways, forming isomers. The appearance of the four signals is consistent with the isomers, and the appearance of the singlet at 2.43 ppm refers to the CH_3 1 hydrogens.

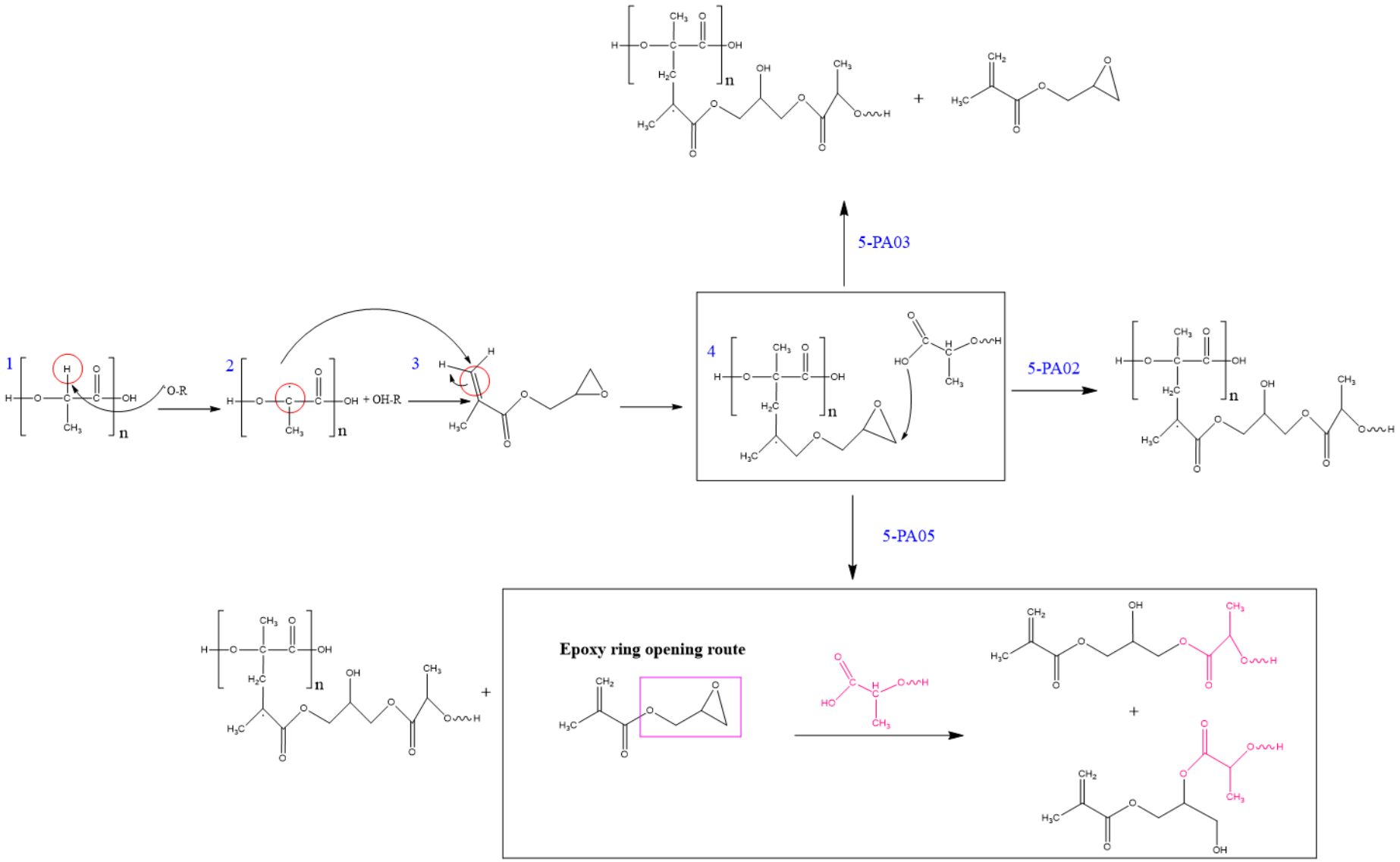
5-PA03
5-PA02
5-PA05
Epoxy ring opening route

To finalize the proposal for a mechanism, NMR spectrum by HSQC will be analyzed (Figure II-SI.8). In this spectrum, it is possible to observe that the hydrogens indicated in Figure II.SI.5 as hydrogens of the branching product do not have any interaction with any carbon of the PLA. This is a strong indication that these hydrogens come from a new product. However, it was not possible to observe any carbon signal from this new product in the ^{13}C spectra. The answer for the non-appearance of these carbons is that, despite the polymer chain is branched, the concentration of GMA branches is low compared to the PLA chain. As the abundance of ^{13}C is ~1.1%, the technique cannot analyze such carbons, and can only observe hydrogens that have an abundance of ~99%. It is also not possible to increase the concentration because the solution became gelled.

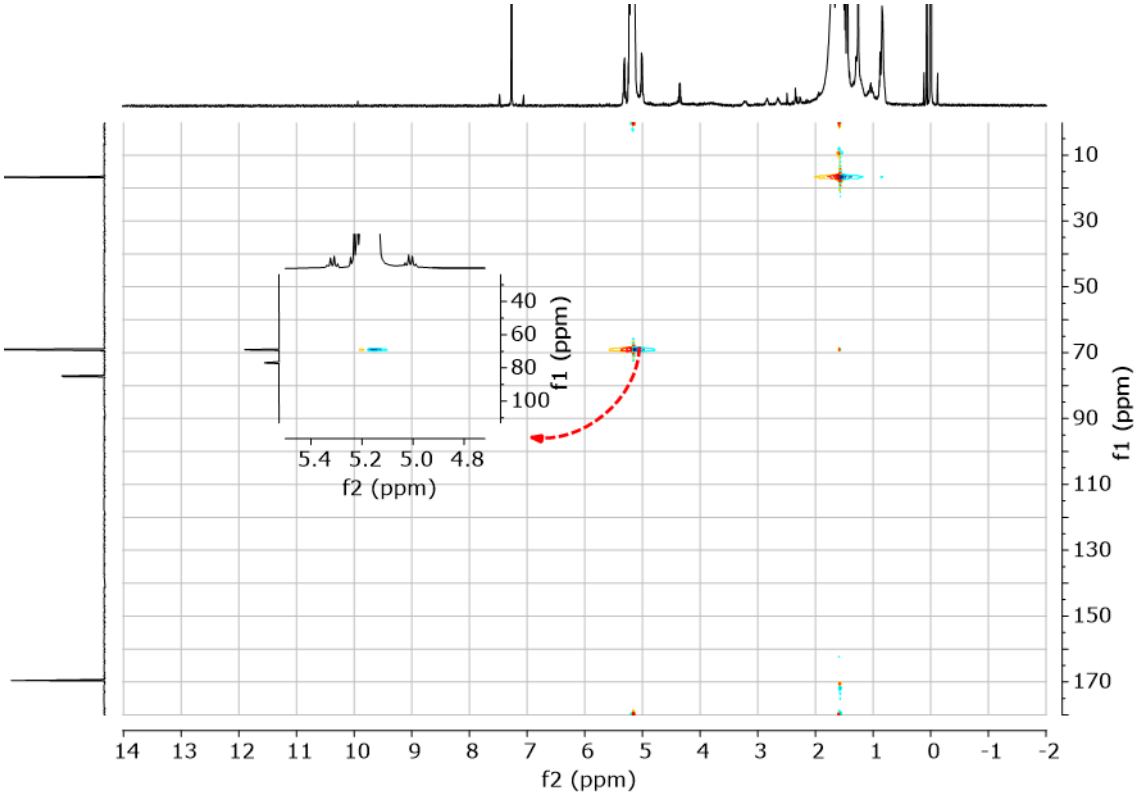

Figure II-SI.8: 1H NMR spectrum of the branching product of PLA plus GMA.

Appendix 3 – Supporting Information Chapter II

DSC curves of neat and modified PLA did not present crystallization during the cooling cycle, only during the heating. As Figure II-SI.9 shows, the Tm peak had shifted to lower temperatures as the molar mass increased. At the same time, the crystallization pick became smaller and broader than neat PLA.

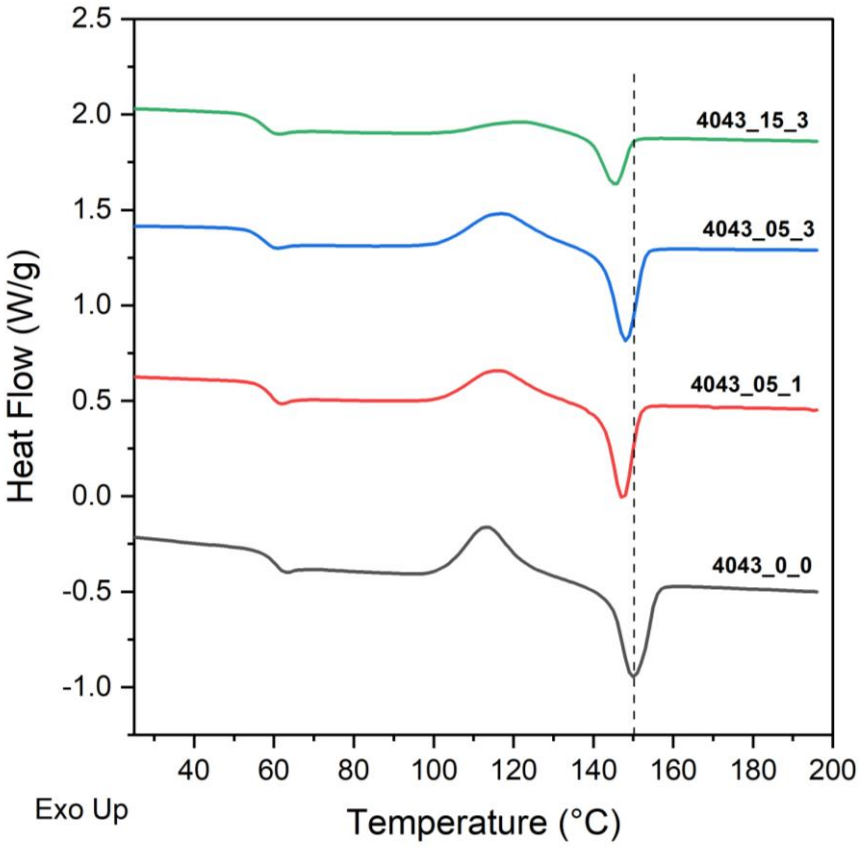

Figure II-SI.9: DSC heating curves for neat and modified PLA, from 25ºC to 200°C, at 10°C/min.

Appendix 4 – Supporting Information Chapter II

Steady-state rheological analysis of the purified samples was performed to determine whether residual GMA was affecting the results. As observed, the behavior of the curves was similar for both purified and non-purified samples. Due to the elimination of residual small molecules, the viscosities of the purified samples were slightly higher than those of the non-purified. This indicates that the rheological behavior of the samples is due to the different structures formed.

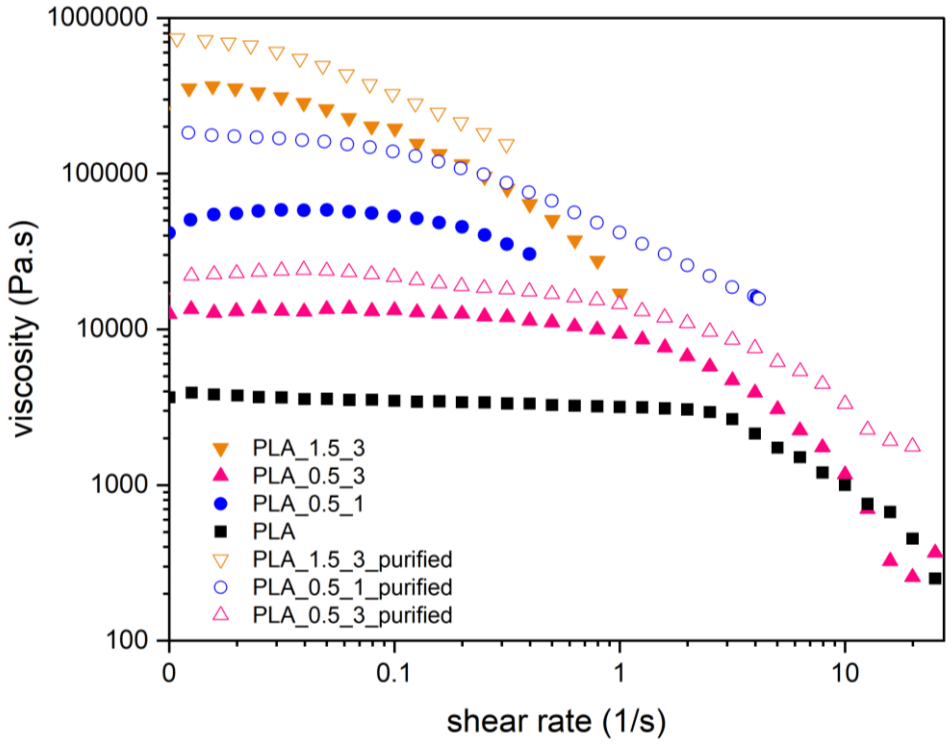

Figure II-SI.10: Apparent viscosity for purified and non-purified PLA samples.

Appendix 5 – Supporting Information Chapter IV

Previous tests carried out in several temperatures to observe the improvement of water resistance for cryogels samples is presented. As it can be observed, without thermal treatment (Figure a) samples were disintegrating in water. However, with the increase in the temperature treatment, the amount of free fibers in the water decreased. At 180°C (Figure f) the samples presented the best water resistance, once it was no longer possible to observe free fibers with the naked eye.

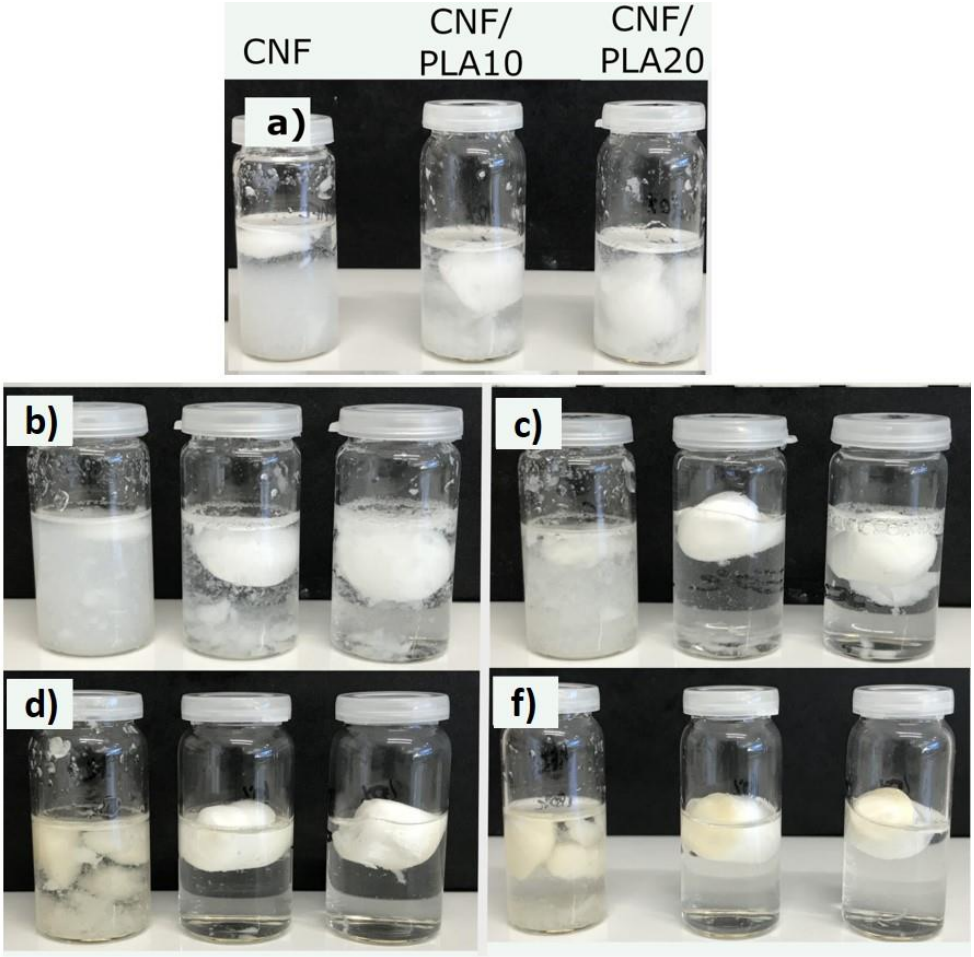

Figure IV-SI.1: a) no thermal treatment; b) 150°C; c) 160°C; d)170°C and; f) 180°C

Appendix 6 - Supporting Information Chapter IV

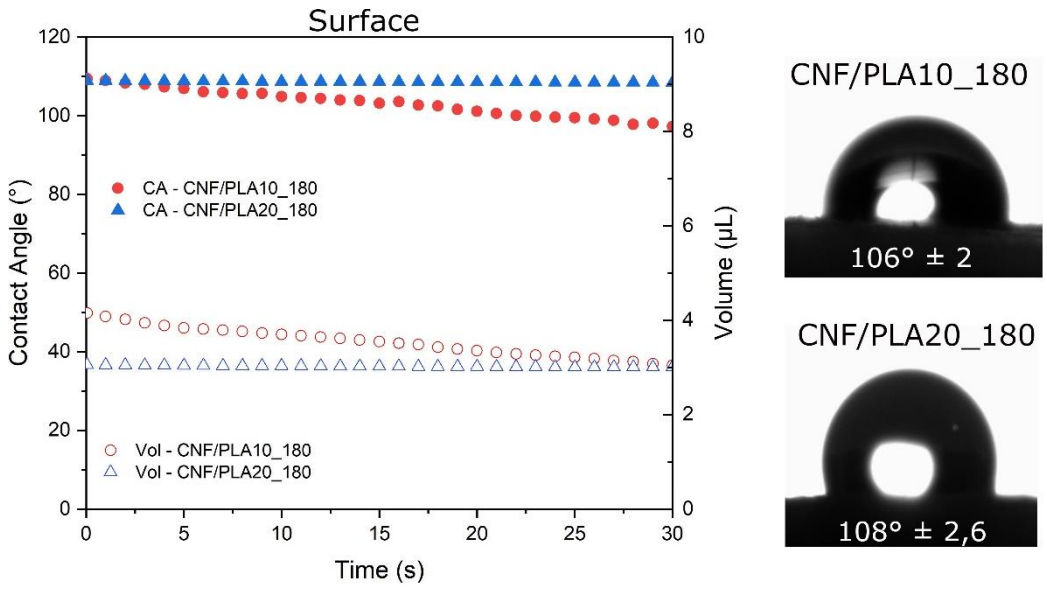

Figure IV-SI.2: Contact angle at the surface for cryogels after thermal treatment.

As it can be observed, on the surface, the CNF/PLA10_180 samples showed a decrease in the contact angle measurement over time, as well as the drop volume, indicating that the liquid was absorbed during the experiment. This may be due to the low concentration of PLA nanoparticles in the sample, unlike the result found for the CNF/PLA20_180 sample, which showed a stable angle and volume during the 30-second experiment. Compared to the cross-sectional measurements, the values found were close.

Extended Portuguese Abastract
Resumo expandido em Português

Materiais poliméricos vem sendo instrumento de crescimento e desenvolvimento da sociedade há mais de 70 anos e ganhou destaque por ser leve, barato, durável e aplicável tanto para fins de consumo como industriais. Desde o fim do século XX, o baixo custo deste material levou ao crescimento do seu mercado, ao mesmo em que tempo que acelerou a cultura de descarte e uso único destes produtos [1].

Desde então, a utilização de produtos plásticos vem crescendo a cada ano. Em 2019, o mundo produziu cerca de 460 milhões de toneladas de plásticos [2], no qual dois terços são destinados a produtos de ciclo de vida curto, os quais se tornam resíduos rapidamente. Isso levou a impactos significativos no ambiente, saúde e economia [3].

Dentro da classe de materiais poliméricos, as espumas são usadas há anos em diversas aplicações. Entretanto, estes materiais produzidos a partir de polímeros de fonte fóssil apresentam alguns desafios pós-consumo, como disposição incorreta dos resíduos e baixa reciclabilidade [4].

Desta forma, a dificuldade na gestão pode levar ao acumulo destes resíduos no ambiente, o que resulta em uma contínua degradação do material devido a fatores externos. Esta degradação gera pequenas partículas atualmente conhecidas como microplásticos [6].

Por esta razão, considerando o esgotamento de recursos não renováveis e as externalidades negativas associadas ao pós-consumo de materiais poliméricos petroquímicos, especialmente aqueles que apresentam desafios em sua gestão, o desenvolvimento e estudo de materiais alternativos se torna uma oportunidade promissora. Neste contexto, os polímeros de fontes renováveis e biodegradáveis/compostáveis são materiais produzidos a partir de recursos de fontes renováveis e que se biodegradam no ambiente ou em condições de compostagem.

O poli(ácido lático) (PLA) é um polímero de fonte renovável, biodegradável em condições de compostagem e biocompatível, produzido em grande escala e

em diversos grades. Por este motivo, o PLA é uma alternativa para a produção de espumas poliméricas. Entretanto, ele apresenta baixa resistência no estado fundido, requisito imprescindível para a produção de espumas com células de tamanho controladas e homogêneas. Deste modo, estratégias como a modificação química do material ou introdução de nanopartículas, podem ser adotadas para aumentar a resistência do fundido do material.

Dentre as diversas opções de reforço para produção de nanocompósitos, a celulose, considerada o polímero mais abundante no planeta, atualmente pode ser utilizada de diversas formas devido a sua organização hierárquica. Uma dessas formas já bem estabelecidas são os nanocristais de celulose (NCC), que podem alterar as propriedades do material. Portanto, o estudo da introdução de NCC na matriz de PLA se torna uma potencial estratégia para entender as propriedades finais do material e suas respectivas estruturas celulares obtidas pela espumação do nanocompósito PLA/NCC.

Além disso, uma vez que a celulose é o polímero mais abundante no planeta, proveniente de fonte renovável, biodegradável e biocompatível, a produção de materiais onde a celulose é o composto principal também pode ser uma alternativa aos problemas citados anteriormente. Entretanto, a celulose não é capaz de ser fundida, o que impede a produção de espuma pelo mesmo método utilizado na produção de espumas poliméricas no estado fundido.

Como alternativa, o método de liofilização permite a produção de um material poroso de matriz celulósica, que é denominado criogél. Os criogeis produzidos a partir da nanofibras de celulose (NFC) apresentam a desvantagem de terem pouca resistência na presença de água, o que leva a possibilidade de novos estudos para sanar este desafio.

Desta forma, dois métodos foram utilizados para exploração da produção de espumas biobaseadas: espumação do PLA e PLA/NCC utilizando-se CO_2 supercrítico e lifofilização para produção de criogeis de NFC.

Portanto, o objetivo geral desta tese de doutorado foi estudar a influência da modificação química, por processamento reativo, e da introdução de nanocristais de celulose (NCC) nas propriedades do poli(ácido lático) (PLA) visando a produção de espumas utilizando o CO_2 supercritico como agente de espumação. Além disso, também foi objetivo propor a produção de um material poroso de matriz celulósica com maior carácter hidrofóbico, sem a necessidade de realizar modificações químicas.

Desta forma, a tese se propôs a atender aos seguintes objetivos específicos:

- Avaliar a influência das diferentes concentrações de reagentes durante a modificação química do PLA nas estruturas químicas formadas e nas propriedades resultantes;
- Modificar quimicamente os nanocristais de celulose para aumentar o caráter hidrofóbico da superfície e melhorar a compatibilidade das partículas com a matriz de PLA;
- Relacionar como as propriedades obtidas no PLA modificado e no nanocompósito PLA/NCC influenciam nas estruturas celulares finais das espumas produzidas.
- Propor um método para aumentar o caráter hidrofóbico de criogel de NFC sem a necessidade de realizar modificações químicas.

Para alcançar os objetivos propostos, a colaboração entre o Laboratório de Polímeros Biodegradáveis da UFScar (Brasil) e o Laboratory of Pulp and Paper Science and Graphic Arts (França) foi imprescindível para alcançar os resultados desenvolvidos durante os 4 anos de doutorado em cotutela. Os resultados foram organizados em 4 diferentes capítulos, como ilustra a Figura 1.

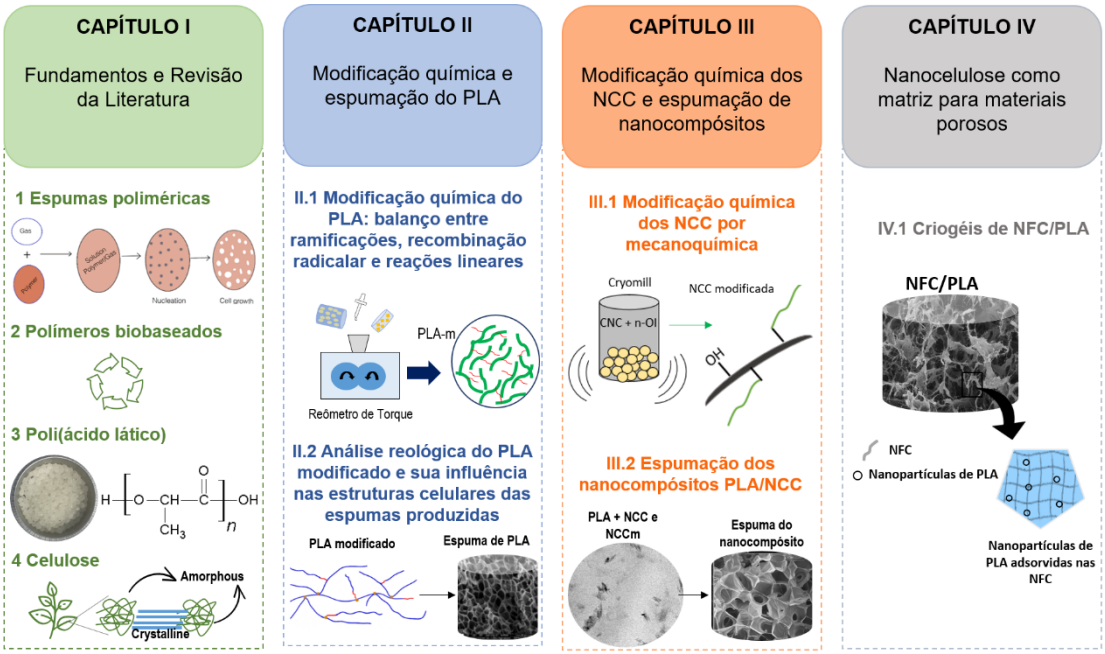

Figura 1 – Resumo da organização da tese.

O **Capítulo I** destinou-se à Fundamentação Teórica sobre os principais temas abordados na tese. Neste capítulo foram apresentados os principais mecanismos do processo de espumação de materiais poliméricos no estado fundido e os diferentes tipos de agentes de espumação que podem ser utilizados, com especial atenção para o agente de espumação CO_2 supercrítico. Além disso, foram apresentadas as principais propriedades necessárias para a produção de espumas poliméricas. Em sequência, foi apresentada uma breve introdução envolvendo as definições e utilização dos bioplásticos, e um detalhamento maior sobre os dos principais materiais que investigados neste trabalho: PLA, celulose nanofibrilada e nanocristais de celulose. Nesta discussão foram apresentados os principais desafios que esses materiais apresentam para seu processamento: a baixa resistência no estado fundido do PLA, a baixa compatibilidade da CNC com matrizes poliméricas de caráter hidrofóbico e a baixa resistência a umidade dos criogéis de CNF.

Neste sentido, o **Capítulo II** se dividiu em duas partes. A **Seção II.1** descreveu a modificação química do PLA, por processamento reativo, utilizando-se metacrilato de glicidila (GMA) em presença de peróxido de dicumila (DCP)

como iniciador da reação. As amostras foram caracterizadas para estudo dos efeitos que essa modificação causou nas propriedades do material e consequentemente nas estruturas celulares das espumas produzidas. Uma descrição detalhada do procedimento da modificação química foi apresentada. Foram propostos mecanismos de reação entre e possíveis estruturas da cadeia do PLA de acordo com as diferentes concentrações de reagentes utilizados. A Figura 2 ilustra as possíveis estruturas formadas na cadeia do PLA durante a modificação química.

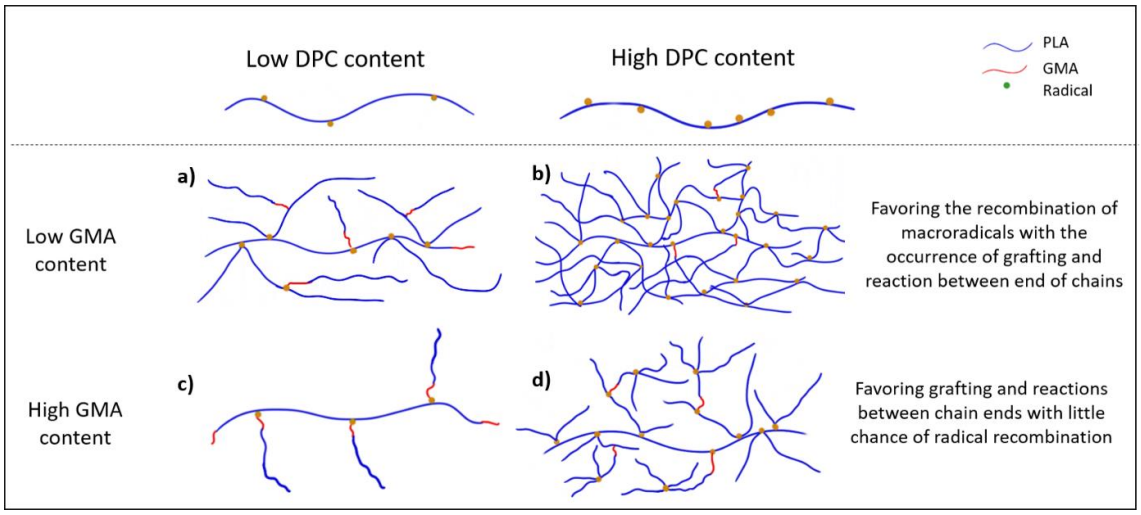

Figura 2 – Diferentes estruturas formadas de acordo com a concentração de GMA e DCP utilizadas na modificação química do PLA.

Como consequência, foi observada mudanças nas propriedades reológicas do material modificado, com aumento expressivo de viscosidade e elasticidade das formulações PLA_0.5_1 e PLA_1.5_3, indicando efetiva extensão de cadeia do material.

Como consequência desses resultados, a **Seção II.2** apresentou as espumas produzidas a partir das amostras modificadas de PLA, como pode ser observado na Figura 3.

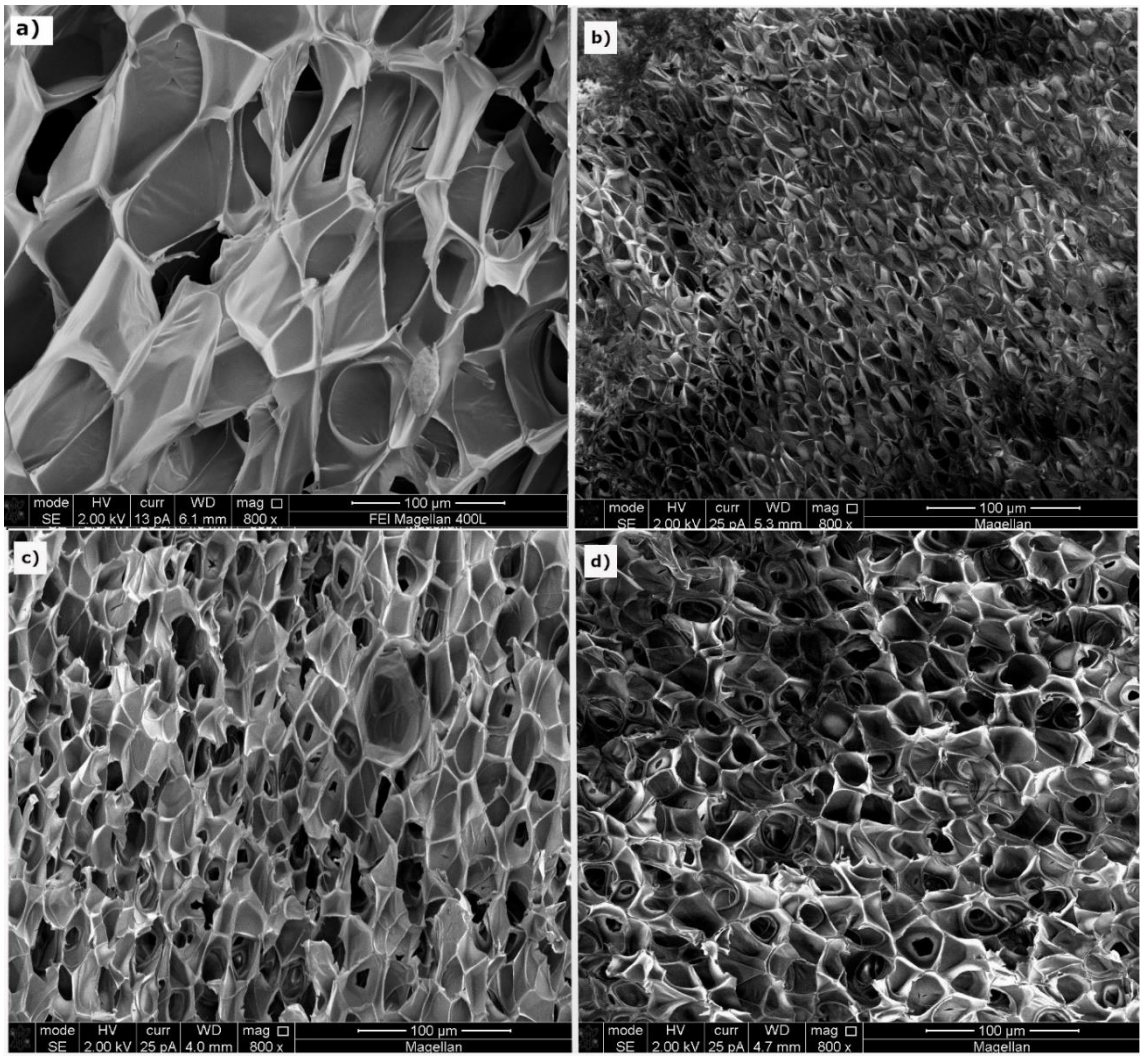

Figura 3 – Comparação entre as espumas obtidas do a) PLa puro; b) PLA_0.5_1; c) PLA_0.5_3; d) PLA_1.5_3.

As estruturas celulares das espumas modificadas apresentaram tamanhos menores em comparação ao PLA puro. Entretanto, as duas amostras que apresentaram os maiores valores de viscosidade e elasticidade, resultaram em células menores e homogêneas. Entre elas, a amostra b) resultou em estruturas ainda menores, o que foi atrelada a cristalinidade do material, que facilitou a nucleação de células durante a espumação.

O **Capítulo III** abordou a estratégia de se adicionar nanocristais de celulose (NCC) no PLA visando o ajuste de propriedades para a produção de espumas. Para isso, a **Seção III.1** foi destinada a apresentação da modificação

química da NCC por mecanoquímica e sua respectiva caracterização. Nesta estratégia, foi utilizado o isocianato octadecil para funcionalizar os NCC, em uma concentração mais baixa do que as apresentadas na literatura. Ainda assim, os resultados mostraram sucesso na funcionalização, com aumento do caráter hidrofóbico demonstrado pela análise de ângulo de contato, e preservação da cristalinidade dos NCC. Entretanto, analise morfológica mostrou que após a modificação química, os NCC sofreram aglomeração, o que pode estar atrelada ao método de mecanoquímica. A Figura 4 ilustra amostras de NCC puro (a), puro depois de ser submetido ao moedor de bolas (b) e modificado (c).

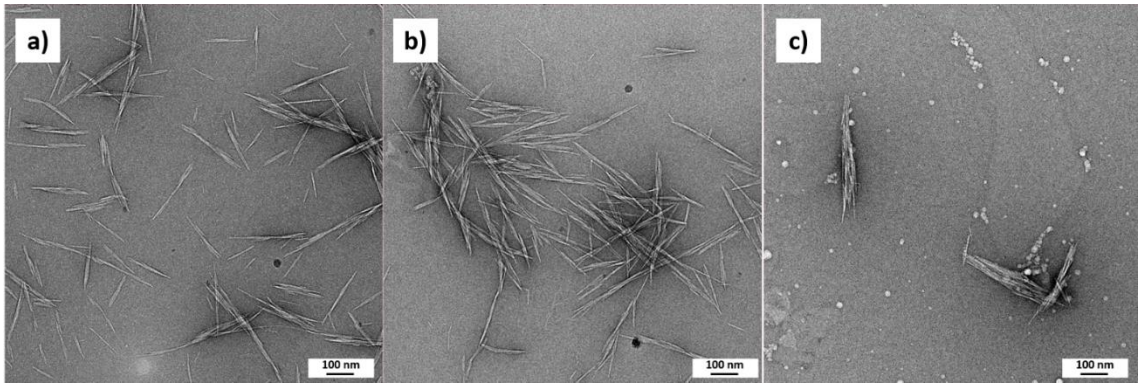

Figura 4 – Comparação entre NCC puro (a), puro depois de ser submetido ao moedor de bolas (b) e modificado (c)

Na **Seção III.2** foi apresentada a produção dos nanocompósitos PLA/NCC, por mistura no estado fundido, assim como sua caracterização. Análise reológica mostrou que não houve percolação reológica dos nanocompósitos, o que deve ser explicado pela baixa dispersão dos NCC na matriz de PLA. A Figura 5 ilustra o comportamento dos módulos de perda e de armazenamento dos nanocompósitos, onde é possível observar que em nenhum caso foi observado sobreposição de G’ em G’’ desde baixas taxas.

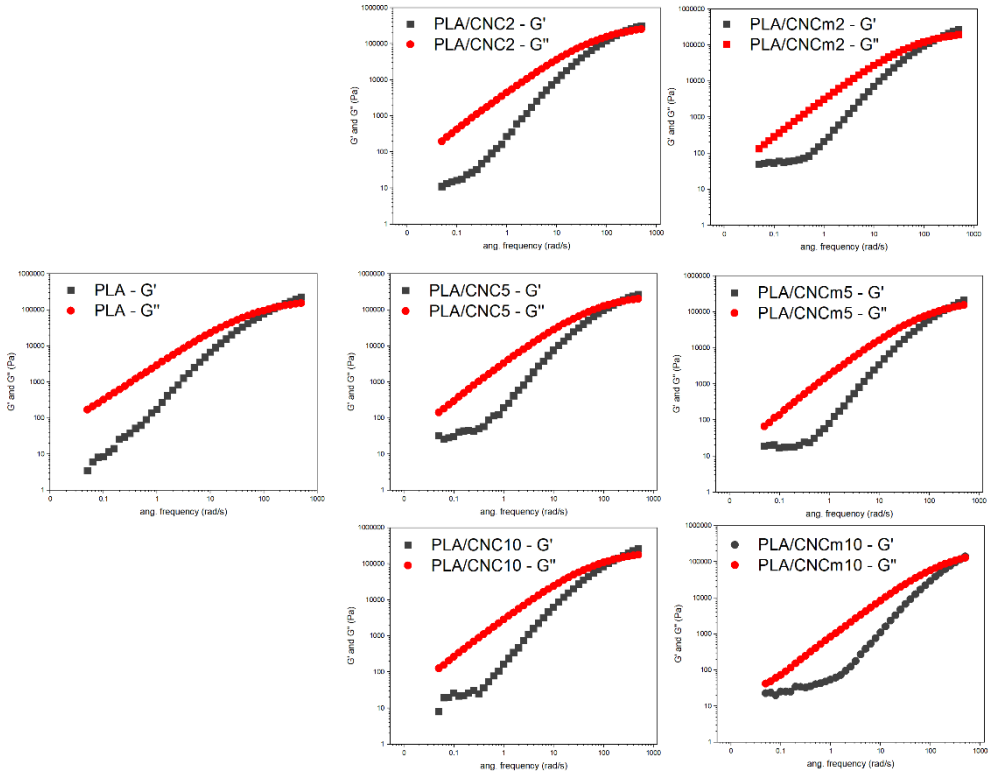

Figura 5 – Curvas de G’ e G’’ por frequência (rad/s) medidas a 180°C, de 0.05 a 500 rad/s.

Por fim, os nanocompósitos foram espumados e suas respectivas estruturas celulares foram observadas. Devido a baixa dispersão de NCC no PLA, as propriedades reológicas não apresentaram diferenças expressivas. Desta forma, o fator que mais foi significativo foi a concentração de NCC nas amostras. As duas formulações contentado 10% resultaram nos efeitos mais distintos. A adição de NCC pura nesta concentração, levou a células menores e alto VER, enquanto que a NCC modificada, que apresentou as menores viscosidades e modulo elástico, resultaram no menor VER. O efeito das cadeias enxertadas na NCC também foi observado durante a cristalização, que mostrou se mais evidente para a formulação de 10%.

Finalmente, o **Capítulo IV** apresentou uma estratégia diferente para produzir material poroso na matriz de nanofibras de celulose (NCF). O desafio

principal de se produzir materiais compostos principalmente por celulose é sua hidrofilicidade elevada, que geralmente é contornada com modificações químicas ou tratamentos superficiais. Como alternativa a esses processos químicos, neste capítulo foi descrita a produção de um criogel a partir de NFC incorporado com nanopartículas de PLA (10 e 20% em peso) e submetido a tratamento térmico, com o objetivo de aumentar a hidrofobicidade dos criogeis, sem necessidade de realizar modificações químicas. Os resultados mostraram que houve elevada adsorção de nanopartículas de PLA na superfície da NFC. Além disso, a introdução das nanoparrticulas de PLA só mostraram efeito quando os criogeis foram submetidos a tratamento térmico em 180°C. Nestes casos, o caráter hidrofóbico foi aumentado, pois as nanoparticulas de PLA foram fundidas e criaram uma espécie de recobrimento nas NFC. Além disso, os criogeis com 10% de nanoparticulas de PLA apresentaram estruturas porosas mais homogêneas e preservadas, o que pode ser explicado pelo fato de que nas amostras com 20% de PLA, menor concentração de NFC estavam disponíveis. A Figura 5 ilustra analise morfológica dos criogeis onde é possível observar as nanoparticulas de PLA antes do tratamento térmico e o recobrimento causado pela fusão do material.

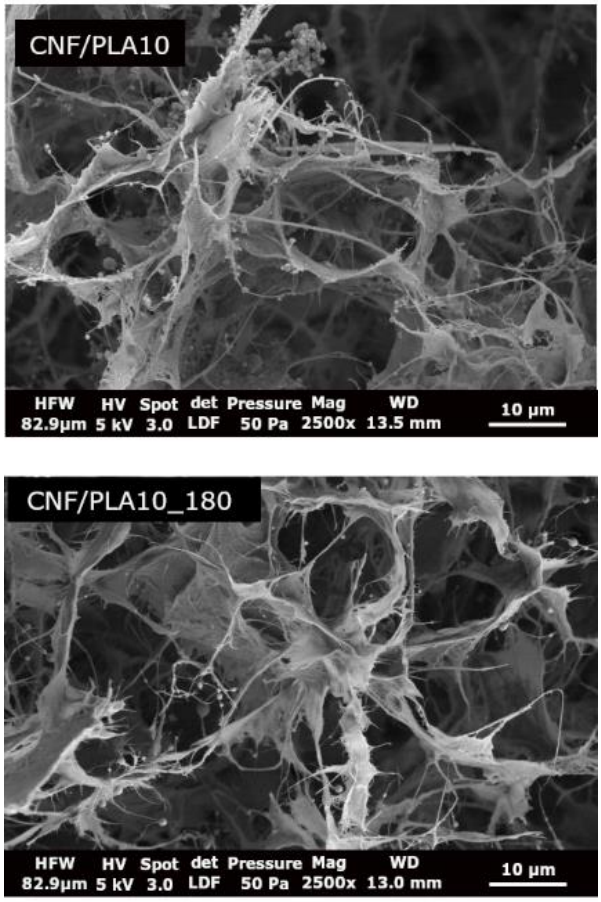

Figura 6 – Criogeis contendo 10% em peso de nanopartículas de PLA, antes e depois de submetidos a tratamento térmico.

Em conclusão, os resultados mostraram que as diferentes concentrações de GMA e DCP na modificação química do PLA levaram a diferentes estruturas celulares, em que uma condição ótima que relaciona elevada viscosidade e elevada cristalinidade resultaram em estruturas celulares menores e homogêneas. Comparativamente, as espumas produzidas pelos nanocompósitos apresentaram tamanhos maiores que as espumas de PLA modificado, evidenciando que as estruturas ramificadas são mais eficientes em produzir espumas com estruturas mais controladas. Além disso, a baixa dispersão da CNC na matriz de PLA limitou a potencial eficiência que as cargas poderiam ter na produção de estruturas controladas.

Apesar disso, foi observado que a modificação na superfície da CNC pode influenciar diretamente na estruturas celulares. As longas cadeias alifáticas do isocianato lubrificaram as cadeias, o que diminui a viscosidade do material de forma geral. Essa diminuição da viscosidade levou a uma espuma de baixa razão de expansão. Neste sentido, é necessário encontrar uma concentração ótima de CNC na matriz para que seja alta o suficiente para formar percolação mas baixa o suficiente para que as concentrações de cadeias enxertadas não diminuam a viscosidade do material durante o processo de espumação.

O trabalho também se propôs em estudar o aumento do caráter hidrofóbico de criogeis de CNF, sendo essa uma contribuição para o entendimento de materiais porosos de matriz celulósica. A introdução de 10 wt% de nanopartículas de PLA foi suficiente para aumentar o ângulo de contato sem grandes mudanças na estrutura porosa do material, comparado ao criogel sem nanoparticulas. Já a introdução de 20 wt%, apesar de ter aumentado o caráter hidrofóbico, resultou em poros rompidos.

Como perspectivas para trabalhos futuros, os seguintes pontos são destacados:

- Estudo de diferentes variáveis de processo de espumação como temperatura, pressão e tempo de saturação, para investigar como esses fatores podem influenciar nas estruturas celulares obtidas;
- Investigação de novos métodos de produção de nanocompósitos PLA/CNC para aumentar a dispersão do reforço na matriz;
- Estudar outras propriedades dos nanocompósitos como biodegradabilidade, propriedades mecânicas, propriedades de barreira;
- Estudo das propriedades finais das espumas como propriedades mecânicas, isolantes, de absorção.
- Estudo da introdução da CNC no PLA modificado com GMA e DCP para investigar se o efeito nucleante das cargas poderia diminuir o tamanho das células.

- Estudo de novas técnicas para realizar o tratamento térmico dos criogeis para evitar a ruptura de poros.

REFERENCES

[1] COWAN, E. et al. Single- use plastic bans: Exploring stakeholder perspectives on best practices for reducing plastic pollution. **Environments - MDPI**, v. 8, n. 8, p. 1–16, 2021.

[2] OECD. **Global Plastics Outlook: Economic Drivers, Environmental Impacts and Policy Options.** Paris: OECD Publishing, 2022.

[3] UNITED NATIONS ENVIRONMENT PROGRAMME. **Turning off the tap. How the world can end plastic pollution and create a circular economy**. Nairobi.

[4] COMBRZYŃSKI, M.; ÖZMEN, Ö. Foamed bioplastics: a review. **International Agrophysics**, v. 35, n. 4, p. 375–388, 2021.

[5] OLIVEIRA, C. T. DE; LUNA, M. M. M.; CAMPOS, L. M. S. Understanding the Brazilian expanded polystyrene supply chain and its reverse logistics towards circular economy. **Journal of Cleaner Production**, v. 235, p. 562–573, 2019.

[6] KUMAR, K. et al. Microplastics and biobased polymers to combat plastics waste. **Chemosphere**, v. 342, 2023.

[7] HARTMANN, N. B. et al. Are We Speaking the Same Language? Recommendations for a Definition and Categorization Framework for Plastic Debris. **Environmental Science and Technology**, v. 53, n. 3, p. 1039–1047, 2019.

[8] INTERNATIONAL UNION OF PURE AND APPLIED CHEMISTRY. **“foam”**IUPAC Compendium of Chemical Terminology, , 2006. Disponível em: <https://doi.org/10.1351/goldbook.F02467>

[9] ASTM D883-20B. **Standard Terminology Relating to Plastics**.

[10] OKOLIEOCHA, C. et al. Microcellular to nanocellular polymer foams: Progress (2004-2015) and future directions - A review. **European Polymer Journal**, v. 73, p. 500–519, 2015.

[11] DONG, M. et al. An overview of polymer foaming assisted by supercritical

fluid. **Advanced Composites and Hybrid Materials**, v. 6, n. 6, p. 1–22, 2023.

[12] BANERJEE, R.; RAY, S. S. Foamability and Special Applications of Microcellular Thermoplastic Polymers: A Review on Recent Advances and Future Direction. **Macromolecular Materials and Engineering**, v. 305, n. 10, p. 1–49, 2020.

[13] ÇANKAYA, N. **Recent Research in Polymerization**. Croatia: INTECH, 2018.

[14] SOUZA, F. M.; DESAI, Y.; GUPTA, R. K. Introduction to Polymeric Foams. In: **Polymeric Foams: Fundamentals and Types of Foams**. Washington, DC: American Chemical Society, 2023. v. 1.

[15] JIN, F. L. et al. Recent trends of foaming in polymer processing: A review. **Polymers**, v. 11, n. 6, 2019.

[16] ANSARI, A. I.; SHEIKH, N. A. A Review on Different Approaches for Foam Fabrication. **Journal of The Institution of Engineers (India): Series C**, v. 104, n. 6, p. 1219–1245, 2023.

[17] BARMOUZ, M.; BEHRAVESH, A. H. The role of foaming process on shape memory behavior of polylactic acid-thermoplastic polyurethane-nano cellulose bio-nanocomposites. **Journal of the Mechanical Behavior of Biomedical Materials**, v. 91, p. 266–277, 2019.

[18] LEE, S.T.; PARK, C.B. **Foam extrusion: Principles and Practice**. 2. ed. New York: CRC Press - Taylor & Francis Group, 2014.

[19] MAIO, E. DI; KIRAN, E. Foaming of polymers with supercritical fluids and perspectives on the current knowledge gaps and challenges. **Journal of Supercritical Fluids**, v. 134, p. 157–166, 2018.

[20] S.T. LEE; N.S. RAMESH. **Polymeric Foams: Mechanisms and Materials**. Boca Raton: CRC Press LLC, 2004.

[21] EAVES, D. **Handbook of polymer foams**. Reino Unido: Rapra Technology Limited, 2004. v. 42

[22] WYPYCH, G. **Handbook of foaming and blowing agents**. Ontario: Elsevier, 2022.

[23] RUIZ, J. A. R. et al. Polymer Foaming With Chemical Blowing Agents: Experiment and Modeling Jos?e. **Polymer Engineering and Science**, v. 55, n. 9, p. 2018–2029, 2015.

[24] WITKOWSKI, A. et al. The analysis of pipeline transportation process for CO2 captured from reference coal-fired 900 MW power plant to sequestration region. **Chemical and Process Engineering - Inzynieria Chemiczna i Procesowa**, v. 35, n. 4, p. 497–514, 2014.

[25] INTERNATIONAL UNION OF PURE AND APPLIED CHEMISTRY (IUPAC). **“supercritical fluid”**IUPAC Compendium of Chemical Terminology, , 2006. Disponível em: <https://doi.org/10.1351/goldbook.S06138>

[26] ROJAS, A. et al. Supercritical impregnation for food applications: a review of the effect of the operational variables on the active compound loading. **Critical reviews in food science and nutrition**, v. v. 60, n. 8, p. 1290–1301, 2020.

[27] CHAMPEAU, M. et al. Drug loading of polymer implants by supercritical CO2 assisted impregnation: A review. **Journal of Controlled Release**, v. 209, p. 248–259, 2015.

[28] SARVER, J. A.; KIRAN, E. Foaming of polymers with carbon dioxide – The year-in-review – 2019. **Journal of Supercritical Fluids**, v. 173, 2021.

[29] LEE, R. E. et al. Highly expanded fine-cell foam of polylactide/polyhydroxyalkanoate/nano-fibrillated polytetrafluoroethylene composites blown with mold-opening injection molding. **International Journal of Biological Macromolecules**, v. 155, p. 286–292, 2020.

[30] FARHANMOGHADDAM, F.; JAVADI, A. Fabrication of poly (lactic acid) foams using supercritical nitrogen. **Cellular Polymers**, v. 39, n. 4, p. 172–182, 2020.

[31] QU, Z. et al. Cellular morphology evolution in nanocellular poly (lactic acid)/thermoplastic polyurethane blending foams in the presence of supercritical

N2. **European Polymer Journal**, v. 116, p. 291–301, 2019.

[32] GENDRON, R. **Thermoplastic Foam Processing: Principles and Development.** Boca Raton: CRC Press, 2005.

[33] SHAFI, M. A.; JOSHI, K.; FLUMERFELT, R. W. Bubble size distributions in freely expanded polymer foams. **Chemical engineering science**, v. 52, n. 4, p. 635–644, 1997.

[34] SHAFI, M. A.; FLUMERFELT, R. W. Initial bubble growth in polymer foam processes. **Chemical engineering science**, v. 52, n. 4, p. 627–633, 1997.

[35] NOFAR, M.; PARK, C. B. Poly (lactic acid) foaming. **Progress in Polymer Science**, v. 39, n. 10, p. 1721–1741, 2014.

[36] SHAU-TARNG LEE; CHUL B. PARK; N.S. RAMESH. **Polymeric Foams: Science and Technology**. Boca Raton: CRC Press - Taylor & Francis Group, 2007.

[37] VILLAMIL JIMÉNEZ, J. A. et al. Foaming of PLA composites by supercritical fluid-assisted processes: A review. **Molecules**, v. 25, n. 15, 2020.

[38] MARTINI-VVEDENSKY, J. E.; SUH, N. P.; WALDMAN, F. A. **Microcellular closed cell foams and their method of manufacture**Google Patents, , 25 Sep. 1984.

[39] STANDAU, T. et al. Chemical modification and foam processing of polylactide (PLA). **Polymers**, v. 11, n. 2, 2019.

[40] ALBUQUERQUE, R. Q. et al. A machine learning investigation of low-density polylactide batch foams. **E-Polymers**, v. 22, n. 1, p. 318–331, 2022.

[41] YU, K. et al. Effects of in-situ crystallization on poly (lactic acid) microcellular foaming: Density functional theory and experiment. **Polymer**, v. 200, 2020.

[42] WANG, G. et al. Lightweight, super-elastic, and thermal-sound insulation bio-based PEBA foams fabricated by high-pressure foam injection molding with mold-opening. **European polymer journal**, v. 103, p. 68–79, 2018.

[43] MOSANENZADEH, S. G. et al. Effect of biopolymer blends on physical and

Acoustical properties of biocomposite foams. **Journal of polymer science. Part B, Polymer physics**, v. 52, n. 15, p. 1002–1013, 2014.

[44] SHAH, V. **Handbook of plastics testing and failure analysis**. 3ª ed. New Jersey: John Wiley & Sons, 2007.

[45] CASTELLÓN, S. M. et al. Modification of different polylactides by reactive extrusion to enhance their melt properties. **AIP Conference Proceedings**, v. 2289, 2020.

[46] LEE, S.-T. **Polymeric foams: Innovations in Processes, Technologies and Products**. Boca Raton: CRC Press, 2017.

[47] LIU, W. et al. Flexibly Controlling the Polycrystallinity and Improving the Foaming Behavior of Polylactic Acid via Three Strategies. **ACS Omega**, v. 7, n. 7, p. 6248–6260, 2022.

[48] LI, J. et al. Crystals in situ induced by supercritical co2 as bubble nucleation sites on spherulitic plla foam structure controlling. **Industrial and Engineering Chemistry Research**, v. 56, n. 39, p. 11111–11124, 2017.

[49] WANG, S. et al. Preparation of high-expansion open-cell polylactic acid foam with superior oil-water separation performance. **International Journal of Biological Macromolecules**, v. 193, p. 1059–1067, 2021.

[50] LI, B. et al. Green fabrication method of layered and open-cell polylactide foams for oil-sorption via pre-crystallization and supercritical CO2-induced melting. **Journal of Supercritical Fluids**, v. 162, p. 1–12, 2020.

[51] CHEN, J. et al. Foaming behavior of poly(lactic acid) with different D-isomer content based on supercritical CO2-induced crystallization. **Journal of Cellular Plastics**, v. 57, n. 5, p. 675–694, 2021.

[52] YANG, Y. et al. Foaming of poly(lactic acid) with supercritical CO2: The combined effect of crystallinity and crystalline morphology on cellular structure. **Journal of Supercritical Fluids**, v. 145, p. 122–132, 2019.

[53] NOFAR, M.; PARK, C. B. **Polylactide foams: fundamentals, manufacturing, and applications**. 1. ed. Oxford: William Andrew, 2017.

[54] VATANSEVER, E.; ARSLAN, D.; NOFAR, M. Polylactide cellulose-based nanocomposites. **International Journal of Biological Macromolecules**, v. 137, p. 912–938, 2019.

[55] Tide will turn against single-use plastic. **C&EN Global Enterprise**, v. 97, n. 2, p. 36, 14 Jan. 2019.

[56] EUROPEAN UNION. DIRECTIVE (EU) 2019/904 OF THE EUROPEAN PARLIAMENT AND OF THE COUNCIL of 5 June 2019 on the reduction of the impact of certain plastic products on the environment. 2019.

[57] GONÇALVES-DIAS, S. L. F. et al. **Single-use plastic in Brazil: policies and laws**. São Paulo: Escola de Artes, Ciências e Humanidades, 2023. v. 2

[58] PRATES, J.-P. Projeto de Lei 2524 de 2022. 2022, p. 1–8.

[59] SHLUSH, E.; DAVIDOVICH-PINHAS, M. Bioplastics for food packaging. **Trends in Food Science and Technology**, v. 125, p. 66–80, 2022.

[60] EUROPEAN BIOPLASTICS; INSTITUTE OF BIOPLASTICS AND BIOCOMPOSITES. **What are bioplastics?** Disponível em: <https://www.european-bioplastics.org/bioplastics/>.

[61] INTERNATIONAL UNION OF PURE AND APPLIED CHEMISTRY (IUPAC). **“biopolymers”**IUPAC Compendium of Chemical Terminology, , 2006. Disponível em: <https://doi.org/10.1351/goldbook.B00661>

[62] ARIF, U. et al. Biocompatible polymers and their potential biomedical applications: A review. **Current pharmaceutical design**, v. 25, n. 34, p. 3608–3619, 2019.

[63] INTERNATIONAL UNION OF PURE AND APPLIED CHEMISTRY (IUPAC). **“biodegradable polymer”**IUPAC Compendium of Chemical Terminology, , 2006. Disponível em: <https://doi.org/10.1351/goldbook.BT07169>

[64] EUROPIAN BIOPLASTICS. **Bioplastics Market Development Update 2023**. Berlin: [s.n.]. Disponível em: <https://docs.european-bioplastics.org/publications/market_data/2023/EUBP_Market_Data_Report_2023.pdf>.

[65] NANDA, S. et al. Innovations in applications and prospects of bioplastics and biopolymers: a review. **Environmental Chemistry Letters**, v. 20, n. 1, p. 379–395, 2022.

[66] SIDDIQUI, S. A. et al. Recent advances in reinforced bioplastics for food packaging - A critical review. **International Journal of Biological Macromolecules**, v. 263, 2024.

[67] NIZAMUDDIN, S.; CHEN, C. Biobased, biodegradable and compostable plastics: chemical nature, biodegradation pathways and environmental strategy. **Environmental Science and Pollution Research**, v. 31, n. 6, p. 8387–8399, 2024.

[68] HOPMANN, C.; SCHIPPERS, S.; HÖFS, C. Influence of recycling of poly(lactic acid) on packaging relevant properties. **Journal of applied polymer science**, v. 132, n. 9, 2015.

[69] JAMSHIDIAN, M. et al. Poly- lactic acid: production, applications, nanocomposites, and release studies. **Comprehensive reviews in food science and food safety**, v. 9, n. 5, p. 552–571, 2010.

[70] KHOURI, N. G. et al. Polylactic acid (PLA): Properties, synthesis, and biomedical applications – A review of the literature. **Journal of Molecular Structure**, v. 1309, 2024.

[71] AURAS, R. et al. **Poly(lactic acid): synthesis, structures, properties, processing and application**. Hoboken: John Wiley & Sons, 2010.

[72] YU, J. et al. PLA bioplastic production: From monomer to the polymer. **European Polymer Journal2**, v. 193, 2023.

[73] SWETHA, T. A. et al. A review on biodegradable polylactic acid (PLA) production from fermentative food waste - Its applications and degradation. **International Journal of Biological Macromolecules**, v. 234, 2023.

[74] GARLOTTA, D. A literature review of poly(lactic acid). **Journal of Polymers and the Environment**, v. 9, n. 2, p. 63–84, 2001.

[75] LIU, H. et al. Super Toughened Poly(lactic acid) Ternary Blends by

Simultaneous Dynamic Vulcanization and Interfacial Compatibilization. **Macromolecules**, v. 43, n. 14, p. 6058–6066, 2010.

[76] BELGACEM, M. N.; GANDINI, A. **Monomers, polymers and composites from renewable resources**. Oxford: Elsevier, 2011.

[77] MARTINEZ, F. A. C. et al. Lactic acid properties, applications and production: A review. **Trends in food science & technology**, v. 30, n. 1, p. 70–83, 2013.

[78] LORENZO, M. L. DI; ANDROSCH, R. **Synthesis, Structure and Properties of Poly (Lactic Acid)**. Cham: Springer International Publishing, 2018.

[79] JAMSHIDI, K.; HYON, S. H.; IKADA, Y. Thermal characterization of polylactides. **Polymer**, v. 29, n. 12, p. 2229–2234, 1988.

[80] LUCAS, N. et al. Polymer biodegradation: Mechanisms and estimation techniques - A review. **Chemosphere**, v. 73, n. 4, p. 429–442, 2008.

[81] JIN, C. et al. Biodegradation Behaviors of Poly(p-dioxanone) in Different Environment Media. **Journal of Polymers and the Environment**, v. 21, p. 1088–1099, 2013.

[82] ASTM D6400-04. Standard specification for compostable plastics. **Annual Book of ASTM Standards**, 2021.

[83] KULIKOWSKAA, D. et al. Composting as a disposal route of PLA materials: kinetics of the aerobic biodegradation. **Desalination and Water Treatment**, v. 206, p. 153–164, 2020.

[84] GUPTA, B.; REVAGADE, N.; HILBORN, J. Poly(lactic acid) fiber: An overview. **Progress in polymer science**, v. 32, n. 4, p. 455–482, 2007.

[85] SAEIDLOU, S. et al. Poly(lactic acid) crystallization. **Progress in Polymer Science**, v. 37, p. 1657–1677, 2012.

[86] ZHANG, Y. et al. Direct evidence for the validity of assessing reaction extent by torque spectrum during reactive processing. **Polymer**, v. 197, 2020.

[87] BETTINI, S. H. P.; AGNELLI, J. A. M. Grafting of maleic anhydride onto polypropylene by reactive processing. II. Effect of rotor speed and reaction time.

Journal of Applied Polymer Science, v. 74, n. 2, p. 256–263, 1999.

[88] AL-MALAIKA, S. **Reactive Modifiers for Polymers.** First ed. London: Blackie Academic & Professional, 1997. v. 1

[89] NGUYEN, T. C.; RUKSAKULPIWAT, C.; RUKSAKULPIWAT, Y. The study on the grafting of glycidyl methacrylate onto Poly(lactic acid) in an internal mixer. **Walailak Journal of Science and Technology**, v. 13, n. 12 Special Issue, p. 1037–1046, 2016.

[90] SCHMELZER, H. G.; KUMPF, R. J. Reactive processing of polymers: A) Reactive processing of engineering thermoplastics; B) Reaction injection molding of polyurethanes. **Journal of Macromolecular Science - Pure and Applied Chemistry**, v. A34, n. 10, p. 2085–2101, 1997.

[91] CASSAGNAU, P.; BOUNOR-LEGARÉ, V.; FENOUILLOT, F. Reactive processing of thermoplastic polymers: A review of the fundamental aspects. **International Polymer Processing**, v. 22, n. 3, p. 218–258, 2007.

[92] HAMIELEC, A. E.; GLOOR, P. E.; ZHU, S. Kinetics of, free radical modification of polyolefins in extruders – chain scission, crosslinking and grafting. **The Canadian Journal of Chemical Engineering**, v. 69, n. 3, p. 611–618, 1991.

[93] CONFERENCE, S. OF P. E. T. **ANTEC 90: Plastics in the Environment : Yesterday, Today & Tomorrow : Conference Proceedings, Dallas, May 7-11**.Technical papers.SPE, 1990. Disponível em: <https://books.google.com.br/books?id=0V0_swEACAAJ>

[94] CORRE, Y. M. et al. Batch foaming of chain extended PLA with supercritical CO2: Influence of the rheological properties and the process parameters on the cellular structure. **Journal of Supercritical Fluids**, v. 58, n. 1, p. 177–188, 2011.

[95] FRENZ, V. et al. Multifunctional polymers as chain extenders and compatibilizers for polycondensates and biopolymers. **Technical Papers, Regional Technical Conference - Society of Plastics Engineers**, v. 3, p. 1678–1682, 2008.

[96] MENG, Q.; HEUZEY, M.-C.; CARREAU, P. J. Control of thermal degradation

of polylactide/clay nanocomposites during melt processing by chain extension reaction. **Polymer degradation and stability**, v. 97, n. 10, p. 2010–2020, 2012.

[97] VILLALOBOS, M. et al. Oligomeric chain extenders for economic reprocessing and recycling of condensation plastics. **Energy**, v. 31, n. 15, p. 3227–3234, 2006.

[98] XU, T.; TANG, Z.; ZHU, J. Synthesis of polylactide-graft-glycidyl methacrylate graft copolymer and its application as a coupling agent in polylactide/bamboo flour biocomposites. **Journal of applied polymer science**, v. 125, n. S2, p. E622–E627, 2012.

[99] LI, P. et al. High performance branched poly(lactide) induced by reactive extrusion with low-content cyclic organic peroxide and multifunctional acrylate coagents. **Polymer**, v. 205, 2020.

[100] GÖTTERMANN, S. et al. Effect of chemical modification on the thermal and rheological properties of polylactide. **Polymer Engineering and Science**, v. 57, n. 11, p. 1242–1251, 2017.

[101] GÖTTERMANN, S. et al. Modifiziertes Polylactid für die Schaumextrusion. **(24. Stuttgarter Kunststoffkolloquium 25.-26. Februar 2015)**, 2015.

[102] GÖTTERMANN, S. et al. Modified standard polylactic acid (PLA) for extrusion foaming. **AIP Conference Proceedings**, v. 1779, 2016.

[103] LI, Y. et al. A Facile and Efficient Method for Preparing Chain Extended Poly(lactic acid) Foams with High Volume Expansion Ratio. **Journal of Polymers and the Environment**, v. 28, n. 1, p. 17–31, 2020.

[104] JIMÉNEZ, J. A. V. et al. Foaming of PLA composites by supercritical fluid-assisted processes: A review. **Molecules**, v. 25, n. 15, 2020.

[105] INTERNATIONAL UNION OF PURE AND APPLIED CHEMISTRY. **nanocomposite**, 2006. Disponível em: <https://doi.org/10.1351/goldbook.NT07243>

[106] BIKIARIS, N. D. et al. Recent Advances in the Investigation of Poly(lactic acid) (PLA) Nanocomposites: Incorporation of Various Nanofillers and their

Properties and Applications. **Polymers**, v. 15, n. 5, 2023.

[107] DESHPANDE, A. P.; KRISHNAN, J. M.; KUMAR, P. B. S. **Rheology of Complex Fluids**. Madras, India: Springer New York LLC, 2010.

[108] HAN, C. D. **Rheology and Processing of Polymeric Materials**. New York: Oxford University Press, Inc., 2007.

[109] ZHAO, J.; MORGAN, A. B.; HARRIS, J. D. Rheological characterization of polystyrene-clay nanocomposites to compare the degree of exfoliation and dispersion. **Polymer**, v. 46, p. 8641–8660, 2005.

[110] KHOSHKAVA, V.; KAMAL, M. R. Effect of cellulose nanocrystals (CNC) particle morphology on dispersion and rheological and mechanical properties of polypropylene/CNC nanocomposites. **ACS Applied Materials and Interfaces**, v. 6, n. 11, p. 8146–8157, 2014.

[111] KHOSRAVI, A. et al. Soft and hard sections from cellulose-reinforced poly(lactic acid)-based food packaging films: A critical review. **Food Packaging and Shelf Life**, v. 23, 2020.

[112] CORDEIRO, N. et al. Natural fibers characterization by inverse gas chromatography. **Carbohydrate Polymers**, v. 84, n. 1, p. 110–117, 2011.

[113] KHALIL, H. P. S. A.; BHAT, A. H.; YUSRA, A. F. I. Green composites from sustainable cellulose nanofibrils: A review. **Carbohydrate polymers**, v. 87, n. 2, p. 963–979, 2012.

[114] JOHN, M. J.; THOMAS, S. Biofibres and biocomposites. **Carbohydrate polymers**, v. 71, n. 3, p. 343–364, 2008.

[115] KLEMM, D. et al. Cellulose: Fascinating biopolymer and sustainable raw material. **Angewandte Chemie - International Edition**, v. 44, n. 22, p. 3358–3393, 2005.

[116] STAUDINGER, H. Über Polymerisation. **Berichte der deutschen chemischen Gesellschaft (A and B Series)**, v. 53, n. 6, p. 1073–1085, 1920.

[117] HUBER, T. et al. A critical review of all-cellulose composites. **Journal of**

Materials Science, v. 47, n. 3, p. 1171–1186, 2012.

[118] NECHYPORCHUK, O.; BELGACEM, M. N.; BRAS, J. Production of cellulose nanofibrils: A review of recent advances. **Industrial Crops and Products**, v. 93, p. 2–25, 2016.

[119] WÜSTENBERG, T. **Cellulose and cellulose derivatives in the food industry: fundamentals and applications**. Pinneberg: John Wiley & Sons, 2014.

[120] FRENCH, A. D. Glucose, not cellobiose, is the repeating unit of cellulose and why that is important. **Cellulose**, v. 24, n. 11, p. 4605–4609, 2017.

[121] KLEMM, D. et al. **Comprehensive cellulose chemistry. Volume 1: Fundamentals and analytical methods.** 1. ed. Weinheim: Wiley-VCH Verlag GmbH, 1998.

[122] HON, D. N.-S. Cellulose: a random walk along its historical path. **Cellulose**, v. 1, p. 1–25, 1994.

[123] WADA, M.; HEUX, L.; SUGIYAMA, J. Polymorphism of cellulose I family: Reinvestigation of cellulose IVl. **Biomacromolecules**, v. 5, n. 4, p. 1385–1391, 2004.

[124] LAVOINE, N. et al. Microfibrillated cellulose - Its barrier properties and applications in cellulosic materials: A review. **Carbohydrate Polymers**, v. 90, n. 2, p. 735–764, 2012.

[125] KENNEDY, J. F. et al. **Cellulose and cellulose derivatives: Cellucon'93 proceedings: Physico-chemical aspects and industrial applications**. Cambridge: Woodhead Publishing Limited, 1995.

[126] LI, T. et al. Developing fibrillated cellulose as a sustainable technological material. **Nature**, v. 590, n. 7844, p. 47–56, 2021.

[127] DUFRESNE, A. Nanocellulose: A new ageless bionanomaterial. **Materials Today**, v. 16, n. 6, p. 220–227, 2013.

[128] TURBAK, A. F.; SNYDER, F. W.; SANDBERG, K. R. Microfibrillated

cellulose, a new cellulose product: properties, uses, and commercial potential. **Journal of Applied Polymer Science: Applied Polymer Symposium**, v. 37, n. 8, p. 815–827, 1983.

[129] FRANCE, K. J. DE; HOARE, T.; CRANSTON, E. D. Review of Hydrogels and Aerogels Containing Nanocellulose. **Chemistry of Materials**, v. 29, n. 11, p. 4609–4631, 2017.

[130] KLEMM, D. et al. Nanocelluloses: A new family of nature-based materials. **Angewandte Chemie - International Edition**, v. 50, n. 24, p. 5438–5466, 2011.

[131] DUFRESNE, A. Cellulose nanomaterials as green nanoreinforcements for polymer nanocomposites. **Philosophical Transactions of the Royal Society A: Mathematical, Physical and Engineering Sciences**, v. 376, n. 2112, 2018.

[132] LIN, N.; DUFRESNE, A. Nanocellulose in biomedicine: Current status and future prospect. **European Polymer Journal**, v. 59, p. 302–325, 2014.

[133] ZINGE, C.; KANDASUBRAMANIAN, B. Nanocellulose based biodegradable polymers. **European Polymer Journal**, v. 133, p. 1–20, 2020.

[134] DHALI, K. et al. A review of nanocellulose as a new material towards environmental sustainability. **Science of the Total Environment**, v. 775, 2021.

[135] TURBAK, A. F.; SNYDER, F. W.; SANDBERG, K. R. **Microfibrillated cellulose, a new cellulose product: properties, uses, and commercial potential**. J Appl Polym Sci Appl Polym Symp. **Anais**...1983

[136] HERRICK, F. W. et al. **Microfibrillated cellulose: morphology and accessibility**. J. Appl. Polym. Sci.: Appl. Polym. Symp.;(United States). **Anais**...ITT Rayonier Inc., Shelton, WA, 1983

[137] ROL, F. et al. Recent advances in surface-modified cellulose nanofibrils. **Progress in Polymer Science**, v. 88, p. 242–264, 2019.

[138] ZIMMERMANN, T.; PÖHLER, E.; GEIGER, T. Cellulose fibrils for polymer reinforcement. **Advanced engineering materials**, v. 6, n. 9, p. 754–761, 2004.

[139] TANIGUCHI, T.; OKAMURA, K. New films produced from microfibrillated

natural fibres. **Polymer International**, v. 47, n. 3, p. 291–294, 1998.

[140] AI, Y. et al. Toward cleaner production of nanocellulose: a review and evaluation. **Green Chemistry**, v. 24, n. 17, p. 6406–6434, 2022.

[141] COPENHAVER, K. et al. Pretreatment of lignocellulosic feedstocks for cellulose nanofibril production. **Cellulose**, v. 29, n. 9, p. 4835–4876, 2022.

[142] YI, T. et al. From cellulose to cellulose nanofibrils—a comprehensive review of the preparation and modification of cellulose nanofibrils. **Materials**, v. 13, n. 22, p. 1–32, 2020.

[143] INTERNATIONAL UNION OF PURE AND APPLIED CHEMISTRY. **“micropore”**IUPAC Compendium of Chemical Terminology, , 2006. Disponível em: <https://doi.org/10.1351/goldbook.M03906>

[144] INTERNATIONAL UNION OF PURE AND APPLIED CHEMISTRY (IUPAC). **“mesopore”**IUPAC Compendium of Chemical Terminology, , 2006. Disponível em: <https://doi.org/10.1351/goldbook.M03853>

[145] INTERNATIONAL UNION OF PURE AND APPLIED CHEMISTRY. **“macropore”**IUPAC Compendium of Chemical Terminology, , 2006. Disponível em: <https://doi.org/10.1351/goldbook.M03672>

[146] TYSHKUNOVA, I. V.; POSHINA, D. N.; SKORIK, Y. A. Cellulose Cryogels as Promising Materials for Biomedical Applications. **International Journal of Molecular Sciences**, v. 23, p. 1–17, 2022.

[147] LAVOINE, N.; BERGSTRÖM, L. Nanocellulose-based foams and aerogels: Processing, properties, and applications. **Journal of Materials Chemistry A**, v. 5, n. 31, p. 16105–16117, 2017.

[148] BUCHTOVÁ, N.; BUDTOVA, T. Cellulose aero-, cryo- and xerogels: towards understanding of morphology control. **Cellulose**, v. 23, n. 4, p. 2585–2595, 2016.

[149] HÜSING, N.; SCHUBERT, U. Aerogels - Airy Materials: Chemistry, Structure, and Properties. **Angewandte Chemie - International Edition**, v. 37, p. 22–45, 1998.

[150] CHARTIER, C. et al. Release Kinetics of Dexamethasone Phosphate from Porous Chitosan: Comparison of Aerogels and Cryogels. **Biomacromolecules**, v. 24, n. 10, p. 4494–4501, 2023.

[151] MOON, R. J. et al. Cellulose nanomaterials review: Structure, properties and nanocomposites. **Chemical Society Reviews**, v. 40, p. 3941–3994, 2011.

[152] QIN, C. et al. MFC/NFC-based foam/aerogel for production of porous materials: Preparation, properties and applications. **Materials**, v. 13, n. 23, p. 1–21, 2020.

[153] HORVAT, G. et al. Hybrid Polylactic-Acid–Pectin Aerogels: Synthesis, Structural Properties, and Drug Release. **Polymers**, v. 15, n. 2, 1 Jan. 2023.

[154] ZHAO, S. et al. Biopolymer Aerogels and Foams: Chemistry, Properties, and Applications. **Angewandte Chemie - International Edition**, v. 57, n. 26, p. 7580–7608, 2018.

[155] WANG, Y. et al. The advances of polysaccharide-based aerogels: Preparation and potential application. **Carbohydrate Polymers**, v. 226, 2019.

[156] KLEMM, D. et al. Nanocellulose as a natural source for groundbreaking applications in materials science: Today's state. **Materials Today**, v. 21, n. 7, p. 720–748, 2018.

[157] FERREIRA, F. V. et al. Nanocellulose-based porous materials: Regulation and pathway to commercialization in regenerative medicine. **Bioactive Materials**, v. 29, p. 151–176, 2023.

[158] MOKHENA, T. C.; JOHN, M. J. Cellulose nanomaterials: new generation materials for solving global issues. **Cellulose.** v. 27, p. 1149-1194, 2020.

[159] HALDAR, D.; PURKAIT, M. K. Micro and nanocrystalline cellulose derivatives of lignocellulosic biomass: A review on synthesis, applications and advancements. **Carbohydrate Polymers**, v. 250, 2020.

[160] VANDERFLEET, O. M.; CRANSTON, E. D. Production routes to tailor the performance of cellulose nanocrystals. **Nature Reviews Materials**, v. 6, n. 2, p. 124–144, 2021.

[161] ILYAS, R. A.; SAPUAN, S. M.; ISHAK, M. R. Isolation and characterization of nanocrystalline cellulose from sugar palm fibres (Arenga Pinnata). **Carbohydrate polymers**, v. 181, p. 1038–1051, 2018.

[162] KIAN, L. K. et al. Isolation and characterization of nanocrystalline cellulose from roselle-derived microcrystalline cellulose. **International journal of biological macromolecules**, v. 114, p. 54–63, 2018.

[163] ANWAR, B. et al. Properties of bacterial cellulose and its nanocrystalline obtained from pineapple peel waste juice. **Fibers and Polymers**, v. 22, p. 1228–1236, 2021.

[164] RAZA, M.; ABU-JDAYIL, B. Cellulose nanocrystals from lignocellulosic feedstock: a review of production technology and surface chemistry modification. **Cellulose**, v. 29, n. 2, p. 685–722, 2022.

[165] TANG, Y.; YANG, H.; VIGNOLINI, S. Recent Progress in Production Methods for Cellulose Nanocrystals: Leading to More Sustainable Processes. **Advanced Sustainable Systems**, v. 6, n. 3, 2022.

[166] LISTYANDA, R. F.; WILDAN, M. W.; ILMAN, M. N. Preparation and characterization of cellulose nanocrystal extracted from ramie fibers by sulfuric acid hydrolysis. **Heliyon**, v. 6, n. 11, 2020.

[167] LEITE, L. S. F. **Preparation and characterization of bionanocomposites based on protein and cellulose nanocrystals by continous casting**. Tese (doutorado em Ciência e Engenharia de Materiais). Universidade Federal de São Carlos. 2020.

[168] MTIBE, A. et al. Recent Developments in Textile-Reinforced Composites and Biocomposites. **Fibres to Smart Textiles**, p. 291–314, 2019.

[169] SHOJAEIARANI, J.; BAJWA, D. S.; CHANDA, S. Cellulose nanocrystal based composites: A review. **Composites Part C: Open Access**, v. 5, 2021.

[170] ZHOU, L. et al. Recent progress on chemical modification of cellulose for high mechanical-performance Poly(lactic acid)/Cellulose composite: A review. **Composites Communications**, v. 23, 2021.

[171] BABAEI-GHAZVINI, A. et al. Cellulose nanocrystals in the development of biodegradable materials: A review on CNC resources, modification, and their hybridization. **International Journal of Biological Macromolecules**, v. 258, 2024.

[172] THOMPSON, L. et al. Cellulose nanocrystals: Production, functionalization and advanced applications. **Reviews on Advanced Materials Science**, v. 58, n. 1, p. 1–16, 2019.

[173] EYLEY, S.; THIELEMANS, W. Surface modification of cellulose nanocrystals. **Nanoscale**, v. 6, n. 14, p. 7764–7779, 2014.

[174] LIN, N.; HUANG, J.; DUFRESNE, A. Preparation, properties and applications of polysaccharide nanocrystals in advanced functional nanomaterials: A review. **Nanoscale**, v. 4, n. 11, p. 3274–3294, 2012.

[175] ABUSHAMMALA, H.; MAO, J. A review of the surface modification of cellulose and nanocellulose using aliphatic and aromatic mono- And di-isocyanates. **Molecules**, v. 24, n. 15, 2019.

[176] GOISSEDET, P. E. C. **United States Patent Office**, 1920.

[177] SIQUEIRA, G.; BRAS, J.; DUFRESNE, A. New process of chemical grafting of cellulose nanoparticles with a long chain isocyanate. **Langmuir**, v. 26, n. 1, p. 402–411, 2010.

[178] STENSTAD, P. et al. Chemical surface modifications of microfibrillated cellulose. **Cellulose**, v. 15, n. 1, p. 35–45, 2008.

[179] MISSOUM, K. **Modification Chimique de Surface de NanoFibrilles de Cellulose (NFC)**. 2012. Université Grenoble Alpes. 2012.

[180] MORELLI, C. L. et al. Supramolecular aromatic interactions to enhance biodegradable film properties through incorporation of functionalized cellulose nanocrystals. **Composites Part A: Applied Science and Manufacturing**, v. 83, p. 80–88, 2016.

[181] ESPINO-PÉREZ, E. et al. Cellulose nanocrystal surface functionalization for the controlled sorption of water and organic vapours. **Cellulose**, v. 23, n. 5, p.

2955–2970, 2016.

[182] PINHEIRO, I. F. et al. Biodegradable PBAT-Based Nanocomposites Reinforced with Functionalized Cellulose Nanocrystals from Pseudobombax munguba: Rheological, Thermal, Mechanical and Biodegradability Properties. **Journal of Polymers and the Environment**, v. 27, n. 4, p. 757–766, 2019.

[183] BITINIS, N. et al. Poly(lactic acid)/natural rubber/cellulose nanocrystal bionanocomposites Part I. Processing and morphology. **Carbohydrate Polymers**, v. 96, n. 2, p. 611–620, 2013.

[184] JAMES, S. L. et al. Mechanochemistry: opportunities for new and cleaner synthesis. **Chemical Society Reviews**, v. 41, p. 413–447, 2012.

[185] INTERNATIONAL UNION OF PURE AND APPLIED CHEMISTRY. **“Mechano-chemical reaction”**IUPAC Compendium of Chemical Terminology, , 2006. Disponível em: <https://doi.org/10.1351/goldbook.MT07141>

[186] PIRAS, C. C.; FERNÁNDEZ-PRIETO, S.; BORGGRAEVE, W. M. DE. Ball milling: A green technology for the preparation and functionalisation of nanocellulose derivatives. **Nanoscale Advances**, v. 1, n. 3, p. 937–947, 2019.

[187] GORRASI, G.; SORRENTINO, A. Mechanical milling as a technology to produce structural and functional bio-nanocomposites. **Green Chemistry**, v. 17, n. 5, p. 2610–2625, 2015.

[188] VATANSEVER, E. et al. **The CNC dispersion quality in various PLA grades**. AIP Conference Proceedings. **Anais**...2023

[189] MA, L. et al. Preparing cellulose nanocrystal/acrylonitrile-butadiene-styrene nanocomposites using the master-batch method. **Carbohydrate polymers**, v. 125, p. 352–359, 2015.

[190] GENG, S. et al. Well-dispersed cellulose nanocrystals in hydrophobic polymers by in situ polymerization for synthesizing highly reinforced bio-nanocomposites. **Nanoscale**, v. 10, n. 25, p. 11797–11807, 2018.

[191] SHOJAEIARANI, J.; BAJWA, D. S.; STARK, N. M. Spin-coating: A new approach for improving dispersion of cellulose nanocrystals and mechanical

properties of poly (lactic acid) composites. **Carbohydrate polymers**, v. 190, p. 139–147, 2018.

[192] MARKETS AND MARKETS. **Nanocelluloses market by type (MFC, NFC, CNC/NCC), Raw material (wood, non-wood), Application (paper&pulp, composites, paints & coating, biomedical & pharmaceuticals, Eletronics & sensors), and region -Global Forecast to 2032**, 2024. Disponível em: <https://www.marketsandmarkets.com/Market-Reports/nano-cellulose-market-56392090.html>

[193] SUZANO. **Celulose Microfibrilada**. Disponível em: <https://www.suzano.com.br/produtos-e-marcas/materias-primas/celulose-microfibrilada>.

[194] BRIZGA, J.; HUBACEK, K.; FENG, K. The Unintended Side Effects of Bioplastics: Carbon, Land, and Water Footprints. **One Earth**, v. 3, n. 1, p. 45–53, 2020.

[195] SOUZA MACHADO, A. A. DE et al. Impacts of Microplastics on the Soil Biophysical Environment. **Environmental Science and Technology**, v. 52, n. 17, p. 9656–9665, 2018.

[196] LI, J.; SONG, Y.; CAI, Y. Focus topics on microplastics in soil: Analytical methods, occurrence, transport, and ecological risks. **Environmental Pollution**, v. 257, 2020.

[197] MOTLOUNG, M. P. et al. Cellulose nanostructure-based biodegradable nanocomposite foams: A brief overview on the recent advancements and perspectives. **Polymers**, v. 11, n. 8, 2019.

[198] DIRLAM, P. T. et al. Polylactide Foams with Tunable Mechanical Properties and Wettability using a Star Polymer Architecture and a Mixture of Surfactants. **ACS Sustainable Chemistry and Engineering**, v. 7, n. 1, p. 1698–1706, 2019.

[199] RIGOLIN, T. R.; COSTA, L. C.; BETTINI, S. H. P. Chemically modified poly(lactic acid): structural approach employing two distinct monomers. **Journal of Polymer Research**, v. 28, n. 4, p. 1–10, 2021.

[200] ZHOU, M. et al. Crystallization, rheology and foam morphology of branched PLA prepared by novel type of chain extender. **Macromolecular Research**, v. 23, n. 3, p. 231–236, 2015.

[201] CUI, W. et al. CO2-assisted fabrication of PLA foams with exceptional compressive property and heat resistance via introducing well-dispersed stereocomplex crystallites. **Journal of CO2 Utilization**, v. 64, 2022.

[202] LI, M. et al. Rheological behavior, crystallization properties, and foaming performance of chain-extended poly (lactic acid) by functionalized epoxy. **RSC Advances**, v. 11, n. 52, p. 32799–32809, 2021.

[203] LI, Y. et al. Nanocellular Foaming Behaviors of Chain-Extended Poly(lactic acid) Induced by Isothermal Crystallization. **ACS Omega**, v. 4, n. 7, p. 12512–12523, 2019.

[204] WANG, X. et al. Microcellular Foaming Behaviors of Poly (Lactic Acid)/Low-Density Polyethylene Blends Induced by Compatibilization Effect. **Journal of Polymers and the Environment**, v. 27, n. 8, p. 1721–1734, 2019.

[205] WANG, X. et al. Multiple actions of poly(ethylene octene) grafted with glycidyl methacrylate on the performance of poly(lactic acid). **RSC Advances**, v. 8, n. 60, p. 34418–34427, 2018.

[206] FORGHANI, E. et al. Compatibility, morphology and mechanical properties of polylactic acid/polyolefin elastomer foams. **Journal of Cellular Plastics**, v. 54, n. 2, p. 235–255, 2016.

[207] FISCHER, E. W.; STERZEL, H. J.; WEGNER, G. Investigation of the structure of solution grown crystals of lactide copolymers by means of chemical reactions. **Kolloid-Zeitschrift & Zeitschrift für Polymere**, v. 251, n. 11, p. 980–990, 1973.

[208] TSUJI, H.; IKADA, Y. Blends of isotactic and atactic poly(lactide)s: 2. Molecular-weight effects of atactic component on crystallization and morphology of equimolar blends from the melt. **Polymer**, v. 37, n. 4, p. 595–602, 1996.

[209] RIGOLIN, T. R. et al. The effect of different peroxides on physical and

chemical properties of poly(lactic acid) modified with maleic anhydride. **Polymer**, v. 179, 2019.

[210] LI, P. et al. Simultaneous Improvement of the Foaming Property and Heat Resistance in Polylactide via One-step Branching Reaction Initiated by Cyclic Organic Peroxide. **Industrial and Engineering Chemistry Research**, v. 59, n. 7, p. 2934–2945, 2020.

[211] SÖDERGÅRD, A.; STOLT, M. Properties of lactic acid based polymers and their correlation with composition. **Progress in polymer science**, v. 27, n. 6, p. 1123–1163, 2002.

[212] BIANCHIN, O. S.; MELO, G. H. F.; BRETAS, R. E. S. Effect of MWCNT carboxyl functionalization on the shear rheological and electrical properties of HMS-PP/MWCNT foams. **Journal of Cellular Plastics**, v. 57, n. 2, p. 210–235, 2021.

[213] TIAN, J.; YU, W.; ZHOU, C. The preparation and rheology characterization of long chain branching polypropylene. **Polymer**, v. 47, n. 23, p. 7962–7969, 2006.

[214] GONÇALVES, L. F. F. F.; REIS, R. L.; FERNANDES, E. M. Forefront Research of Foaming Strategies on Biodegradable Polymers and Their Composites by Thermal or Melt-Based Processing Technologies: Advances and Perspectives. **Polymers**, v. 16, n. 9, 2024.

[215] VENKATESAN, K. B.; KARKHANIS, S. S.; MATUANA, L. M. Microcellular foaming of poly(lactic acid) branched with food-grade chain extenders. **Journal of Applied Polymer Science**, v. 138, n. 29, 2021.

[216] LI, P. et al. Ultrahigh performance polylactide achieved by the design of molecular structure. **Materials and Design**, v. 206, 2021.

[217] LI, P. et al. Fully biodegradable polylactide foams with ultrahigh expansion ratio and heat resistance for green packaging. **International Journal of Biological Macromolecules**, v. 183, p. 222–234, 2021.

[218] BRÜTTING, C. et al. Amorphous polylactide bead foam–effect of talc and

chain extension on foaming behavior and compression properties. **Journal of Renewable Materials**, v. 9, n. 11, p. 1859–1868, 2021.

[219] NI, J. et al. Morphological evolution of PLA foam from microcellular to nanocellular induced by cold crystallization assisted by supercritical CO2. **Journal of Supercritical Fluids**, v. 158, 2020.

[220] YAN, Z. et al. Green Method to Widen the Foaming Processing Window of PLA by Introducing Stereocomplex Crystallites. **Industrial and Engineering Chemistry Research**, v. 58, n. 47, p. 21466–21475, 2019.

[221] REN, Q. et al. Solid state foaming of poly(lactic acid) blown with compressed CO 2: Influences of long chain branching and induced crystallization on foam expansion and cell morphology. **Industrial and Engineering Chemistry Research**, v. 52, n. 37, p. 13411–13421, 2013.

[222] YAN, Z. et al. Green and High-Expansion PLLA/PDLA Foams with Excellent Thermal Insulation and Enhanced Compressive Properties. **Industrial and Engineering Chemistry Research**, v. 59, n. 43, p. 19244–19251, 2020.

[223] KUSKA, R. et al. Thermal analysis of polylactic acid under high CO2 pressure applied in supercritical impregnation and foaming process design. **Journal of Supercritical Fluids**, v. 144, p. 71–80, 2019.

[224] LI, B. et al. A green strategy to regulate cellular structure and crystallization of poly(lactic acid) foams based on pre-isothermal cold crystallization and CO2 foaming. **International Journal of Biological Macromolecules**, v. 129, p. 171–180, 2019.

[225] WANG, G. et al. Low-density and structure-tunable microcellular PMMA foams with improved thermal-insulation and compressive mechanical properties. **European Polymer Journal**, v. 95, p. 382–393, 2017.

[226] WANG, L. et al. Morphologies and properties of epoxy/multi-walled carbon nanotube nanocomposite foams prepared through the free-foaming and limited-foaming process. **Composites Science and Technology**, v. 182, 2019.

[227] NOURI, S.; DUBOIS, C.; LAFLEUR, P. G. Effect of chemical and physical

branching on rheological behavior of polylactide. **Journal of Rheology**, v. 59, n. 4, p. 1045–1063, 2015.

[228] TIWARY, P.; NAJAFI, N.; KONTOPOULOU, M. Advances in peroxide-initiated graft modification of thermoplastic biopolyesters by reactive extrusion. **Canadian Journal of Chemical Engineering**, v. 99, n. 9, p. 1870–1884, 2021.

[229] WANG, Y. et al. Rheological and Topological Characterizations of Electron Beam Irradiation Prepared Long-Chain Branched Polylactic Acid. **Journal of Applied Polymer Science**, v. 122, p. 1857–1865, 2011.

[230] PANG, Y. et al. A comprehensive review of cell structure variation and general rules for polymer microcellular foams. **Chemical Engineering Journal**, v. 430, 2022.

[231] HABIBI, Y.; LUCIA, L. A.; ROJAS, O. J. Cellulose nanocrystals: Chemistry, self-assembly, and applications. **Chemical Reviews**, v. 110, n. 6, p. 3479–3500, 2010.

[232] ZHANG, H. C. et al. Recent Developments of Nanocellulose and its Applications in Polymeric Composites. **ES Food and Agroforestry**, v. 9, p. 1–14, 2022.

[233] PORNBENCHA, K. et al. Functionalization of cellulose nanocrystals extracted from pineapple leaves as a UV-absorbing agent in poly(lactic acid). **RSC Advances**, v. 13, n. 22, p. 15311–15321, 2023.

[234] SZEFER, E. et al. The application of cellulose nanocrystals modified with succinic anhydride under the microwave irradiation for preparation of polylactic acid nanocomposites. **Journal of Renewable Materials**, v. 9, n. 6, p. 1127–1142, 2021.

[235] DUNLOP, M. J. et al. Polylactic Acid Cellulose Nanocomposite Films Comprised of and Octadecylamine. **Polymers**, v. 13, p. 17, 2021.

[236] FARAJ, H. et al. Gas barrier properties of polylactide/cellulose nanocrystals nanocomposites. **Polymer Testing**, v. 113, 2022.

[237] PINHEIRO, I. F. et al. Mechanical, rheological and degradation properties

of PBAT nanocomposites reinforced by functionalized cellulose nanocrystals. **European Polymer Journal**, v. 97, p. 356–365, 2017.

[238] GRISHKEWICH, N. et al. Recent advances in the application of cellulose nanocrystals. **Current Opinion in Colloid and Interface Science**, v. 29, p. 32–45, 2017.

[239] KURNIAWAN, T. W. et al. Cellulose Nanocrystals (CNCs) and Cellulose Nanofibers (CNFs) as Adsorbents of Heavy Metal Ions. **Journal of Chemistry**, v. 2023, 2023.

[240] ZHANG, Y. et al. Preparation methods of cellulose nanocrystals and its application in treatment of environmental pollution: A mini-review. **Colloid and Interface Science Communications**, v. 53, p. 12, 2023.

[241] DURAIRAJ, A. et al. Cellulose Nanocrystals (CNC)-Based Functional Materials for Supercapacitor Applications. **Nanomaterials**, v. 12, n. 11, p. 1–25, 2022.

[242] NASSERI, R. et al. Cellulose nanocrystals in smart and stimuli-responsive materials: a review. **Materials Today Advances**, v. 5, 2020.

[243] DOUARD, L.; BELGACEM, M. N.; BRAS, J. Extraction of Carboxylated Nanocellulose by Combining Mechanochemistry and NADES. **ACS Sustainable Chemistry and Engineering**, v. 10, n. 39, p. 13017–13025, 2022.

[244] KUGA, S.; WU, M. Mechanochemistry of cellulose. **Cellulose**, v. 26, n. 1, p. 215–225, 2019.

[245] GAO, A. et al. Efficient extraction of cellulose nanocrystals from waste Calotropis gigantea fiber by SO42-/TiO2 nano-solid superacid catalyst combined with ball milling exfoliation. **Industrial Crops and Products**, v. 152, 2020.

[246] SONG, K. et al. A green and environmental benign method to extract cellulose nanocrystal by ball mill assisted solid acid hydrolysis. **Journal of Cleaner Production**, v. 196, p. 1169–1175, 2018.

[247] LU, Q. L. et al. One-pot tandem reactions for the preparation of esterified cellulose nanocrystals with 4-dimethylaminopyridine as a catalyst. **RSC**

Advances, v. 5, n. 69, p. 56198–56204, 2015.

[248] TANG, L. et al. Organic solvent-free and efficient manufacture of functionalized cellulose nanocrystals via one-pot tandem reactions. **Green Chemistry**, v. 15, n. 9, p. 2369–2373, 2013.

[249] PARK, S. et al. Cellulose crystallinity index: Measurement techniques and their impact on interpreting cellulase performance. **Biotechnology for Biofuels**, v. 3, p. 1–10, 2010.

[250] MISSOUM, K.; BRAS, J.; BELGACEM, M. N. Organization of aliphatic chains grafted on nanofibrillated cellulose and influence on final properties. **Cellulose**, v. 19, n. 6, p. 1957–1973, 2012.

[251] DOUARD, L. **Surface modification of cellulose and nanocelluloses by innovative green process**. 2022. Université Grenoble Alpes. 2022.

[252] ESPINO-PÉREZ, E. et al. Influence of chemical surface modification of cellulose nanowhiskers on thermal, mechanical, and barrier properties of poly(lactide) based bionanocomposites. **European Polymer Journal**, v. 49, n. 10, p. 3144–3154, 2013.

[253] CELEBI, H.; ILGAR, M.; SEYHAN, A. T. Evaluation of the effect of isocyanate modification on the thermal and rheological properties of poly(ε-caprolactone)/cellulose composites. **Polymer Bulletin**, v. 79, n. 7, p. 4941–4955, 2022.

[254] ROJAS, A. et al. Foaming with scCO2 and Impregnation with Cinnamaldehyde of PLA Nanocomposites for Food Packaging. **Processes**, v. 10, n. 376, p. 16, 2022.

[255] ERYILDIZ, M.; ALTAN, M. Polylactide/halloysite nanocomposite foams: Particle dispersion and mechanical strength. **Acta Physica Polonica A**, v. 135, n. 4, p. 619–621, 2019.

[256] MAHDAVI, M.; YOUSEFZADE, O.; GARMABI, H. A simple method for preparation of microcellular PLA/calcium carbonate nanocomposite using super critical nitrogen as a blowing agent: Control of microstructure. **Advances in**

Polymer Technology, v. 37, n. 8, p. 3017–3026, 2018.

[257] JI, G. et al. Microcellular foaming of poly(lactic acid)/silica nanocomposites in compressed CO2: Critical influence of crystallite size on cell morphology and foam expansion. **Industrial and Engineering Chemistry Research**, v. 52, n. 19, p. 6390–6398, 2013.

[258] QIU, Y. et al. Cyclic tensile properties of the polylactide nanocomposite foams containing cellulose nanocrystals. **Cellulose**, v. 25, n. 3, p. 1795–1807, 2018.

[259] ZHANG, Y. et al. Foaming of Polylactic Acid/Cellulose Nanocrystal Composites: Pickering Emulsion Templating for High-Homogeneity Filler Dispersions. **ACS Applied Polymer Materials**, v. 4, n. 1, p. 111–120, 2022.

[260] SADEGHI, B. et al. Impacts of cellulose nanofibers on the morphological behavior and dynamic mechanical thermal properties of extruded polylactic acid/cellulose nanofibril nanocomposite foam. **Journal of Applied Polymer Science**, v. 139, n. 8, 2022.

[261] CHO, S. Y. et al. Influence of cellulose nanofibers on the morphology and physical properties of poly(lactic acid) foaming by supercritical carbon dioxide. **Macromolecular Research**, v. 21, n. 5, p. 529–533, 2013.

[262] DLOUHÁ, J.; SURYANEGARA, L.; YANO, H. The role of cellulose nanofibres in supercritical foaming of polylactic acid and their effect on the foam morphology. **Soft Matter**, v. 8, n. 33, p. 8704–8713, 2012.

[263] VADAS, D. et al. Flame retardancy of microcellular poly(lactic acid) foams prepared by supercritical CO2-assisted extrusion. **Polymer Degradation and Stability**, v. 153, p. 100–108, 2018.

[264] KOTHAVADE, P. A.; SHANMUGANATHAN, K. Mechanical Properties of PLA/Nanocellulose Composites. **Polylactic Acid-Based Nanocellulose and Cellulose Composites**, p. 181–206, 2022.

[265] REN, Q. et al. Cellulose nanofiber reinforced poly (lactic acid) with enhanced rheology, crystallization and foaming ability. **Carbohydrate Polymers**,

v. 286, 2022.

[266] REN, Q. et al. Light and strong poly (lactic acid)/ cellulose nanofiber nanocomposite foams with enhanced rheological and crystallization property. **Journal of Supercritical Fluids**, v. 190, 2022.

[267] BORUVKA, M. et al. Solid and microcellular polylactide nucleated with PLA stereocomplex and cellulose nanocrystals. **Journal of Thermal Analysis and Calorimetry**, v. 142, n. 2, p. 695–713, 2020.

[268] BORKOTOKY, S. S.; CHAKRABORTY, G.; KATIYAR, V. Thermal degradation behaviour and crystallization kinetics of poly (lactic acid) and cellulose nanocrystals (CNC) based microcellular composite foams. **International Journal of Biological Macromolecules**, v. 118, p. 1518–1531, 2018.

[269] BORKOTOKY, S. S.; DHAR, P.; KATIYAR, V. Biodegradable poly (lactic acid)/Cellulose nanocrystals (CNCs) composite microcellular foam: Effect of nanofillers on foam cellular morphology, thermal and wettability behavior. **International Journal of Biological Macromolecules**, v. 106, p. 433–446, 2018.

[270] KWEON, M. S. et al. Tuning high and low temperature foaming behavior of linear and long-chain branched polypropylene via partial and complete melting. **Polymers**, v. 14, n. 1, 2022.

[271] SILVERSTEIN, R. M.; WEBSTER, F. X. **Spectrometric Identification Of Organic Compounds**. 6. ed. New York: John Wiley & Sons, 1996.

[272] BRETAS, R. E. S.; D'ÁVILA, M. A. **Reologia de polímeros fundidos**. São Carlos: Editora da UFSCar, 2005.

[273] VATANSEVER, E.; ARSLAN, D.; NOFAR, M. Polylactide cellulose-based nanocomposites. **International Journal of Biological Macromolecules**, v. 137, p. 912–938, 2019.

[274] BAGHERIASL, D. et al. Shear rheology of polylactide (PLA)–cellulose nanocrystal (CNC) nanocomposites. **Cellulose**, v. 23, n. 3, p. 1885–1897, 2016.

[275] SIQUEIRA, G.; BRAS, J.; DUFRESNE, A. Cellulosic bionanocomposites: A review of preparation, properties and applications. **Polymers**, v. 2, n. 4, p. 728–765, 2010.

[276] SAMIR, M. A. S. A. et al. Cellulose nanocrystals reinforced poly (oxyethylene). **Polymer**, v. 45, n. 12, p. 4149–4157, 2004.

[277] LU, J.; WANG, T.; DRZAL, L. T. Preparation and properties of microfibrillated cellulose polyvinyl alcohol composite materials. **Composites Part A: Applied Science and Manufacturing**, v. 39, n. 5, p. 738–746, 2008.

[278] GRUNERT, M.; WINTER, W. T. Nanocomposites of cellulose acetate butyrate reinforced with cellulose nanocrystals. **Journal of Polymers and the Environment**, v. 10, p. 27–30, 2002.

[279] WARDAK, M. H. et al. Development of edible films and partial coating, a novel coating technique for tomato fruits, using citric acid-crosslinked starch and cellulose nanofiber. **Progress in Organic Coatings**, v. 187, 2024.

[280] LAVOINE, N.; DESLOGES, I.; BRAS, J. Microfibrillated cellulose coatings as new release systems for active packaging. **Carbohydrate Polymers**, v. 103, n. 1, p. 528–537, 2014.

[281] HU, X. et al. Water-resistant nanocellulose/gelatin biomass aerogel for anionic/cationic dye adsorption. **Separation and Purification Technology**, v. 330, p. 1–10, 2024.

[282] DOMINGUEZ, C. V. R.; WAGNER, J. R. .; PORFIRI, M. C. Nanofibers from soybean hull insoluble polysaccharides as Pickering stabilizers in oil-in-water emulsions formulated under acidic conditions. **Journal of the Science of Food and Agriculture**, v. 104, n. 1, p. 125–133, 2024.

[283] CURVELLO, R.; RAGHUWANSHI, V. S.; GARNIER, G. Engineering nanocellulose hydrogels for biomedical applications. **Advances in colloid and interface science**, v. 267, p. 47–61, 2019.

[284] HOENG, F. et al. Rheology of cellulose nanofibrils/silver nanowires suspension for the production of transparent and conductive electrodes by screen

printing. **Applied Surface Science**, v. 394, p. 160–168, 2017.

[285] BUDTOVA, T. Cellulose II aerogels: a review. **Cellulose**, v. 26, n. 1, p. 81–121, 2019.

[286] DARPENTIGNY, C. et al. Ice-templated freeze-dried cryogels from tunicate cellulose nanocrystals with high specific surface area and anisotropic morphological and mechanical properties. **Cellulose**, v. 27, p. 233–247, 2020.

[287] JOSSET, S. et al. Microfibrillated cellulose foams obtained by a straightforward freeze–thawing–drying procedure. **Cellulose**, v. 24, n. 9, p. 3825–3842, 2017.

[288] MICHEL, B. et al. Production and mechanical characterisation of TEMPO-oxidised cellulose nanofibrils/β-cyclodextrin films and cryogels. **Molecules**, v. 25, n. 10, p. 1–18, 2020.

[289] HO, K. T. H. et al. **Functionalization of cellulose cryogels cross-linked by tetraethylenepentamine for heavy metal removal and oil adsorption**. AIP. **Anais**...2023

[290] CAO, S. et al. Injectable and photothermal antibacterial bacterial cellulose cryogel for rapid hemostasis and repair of irregular and deep skin wounds. **Carbohydrate Polymers**, v. 320, p. 1–12, 2023.

[291] LI, Y. et al. Biocompatible Cryogel with Good Breathability, Exudate Management, Antibacterial and Immunomodulatory Properties for Infected Diabetic Wound Healing. **Advanced Science**, v. 10, n. 31, p. 1–12, 2023.

[292] LEI, C. et al. Cellulose cryogels from herbal residues for oily wastewater purification. **International Journal of Biological Macromolecules**, v. 252, p. 1–9, 2023.

[293] LE, W. T. et al. Leakage-free porous cellulose-based phase change cryogels for sound and thermal insulation. **Solar Energy Materials and Solar Cells**, v. 256, p. 1–11, 2023.

[294] LIU, Y. et al. Numerical investigation of heat transfer mechanisms in microfibrillated cellulose cryogels: effects of concentration, porosity, and

thickness. **Cellulose**, v. 30, n. 16, p. 10025–10038, 2023.

[295] WIESEMÜLLER, F. et al. Biopolymer Cryogels for Transient Ecology-Drones. **Advanced Intelligent Systems**, v. 5, n. 7, 2023.

[296] LAZZARI, L. K. et al. Sorption capacity of hydrophobic cellulose cryogels silanized by two different methods. **Cellulose**, v. 24, n. 8, p. 3421–3431, 2017.

[297] YOUSEFI, B. et al. Preparation and characterization of morphological and mechanical properties of cellulose cryogel nanofibers reinforced by different polyamide resins. **Journal of Polymer Research**, v. 30, n. 8, p. 1–15, 2023.

[298] JUAN, L. T. et al. Functionalized Cellulose Nanofibers as Crosslinkers to Produce Chitosan Self-Healing Hydrogel and Shape Memory Cryogel. **ACS Applied Materials and Interfaces**, v. 14, n. 32, p. 36353–36365, 2022.

[299] GUO, R. et al. Processable Pickering emulsion for composite cryogel with cellulose nanofibrils and nanochitin. **Carbohydrate Polymers**, v. 334, 2024.

[300] JUNG, L. S. et al. Quantitative interpretation of the response of surface plasmon resonance sensors to adsorbed films. **Langmuir**, v. 14, n. 19, p. 5636–5648, 1998.

[301] GICQUEL, E. **Development of stimuli-responsive cellulose nanocrystals hydrogels for smart applications**. 2017. 329 f. Université Grenoble Alpes. 2017.

[302] KIM, C. T. C. G. SPR microscopy and its applications to high-throughput analyses of biomolecular binding events and their kinetics. **Biomaterials**, v. 28, p. 2380–2392, 2007.

[303] ZHU, G. et al. Dual-enhancement effect of electrostatic adsorption and chemical crosslinking for nanocellulose-based aerogels. **Industrial Crops and Products**, v. 139, p. 1–9, 2019.

[304] SUN, C. True density of microcrystalline cellulose. **Journal of Pharmaceutical Sciences**, v. 94, n. 10, p. 2132–2134, 2005.

[305] HASSAN, M. L. et al. Enzyme-assisted isolation of microfibrillated cellulose

from date palm fruit stalks. **Industrial Crops and Products**, v. 55, p. 102–108, 2014.

[306] DESMAISONS, J. et al. A new quality index for benchmarking of different cellulose nanofibrils. **Carbohydrate Polymers**, v. 174, p. 318–329, 2017.

[307] TADROS, T. et al. Formation and stability of nano-emulsions. **Advances in Colloid and Interface Science**, v. 108–109, p. 303–318, 2004.

[308] DELMAS, T. et al. How to prepare and stabilize very small nanoemulsions. **Langmuir**, v. 27, n. 5, p. 1683–1692, 2011.

[309] GUPTA, A. et al. Nanoemulsions: Formation, properties and applications. **Soft Matter**, v. 12, n. 11, p. 2826–2841, 2016.

[310] MASON, T. G. et al. Nanoemulsions: Formation, structure, and physical properties. **Journal of Physics Condensed Matter**, v. 18, n. 41, 2006.

[311] RUIZ, E. et al. Study of sonication parameters on PLA nanoparticles preparation by simple emulsion-evaporation solvent technique. **European Polymer Journal**, v. 173, p. 1–11, 2022.

[312] MISSOUM, K.; BRAS, J.; BELGACEM, M. N. **Method for forming a hydrophobic layer.** United States of America, 2016. Disponível em: <https://patents.google.com/patent/US20160168696A1/en>

[313] Le GARS, M. et al. High-barrier and antioxidant poly(lactic acid)/nanocellulose multilayered materials for packaging. **ACS Omega**, v. 5, n. 36, p. 22816–22826, 2020.

[314] Le GARS, M. **Surface modifications of cellulose nanocrystals for biobased food packaging applications**. 2020. 349 f. Université Grenoble Alpes. 2020.